

Dissertation zur Erlangung des Doktorgrades
der Fakultät für Chemie und Pharmazie
der Ludwig-Maximilians-Universität München

Investigations into *s*-Heptazine-Based Carbon Nitride Precursors

Andreas Sattler
aus
Augsburg
2010

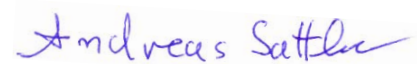
Erklärung

Diese Dissertation wurde im Sinne von § 13 Abs. 3 bzw. 4 der Promotionsordnung vom 29. Januar 1998 von Herrn Prof. Dr. Wolfgang Schnick betreut.

Ehrenwörtliche Versicherung

Diese Dissertation wurde selbstständig, ohne unerlaubte Hilfe erarbeitet.

München, den 12.02.2010



Andreas Sattler

Dissertation eingereicht am 15.02.2010

1. Gutachter: Prof. Dr. Wolfgang Schnick

2. Gutachter: Prof. Dr. Dirk Johrendt

Mündliche Prüfung am 20. April 2010

*Für meine Familie und Freunde
Und für alle denen dies Information und Hilfe sein mag*

Acknowledgements

First of all, I would like to express my gratitude to Prof. Dr. Wolfgang Schnick for having granted me the opportunity to work in his research group. His guidance and expertise have been invaluable for the present work.

I am most grateful to Prof. Dr. Dirk Johrendt for his willingness to be the co-referee of this thesis.

I thank Prof. Dr. Bettina V. Lotsch, Prof. Dr. Jürgen Senker, Prof. Dr. Konstantin Karaghiosoff and Priv. Doz. Dr. Klaus Müller-Buschbaum for being available as examiners in my viva-voce.

The past and present members of the work group and other members of the department, whose company I have had the honor to enjoy, have helped and supported me in a multitude of ways. Working with these fine colleagues has become a part of my life that I will look back upon often and happily. I would like to address special thanks and gratitude to:

My predecessors Dr. Barbara Jürgens and Prof. Dr. Bettina V. Lotsch and my successors Sophia Makowski and Eva Wirnhier working on carbon nitride chemistry. I want to express my gratitude for contributing in many discussions and for every-day help, ideas and inspirations they have offered. After the interlude represented by my works the research topic will be in female hands exclusively once more.

All past and present members of laboratory D.2.103: Sophia Makowski and Eva Wirnhier, Cordula Braun, Yamini Avadhut, Dr. Sabine Beyer, Stefanie Hering, Christian Minke, Stefan „Superflip“ Sedlmaier, Theresa Soltner, Dr. Johannes Weber are all thanked for contributing to this fine working environment. Christian Minke for conducting solid-state NMR and REM measurements; as well as for his willingness to compete in several word-play duels and for his helpful suggestions on improving the energy efficiency of our laboratory. Dr. Stefan Rannabauer, who very much inspired my interest in solid-state chemistry during my research practicum.

I also want to express thanks to all my cooperation partners, especially: Prof. Dr. Jürgen Senker and his co-workers Daniel Gunzelmann, Dr. Jan Seyfarth and Dr. Lena Seyfarth for their expertise concerning solid-state NMR spectroscopy. As well as the PZZ team aka Dr. Sandro Pagano, Dr. Martin Zeuner and Alexander Zurawski who have worked with me on melamine melem adduct phases.

My bachelor and research practicum students Lucia R. Lorenz, Michael R. Budde, Nicole Braml, Stefanie Schönberger, Simon Welzmilller whose drive and ambition have helped and supported this work a great deal.

Dr. Oliver Oeckler for his invaluable help concerning crystallographic problems. As well as for providing additional insights concerning several aspects of science and life in general like the many flaws of spectroscopy making it vastly inferior to diffraction, the needlessness of noodles and the meaning of “rüftig” just to mention some select examples.

Thomas Miller, Dr. Peter Mayer and Sandra Albrecht for measuring single-crystal data.

Those who have been my fellow students all the way from undergraduate, especially: Daniel Bichler, Nina Hahn, Dr. Juliane A. Kechele, Phillipp Lorenz, Dr. S. Rebecca Römer, and Marc Thormählen.

The other current members and alumni of solid-state chemistry (and associated groups) at LMU (in alphabetical order) Dr. Ulrich Baisch, Dr. Sascha Correll, Rainer Frankovsky, Cora Hecht, Elsbeth Hermanns, Frauke Hintze, Christoph Höller, Dr. Henning Höppe, Dr. Petra Jakubcova, Sebastian Junggeburth, Dr. Friedrich Karau, Dr. Alexandra Lieb, Catrin Löhnert, Saskia Lupart, Dr. Helen Müller, Dr. Abanti Nag, Dr. Regina Pocha, Florian „FloPu“ Pucher, Tobias Rosenthal, Marianne Rotter, Christoph „Rybi“ Rybak, Dr. Jörn Schmedt auf der Günne, Christian Schmolke, Matthias Schneider, Sebastian Schneider, Markus Seibald, Dr. Florian Stadler, Dr. Michael Tauchert, Marcus Tegel, Dr. Sabarinathan Venkatachalam, Wolfgang Wunschheim and Veronika Zinth.

The other members of the department who have assisted me concerning analysis, administrative tasks and in many other ways. Dr. Markus Döblinger (TEM and ED), Dr. Bernhard Kempf, Robert Eicher and Gertraud Käser (elemental analysis), Armin Andres (mass spectroscopy), Irmgard Peter (IR), Helmut „Piko“ Hartl (ICP–AES), Prof. Dr. Konstantin Karaghiosoff and Peter Mayer (solution-state NMR), and those working at the precision mechanics and the glassblower workshops.

Univ.- Prof. Dr. Hubert Huppertz and the past and present members of his group, which is now located at Innsbruck, whom I got to know during their time in Munich. Especially I would like to name, Dr. Johanna Knyrim, Dr. Gunter Heymann, Sonja Herlinka, Constantin Beyer and Dr. Holger Emme.

And last, but not least, to all my friends, family and others who, though in a mostly non-chemical way, have helped me immeasurably.

Science may set limits to knowledge, but should not set limits to imagination.

Bertrand Russell (1872 - 1970)

Contents

Contents.....	1
1. Introduction	4
1.1 Basic Concepts and Current State of Research	4
1.2 Carbon Nitride Compounds – a Historical Outline	13
1.3 Goals of this Study	18
2. Experimental Methods.....	19
2.1 Preparative Methods.....	19
2.1.1 Vacuum and Inert Gas Line	19
2.1.2 Furnaces	19
2.1.3 Glove-Box	19
2.1.4 Operation Techniques	20
2.2 Analytical Methods	21
2.2.1 Diffraction Techniques.....	21
2.2.2 Spectroscopic Methods	23
2.2.4 Thermal Analysis	24
2.2.5 Elemental Analysis.....	24
2.2.6 Mass Spectroscopy.....	25
2.2.7 Magnetic Measurements	25
3. The Formation of Melem.....	26
3.1 Introduction	26
3.2 Melamine Melem Adduct Phases.....	26
3.3 Oxygen-Containing Precursors – A Strategy Towards Oxo-Amino Heptazines?	38
3.4 Enhancing the Synthesis of Melem.....	41
4. The Formation of Melam.....	43
4.1 The Melamium Adduct $C_6N_{11}H_{10}Cl \cdot 0.5NH_4Cl$	43
4.2 The Melamium Melamine Adduct $C_6N_{11}H_{10}SCN \cdot 2C_3N_3(NH_2)_3$	48
4.3 On the Potential of Thiourea as a Carbon Nitride Precursor.....	52
5. Melemium Salts	53
5.1 Introduction	53
5.2 Melemium Melem Perchlorate.....	53
5.3 Melemium Diperchlorate Sesquihydrate.....	58
5.3 Melemium Methylsulfonates.....	61
5.4 The Melemium Hydrogensulfate $H_3C_6N_7(NH_2)_3(HSO_4)_3$	68

6. Melon	73
6.1 Introduction	73
6.2 Synthesis by Condensation of Melamine	75
6.3 Synthesis by Reaction of NaSCN with Chlorine	81
6.4 The Pharaoh's Serpents – “Melon“ by Pyrolysis of Hg(SCN) ₂	86
7. Cyameluric Acid and its Salts	90
7.1 Introduction	90
7.2 Cyameluric Acid Trihydrate H ₃ C ₆ N ₇ O ₃ · 3H ₂ O.....	92
7.2.1 General Aspects and Synthesis	92
7.2.2 Crystal Structure of H ₃ C ₆ N ₇ O ₃ · 3H ₂ O.....	93
7.2.3 Properties.....	98
7.2 Sodium Dihydrogencyamelurate Tetrahydrate - NaH ₂ C ₆ N ₇ O ₃ · 4H ₂ O.....	100
7.3 Metal(II) Cyamelurates	104
7.4 The Cyameluric Acid Adduct H ₃ C ₆ N ₇ O ₃ · H ₂ NMe ₂ Cl · H ₂ O	113
7.5 A New Sodium Cyamelurate.....	118
8. Tricyanomelaminates and Melonates	122
8.1 Formation and Decomposition of Melonates in Salt Melts.....	122
8.1.1 General Aspects and Synthetic Procedures	122
8.1.2 Thermal Analysis	123
8.1.3 Mechanistic Considerations	127
8.2 Anhydrous Potassium Melonate - K ₃ C ₆ N ₇ (NCN) ₃	131
9. Other Reactions of Heptazines	135
9.1 Cyameluric Chloride C ₆ N ₇ Cl ₃	135
9.2 Synthetic Attempts towards Cyameluric Cyanide	137
9.3 Decomposition of Heptazines in Aqueous Solution	139
9.4 N-Guanyllammelin Dihydrochloride.....	141
9.5 Additional Derivatization Reactions of Heptazines	145
10. Discussion and Outlook	147
10.1 Structuring and Understanding the Thermal Condensation of C/N/H Precursors	147
10.2 The Importance of Adduct Phases Containing Carbon Nitride Precursors.....	149
10.3 Comparison of Structural and Spectroscopic Data	151
10.4 Additional Goals and Possible Applications.....	156
11. Summary	157
11.1 The Condensation of Carbon Nitride Precursors	157
11.2 Investigations of Heptazine-based Compounds	158
11.3 Chemical Reactivity of Heptazines	160

12. Appendix	161
12.1 Synthesis.....	161
12.1.1 $C_6N_7(NH_2)_3$	161
12.1.2 $2C_3N_3(NH_2)_3 \cdot C_6N_7(NH_2)_3$	162
12.1.3 $C_3N_3(NH_2)_3 \cdot C_6N_7(NH_2)_3$	162
12.1.4 $C_3N_3(NH_2)_3 \cdot 3C_6N_7(NH_2)_3$	162
12.1.5 Attempts to Synthesize Adduct Phases from Solution.....	163
12.1.6 $C_6N_{11}H_{10}Cl \cdot 0.5NH_4Cl$	163
12.1.7 $C_6N_{11}N_{10}SCN \cdot 2C_3N_3(NH_2)_3$	164
12.1.8 $HC_6N_7(NH_2)_3ClO_4 \cdot C_6N_7(NH_2)_3$	164
12.1.9 $H_2C_6N_7(NH_2)_3(ClO_4)_2 \cdot 1.5H_2O$	164
12.1.10 $HC_6N_7(NH_2)_3H_2C_6N_7(NH_2)_3(SO_3Me)_3 \cdot H_2O$	164
12.1.11 $H_2C_6N_7(NH_2)_3(SO_3Me)_2 \cdot H_2O$	165
12.1.12 $H_3C_6N_7(NH_2)_3(HSO_4)_3$	165
12.1.13 $C_6N_7(NH_2)(NH)$, Raw Melon from Melamine.....	165
12.1.14 $C_6N_7(NH_2)(NH)$, Highly Crystalline Melon.....	166
12.1.15 “Melon” from Sodium Thiocyanate.....	166
12.1.16 “Melon” from Mercury(II) Thiocyanate.....	166
12.1.17 $H_3C_6N_7O_3 \cdot 3H_2O$	167
12.1.18 $Na[H_2(C_6N_7)O_3] \cdot 4H_2O$	167
12.1.19 $CaNH_4(H_2C_6N_7O_3)(HC_6N_7O_3) \cdot 6H_2O$	168
12.1.20 $[Cu(NH_3)_2]_3(C_6N_7O_3)_2 \cdot 2H_2O$	168
12.1.21 $(NH_4)_2[Zn(H_2O)_6](HC_6N_7O_3)_2 \cdot 2H_2O$	168
12.1.22 $H_3C_6N_7O_3 \cdot H_2NMe_2Cl \cdot H_2O$	168
12.1.23 $K_3C_6N_7(NCN)_3$ from a Thiocyanate Melt.....	169
12.1.24 $K_3C_6N_7(NCN)_3$ from a Cyanate Melt.....	170
12.1.25 $K_3C_3N_3(NCN)_3$ from a Cyanate Melt.....	170
12.1.26 $Na_3C_3N_3(NCN)_3$ from a Cyanate Melt.....	171
12.1.27 $Na_3C_6N_7(NCN)_3$ from a Thiocyanate Melt.....	171
12.1.28 Reactivity in KSCN melts.....	172
12.1.29 $H_2(C_3N_3)=O(NH_2)NHC(NH_2)_2Cl_2$	172
12.1.30 $C_6N_7O_3 \cdot 4.5H_2O$	172
12.1.31 $C_6N_7O_3 \cdot 4H_2O$	173
12.1.32 $C_6N_7Cl_3$	173
12.2 Chemicals.....	174
12.3 Abbreviations and Acronyms.....	176
12.4 List of Publications.....	178
12.5 Deposition Numbers.....	181
12.6 Crystallographic Data.....	182
12.6.1 $C_6N_{11}H_{10}Cl \cdot 0.5NH_4Cl$	182
12.6.2 $C_6N_{11}H_{10}SCN \cdot 2C_3N_3(NH_2)_3$	184
12.6.3 $H_2C_6N_7(NH_2)_3(ClO_4)_2 \cdot 1.5H_2O$	187
12.6.4 $H_3C_6N_7(NH_2)_3(HSO_4)_3$	191
12.6.5 $Na_3C_6N_7O_3 \cdot 4H_2O$	193
12.6.6 $H_2(C_3N_3)=O(NH_2)NHC(NH_2)_2Cl_2$	194
12.7 Curriculum Vitae.....	195
Bibliography	196

1. Introduction

1.1 Basic Concepts and Current State of Research

Nitridic materials constitute a continuously emerging field of chemistry.^[1-3] Since nitrides cannot be collected from exploitable natural deposits and in general require a more complex synthesis than oxides, the natural abundance of oxidic materials has allowed the properties of many oxides to be investigated much earlier than has been the case for nitrides. Especially the polymorphs of Si_3N_4 are famous as resilient and hard high-performance ceramics. Nitridosilicates and oxonitridosilicates have also found applications, luminescent materials for light emitting diodes (LEDs) being a very prominent example.^[4] The nitrides of many other elements, however, just as well hold the potential for a manifold of properties and applications. The chemical nature of nitride materials is a very versatile one. There are various examples of covalent, metallic or salt-like compounds. Covalently bonded examples both occur in molecular species as well as in solid-state compounds. In this respect the nitrides of carbon will be addressed as an interesting example of covalent nitrides with a great potential for applications, which will be the main topic of this thesis.

Some organic nitriles and cyanogen are, so far, the only strictly binary examples of carbon nitrides (Scheme 1) that have so far been synthesized on a bulk scale. These compounds are, however, usually not counted among carbon nitrides. A condensed solid carbon nitride in which carbon(+IV) and nitrogen(-III) atoms are alternating can be expected to exhibit the formula C_3N_4 . Such a compound has been in the focus of interest for a while and many possible structures have been brought up. Molecular propositions for C_3N_4 (cf. Figure 1) have also been discussed. The depicted example shows a molecule of formula $\text{N}(\text{CN})_3$ that might best be called “tricyanamide”. There have been some attempts to obtain this molecule and some theoretical calculations.^[5] The synthesis of $\text{N}(\text{CN})_3$, however, has not been successful. This compound is thus not of central interest for this theses which will primarily focus on polymeric or highly linked solid-state structures. Carbon nitrides have a vast

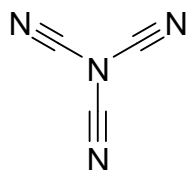
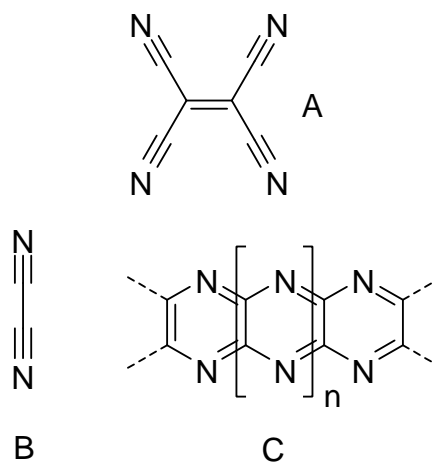


Figure 1. $\text{N}(\text{CN})_3$ a possible structure of the postulated molecular C_3N_4 .

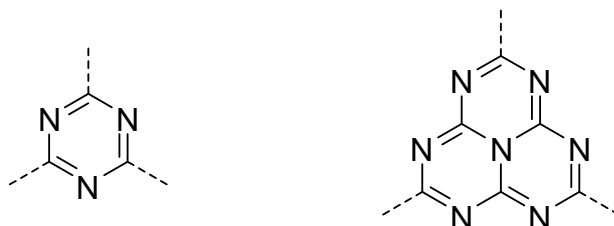


Scheme 1. Selected examples of common molecular carbon nitrides. Tetracyanoethylen, A cyanogen B, and its reported polymerization product C.

potential of possible applications. The most prominent property discussed for C_3N_4 is its possible hardness. Initial calculations even suggested that the hardness of C_3N_4 could surmount the one of diamond, thus rendering this compound the world’s hardest material.^[6-8]

The compounds discussed as follows regularly feature characteristic heterocycles. One is the *s*-triazine (*sym*-triazine; 1,3,5-triazine) core or cyanuric nucleus

[C₃N₃], the other is the *s*-heptazine (tri-*s*-triazine, *sym*-heptazine, heptaazaphenalene) core also known as cyameluric nucleus [C₆N₇] (cf. Scheme 2).^[9] These structural motifs are necessary for understanding the structure and nomenclature of carbon nitrides and will be addressed in more detail as follows.



Scheme 2. The structure of the triazine (left) and the heptazine core (right).

Two basic types of carbon nitride networks have been discussed in the literature. First there are three-dimensionally cross-linked networks. Such propositions have particularly been brought up for ultra-hard C₃N₄ modifications. These phases are expected to exhibit high bulk modulus. High-pressure conditions are discussed for obtaining such compounds as expected for dense and hard materials.^[10] Despite considerable efforts undertaken in this direction, no well defined sample has been yielded, yet. This leaves the actual structure and properties of such compounds subject to some uncertainty. A lot of theoretical work has, however, been conducted for several possible C₃N₄ modifications, thus preferable structural propositions are already well investigated. This field cannot be covered in all due detail, in the following. In this regard some very informative reviews on the topic are recommended for further information.^[10,11] The high-pressure synthesis of carbon nitride imide C₂N₂(NH) has been described,^[12] displaying a very interesting recent advance towards 3D carbon nitride networks. This is a compound already quite close to the composition C₃N₄.^[a] It crystallizes in a defect Wurtzite structure (cf. Figure 2) like the one of Sinoite. It may be noted that Sinoite (Si₂N₂O), found in meteorites, is the only naturally occurring oxonitrido silicate known.

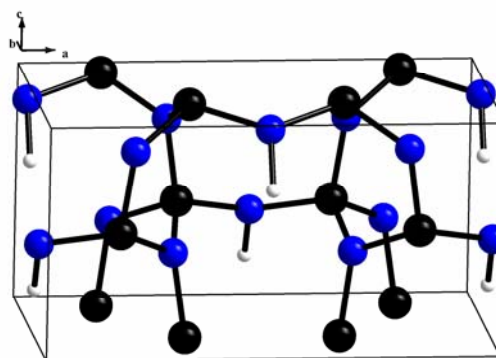


Figure 2. The crystal structure of C₂N₂(NH).

Possible layered modifications of C₃N₄ are called graphitic carbon nitride (g-C₃N₄) referring to the layered structure of graphite. Such 2D carbon nitride structures have received even more synthetic interest than 3D C/N networks. This is probably due to the fact that for accessing such compounds there are no specific requirements concerning pressure. Thus, technical prerequisites usually constitute a significantly less demanding issue. Furthermore, graphitic carbon nitride (g-C₃N₄) also possibly constitutes a suitable precursor for structures displaying 3D cross-linking accessible under high-pressure conditions. This is to some degree referring to a possible analogy to the graphite / diamond system. Several methods like conventional bulk synthesis (e.g. precursor pyrolysis), CVD (chemical vapor deposition), molecular beam epitaxy and others have been employed.^[2] Central parts of this work aim at an-

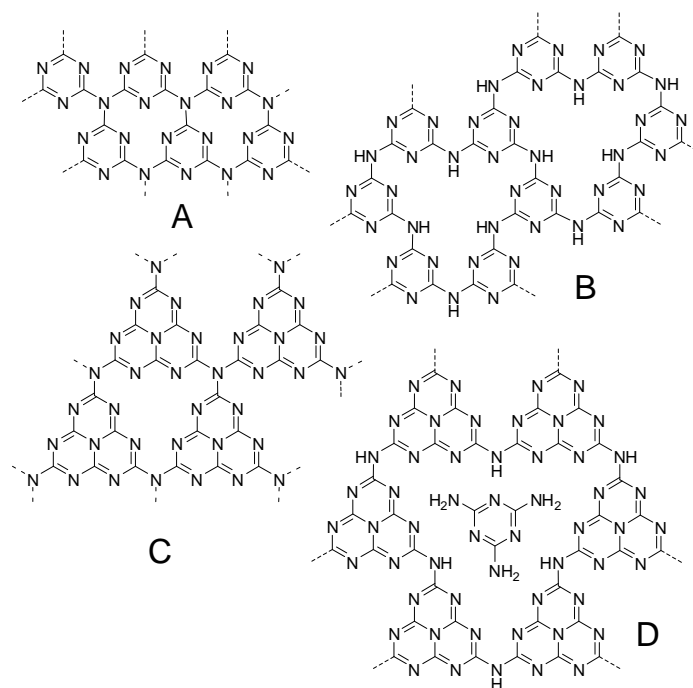
[a] Interestingly the empirical formula of C₂N₂(NH) ≡ C₂N₃H is identical to the one of the polymer melon C₆N₇(NH)(NH₂) ≡ C₆N₉H₃ ≡ 3C₂N₃H (which will be addressed later on, cf. Scheme 7). The compound can thus formally be regarded as a high-pressure modification of melon.

swering synthetic questions. Thus, in the following mainly synthesis on a bulk scale will be addressed. The term $g\text{-C}_3\text{N}_4$ already hints at the fact that in order to understand such compounds it is best to formally derive them from the structure of graphite. Some structures of layered 2D carbon nitrides are depicted in Scheme 3. Though there is quite an impressive amount of work concerning triazine-based $g\text{-C}_3\text{N}_4$ (cf. Scheme 3 structure A) a compound of this structure has never been unequivocally characterized. The existence of such networks can, however, not be completely ruled out.^[7,13,14] The synthesis of a $g\text{-C}_3\text{N}_4$ network displaying structure C (cf. Scheme 3) has recently been claimed by *Antonietti et al.*^[15] New investigations, however, have yielded different results,

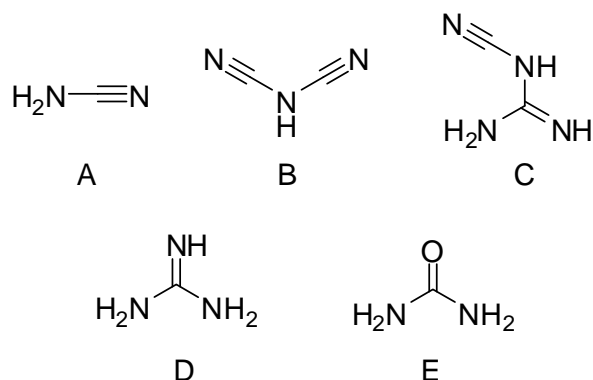
once again putting the quest for structure C back into the focus of interest. Under the respective synthetic conditions chosen another triazine-based network B is found instead.^[16] Such networks are termed polytriazine imide (PTI). As of now, two compounds displaying such a structure have been described. One is intercalated with LiCl ^[16] while the other incorporates HCl .^[14] It does not seem likely that the networks can be completely liberated of these or other substances filling the voids within the structure. A heptazine-based analogue structure, polyheptazine imide (PHI) has also been recently described.^[17] This novel network incorporates melamine molecules tightly fixed by H-bonding interactions as can be seen in Scheme 3 D. Other recent investigations into nitrogen-rich carbon nitrides have also been reported in the literature.^[13,18] A significant amount of work has been invested into the investigation and study of preferable building blocks and motifs of $g\text{-C}_3\text{N}_4$. Heptazine-based models for $g\text{-C}_3\text{N}_4$ have been discussed for a considerable amount of time^[19] and proven to be energetically favorable over triazine-based ones by theoretical calculations.^[20,21]

The term C/N/H compounds will be frequently used and needs some clarification. The expression as used in this work does not refer to any compound incorporating carbon, nitrogen and possibly hydrogen atoms whatsoever. Instead only compounds expressing a high degree of covalent C-N bonds, atomic ratio C : N that is favorable for the formation of carbon nitride materials and a lack of typical organic (i.e. expressing C-H and C-C bonds) moieties are meant. These compounds comprise some useful starting materials and precursors for the synthesis of carbon nitrides and are thus of great interest for this field of chemistry.

In order to provide an overview on the state of synthesis, certain basic C/N/H compounds must be addressed as they are fundamental for understanding carbon nitride chemistry. Many of these were assigned non-systematical names which, though often non-intuitive, are frequently used. Thus, nomenclature can be confusing to those not profoundly familiar with these compounds. A summary of the compounds necessary for a complete understanding of the following sections will be provided as follows.



Scheme 3. Structure of some exemplary carbon nitride networks. A possible model for s -triazine-based $g\text{-C}_3\text{N}_4$ A, polytriazine imide B, heptazine-based $g\text{-C}_3\text{N}_4$ C, polyheptazine imide D.

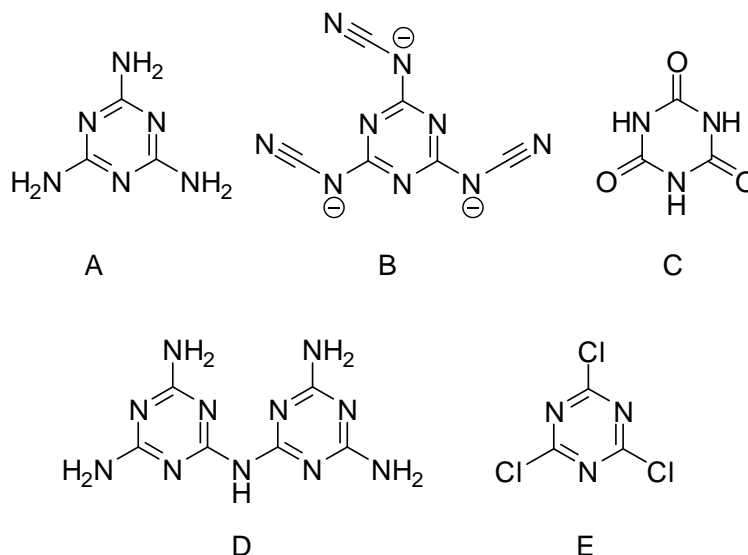


Scheme 4. Structures of some small acyclic C/N/H molecules (from upper left to lower right). Cyanamide (NH_2CN , A), dicyanamide ($\text{NH}(\text{CN})_2$, B), dicyandiamide (cyanoguanidine, $\text{C}_2\text{N}_4\text{H}_4$, C), guanidine ($\text{CNH}(\text{NH}_2)_2$, D) and urea ($\text{CO}(\text{NH}_2)_2$, E).

For the sake of clarity C/N/H molecules (and some additional, very important compounds featuring further non-nitrogen heteroatoms) will be divided into three groups. The first of which comprises small acyclic molecules. A small overview of such compounds is provided by Scheme 4. Especially cyanamide (Scheme 4 A), dicyanamide (Scheme 4 B) and dicyandiamide (Scheme 4 C) have been extensively investigated during preliminary works. The sheer amount of cyanamide / carbodiimide compounds existing is too large as to offer a comprehensive overview in this context. In the case of dicyanamide a large variety of metal^[22-24,107] and nonmetal salts (ammonium,^[25-27,108] hydrazinium and N-alkylhydrazinium,^[28] guanidinium,^[29,108] or

guanylurea^[30,108] compounds) have been prepared and studied. As was already stated, the thermal reactivity of these compounds has been proven to be particularly interesting. Polymerization and condensation reactions enable the synthesis of larger molecular species and ultimately polymers and networks. Especially dicyandiamide still holds considerable importance as a precursor and was used in some recent investigations.

Triazine-based compounds, which are the next group of C/N/H molecules discussed, play an important role for carbon nitride chemistry. The triazine motif is part of many, both actually studied and postulated network structures (cf. Scheme 3). Some important triazine-based molecular compounds are depicted in Scheme 5.



Scheme 5. Molecular structure of some *s*-triazine derivatives (from upper left to lower right). Melamine ($\text{C}_3\text{N}_3(\text{NH}_2)_3$, A), the tricyanomelaminatone anion ($\text{C}_3\text{N}_3(\text{NCN})_3^{3-}$, B), cyanuric acid ($\text{H}_3\text{C}_3\text{N}_3\text{O}_3$, C), melam ($\text{C}_6\text{N}_{11}\text{H}_9 \equiv (\text{NH}_2)_2(\text{C}_3\text{N}_3)\text{NH}(\text{C}_3\text{N}_3)(\text{NH}_2)_2$, D) and cyanuric chloride ($\text{C}_3\text{N}_3\text{Cl}_3$, E).

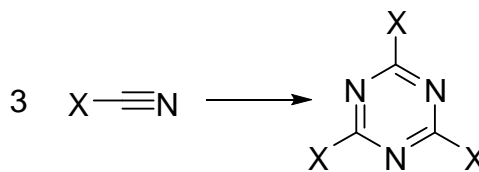
All triazines can formally be regarded trimerization products of the respective cyanides. Such trimerization reactions are a very convenient and versatile tool for preparing triazines and are commonly found as will be shown below. One must, however, be careful not to confuse this formalism with actual reactivity, as a preference for a concerted cyclotrimerization is

not necessarily found. The thermal “trimerization” of cyanamide to melamine e.g. proceeds via dicyandiamide, which is intermediately formed. This compound in fact remains stable over a considerable temperature range and is ultimately transformed to melamine. Especially the conversion of ammonium dicyanamide to dicyandiamide has been the subject of in depth investigations.^[27] Melamine (cf. Scheme 5 A) is a triazine-based molecule of great importance featuring a manifold of industrial uses. Thus melamine is manufactured on megaton scale and readily available in high purity. It accordingly constitutes a convenient basic starting material for carbon nitride chemistry. The technical synthesis of melamine starts from urea. Melamine can, however, be yielded starting from many other small C/N/H molecules as well.^[26,29,31,32] Melamine thus obviously constitutes a thermodynamic sink favorable over a wide range of conditions.

Tricyanomelaminates (Scheme 5 B) are trimerization products of certain dicyanamides and have also been subject to detailed investigations. Especially alkali metal tricyanomelaminates prepared by cyclotrimerization have been well studied regarding their structure and properties.^[22] Non-metal tricyanomelaminates have been investigated as precursors for C_3N_4 .^[33]

The molecule melam consisting of two triazine rings has been subject to much speculation over the course of years. Its existence and structure have not been established free of doubt until very recently.^[34]

Heptazine^[b]-based compounds are the primary interest of this thesis. It has already been stated that the heptazine core is known under a variety of appellations. According to IUPAC nomenclature it should be termed heptaaza phenalene (referring to the respective hydrocarbon cf. Figure 3). This is, however, sparsely done. The expression tri-*s*-triazine (three fused triazine rings) is also quite common. The prefix “*s*” or “*sym*” (uncommon) is short for symmetric and expresses, that the seven nitrogen atoms are arranged in a way that allows for maximum symmetry. The *s*-heptazine motif is of great importance for carbon nitride networks as heptazine-based *g*- C_3N_4 was calculated to be thermodynamically favorable over the respective triazine-based form as was already mentioned.^[20,21] A variety of heptazine-based molecular species have been prepared and studied (cf. Scheme 3). Structural data of some of those compounds has become available recently (references are given separately for each compound as follows). Some of these structures are contents of this work and will be dealt with in the respective sections.



Scheme 6. The trimerization of nitriles to triazines.

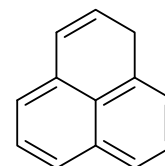
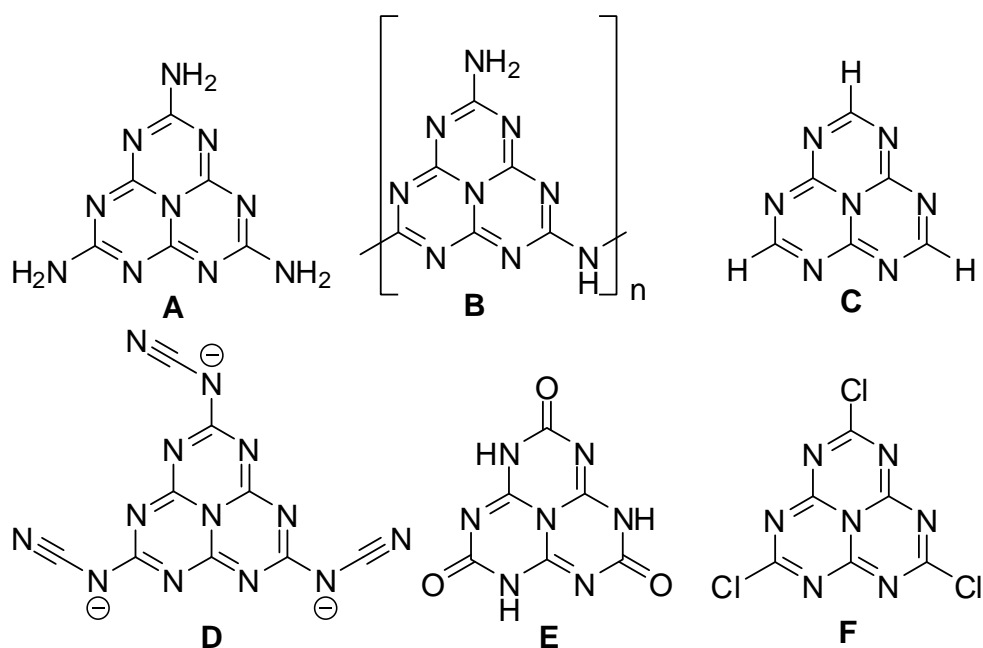


Figure 3. The Phenalene molecule $C_{13}H_{14}$.

[b] This name, as well as the expression cyameluric nucleus, will be preferably used in this thesis. All synonymous expressions are only mentioned to allow better comparability with other literature.

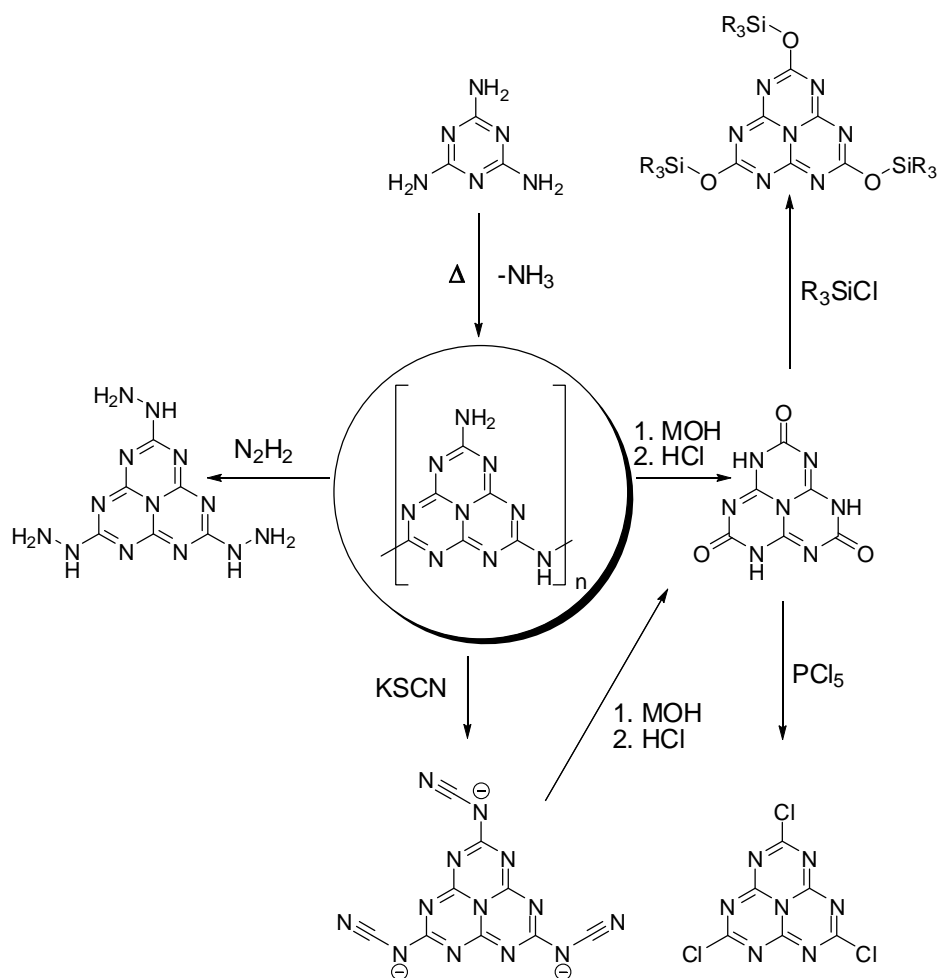


Scheme 7. Molecular structure of some *s*-heptazine derivatives (from upper left to lower right). melem ($C_6N_7(NH_2)_3$, A), melon ($C_6N_7(NH)(NH_2)$, B), *s*-heptazine (tri-*s*-triazine, $C_6N_7H_3$, C), the melonate anion (tricyanomelemate, $C_6N_7(NCN)_3^{3-}$, D), cyameluric acid ($H_3C_6N_7O_3$, E), and cyameluric chloride (trichloro-*s*-heptazine, $C_6N_7Cl_3$, F).

The molecule melem^[35] (Scheme 7 A) is of crucial importance for this thesis as it constitutes an intermediate playing a key role in the thermal condensation of C/N/H compounds. Melem is thus a favorable access to the cyameluric nucleus. Some salts of melem have also been described recently^[36] and further ones will be addressed in this thesis (cf. Chapter 5).^[37, 38]

The heptazine-based polymer melon, though known for a long time, has not been well investigated until very recently. Structure elucidation by electron diffraction has revealed a linear 1D polymer (Scheme 7 B).^[39]

The reactivity of heptazines will be discussed in more detail in the respective sections of this thesis. Thus, this paragraph is only providing a brief overview and does not include works conducted as part of this thesis. Melem and melon are known to offer a range of further derivatization reactions. Based on this chemistry cyameluric acid and its salts,^[40-43] melonates,^[44-47] cyameluric chloride^[20,48] and azide^[49] have all been described (cf. Scheme 8), thus pointing the way towards a further exploration of the interesting reactivity of heptazines. The compound *s*-heptazine (tri-*s*-triazine) has also been prepared and studied.^[50] Its reactivity is, however, difficult to control and no derivatization reactions have been reported so far starting from this compound. The reactivity depicted in Scheme 8 provides an overview covering many basic reactions of heptazines. Melon has been chosen as heptazine source for this visualization. It can, however, well be replaced by melem in many cases if desirable. A hydrazine derivative of heptazine, $C_6N_7(NHNH_2)_3$, has also been reported recently.^[51]

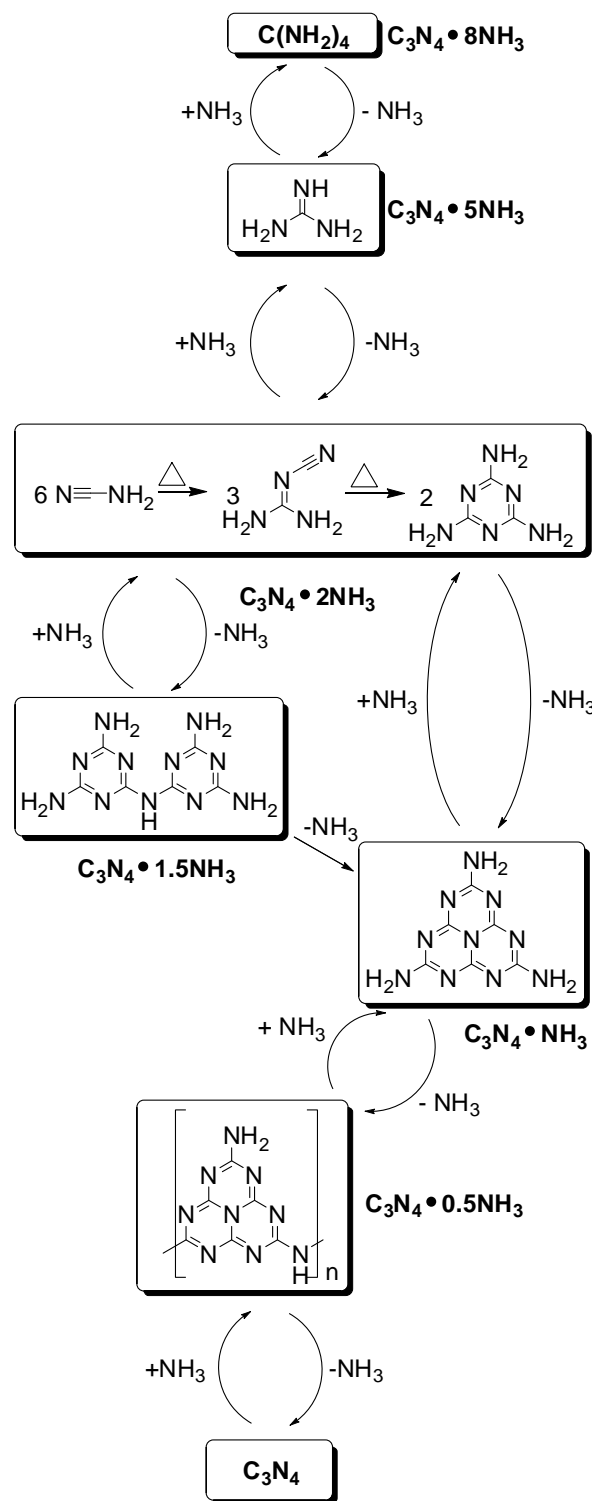


Scheme 8. A selection of some established derivatization reactions of the cyameluric nucleus. All reactions are based on melon (center) readily accessible by thermal condensation of melamine.

Organic heptazine derivatives have caused considerable interest as well. Some basic work on this topic has already been conducted back in the 1960s.^[52] Many derivatizations use the reactive heptazine compound cyameluric chloride which reacts much like an organic acid chloride. Nucleophilic substitutions are described in the literature and $\text{C}_6\text{N}_7\text{Cl}_3$ can even be used in Friedel-Crafts reactions. Molecules like amines $\text{C}_6\text{N}_7(\text{NEt}_2)_3$ ^[53] or ethers like $\text{C}_6\text{N}_7(\text{OSiMe}_3)_3$ ^[54] or $\text{C}_6\text{N}_7(\text{OPh})_3$ ^[55] and some metal-organic compounds have been prepared and thoroughly characterized recently. The ethers are also sometimes referred to as esters of cyameluric acid.

The compounds listed above have found a vast variety of applications. It is thus hardly possible to give complete summary of all these uses. However, a rough overview covering some selected aspects will be provided in the following. The most common one of these compounds is probably urea, which among others has found use as fertilizer, component of resins and for the synthesis of other chemicals. Melamine has caught public attention as an illegal additive in milk causing food poisoning and even fatalities among infants.^[56] Apart from such misuse melamine features a lot of beneficial applications. As was hinted at before, melamine has also found use in plastics,^[57] varnish products, concrete additives or flame retardants.^[58] Additional applications for some C/N/H compounds include (carbo)nitridation agents for metals.^[59] Cyanamide is also commonly used as an alcohol deterrent drug.^[60] Several other properties of carbon nitrides are subject to current investigations and may well find use in the future. Some prominent examples are catalysis,^[15,61-63] organic semiconductors^[64] or coatings for plastics.^[65]

It has already been mentioned, that many C/N/H compounds can be prepared by thermal condensation. The concept of ammonocarbonic acids^[66] can be very helpful for understanding this initial condensation process observed for carbon nitrides. This concept was devised by *Franklin* and stresses a formal relationship between the ammonocarbonic acid / ammonia and the carbon acid / water systems. In theory any ammonocarbonic acid releasing all ammonia by undergoing condensation is thus successively transformed into the carbon nitride C_3N_4 . Carbon nitride can accordingly be considered the final deammonation product of all ammonocarbonic acids. Hence the empirical formula of ammonocarbonic acids matches the one of ammonia adducts of C_3N_4 which is very useful for assessing the progress of condensation reactions. The opposite to C_3N_4 expressing the highest possible degree of ammonation is constituted by the compound tetraamino carbon, $C(NH_2)_4$, which has not yet been synthesized. Scheme 9 gives an overview of the application of the ammonocarbonic acid concept on the condensation of some previously mentioned C/N/H compounds. The concept is, however, a strictly formal one by nature. No predictions of reactivity or structure are possible.^[c] It is not necessarily achievable to readily transform any ammonocarbonic acid into any other one. Unfortunately, it has not been possible to synthesize pure C_3N_4 by thermal deammonation of melamine or any other ammonocarbonic acid, as yet. The condensation product closest to the binary nitride that can be obtained this way is melon. In some cases, however, samples displaying a significant degree of residual hydrogen in the range typical for melon have been termed C_3N_4 , making this matter somewhat confusing. For more in depth considerations of the condensation of C/N/H precursors please refer to the Chapters 3, 4 and 6 of this thesis.



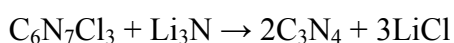
Scheme 9. The concept of ammonocarbonic acids applied on the condensation of C/N/H compounds.

[c] This is obvious since at the time *Franklin* presented this concept the molecular structure of heptazines had not been correctly elucidated. All statements only apply to the composition of the empirical formula of ammonocarbonic acids.

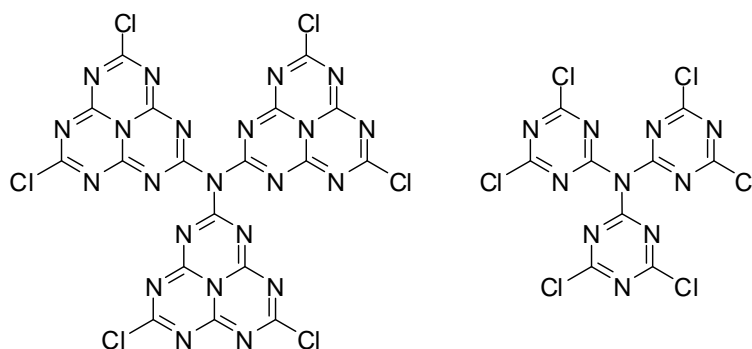
A lot of different precursor compounds and experimental conditions have been investigated aiming to prepare C_3N_4 by thermal condensation. Despite these efforts it has not been possible to yield bulk samples of C_3N_4 as yet. Products regularly contain significant amounts of residual hydrogen. Conditions and precursors need to be carefully considered as the synthesis is far from straightforward. Other molecular precursors forming carbon nitrides upon thermal decomposition include compounds like triazido-*s*-heptazine.^[67] Another possible route to carbon nitride networks is the reaction of the chlorides of cyanuric acid ($C_3N_3Cl_3$) or cyameluric acid ($C_6N_7Cl_3$) with suitable nitrogen sources like Li_3N . Such reaction conditions were used to synthesize molecular compounds like $N(C_3N_3Cl_2)_3$ ^[68] and $N(C_6N_7Cl_2)_3$ ^[69] displayed in Scheme 10. This method has also been reported to yield interesting nano-tubular carbon nitride materials.^[70]



Eq. 1.1

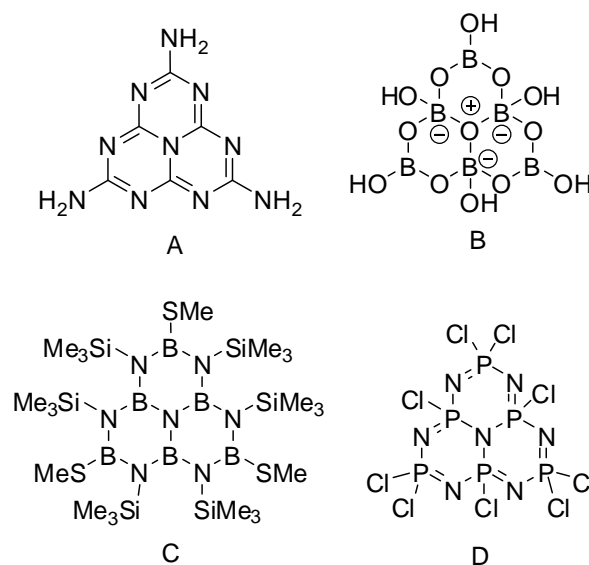


Eq. 1.2



Scheme 10. Some molecular species yielded by the reaction of cyameluric and cyanuric acid with a suitable nitrogen source.

The existence of some interesting substituted analogs of the cyameluric nucleus should also be noted. Examples of such compounds are displayed in Scheme 11. Compounds displaying $[B_6N_7]$, $[P_6N_7]$ or $[B_6O_7]$ nuclei have been described in the literature. Examples of such molecules are $B_6N_7(SiMe_3)_6(SMe)_3$ ^[71] and $P_6N_7Cl_9$.^[72] The depicted hexaborate anion (Scheme 11 B, $B_6N_7(OH)_6^{2-}$) is only known in form of its salts.^[73] This finding demonstrates that the cyameluric nucleus is not an odd curiosity only found for carbon nitrides. On the contrary tricyclic $[X_6Y_7]$ motifs are realized in other systems just as well. The chemical and thermal stability of the cyameluric nucleus, however, vastly surmounts the ones of its depicted derivatives. B/O is isoelectronic to C/N and the hexaborate ion does show some chemical stability. The other compounds (C and D), however, are very sensitive and prone to decomposition.



Scheme 11. Melem (A) and some examples of substitution variants of the heptazine core found for B/O (B), B/N (C) and P/N (D) molecules.

1.2 Carbon Nitride Compounds – a Historical Outline

It is always hard to pinpoint gradual progressions and developments. It is thus not possible to link the transition of chemistry into an exact empirical science to a certain date. One must rather accept that this was a slow process, the beginning of which took place in the 17th and 18th century. Though the history of carbon nitrides is a long one it does not date back this far. The chemistry of these compounds unfolded during the 19th century. The discovery of melon by the Swedish chemist *Jöns Jacob Berzelius* (Figure 4) in 1830 probably is the best moment to begin with a revision of the heptazine-based compounds and other C/N/H molecules. Melon was yielded after the pyrolysis of mercury thiocyanate. Surprisingly, $\text{Hg}(\text{SCN})_2$ was one of the first thiocyanate salts known. It can easily be ignited and slowly burns while forming bizarre structures resembling snakes. This experiment was thus frequently used for show and entertainment purposes and became famous as the Pharaoh's serpents. It was, however, in the meantime widely abandoned due to toxicity reasons. Melon prepared by this reaction has to be counted among the first polymers synthesized. The compound was later reported to be yielded by other procedures like pyrolysis of ammonium thiocyanate or heating of the reaction product of thiocyanate and chlorine as well.



Figure 4. Jöns Jakob Berzelius.

Special credit must in this regard be assigned to the works of *Justus v. Liebig* (Figure 5) since 1834.^[74] He identified several triazine and heptazine-based molecular compounds like melamine, melam, melem, ameline and amelide. Much of this was based on the pyrolysis of ammonium thiocyanate.^[d] His extensive works on these compounds^[75-78] often yielded products of higher purity, and thus allowed the first reliable characterizations by elemental analysis for several C/N/H compounds. *Liebig* retained his interest in these C/N/H compounds for decades and conducted some pioneering investigations. However, *Liebig's* assumptions were not always correct. Especially the discussion concerning the empirical formula of melon and the nature of melonates involving himself and *Henneberg* on the one side and *Völckel* as well as *Laurent* and *Gerhardt* on the other has to be mentioned in this respect. It endured for several years and ultimately disproved *Liebig's* initial statements.

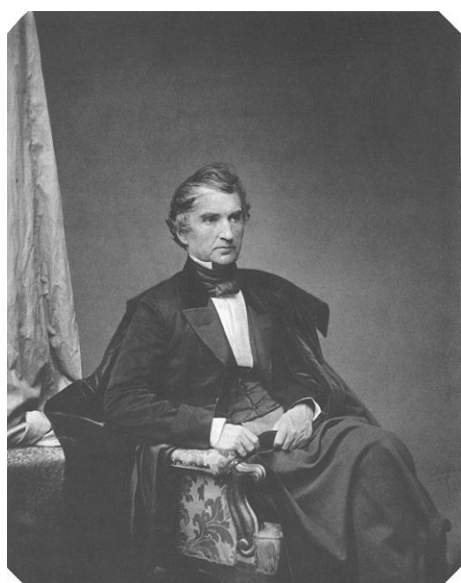


Figure 5. Justus von Liebig.

In the course of his works *Liebig* coined the specific names of many C/N/H molecules like “melamine”, “melon” or “melem”. According to *Liebig's* own statements, the names were arbitrarily chosen and cannot be

[d] Usually mixtures of NH_4Cl and KSCN were used instead of pure NH_4SCN .

related to color or properties of the respective compounds.^[e]

Another important progress was the discovery of potassium hydromelionate, $\text{K}_3\text{C}_6\text{N}_7(\text{NCN})_3$, in 1835 by *Leopold Gmelin* (Figure 6).^[79] The initial synthesis was conducted starting from potassium hexacyanoferrate^[f] and elemental sulfur, which were heated in an iron crucible. The assignment of the name hydromelionate originated from the finding, that the respective hydromelonic acid was reported to transform into melon and release water upon heating. Thus it was initially considered to be a hydrate of melon. Later *Liebig* developed improved synthetic routes to potassium melonate starting from melon and KSCN or $\text{BiCl}_3/\text{SbCl}_3$ and KSCN . Cyameluric acid ($\text{H}_3\text{C}_6\text{N}_7\text{O}_3$) was discovered much later by *Henneberg* as a hydrolysis product of potassium melonate.^[80]

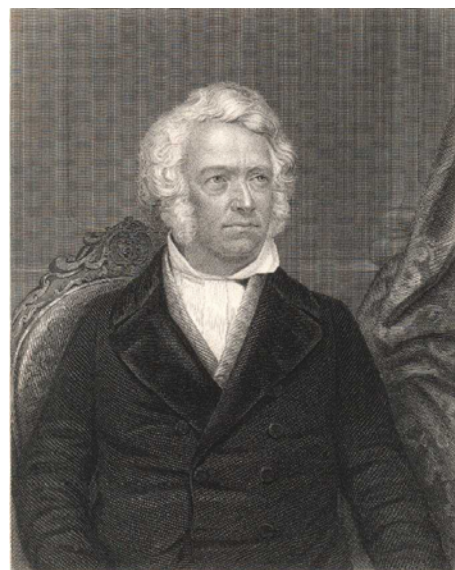


Figure 6. Leopold Gmelin.

The structure of many of the above-mentioned compounds, however, remained unclear. In the course of the mid 19th century these C/N/H molecules were a matter of great scientific interest. They were mentioned in many textbooks and considered to be of fundamental importance.^[g] Structures, formulas and synthetic procedures were controversially discussed. The low solubility substantially impeded both easy purification and thorough characterization especially for all heptazine-based compounds. These molecules also did not show characteristic melting or boiling points and could not be transformed into derivatives which could easily be characterized. As a result possibilities for investigating these compounds were very limited and over the years interest dwindled. Considering analytical methods of that time, the knowledge accumulated was, however, quite impressive. This is illustrated by late 19th century literature.^[81] In the early 20th century names like melon, melem or cyameluric acid were merely footnotes if they were mentioned at all. *Franklin's* introduction of the ammonocarbonic acid concept in 1922 finally brought these compounds into consideration once more. Beginning in the 1920s many C/N/H compounds were (re)investigated. One might refer to the works of *Burdick*^[82] or *Madelung and Kern*^[24,83] and additional investigations by *Franklin*^[84] for an overview concerning the research of this period.

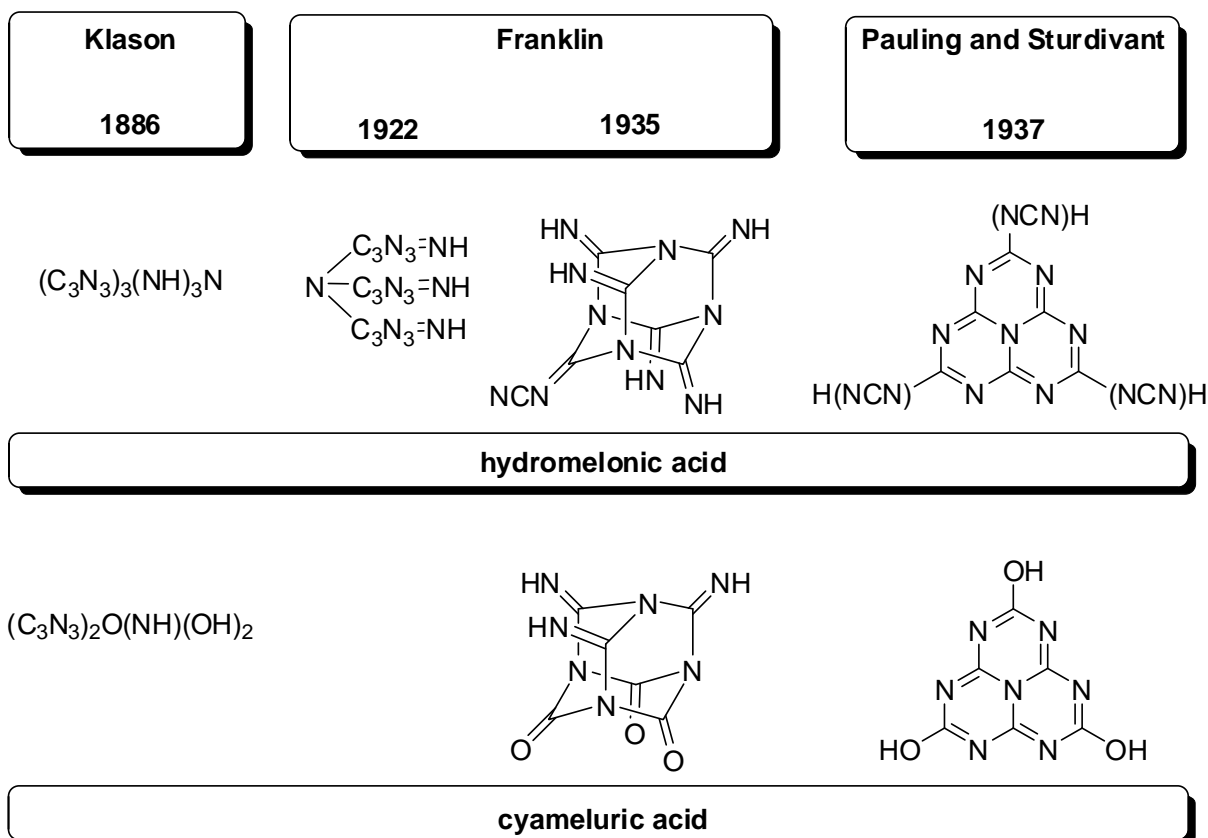
The structure of triazines has been correctly assumed for a considerably long time. It was already elucidated during the 19th century and finally proven by early single-crystal XRD investigations of compounds like melamine^[85] and cyanuric acid.^[86] The heptazine core and thus the structure of many basic C/N/H molecules, however, remained subject of speculation and uncertainty for more than a century. Many structural propositions were put forward in this respect. Though several formulas seem rather odd to a modern days chemist one should, however, be very mindful not to disqualify such propositions. I will only present structural propo-

[e] "Ich enthalte mich, Gründe für die Namen anzuführen, denen man in dieser Abhandlung begegnet; sie sind, wenn man will, aus der Luft gegriffen, was den Zweck genau so gut erfüllt, als wären sie von der Farbe oder einer Eigenschaft abgeleitet."^[74]

[f] Hexacyanoferrates were one of *Gmelin's* most prominent fields of expertise.

[g] In fact much of the scientific discussion is referring to textbooks and claims made therein. These works are not to be neglected in comparison to journal articles. In comparison to journal articles they are, however, difficult to find, overview and to come by as they are not included in standard-issue scientific search engines, hardly accessible via libraries, not available on the internet and often poorly referenced in the respective literature.

sitions for hydromelonic acid and cyameluric acid since these compounds have played the most important role in the structural discussion (cf. Scheme 12).



Scheme 12. Some propositions issued for the molecular structure of heptazines. The compounds hydromelonic acid (top) and cyameluric acid (bottom) are depicted. Franklin's propositions have been fitted into presentations offering a better overview of the steric arrangement.

The realization that all heptazines probably bear one common nucleus has developed in the early 20th century. The structural propositions brought forward by *Klason* in the late 19th century are mainly based on interpretations of elemental analytical data and decomposition reactions. Both compounds were, at the time, considered to consist primarily of cyanide (not depicted in Scheme 12) or triazine moieties linked by nitride, imide or oxide groups in various ways. After initially offering formulas that can only be considered some interpretation of *Klason's* propositions, *Franklin* finally developed the theory that hydromelonic acid and cyameluric acid could be described as substituted derivatives of hexamethylenetetramine (Figure 7). The hydrogen atoms of the CH₂ groups of this compound were considered to be replaced by a respective amount of =O, =NH or =NCN moieties. *Pauling* and *Sturdivant* presented another structural proposition, based on quantum chemical considerations^[h] and chemical properties.^[9] They proposed the cyameluric nucleus as the characteristic motif of cyameluric acid and hydromelonic acid. They developed this explanation by assuming structural similarities between cyameluric acid and melonates on the one hand side and cyanuric acid and tri-cyanomelaminates (both of which were already studied

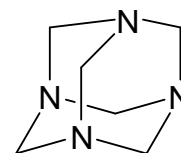


Figure 7. Molecular structure of hexamethylenetetramine.

[h] Stabilization by resonance of the cyameluric nucleus was assessed by Hückel calculations to account for ca. 150 kcal mol⁻¹.

at the time)^[86,66,87] on the other.

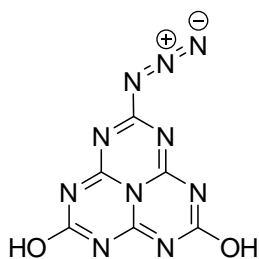


Figure 8. 2,6-Dihydroxy-10-azido heptazine: Pauling's mystery molecule.

Apparently *Pauling* permanently retained his interest for the cyameluric nucleus, for when he died in 1994 he left the structure of a heptazine-based compound on his chalkboard. It depicted the molecule 2,6-dihydroxy-10-azido heptazine (Figure 8), which thus became famous as *Pauling's* "mystery molecule". Much interest in this molecule as well as heptazines as a whole was caused by a competition issued by Chemical & Engineering News (C&EN) aiming to resolve the potential utility of *Pauling's* molecule.^[88] The two applications most commonly assumed in this regard are anti-cancer activity and use as a labeling agent for biological molecules. Some other ideas have, however, also been stated.

During the second half of the 20th century the extensive works of the Russian chemist *Finkel'shtein* on heptazines and the condensation reactions leading to their formation have to be mentioned.^[89] He was the first to comprehensively study the spectroscopic properties of heptazine-based compounds and other C/N/H molecules (IR and UV/vis). He also conducted investigations into acid and base properties and into technical uses of such compounds. It might be helpful to add, that his works are in part available as English translations (translated references will be provided wherever possible).

Other important developments during this time were the synthesis and characterization of tri-*s*-triazine C₆N₇H₃^[50] and the first syntheses of organic heptazine derivatives starting from cyameluric chloride.^[52]

During recent investigations structural characterizations have been commonly applied on heptazine-based compounds, offering final clarity about this structural element. Nowadays molecular structures are well established by several single-crystal XRD investigations.

Current interest in carbon nitrides is often related to the binary carbon nitride expressing the formula C₃N₄ and theoretical studies thereof. Apart from being a new binary compound the cubic modification c-C₃N₄ was predicted to show exceptional hardness even possibly surmounting the one of diamond. Especially the works of *Liu* and *Cohen*^[6] started what is often referred to as a "harder than diamond fever". Thus the quest for such a novel hardest material dramatically quickened interest in this field of research. Publication numbers (cf. Figure 10) show that, however, the mentioned calculations do not mark the beginning of interest into carbon nitrides.

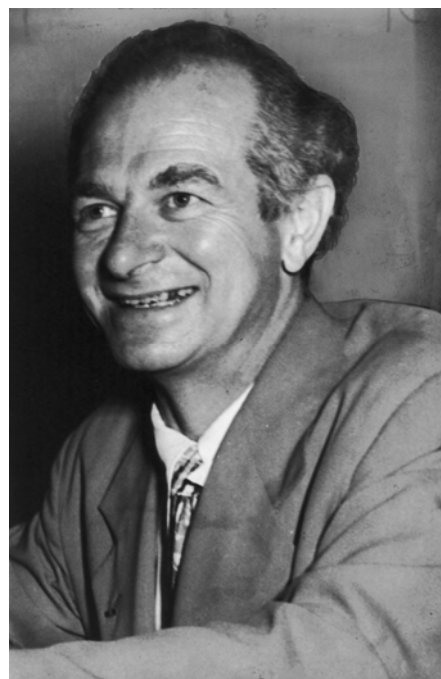


Figure 9. Linus Pauling.

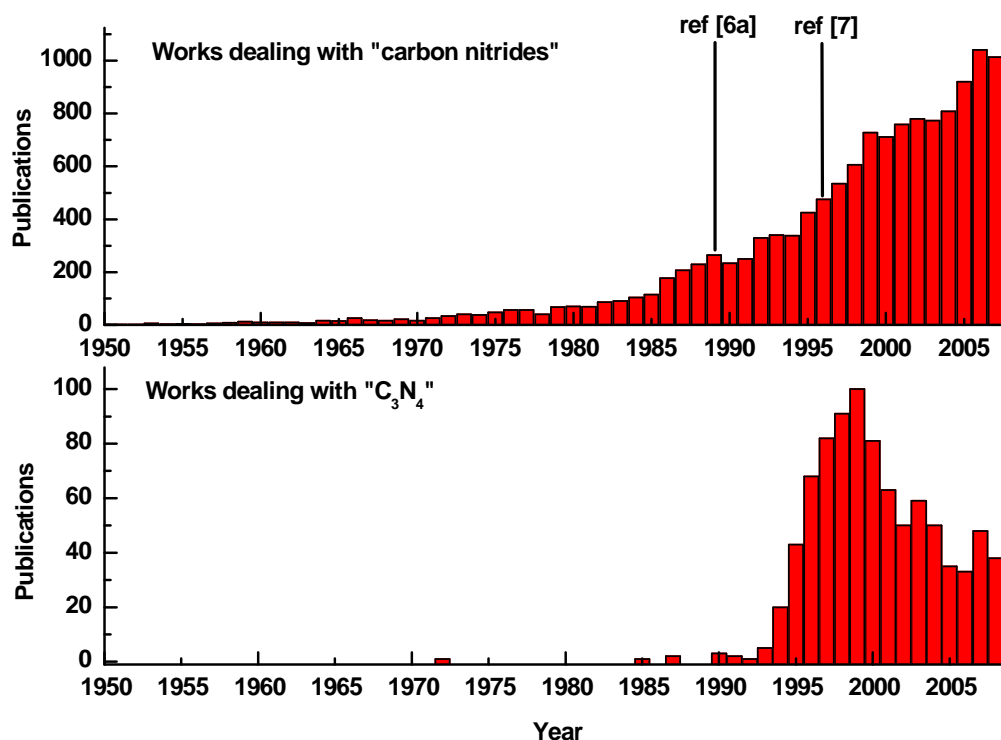


Figure 10. Frequency of works on “carbon nitrides” and “ C_3N_4 ”. Data is summarized until the year 2008. All data is based on the databases accessible by the SciFinder software.^[90]

Research concerning carbon nitrides has been growing steadily over the course of years. Some degree of interest has already originated back in the 1970s and an increase following the usual exponential progression can be observed. The publications dealing with so-called C_3N_4 , on the other hand, show a sudden drastic increase in the mid 1990s. Preceding works in this respect are quite rare. The highest numbers were hit in 1999 from whereon a notable decrease in research activity can be observed. Thus the beginning interest in C_3N_4 corresponds very well with the theoretical calculations concerning this compound. It is also an interesting fact that C_3N_4 related topics only account for one tenth of the publication numbers that are observed for carbon nitrides. This is since this topic is much wider e.g. incorporating systems like B/C/N or Si/C/N. One must also be mindful not to omit that certain changes in wording have taken place and expressions have evolved. It is thus impossible to summarize all 19th and early 20th century literature concerning carbon nitrides and their precursors under one or two keywords as such plainly did not exist or were not commonly used at the respective time.

C_3N_4 certainly is of great interest but carbon nitride materials are not limited to solely pursuing the synthesis of this compound. Hardness certainly remains a desirable property for carbon nitride materials. But as data shows, the progress in C/N chemistry moves on. Accordingly, interest for additional properties emerges. Very prominent ones are catalysis, gas storage/sorption or organic semiconductors. It can also be observed, that the chemistry of carbon nitrides is to some degree crossing over into the field of covalent organic frameworks (COFs).

1.3 Goals of this Study

Despite of the considerable recognition, carbon nitrides have recently received, a lot of uncertainties still remain. Especially heptazine-based compounds were not sufficiently studied. Although some basic concepts concerning their reactivity, structure and properties have been described long ago, the lack of analytical data was a significant problem. This has impeded any in depth understanding of many aspects, for a long time. Thus, the aim of this thesis covers several aspects of the chemistry of heptazines.

- First structural investigations of heptazine-based compounds have already been conducted, but a lot of compounds were not yet structurally investigated. Establishing solid-state structural data for various heptazines is thus desirable as such but also as a reference for other analytical methods.
- New heptazine-based compounds constituted interesting goals for our synthetic efforts as only a very limited amount of different heptazines had yet been prepared.
- Despite of numerous preceding investigations, the thermal condensation of C/N/H compounds was yet to be fully understood. Thus further investigations into the formation of heptazines starting from smaller molecules were needed.
- The potential of heptazine-based compounds as precursors for carbon nitride had to be investigated especially after calculations had shown heptazine-based g-C₃N₄ to be energetically favorable over the triazine-based variant.
- The laboratory synthesis of analytically pure samples of some heptazines, like melem, was only established for small amounts (about 50 mg). Convenient access to larger quantities was, however, desirable as such compounds are important starting materials for other reactions of heptazines.

As can be seen regarding the abovementioned points comprehensive investigations of heptazines were needed in order to assess the potential of these compounds for carbon nitride chemistry. Thus studying the reactivity and structure of heptazine-based molecules and their condensation products constitutes the primary goal of this thesis.

2. Experimental Methods

2.1 Preparative Methods

2.1.1 Vacuum and Inert Gas Line

Thermolyses and other reactions and manipulations of air-sensitive compounds were carried out using inert atmosphere of dry argon. Argon (purity gage 4.8, Messer or Air Liquide) was thus successively passed through columns filled with so-called BTS catalyst^[91] (copper dispersed on a ceramic carrier matrix, Fluka), blue silica gel (Merck), molecular sieve (porewidth 0.3 nm, Merck) and granulated phosphorus pentoxide (Granulopent[®], Roth) for purification purposes. Residual traces of oxygen and nitrogen were removed by passing the gas through a tube filled with titanium sponge (99.5 %, Alfa) maintained at a temperature of 700 °C. Argon was distributed via an inert gas line combined with a vacuum line. Evacuation of the latter was accomplished using a rotary vane pump (RZ8, suction capacity 8.6 m³ h⁻¹, Vacuubrand).

2.1.2 Furnaces

Reactions at elevated temperatures were performed using electrical furnaces if not stated otherwise.

Ampoules were heated in a tubular furnace with electric resistance heating. The programmable controller (Eurotherm) allowed for maximum continuous operation temperatures of 1200 °C and heating rates of ≥ 0.01 K min⁻¹. The temperature was measured using a built in thermocouple.

Thermal conversions under air were carried out using muffle furnaces (Nabertherm) allowing for a maximum continuous operation temperature of 1000 °C. Defined heating or cooling ramps were impossible using this setup. A variety of different reaction vessels were used. Crucibles made of porcelain or of alumina and porcelain evaporation dishes are the most common examples. Please refer to the respective parts of the experimental section, for further data concerning the individual experiments.

2.1.3 Glove-Box

For manipulation and storage of hygroscopic or air-sensitive compounds under argon (purity grade 4.8, Messer or Air Liquide) a glove-box (MB150-G1 and UniLab, O₂ < 1 ppm, H₂O < 1 ppm, MBraun) was used. A glove-box equipped with a polarization microscope was used for selecting single-crystals of air-sensitive compounds.

2.1.4 Operation Techniques

Manipulations of air-sensitive compounds were carried out using Schlenck techniques. Glassware was dried in vacuo and purged with argon for three times in succession prior to use.

Predried Duran[®] ampoules were filled with the respective starting materials (mixtures were well ground before use) and sealed either under argon or vacuum using a fan burner (operated with natural gas and oxygen). Ampoules were placed at the centre of a vertical tubular furnace and subjected to their respective temperature program. The furnace tube was sealed using mineral wool.

Two types of ampoules were commonly used in experiments. Large ampoules ($\varnothing_{ext.} = 16$ mm, wall thickness = 2 mm, length ≈ 12 cm) or small ampoules ($\varnothing_{ext.} = 10$ mm, wall thickness = 1.5 mm, length ≈ 10 cm) were chosen depending on desirable sample sizes and reaction conditions (cf. Figure 11).

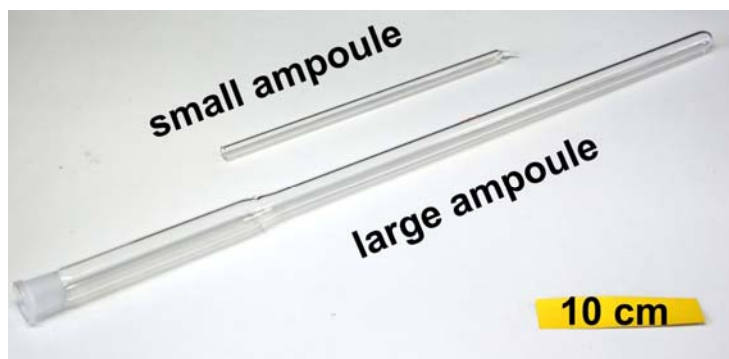


Figure 11. Ampoules used in this work.

2.2 Analytical Methods

2.2.1 Diffraction Techniques

2.2.1.1 General and Theoretical Aspects

Due to the complexity of the matter, a comprehensive revision of crystallographic fundamentals will not be given in this work. For a detailed theoretical consideration of diffraction methods please refer to standard works in the literature.^[92,93]

Ever since *Max von Laue* discovered the interactions of X-rays with crystalline matter in 1912 crystallography has had an enormous impact on the way the nature of chemical compounds is perceived and understood. Especially structural investigations by X-ray diffraction have developed into a powerful and versatile tool for chemists. Though X-rays are used for the vast majority of diffraction experiments electron and neutron diffraction are valuable tools for obtaining structural information as well. In order to facilitate diffraction experiments the respective wavelengths need to be in the dimension of the structures studied. Analyzing position and intensity of the resulting diffraction peaks allows structural information to be extracted.

2.2.1.2 Single-Crystal X-Ray Diffraction

Structure elucidation by single-crystal X-ray diffraction (XRD) is of central importance in this thesis. A crop of crystals on a microscope slide or a small Petri dish was covered with a thin film of paraffin. Suitable crystals were selected using a polarization microscope MZ 6 (Leica). Single-crystals were fixed on a glass stick or within a glass capillary (Hilgenberg, $\varnothing_{\text{ext.}} = 0.3 - 0.5$ mm). Crystals of air-sensitive compounds were collected in a glove-box. Glass capillaries were sealed with grease under Argon and immediately sealed with a pitch after locking them out of the glove-box. The quality of these crystals was checked using a Laue or Precession camera in Laue mode (Buerger Precession camera 205, Huber). White Mo- K_{α} radiation was used for operating the camera (Röntgengenerator Kristalloflex 760, Siemens). The Laue diagrams were recorded with imaging plates readable with a laserscanner (BAS 2500 Bio Imaging Analyser, Fuji). The programs BASREADER^[94] and Tina^[95] were used for evaluation of the diagrams. Crystals displaying good diffraction patterns were selected for the actual measurement.

The datasets presented in this thesis were measured on a Kappa-CCD (Bruker AXS / Nonius) or a IPDS-1 diffractometer (STOE & Cie) equipped with a 600 Series CRYOSTREAM Cooler (Oxford Cryosystems). The measurements were usually conducted at a temperature of 200 K. Actual temperatures for individual measurements are given in the respective sections. The raw data were reduced using the software specific to the respective instruments. Lorenz- and polarization corrections were applied to all data. Extinction correction was applied if appropriate. Diffraction intensities of Kappa-CCD Data were scaled using the SCALEPACK software package.^[96] No additional absorption correction was applied in these cases. A numerical absorption correction was usually applied to IPDS data. Analysis of datasets including determination of possible space groups was carried out with the program XPREP.^[97] The GUI provided by WINGX^[98] was commonly used. Evaluation and verification of the structure models and the selected space groups was done using the program PLATON (including ADDSYM and MISSYM).^[99] Visualizations of crystal structures as given in this work were produced using the program DIAMOND.^[100]

Crystal structures were solved by direct methods (SHELXS-97^[101] or different versions of SIR)^[102] and refined against F^2 on all data by full-matrix-least-squares (SHELXL-97).^[101] All hydrogen atoms were located using difference Fourier-syntheses whenever possible. Restraints were used to ensure plausible bond lengths involving H atoms if necessary. Crystallographic data, selected distances and angles are presented in the respective sections. Further details on the crystal structure can be obtained free of charge on application to Cambridge Crystallographic Data Centre, 12 Union Road, Cambridge CB2 1EZ (UK) (fax: +(44) 1223-336-033); e-mail (fileserv@ccdc.cam.ac.uk). The respective CSD numbers are summarized in Section 12.5.

The quality of structural models was judged based on R -indices and the goodness of fit (GooF). The evaluation is based on a comparison of structure amplitudes calculated according to the structure model F_{ci} with those measured experimentally F_{oi} . The weighted R value on F^2 ($wR2$) and the goodness of fit are minimized during the course of the refinement.

Intergrowth of two crystals is called twinning. A considerable fraction of crystals studied in this work features some sort of twinning. Thus general procedures used for twin refinement are discussed in the following. The treatment of twinned crystals in this work distinguishes between two different cases. For merohedral twins all reflections contain intensity of all individuals. A twin law (a 3×3 matrix) describes the transformation of one individual into the other one with a symmetry operation. If this twin law is known it can be used as part of the refinement. The relative size of the two individuals is refined as an additional parameter (BASF) in this case. The data is given in the respective section. The rest of the refinement is identical with the procedures used for non-twinned structures. For non-merohedral twinning there is no twinning law corresponding to a reasonable symmetry operation. Thus the reflections of the two individuals had to be separated. The data separation was carried out using the software TWIN provided by the Stoe IPDS diffractometer software package.^[103] Thus the structure of non-merohedral twins could only be solved if measured using this device. Overlapping signals are a significant problem in this context and were usually excluded from the refinement at the cost of a low overall completeness of the dataset. The separated datasets can be solved and refined like any normal X-ray data originating from a non-twinned crystal.

2.2.1.3 X-ray Diffraction of powders

X-ray powder diffraction patterns (PXRD) were recorded on a Huber G670 Guinier Imaging Plate or a Stoe STADI P diffractometer. The latter one could be operated in both, transmission or Debye-Scherrer geometry. Measurements were conducted using monochromatic Cu- $K_{\alpha 1}$ radiation at room temperature. Theoretical powder diffraction patterns were simulated from single-crystal data using the Win XPOW software package.^[104]

2.2.2 Spectroscopic Methods

2.2.2.1 Vibrational spectroscopy

Fourier-transformed infra-red (FTIR) spectra were usually recorded in reflection geometry on a Spektrum BX II FTIR spectrometer (Perkin Elmer) equipped with a DuraSampler diamond ATR (attenuated total reflectance) unit. All spectra were corrected of baseline and ATR specific effects. All measurements involving IR spectroscopy were conducted at room temperature if not stated otherwise.

Measurements of (mostly air-sensitive) samples prepared as KBr pellets were conducted on an IFS 66v/S FTIR spectrometer (Bruker).

Raman spectra were measured on an IFS 66v/S FTIR spectrometer equipped with a Raman-module FRA 106/S (Bruker). A frequency-doubled Nd-YAG laser was used for excitation. All measurements were conducted at room temperature if not stated otherwise. Data evaluation was carried out using the OPUS program package (Bruker).^[105]

Signal shapes and intensities of the signals are addressed using the following abbreviations: s = strong, m = medium, w = weak, vw = very weak, br = broad, vbr = very broad, sh = shoulder.

2.2.2.2 NMR Spectroscopy

Solution-state NMR spectra were recorded on an Eclipse EX-400 spectrometer (JEOL, 400 MHz). Chemical shifts are referenced with respect to tetramethylsilane (TMS) (^1H , ^{13}C) and nitromethane (^{14}N) as external standards. Various deuterated solvents were used depending on the solubility of the respective compound.

Solid-state NMR spectra were recorded at room temperature on a DSX 500 Avance (Bruker) FT-NMR spectrometer with an external magnetic field of 11.4 T. Magic angle spinning (MAS) spectra were recorded using double resonance probes (Bruker) operated with 2.5 mm (^1H) and 4.0 mm (^{13}C , ^{15}N) ZrO_2 rotors. The rotation frequencies were 6 kHz (^{15}N , ^{13}C) or 12 kHz (^1H). The repeating times were 128 and 64 s for ^1H and ^{13}C spectra. Cross-polarization (CP) experiments were used for all ^{15}N and some ^{13}C measurements. The repeating time was 64 s in this case. Chemical shifts are referenced with respect to TMS (^1H , ^{13}C) and nitromethane (^{15}N) as external standards.

2.2.3 Electron Microscopy

Scanning electron microscopy (SEM) was conducted on a JSM-6500F electron microscope (JEOL). Nonconductive samples were sputtered with carbon prior to use. The microscope was equipped with a model 7418 EDX detector (Oxford Instruments) allowing elemental analysis.

Electron diffraction (ED) and transmission electron microscopy (TEM) measurements were carried out on a JEOL 2001 instrument equipped with a tungsten cathode operating at 200 kV. The images were recorded using a TVIPS CCD camera (F114). The sample was dispersed by sonification in ethanolic suspension for 30 minutes. A small amount of the suspension was dispersed on a carbon-coated copper grid in air. After drying, the grids were mounted on a single-tilt holder with a maximum tilt angle of 30° and subsequently transferred into the microscope.

2.2.4 Thermal Analysis

2.2.4.1 DTA/TG

Simultaneous differential thermal analysis and thermogravimetric (DTA/TG) measurements were performed using a Setaram TG-92 simultaneous thermal analyzer equipped with a protected (i.e. alumina covered) DTA/TG rod (P-type thermocouple, maximum operating temperature = 1600 °C). Temperature calibration was achieved in reference to melting points of metal standards. The measurements were conducted in an atmosphere of streaming helium at scanning rates ranging between 3 and 10 K min⁻¹ using 100 µL alumina crucibles. Data collection and evaluation was conducted using device-specific software. Curves were corrected for baseline effects by subtraction of blank measurements wherever appropriate.

2.2.4.2 DSC

Differential scanning calorimetry (DSC) was measured on a DSC 141 (Setaram) calorimeter. Aluminium crucibles were heated under streaming nitrogen. Data collection and evaluation was conducted using device-specific software.

2.2.5 Elemental Analysis

Various elemental analysis methods were used in this work.

2.2.5.1 C/N/H Analysis

Determination of the elements H, C, N and S by combustion analysis was carried out by the micro analytical laboratory of the Department of Chemistry and Biochemistry, LMU Munich. The commercial elemental analyzer system vario EL (Elementar) was used in this respect. Analyzes of sulfur-containing samples were conducted using a vario micro cube (Elementar).

2.2.5.2 ICP-AES

Analyses for metal contents were conducted on a VISTA RL CCD simultaneous inductively coupled plasma - atomic emission spectrometry (ICP-AES) analyzer system (Varian). The wavelengths are summarized in Table 1.

Table 1. Wavelengths (in nm) used for ICP-AES analysis.

Element	Wavelength(s)	
K	766.491	
Na	588.995	
Fe	238.204	
Hg	184.887	194.164
S	180.669	181.972
Zn	213.857	

2.2.6 Mass Spectroscopy

Mass spectra were obtained using a MStation JMS-700 spectrometer (JEOL) with a mass resolution of $\geq 1 \text{ u e}^{-1}$. Ionization was achieved by fast atom bombardment (FAB) (for anionic molecules) or by direct electron impact (DEI) (for all other compounds). Evaluation of results was achieved using device-specific software.

2.2.7 Magnetic Measurements

Magnetic measurements were performed using a SQUID magnetometer (MPMS-XL5, Quantum Design Inc.). The data were corrected for sample holder and core diamagnetism by diamagnetic increments^[144] and fitted to a Curie-Weiss law.

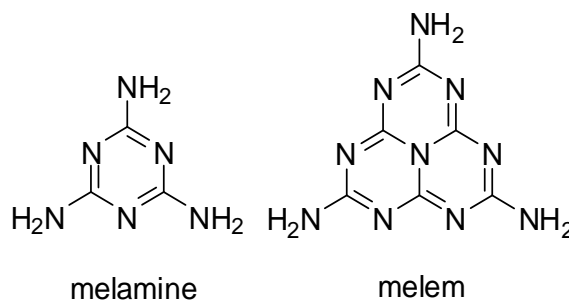
3. The Formation of Melem

3.1 Introduction

Contents of this section have already been published in advance to this thesis.^[106] Melem, $C_6N_7(NH_2)_3$, (cf. Scheme 13) is a key heptazine-based molecule of considerable importance for the chemistry of carbon nitrides (cf. Section 1.1). It was among the first heptazine derivatives to receive detailed structural and spectroscopic investigations.^[35] However, upon starting this thesis, synthetic procedures only allowed for small amounts of melem to be readily prepared.^[i]

In addition the condensation process of small C/N/H molecules like melamine, $C_3N_3(NH_2)_3$, was far from being understood.

Though much progress has been made by preceding works in the last years a lot of questions concerning the species occurring during the condensation of C/N/H precursors still remained upon starting this thesis. Very prominent examples are the phases occurring at reaction temperatures ranging between the formation temperatures of melamine and melem (i.e. approximately 300 to 400 °C). In older literature the occurrence of pure melam as bulk material has often been postulated in this regard. This can, however, meanwhile be excluded based on actual investigations (cf. Chapter 4).^[34] The following chapter will focus on understanding the formation of melem and using this knowledge in order to enhance the laboratory synthesis of this compound.



Scheme 13. Molecular structures of melamine (left) and melem (right).

3.2 Melamine Melem Adduct Phases

Though some phases being discovered as new powder XRD patterns were observed for products synthesized in the abovementioned thermal range^[107] reliable characterization proved to be difficult. As can be easily rationalized by referring to the ammonocarbonic acid formalism^[66] mixtures or molecular adducts of melamine and melem are not discernable from melam by elemental analysis alone (cf. Section 1.1, Scheme 9). The analytical formula of melam ($C_6N_{11}H_9$) can be formulated as $2C_3N_4 \cdot 1.5NH_3$. Thus, a mixture of 2 equivalents melamine ($C_3N_6H_6 \equiv C_3N_4 \cdot 2NH_3$) and 1 melem ($C_6N_{10}H_6 \equiv 2C_3N_4 \cdot 2NH_3$) is not distinguishable from pure melam. Efforts aimed at resolving this issue finally resulted in proposing the chemical nature of the abovementioned compounds as adducts of melamine and melem.^[34] The stoichiometric compositions of 2melamine · melem and melamine · 2melem were allocated to the two phases known at this time based on elemental analyses.^[34,108]

[i] An average ampoule synthesis only yielded around 50 mg of melem.

Three molecular adducts of melamine and melem were identified during the thermal condensation of melamine as part of the present work. Upon cooling to room temperature it was possible to yield the three adducts in crystalline form, thus allowing the structures to be studied using single-crystal XRD. The respective compositions were found to be $2\text{C}_3\text{N}_3(\text{NH}_2)_3 \cdot \text{C}_6\text{N}_7(\text{NH}_2)_3$, $\text{C}_3\text{N}_3(\text{NH}_2)_3 \cdot \text{C}_6\text{N}_7(\text{NH}_2)_3$ and $\text{C}_3\text{N}_3(\text{NH}_2)_3 \cdot 3\text{C}_6\text{N}_7(\text{NH}_2)_3$ (cf. Table 2, Table 3). As follows compositions of these adducts will be addressed as molar ratio of melamine to melem (2:1, 1:1, and 1:3). All three compounds were synthesized at temperatures ranging from 350 to 400 °C with reaction times of at least 7 days. Please refer to Section 12.1.2 - 12.1.4 for further experimental details.

Table 2. Composition and conditions of synthesis for melamine melem adducts. Comparison of literature values to the data found in this work.

Compound	$2\text{C}_3\text{N}_3(\text{NH}_2)_3 \cdot \text{C}_6\text{N}_7(\text{NH}_2)_3$	$\text{C}_3\text{N}_3(\text{NH}_2)_3 \cdot \text{C}_6\text{N}_7(\text{NH}_2)_3$	$\text{C}_3\text{N}_3(\text{NH}_2)_3 \cdot 3\text{C}_6\text{N}_7(\text{NH}_2)_3$
Molar ratio	2:1	1:1	1:3
	Temperatures / °C		
With Eu	350	370	390
Without Eu	360-390	not found	>400
Reported temperature ^[34]	390 ^[a]	-	390 ^[b]
Reported temperature ^[107]	395-410 ^[c]	-	405-425 ^[c]

[a] 200 mg of melamine 2.5 h reaction time;

[b] 200 mg of melamine, 14 h reaction time;

[c] 80 mg of melamine, over night reaction.

Comparing the current results with preceding works from our group^[34,107,108] it is evident that the 2:1 adduct is identical with the 2:1 adduct suggested in the literature. The postulated 1:2 adduct actually has the composition of 1:3. Since the 1:1 adduct only is formed under very distinct conditions it has not been observed so far. Powder XRD data were used to decide whether the adducts described in this work are identical with the ones previously reported. Temperature is by far the most important factor directing the formation of a certain adduct. Melamine-rich adducts are formed at lower temperatures while melem-rich ones are found at elevated temperatures (cf. Table 2). This observation is in accordance with the general trend that melem is formed at higher temperatures compared to melamine.

For better comparability with the abovementioned prior results^[34,35,107,108] the differences in the experimental setup (cf. Sections 12.1.2 – 12.1.4) and the resulting effects are briefly discussed. The experiments, presented as follows, were conducted in ampoules sealed under vacuum while preceding studies used an inert gas atmosphere with an atmospheric pressure of argon (at RT). The amount of starting material used for most experiments was significantly increased while the free volume within the ampoule was decreased. This should result in increased overall pressures despite of the initial vacuum conditions. Upon opening significant pressure of ammonia was released, supporting this assumption.

Prolonged reaction times were found to be fundamental for good crystal growth as well as complete thermodynamic equilibration. Thus reaction times were increased from typical over-night reaction to about a week for the thermal condensation step at elevated temperatures only. By comparison of the experiments conducted as part of this thesis and in the abovementioned works^[34,107,108] some general trends concerning reaction times become evident. From the data at hand it seems favorable that full equilibration between melamine and melem is reached most likely after about two to three days. Increasing the reaction time up to seven days, as used for most experiments in this work, does not result in increasing the quality of the products (in terms of phase purity). Prolonging the tempering steps, however, still allows for

better crystal growth as do the slow cooling ramps chosen. No adverse effects were caused by fast initial heating rates. Thus the time used for the heating period was significantly decreased.

The influence of additives acting as ammonia scavengers was also studied. Elemental europium, which is known to react with ammonia yielding europium amide, was used for this purpose (cf. Equation 3.1). This synthetic approach of controlling ammonia pressure has already been used in our group for differing systems.^[109]



Catalytic amounts of mercury were added to increase the reactivity of the metal by amalgamation. By this approach the reaction temperatures can be reduced by 10 to 30 °C for phase pure synthesis in comparison to a metal-free setup (cf. Table 2). This can easily be explained by *Le Chatelier's* principle. However, a catalytic effect of europium upon the condensation cannot be excluded because no detailed experiments were done on the kinetic aspects of the condensation reaction. Attempts to prepare the 1:1 adduct in a metal-free setup were not successful. This could be a crucial point to the synthesis, since proceeding works did not find this adduct starting from pure melamine either.

It must be stated that an essential factor in the successful preparation of melamine melem adducts is a homogeneous temperature distribution within the ampoule. If significant temperature gradients are present, phase separation into melem and melamine can easily occur even if no part of the ampoule is outside the temperature range given for the formation of the reported adducts. A mixture of phases was also found when reaction temperatures were ranging between the ideal syntheses conditions of the individual adducts even if temperature gradients were marginal.^[j] A separation of phases however in most cases still allowed mechanical separation of the reaction products since they were found as pure compounds at different regions reflecting temperature distribution.

It was not possible to prepare the three reported melamine melem adducts from solution since the formation of solvates often seems to be more favorable. This is the case for solvents allowing a notable solubility of melem like water or DMSO. The fact that the solubility of melamine is significantly higher than the one of melem also proved disadvantageous (cf. Section 12.1.5 for additional data on the experiments).

Experiments aiming to prepare melamine melem adducts from mixtures of melem and melamine, at lower temperatures were also conducted. The molar ratios found for the respective adducts were used for these experiments. Upon heating to a temperature of 300 °C in sealed glass ampoules, the adduct phases were not formed. This finding can be interpreted by assuming that gas phase mobility of melamine alone is not sufficient to allow formation of adduct phases. Melem is not affected thus rendering a synthesis of the adduct phases at low temperatures impossible. However, once a sufficient temperature is reached condensation of melamine sets in due to the missing initial partial pressure of ammonia. Melem is formed as melamine is consumed this way and a dynamic equilibrium between the two species is reached also depending on temperature and volume of the reaction vessel. Thus the molar ratio given by the initial weight cannot be maintained under conditions suitable for the formation of the adducts and using heterogeneous mixtures of melem and melamine as starting ma-

[j] The furnaces used for the respective experiments show a temperature gradient ranging between 4 and 5 °C per 10 cm length.

terials does in no way increase phase purity of the products. The formation of adducts already occurs at rather low temperatures (350 °C, cf. Table 2). At such conditions melem does not evaporate to a significant degree.^[k] Therefore, the in-situ generation of melem from melamine in the solid offers distribution of the two compounds on a molecular level.

Table 3. Crystallographic data and details of the structure refinements for melamine melem adduct phases.

Formula	$2\text{C}_3\text{N}_3(\text{NH}_2)_3 \cdot \text{C}_6\text{N}_7(\text{NH}_2)_3$	$\text{C}_3\text{N}_3(\text{NH}_2)_3 \cdot \text{C}_6\text{N}_7(\text{NH}_2)_3$	$\text{C}_3\text{N}_3(\text{NH}_2)_3 \cdot 3\text{C}_6\text{N}_7(\text{NH}_2)_3$
Crystal system	monoclinic	orthorhombic	monoclinic
Space group	<i>C2/c</i> (no. 15)	<i>Pcca</i> (no. 54)	<i>C2/c</i> (no. 15)
Lattice parameters / Å, °	$a = 21.526(4)$ $b = 12.595(3)$ $c = 6.8483(14)$ $\beta = 94.80(3)$	$a = 7.3280(2)$ $b = 7.4842(2)$ $c = 24.9167(8)$	$a = 14.370(3)$ $b = 25.809(5)$ $c = 8.1560(16)$ $\beta = 94.62(3)$
Volume / Å ³	1850.2(7)	1366.54(7)	3015.0(10)
Z	4	4	4
Diffractometer		Kappa-CCD	
Radiation, monochromator		Mo-K α ($\lambda = 71.073$ pm), graphite	
Temperature / K		200 K	
Structure solution		SHELXS-97 ^[101] (direct methods)	
Structure refinement		SHELXL-97 ^[101] (full-matrix least-squares on F ²)	
Corrections applied	Lorentz, polarization, SCALEPACK, ^[96] extinction	Lorentz, polarization, SCALEPACK ^[96]	
Data / restraints / parameters	2109 / 0 / 193	1423 / 0 / 142	3458 / 0 / 299
R-indices	$R1 = 0.0737$ all data $R1 = 0.0475$ $F_o^2 > 2\sigma(F_o^2)$ (1494 reflections) $wR2 = 0.1298$ all data $wR2 = 0.1167$ $F_o^2 > 2\sigma(F_o^2)$	$R1 = 0.0714$ all data $R1 = 0.0537$ $F_o^2 > 2\sigma(F_o^2)$ (1066 reflections) $wR2 = 0.1412$ all data $wR2 = 0.1312$ $F_o^2 > 2\sigma(F_o^2)$	$R1 = 0.0733$ all data $R1 = 0.0547$ $F_o^2 > 2\sigma(F_o^2)$ (2618 reflections) $wR2 = 0.1470$ all data $wR2 = 0.1347$ $F_o^2 > 2\sigma(F_o^2)$
Goof	1.048	1.031	1.038
Weighting scheme	$w^{-1} = \sigma^2(F_o^2) + (0.0765P)^2$ where $P = (F_o^2 + 2F_c^2) / 3$	$w^{-1} = \sigma^2(F_o^2) + (0.0962P)^2$ where $P = (F_o^2 + 2F_c^2) / 3$	$w^{-1} = \sigma^2(F_o^2) + (0.0765P)^2$ where $P = (F_o^2 + 2F_c^2) / 3$
Largest peak deepest hole / e Å ⁻³	0.332 / -0.247	0.652 / -0.263	0.385 / -0.324

The crystallographic studies reveal the exact composition of the three adduct phases as stated in the preceding paragraph (cf. Table 3). They are solely composed of melamine and melem (cf. Scheme 13) in the respective molar ratios. The molecular structures of melamine and melem in the adduct phases agree quite well with the data found for the pure compounds.^[35,110] Their molecular structure corresponds well with the stoichiometric formula given in Scheme 13. All three compounds form extensive hydrogen-bonding networks in the solid.

[k] Some degree of sublimation of melem has been observed occurring above 400 °C.^[35b] Thermal analysis conducted for melem as part of this thesis (cf. Section 3.4, Figure 23) shows no significant thermal event below 500 °C.

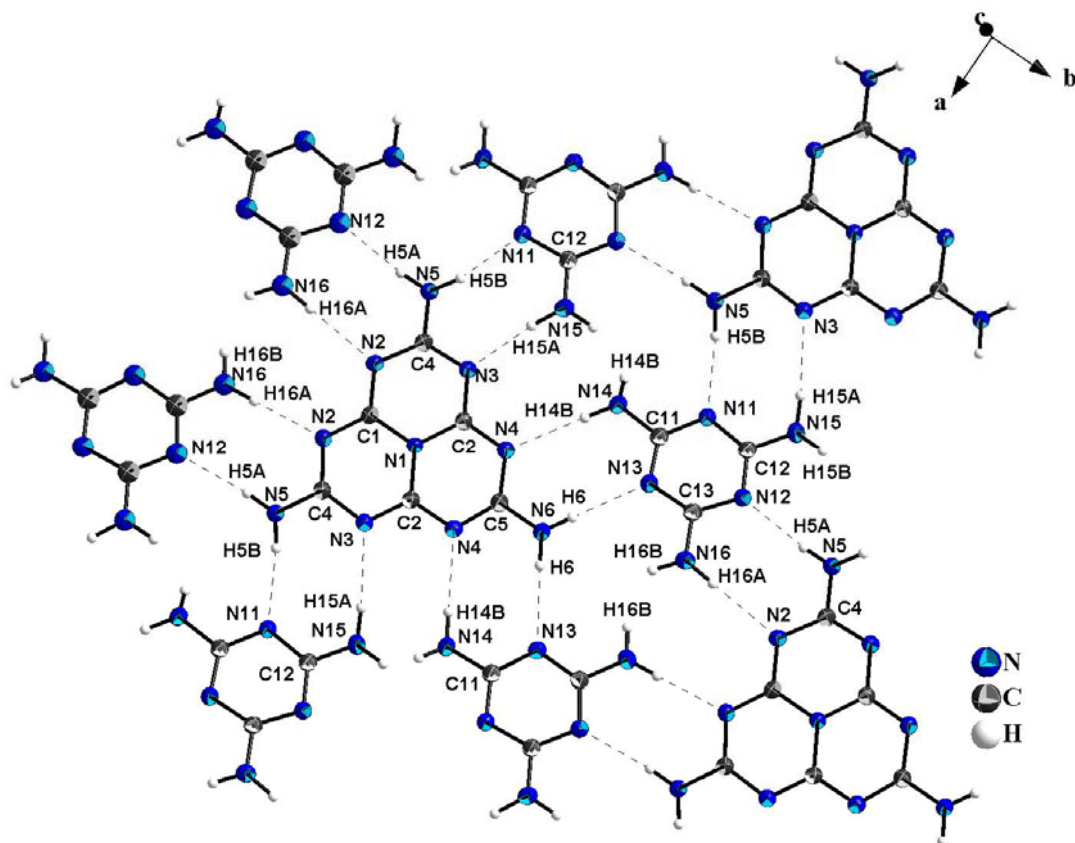


Figure 12. Hydrogen-bonding interactions in $2\text{C}_3\text{N}_3(\text{NH}_2)_3 \cdot \text{C}_6\text{N}_7(\text{NH}_2)_3$. Ellipsoids for non-hydrogen atoms are drawn at the 50 % probability level.

In the lower part of the temperature range studied an adduct displaying a molar ratio melamine to melem of 2:1 is found. The compound crystallizes in the monoclinic space group $C2/c$ with one melamine and half of a melem molecule within the asymmetric unit. The melem molecules are connected to six neighboring melamine molecules via several hydrogen-bonds. The melamine molecules are then again linked to three melem molecules as is necessary by stoichiometry. A layer-like structure is assembled due to the fact that the vast majority of H-bonds are found in the plane perpendicular to c (cf. Figure 12). The layers, however, also have some bonding interactions connecting them to each other (cf. Figure 13).

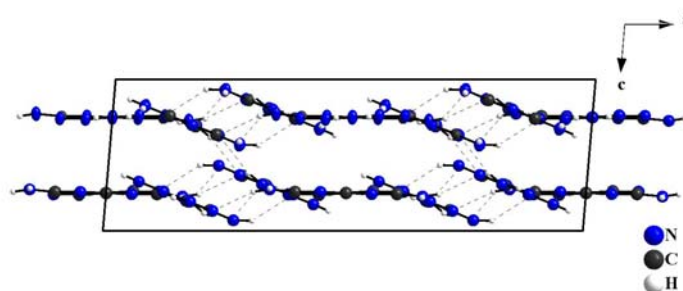


Figure 13. Unit cell and layer-like arrangement for $2\text{C}_3\text{N}_3(\text{NH}_2)_3 \cdot \text{C}_6\text{N}_7(\text{NH}_2)_3$. View along b .

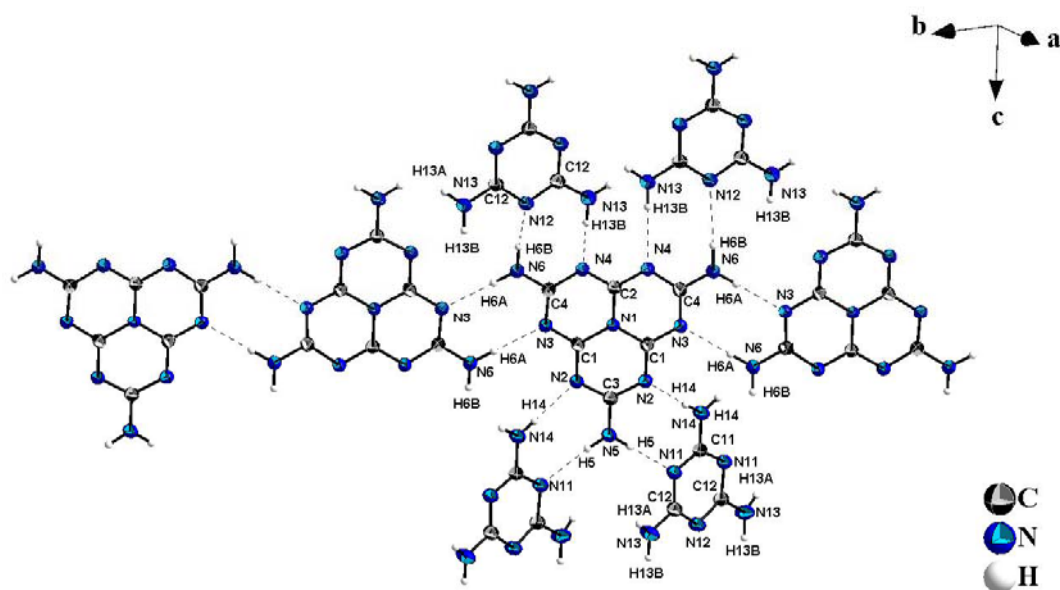


Figure 14. Hydrogen-bonding interactions in $C_3N_3(NH_2)_3 \cdot C_6N_7(NH_2)_3$. Ellipsoids for non-hydrogen atoms are drawn at the 50 % probability level.

In the mid temperature range formation of an equimolar adduct, melamine · melem, is predominant, if Eu metal is present. The compound crystallizes in the orthorhombic space group $Pcca$ with half a molecule of both melem and melamine in the asymmetric unit. Strands of hydrogen-bonded melem molecules are found running along $[1\ 2\ 0]$ and $[1\ \bar{2}\ 0]$ (cf. Figure 14). These molecules are inter-linked by melamine molecules (cf. Figure 14, Figure 15). The melem molecules within parallel strands are stacked at a distance of 3.5 Å.

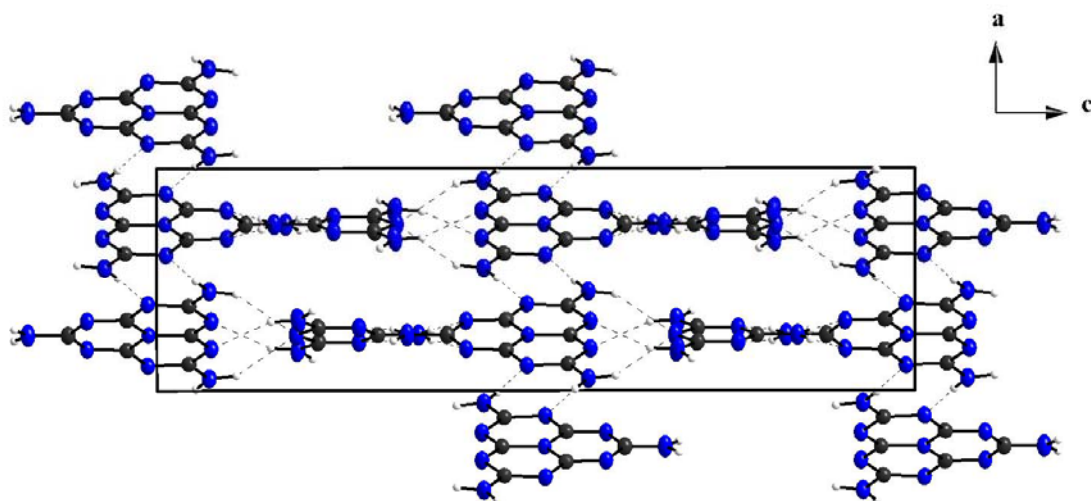


Figure 15. Unit cell and arrangement of hydrogen-bonded melem strands for $C_3N_3(NH_2)_3 \cdot C_6N_7(NH_2)_3$. View along b .

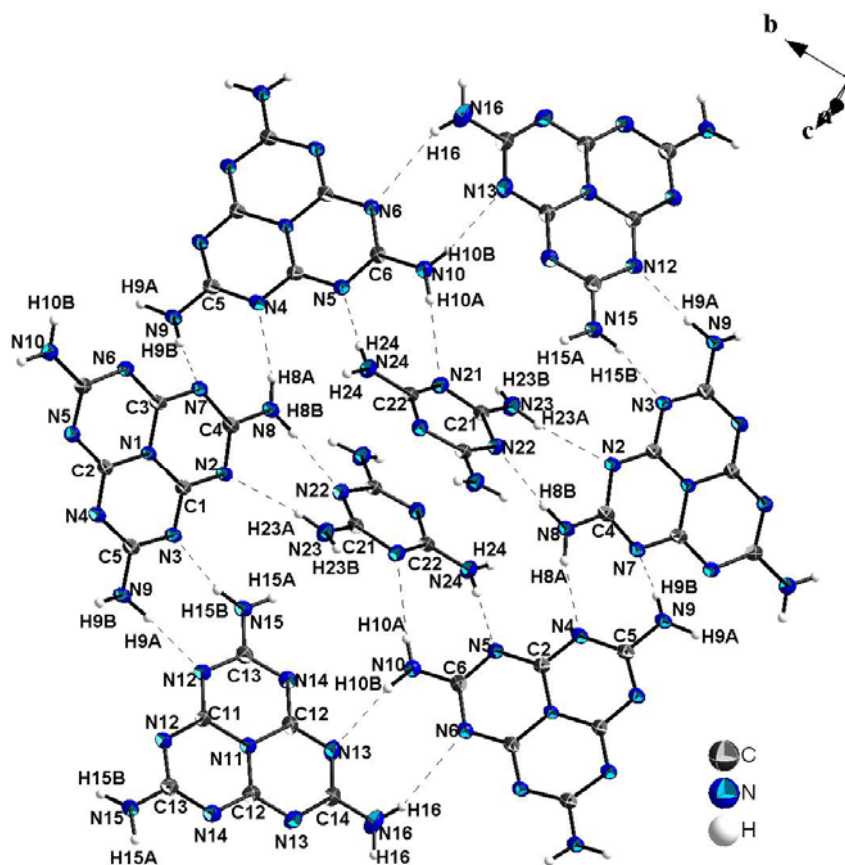


Figure 16. Hydrogen-bonding interactions in $C_3N_3(NH_2)_3 \cdot 3C_6N_7(NH_2)_3$. Ellipsoids for non-hydrogen atoms are drawn at the 50 % probability level.

For the high-temperature adduct a rather complex H-bonding pattern has been found. This compound crystallizes in the monoclinic space group $C2/c$ with 1.5 molecules of melem and one melamine molecule within the asymmetric unit. Its structure is illustrated in Figure 16 to Figure 18.

The melamine molecules are located in a tube-like structure formed by stacking of rings of six hydrogen-bonded melem molecules running along c . The parallel heptazine cores are stacked at a distance ranging from 3.4 to 3.5 Å. Each melamine molecule establishes H-bonds to two pairs of melem molecules located in the center of two separate melem “rings”, thus cross-linking them. As a second motif H-bonded helices of melem molecules found along c have to be mentioned (cf. Figure 17, Figure 18). Each “helix” also partially overlaps with three dif-

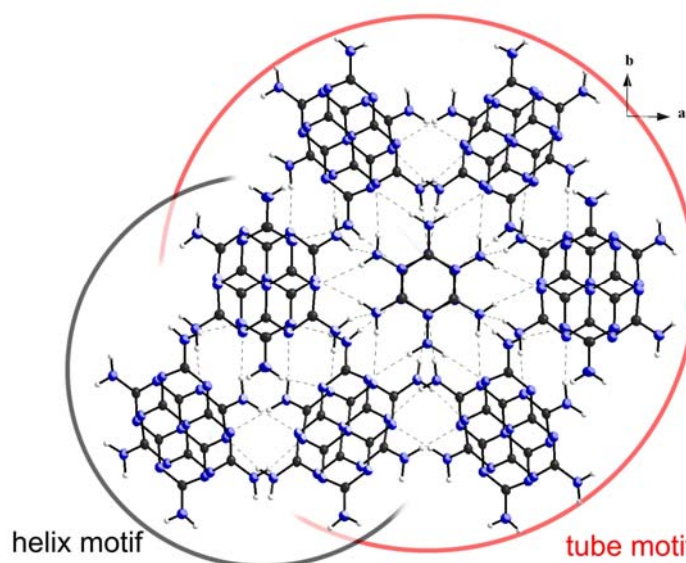


Figure 17. Unit cell and melem rings with central melamine molecule for $C_3N_3(NH_2)_3 \cdot 3C_6N_7(NH_2)_3$. View along c .

ferent “tubes” just as each “tube” is also part of six “helices”.

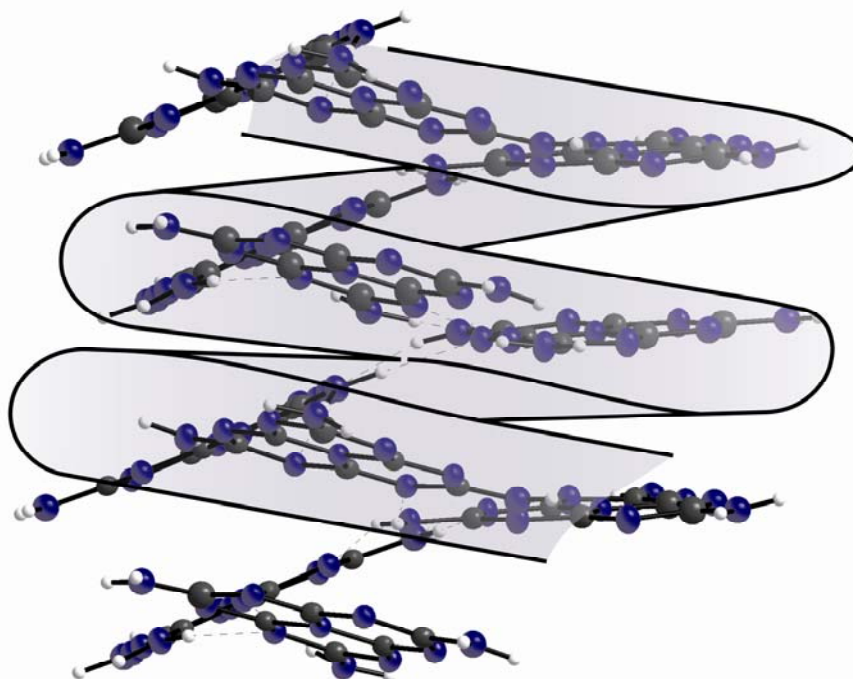


Figure 18. Hydrogen-bonded melem helices in $C_3N_3(NH_2)_3 \cdot 3C_6N_7(NH_2)_3$.

It is obvious that the hydrogen-bonding interaction is of foremost importance for the stability and structure of the melamine melem adducts discussed. For details on H-bonding networks refer to Table 4. The average length calculated for donor-acceptor distances in N-H \cdots N bridges is 3.1 Å (averaged over all three melamine melem adducts). The standard deviation of individual lengths from this value is 0.15 Å resulting in a rather homogeneous distance distribution. Most H-bonds are nearly linear displaying (donor hydrogen acceptor) DHA angles of about 170° or more while a small percentage of them also deviate notably from linearity. In 2melamine · melem and melamine · 3melem, a type of H-bonds, uncommon in compounds incorporating melem or melamine, is also observed. These interactions are found between two NH₂ groups with the amino nitrogen atoms also acting as a H-bond acceptor. Angles (111.7 to 137.8°) found for such contacts are not very favorable and so these bonds are probably rather weak by nature.

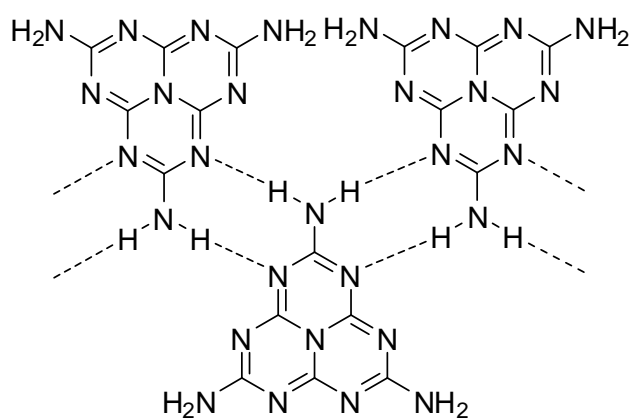
For pure melamine the D-A distances range between 3.02 and 3.11 Å and DHA angles between 166 and 175° are reported.^[110] For melem distances were found to be between 2.97 and 3.23 Å and angles range from 166 to 172°.^[35b] Thus the average H-bonds for the title adducts are not significantly more favorable than the ones found in pure melem or melamine.

The H-bonding network, however, is denser.^[1] For 2melamine · melem and melamine · 3melem all H atoms participate in H-bonding and for melamine · melem only one (of six) does not. For melem one H atom (of six) does not participate in H-bridges and another one only participates in a very long H-bonding interaction. For melamine two of six H atoms do not form proper H-bonds.

Energetic assumptions for individual H-bonds based on geometric considerations are only approximate by nature. But since the data at hand is very consistent regarding this point certain conclusions can, however, be drawn. The crucial point favoring the formation of molecular adducts in the melamine melem system probably is due to the construction of denser H-bonding networks. The average strength of the H-bonds remains virtually the same for most interactions but the number of nonexistent or weak bonds is notably lower for the three adducts than for the pure compounds. Thus, it is hardly surprising that the adduct melamine · melem which has a rather narrow field of existence in comparison to 2melamine · melem and melamine · 3melem is the only adduct without a complete H-bonding network involving any H atoms present. In addition entropy also possibly favors the formation of melamine melem adducts.

The variety of different H-bonding networks shown can however be easily broken down by analyzing the occurring structural motifs. By doing so it becomes evident that there is but one basic hydrogen-bonding motif. Most structural diversity observed for adducts of melamine and melem as well as in the pure compounds can thus easily be explained by the drive to express this motif as often as possible.

This motif of an amino moiety acting as a hydrogen bridge donor to nitrogen atoms of two separate heptazine cores is depicted in Scheme 14. As each molecule also acts as a hydrogen bridge acceptor and a donor a strand-like structure is realized. Although only shown for three melem molecules, melamine can just as well participate in this arrangement. Arranging the molecules into a crystal is thus finding a structural



Scheme 14. Dominant hydrogen-bonding motif shown for melem molecules.

[1] This corresponds well with the finding that the molar volumes of melamine melem adducts are lower (and thus more dense) than that of a mixture consisting of melamine and melem at the respective ratio. The molar volumes of melamine, melem and the adduct phases are calculated from density and molar weight of the compounds. They are divided by the amount of molecules per formula unit to describe the space used by one molecule. The values found for the adduct phases are compared with the weighted averages of V_m of melamine and melem that correspond to the respective molar ratio of each adduct. Thus it becomes evident, that the adducts are slightly more dense than a mixture of the pure components would possibly be.

Formula	density / g cm ⁻³	M / g mol ⁻¹	V_m / dm ³ mol ⁻¹	(V_m / molecules per formula unit) / dm ³ mol ⁻¹	estimate of V_m based on averaged values of melamine and melem / dm ³ mol ⁻¹
melamine	1.574	126.12	0.08013	0.08013	-
2melamine · melem	1.689	470.42	0.2785	0.0928	0.0957
melamine · melem	1.674	304.30	0.1818	0.0909	0.1034
melamine · 3melem	1.720	780.66	0.4539	0.1135	0.1151
melem	1.722	218.18	0.1267	0.1267	-

arrangement in which, in the best case, all three amino groups of each molecule can express this motif. For melem the problem about this is steric hindrance by the extended heptazine core. For melamine only three ring nitrogen atoms form hydrogen-bonds with one of the six hydrogen atoms of the amino groups. Thus not each H atom can participate in this H-bonding motif.

Table 4. Hydrogen-bonds (in ° and Å) for 2melamine · melem, melamine · melem and melamine · 3melem (D = donor, H = hydrogen, A = acceptor).

D-H...A	∠DHA	d(D...A)	D-H...A	∠DHA	d(D...A)
2melamine · melem					
N5-H5A...N12	174.2	2.95	N15-H15A...N3	149.2	3.25
N5-H5B...N11	161.1	3.05	N15-H15B...N14	131.1	3.06
N6-H6...N13	178.6	3.02	N16-H16A...N2	175.3	3.07
N14-H14A...N11	166.0	3.09	N16-H16B...N16	111.7	3.11
N14-H14B...N4	177.0	3.08			
melamine · melem					
N5-H5...N11	169.5	3.06	N13-H13B...N4	155.5	3.04
N6-H6A...N3	176.4	2.93	N14-H14...N2	176.4	3.09
N6-H6B...N12	149.8	3.25			
melamine · 3melem					
N8-H8A...N4	166.4	3.01	N15-H15A...N23	137.8	3.02
N8-H8B...N22	172.2	3.26	N15-H15B...N3	162.9	2.90
N9-H9A...N12	174.0	3.09	N16-H16...N6	154.8	3.55
N9-H9B...N7	170.4	2.89	N23-H23B...N14	170.0	3.31
N10-H10B...N13	169.9	3.20	N23-H23A...N2	172.5	3.15
N10-H10A...N21	176.0	3.30	N24-H24...N5	175.3	3.07

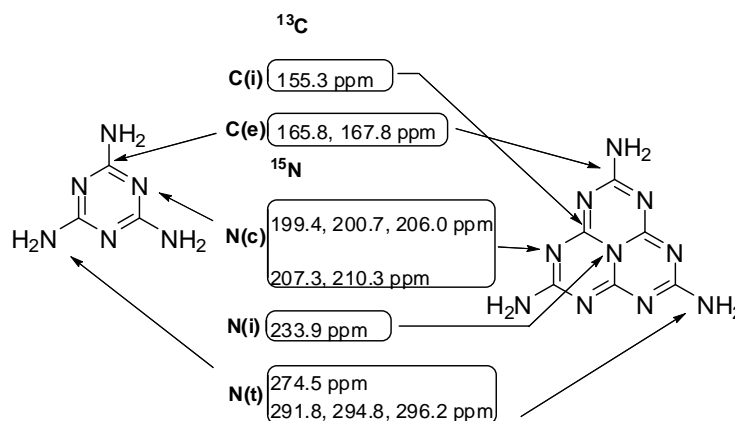
The melamine melem adducts, however, can achieve complete or almost complete networks by combining the different H-bonding properties of their components. A revision of the adduct phases' H-bonding networks (Figure 12 - Figure 16) confirms this consideration. Some H atoms are not able to participate in this preferred motif. They are, however, found in H-bonding interactions between two NH₂ groups, a feature not found for pure melamine and melem. Although stabilization by these bonds is probably low due to unfavorable angles, such an interaction is still much better than being unable to establish H-bonds at all.

Regarding the aminogroups of both melem and melamine molecules in the investigated adduct phases a number of interesting questions arise. As the crystal structure of melamine has been investigated by neutron diffraction hydrogen localization at the NH₂ groups is unambiguous.^[110] For melem, the chemical nature of the NH₂ groups has been thoroughly investigated using solid-state NMR spectroscopy.^[35a] It has been shown that the aminogroups are existent as such and a tautomerism into C=NH (and a protonation site at the heptazine core) does not occur for this compound. Such a tautomerism should also result in an alteration of bond lengths and angles within the cyameluric nucleus and a detectable shift of NMR resonances as has been shown for salts of melem expressing protonation at the cyameluric nucleus.^[36,111] Further respective melemium salts will be dealt with in Chapter 5. As no unusual values were observed here, the sole presence of C-NH₂ was concluded. It must however be noted, that a comparable tautomerism is observed for other heptazines like cyameluric acid (cf. Chapter 7 for results observed as part of this thesis).^[40,41] The NH₂ groups all favor coplanarity with the cyameluric nucleus. The central nitrogen atom shows the structural features expected for sp² hybridization. This has been observed for melem and its salts as well.^[35b,36]

Notable tilts and bending of the NH₂ groups typically lead to stronger H-bonding. This finding is also in accordance with single-crystal data of melamine^[110] and melem.^[35]

Solid-state NMR spectroscopic investigations were focused on the compound $2\text{C}_3\text{N}_3(\text{NH}_2)_3 \cdot \text{C}_6\text{N}_7(\text{NH}_2)_3$ since it is most easily obtained in large quantities. The assignment of NMR resonances in this paragraph is primarily based on spectroscopic investigations conducted for melamine,^[107] melem^[35a,107] and melemium salts.^[36,111] The ¹H-NMR spectrum only displays one resonance at 7.13 ppm, originating from NH₂ protons in melamine and melem molecules alike. Due to the strong homonuclear coupling

between the protons in the individual NH₂ groups the proton resonance remains broad and featureless even at high rotation frequencies and no further differentiation is possible. The ¹³C-NMR spectrum shows three peaks at 155.3, 165.8 and 167.8 ppm (cf. Figure 19). The first resonance is to be assigned to the C(i) atoms of the melem molecule (155.1 to 156.0 ppm for the pure compound) while the later ones comprise the C(e) atoms of melem (167.5 and 169.2 ppm for pure melem) and the carbon atoms of melamine (found at 166.2 and 167.8 ppm in pure melamine) (cf. Scheme 15). Regarding the high-field shift of the melamine resonances the resonances at 165.8 and 167.8 ppm may be assigned to C(melamine) and C(e), (melem). However, individual crystallographic positions could not be resolved.



Scheme 15. Allocation of NMR resonances and labeling of atom-types for melamine and melem molecules. Data were collected for the adduct $2\text{C}_3\text{N}_3(\text{NH}_2)_3 \cdot \text{C}_6\text{N}_7(\text{NH}_2)_3$.

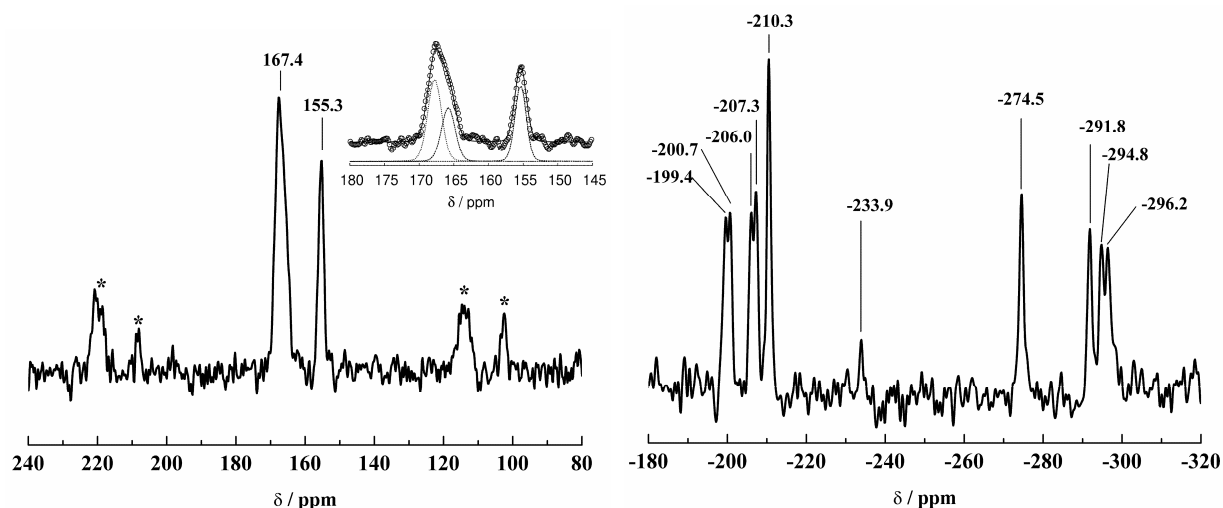


Figure 19. ¹³C-MAS solid-state NMR spectrum for $2\text{C}_3\text{N}_3(\text{NH}_2)_3 \cdot \text{C}_6\text{N}_7(\text{NH}_2)_3$. Sidebands are labeled with *.

Figure 20. ¹⁵N-MAS solid-state NMR spectrum for $2\text{C}_3\text{N}_3(\text{NH}_2)_3 \cdot \text{C}_6\text{N}_7(\text{NH}_2)_3$.

The ¹⁵N solid-state NMR spectrum (cf. Figure 20) of $2\text{C}_3\text{N}_3(\text{NH}_2)_3 \cdot \text{C}_6\text{N}_7(\text{NH}_2)_3$ shows three groups of signals. Peaks between -199.4 and -210.3 ppm can be attributed to nitrogen

atoms of the cyanuric and the cyameluric (N(c)) nuclei. Five resonances with an intensity ratio of 1:1:1:1:2 could be resolved. For melamine values from -208.8 to -211.0 ppm have been reported while literature values range from -197.1 to -205.3 ppm for melem. Thus it is reasonable to assign the high-field resonances at -199.6, -200.7 and -206.0 ppm to the adduct's melem molecules and those at -207.3 and -210.3 ppm to melamine. Since the resonance at -210.3 ppm shows twice the intensity of the other ones all six crystallographically independent N(c) nitrogen atoms can be assigned. The weak signal at -233.9 ppm belongs to the N(i) atom of the melem molecule (-234.2 ppm for pure melem). In the frequency region of the NH₂ groups four resonances can be distinguished. The peak at -274.5 ppm originates from the NH₂ groups of melem (-267.1 to -281.2 ppm for pure melem). It is not split into the two crystallographically possible independent signals demonstrating the similarity of the H-bonds formed by the NH₂ groups of melem. In contrast the H-bond network of the NH₂ groups of the melamine molecules (found at -291.4, -295.1 and -298.7 ppm for pure melamine) differs significantly in strength and geometry (cf. Tab. 3). As a consequence all three independent melamine N(t) atoms can be resolved at -291.8, -294.8 and -296.2 ppm. (cf. Scheme 15).

The multi-nuclear NMR spectroscopic investigation fully supports the structural data derived from the single-crystal X-ray diffraction experiments. The synthetic insight gained by the presented results will most certainly prove helpful in discovering new phases and preparing new or hardly accessible compounds on a bulk scale.

IR spectroscopy shows that the adduct phases exhibit vibrations at the typical wavenumbers expected for melamine or melem (cf. Figure 21). An important feature found for the adduct phases is that although both melem and melamine are present in the compound only one characteristic triazine / heptazine deformation signal is observed around 800 cm⁻¹. This illustrates that the presence or absence of mixed triazine / heptazine systems cannot be related to the number of IR active vibrations in this area. This finding will prove useful for the discussion of vibrational spectroscopy of melon and other condensed phases (cf. Chapter 6).

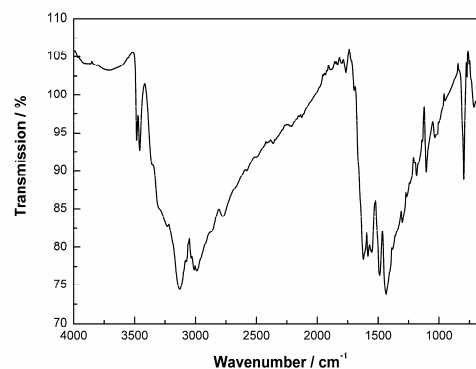
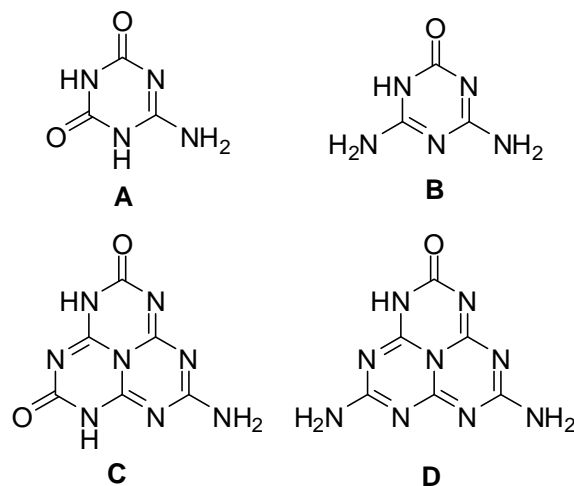


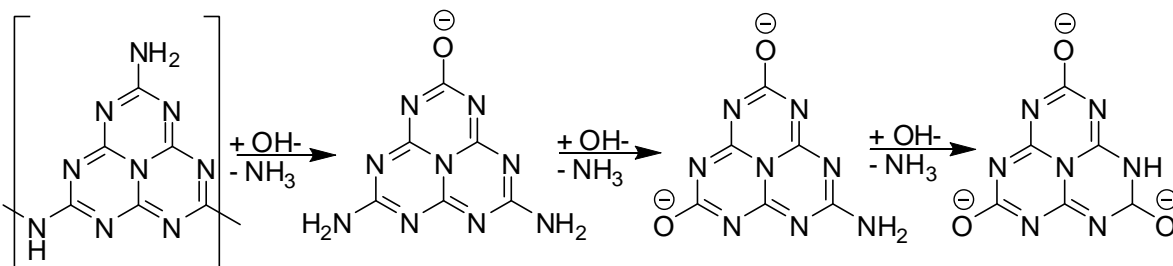
Figure 21. FTIR spectrum (ATR) of the adduct 2melamine · melem.

3.3 Oxygen-Containing Precursors – A Strategy Towards Oxo-Amino Heptazines?

The term oxo-amino heptazines refers to the compounds 2,6-dioxo-10-amino-*s*-heptazine (C) and 2-oxo-6,10-diamino-*s*-heptazine (D) (cf. Scheme 16). Not much has been reported concerning such compounds, as yet. The triazine-based molecules ammeline (A) and ammelide (B) are, however, well known compounds. So far all well described *s*-heptazine derivatives are substituted with three identical functional groups. The most important reason for interest in oxo-amino heptazines thus is the fact that, as they are substituted with two different functionalities these compounds are valuable for overcoming the synthetic limitations of heptazines. The synthesis of oxo-amino heptazines by a selective stepwise alkaline hydrolysis of melon / melem (cf. Scheme 17) has been reported by *Finkel'shtein et al.*^[112] The reactivity has been claimed to be tunable by adjusting concentration of the respective hydroxide base and reaction time.



Scheme 16. The triazine-based compounds ammeline (A) and ammelide (B) and their respective heptazine-based analogs (C) and (D). All compounds are presented as keto-like tautomers.



Scheme 17. Model of a selective hydrolysis of melon as proposed by *Finkel'shtein et al.*^[112]

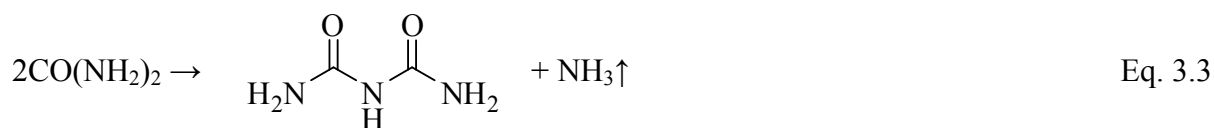
During experiments conducted as part of this theses it was, however, impossible to reproduce these results. Cyamelurates were the only hydrolysis products observed regardless of reaction conditions. Thus, the claimed compounds 2,6-dioxo-10-amino-*s*-heptazine and 2-oxo-6,10-diamino-*s*-heptazine (cf. Scheme 16, compounds C and D) are possibly only mixtures of cyameluric acid with unreacted starting material. In the original contribution the resulting products were only analyzed by methods like elemental analysis or IR spectroscopy. Thus, it was not possible to definitely distinguish between mixtures (or adducts) of cyamelu-

ric acid and melem on the one hand and partial amides of cyameluric acid on the other.^[m] Thus other ways of obtaining such partial hydrolysis products of melem need to be investigated.

The condensation of oxygen-containing precursor compounds presented itself as one such possibility. Although a multitude of different compounds can be transformed into melamine upon heating urea is of central importance, in this respect. This is due to the fact that the industrial synthesis of melamine is primarily conducted using urea as starting material. The reaction is usually carried out in the gas phase using a suitable steel reactor, however, other processes are reported as well.^[113] The following reaction equation is commonly offered for this process.^[114]



One has to bear in mind that the final reaction products, apart from melamine, are carbon dioxide and ammonia and water is not found. However, some differing reactivity of urea, leading to oxygen-containing molecules is also known. Compounds like biurea (Eq. 3.3) or cyanuric acid (Eq. 3.4) are prominent examples.



Thus, the nature of the condensation products formed starting from urea is highly variable and dependent on the respective reaction conditions.

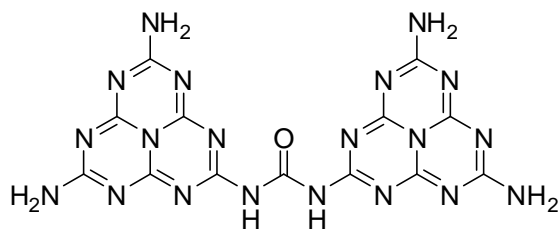


Figure 22. So-called “dimelemon”. A compound reported to be accessible by pyrolysis of urea-containing precursor mixtures.

Preliminary investigations have already covered some aspects of such condensation reactions on a laboratory scale. *Finkel'shtein* et al. have patented the synthesis of melem starting from mixtures of urea and melamine.^[115] Additional patents describing the synthesis of melem from various mixtures of melamine and dicyandiamide^[116] or from a range of other starting materials, also including compounds incorporating notable amounts of oxygen like cyanuric acid,^[117] have also been filed. Reaction temperatures

[m] Mixtures of melem and cyameluric acid display the same analytical composition as do oxo-amino heptazines. These compounds are thus not discernable by elemental analysis. IR absorption bands of partial hydrolysis products should also mostly match a combination of the ones observed for melem and cyameluric acid. This shows some parallels to the analytical problems already discussed for discerning melamine melem adduct phases from melam (cf. Section 3.1).

of 380 to 450 °C are usually reported therein. Other claims proposing the formation of oxygen-containing molecules by thermal condensation of urea-containing precursor mixtures have also been made. The bis-melemyl-substituted urea (“dimelemon“ Figure 22) has been claimed to occur during the pyrolysis of urea at 350 to 400 °C. However a yield of merely 6 - 8 % was reported.^[118] Some additional studies concerning absorption properties of this compound are also reported from the same source.^[119]

Other examples of oxygen-containing precursor compounds yielding oxygen-free products (usually melamine) upon heating have been reported as well.^[32] Examples from the literature are ammonium cyanoureate, $\text{NH}_4[\text{H}_2\text{NC}(=\text{O})\text{NCN}]$,^[120] or guanylurea dicyanamide, $\text{H}_2\text{NC}(=\text{O})\text{NHC}(\text{NH}_2)\text{NCN}$.^[121] The revision of literature data shows that there are reports on C/N/O/H compounds forming both oxygen-containing and non-oxygen-containing species upon heating. Thus, some experiments were conducted to allow a better assessment of the reactivity of such compounds under pyrolysis conditions regularly used in this thesis as well as in preceding works from our work group. Long reaction times comparable to the conditions used for obtaining the melem melamine adduct phases were chosen.

It could be observed that only oxygen-free products were yielded by this approach. The occurrence of oxygen-containing heptazine-based products could not be verified. Accordingly it is most likely that C/N/O/H compounds are only accessible by thermal contestation of suitable precursors if the reaction conditions are outside of the chemical equilibrium. If temperatures and reaction times are sufficient for the reaction to fully equilibrate such compounds decompose to form C/N/H compounds, NH_3 and CO_2 . Thus, oxygen-containing precursors work well for preparing C/N molecules by condensation reactions within an ampoule. Mixed oxo-amino compounds, however, cannot readily synthesized by such reactions.

Alkaline hydrolysis of melem and melamine also does, in contradiction to other reports, not seem to progress stepwise. Thus this method is not suitable for preparing oxo-amino heptazines. Other reaction patterns present themselves as much more promising routes for obtaining oxo-amino heptazines. Possible methods might be hydrothermal reactions or other means of hydrolysis as well as a precursor approach operating at low temperatures (< 200 °C).

3.4 Enhancing the Synthesis of Melem

As reported in prior contributions, melem was prepared by heating melamine in sealed glass ampoules.^[35,36,107,111] In order to allow the synthesis of larger quantities of melem an alternative synthesis, based on synthetic protocols used for the polymer melon and observations for the synthesis of melem in open systems, was devised.^[122] Melamine was heated in a loosely covered crucible. In contrast to the synthesis of melon pure melem is rarely ever yielded this way. Usually reaction products contain both melamine and melem. This is consistent with observations made by *Finkel'shtein* upon heating of melamine.

Additional purification is possible by boiling in water (or dilute acetic acid) to remove non-reacted melamine and yielding melem as a hydrate of formula $C_6N_7(NH_2)_3 \cdot 1.5H_2O$. This compound was already identified some time ago but unfortunately, its structure remains unresolved as yet.^[111] One might add that the synthesis of suitable melem samples in this way requires some adjustments of synthetic conditions, first of all furnace temperature, size and form of the crucible etc..

For a typical reaction 20 to 60 g of melamine were heated in a loosely covered crucible (cf. Section 12.1.1 for further experimental details). Although, it is well possible to conduct the reaction in a smaller scale yields generally tend to be lower if doing so. Mixtures also containing dicyandiamide or urea were also investigated. Melem-containing samples could be prepared this way, however, the beneficial effect on product quality claimed by *Finkelsh'tein*^[115,116] was not observed in this setup. A temperature of 300 to 400 °C was typically maintained over night. Higher temperatures resulted in the presence of higher condensation products easily detectable by a slightly yellow color of the product. Low reaction temperatures (less than 350 °C) caused low yields due to the incorporation of significant amounts of melamine in the product as well as losses due to sublimation of unreacted melamine (this is since sublimation still occurs to a notable degree while condensation is very much slowed down). This is consistent with DTA/TG investigations conducted in open crucibles (cf. Figure 23). The measurements show that upon gradual heating in an open system about 90 % of the initial weight is lost in the case of pure melamine, whereas for melem sublimation is only of subordinate importance. Based on the experiments conducted for melamine a sublimation temperature of 325 °C was found. The thermal events observed for melem above 500 °C (onset) could not be unequivocally assigned to sublimation and / or condensation of the molecule. However, a certain gas phase mobility of the respective molecules is already found at lower temperatures. Due to the issues concerning sublimation slow heating of the crucible is thus not advisable.

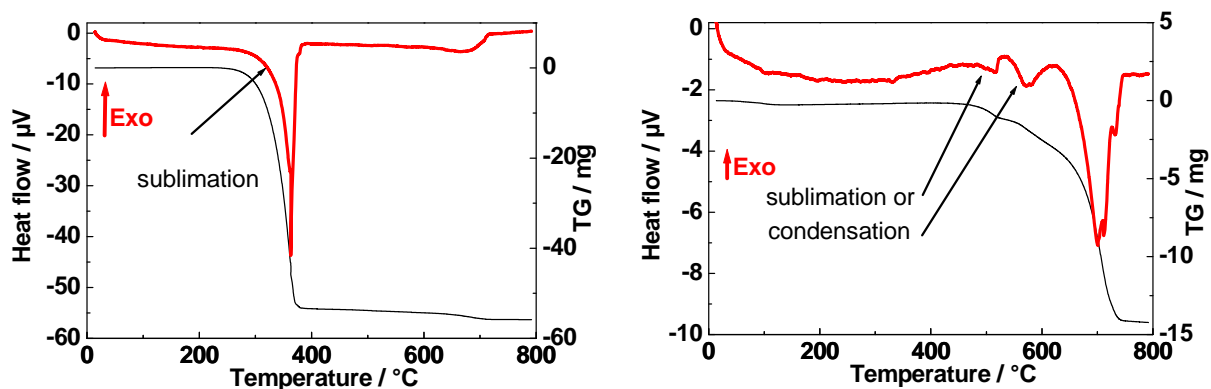


Figure 23. DTA/TG diagrams of melamine (left) and melem (right). Heat flow is drawn in bold (red) TG is drawn in narrow (black). Measurements were conducted at a scanning rate of $5^{\circ}\text{C min}^{-1}$. Initial weights were melamine = 57.83 mg and melem = 15.34 mg.

The resulting condensation products of melamine (found between 350 and 400 $^{\circ}\text{C}$) mainly consist of inhomogeneous mixtures of adduct phases and melem. The XRD pattern does, however, not necessarily match any of the three adducts studied by single-crystal XRD (cf. Section 3.2). This can be seen as an indication towards the existence of additional phases. In order to remove melamine from the product further heating is very problematic since the adducts retain melamine quite easily and further condensation of melem sets in before significant amounts of pure melem are formed. Melamine is best removed by boiling / washing with hot water or hot aqueous acetic acid. Prolonged boiling can also partially remove further condensation products as they tend to be more susceptible to hydrolysis than is melem (cf. Chapter 9). The melem hydrate is yielded this way and can be dried to yield melem. Even if synthetically pure, the dried product hardly ever shows crystallinity (cf. Section 12.1.1).

4. The Formation of Melam

4.1 The Melamium Adduct $C_6N_{11}H_{10}Cl \cdot 0.5NH_4Cl$

Historically, melam, $C_6N_{11}H_9 \equiv (NH_2)_2C_3N_3(NH)C_3N_3(NH_2)_2$, was one of the first C/N/H compounds to be mentioned. It is the initial compound reported in *Liebig's* first publication dealing with carbon nitride molecules.^[74] However, this compound has repeatedly puzzled researchers for one and a half century. Questions concerning the actual existence and structure of melam were not sufficiently solved until very recently.^[34] It

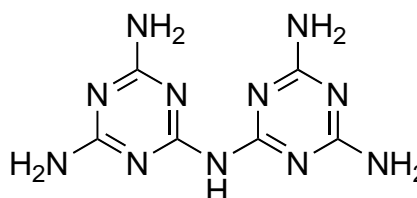


Figure 24. The molecular structure of melam ($C_6N_{11}H_9$).

is, however, finally evident that melam is existent as such and favors the molecular structure depicted in Figure 24. Though melam has been yielded by condensation of pure melamine, it remains but an intermediary product, as the formation of melem or melamine melem adduct phases is energetically preferential. The general trend that, in the course of a pyrolysis experiment of C/N/H precursors, the presence of acids generally favors the generation of melam(ium)-containing species has been reported by some Russian researchers involving *Finkel'shtein*.^[123] This method has found much use for obtaining melam. As will be shown in the following all reported synthesis conditions can be regarded as examples of this method.

Melamium adducts of the formula $C_6N_{11}H_{10}Cl \cdot 0.5NH_4X$ ($X = Cl, Br$) have first been described by *Jürgens*.^[107] The compound $C_6N_{11}H_{10}Cl \cdot 0.5NH_4Cl$ has been reported to be accessible by reaction of ammonium chloride and various small C/N/H molecules or ions (e.g. melamine, tricyanomelaminates, dicyandiamide) in sealed glass ampoules. Such melamium compounds have also received attention from other groups as well.^[124] Despite of the detailed characterizations and investigations conducted by *Jürgens* the structure of these compounds could not be resolved and their chemical nature was not established free of doubt. Based on the success in crystal growth achieved for the melamine melem adduct phases (cf. Chapter 3) the reported synthesis conditions were modified for substantially longer reaction times and slower cooling ramps. It was thus possible to reproduce the synthesis and grow crystals suitable for single-crystal XRD (cf. Section 12.1.6 for experimental details). The crystals prepared this way, however, show an inherent tendency for twinning. Although the twinning is non-merohedral, it was not possible to select a single individual. The crystal which served for the present structural investigation consisted of a total of three individuals. With that largest of them accounting for almost 90 % of diffraction intensity, the sizes of these individuals were very different. Only non-overlapping reflections of the largest individual were used during the structure elucidation, all other data was discarded (cf. Section 2.2.1 for further details on the general data handling procedure used). Although this method resulted in a low overall

4.1 The Melamium Adduct $C_6N_{11}H_{10}Cl \cdot 0.5NH_4Cl$

completeness of the dataset,^[n] the quality and plausibility of the resulting structural model, which will be presented as follows, leaves little room for doubts concerning the structural investigations.

Table 5. Crystallographic data and details of the structure refinement for $C_6N_{11}H_{10}Cl \cdot 0.5NH_4Cl$.

Formula	$C_6N_{11}H_{10}Cl \cdot 0.5NH_4Cl$	
Formula weight	298.45	
Crystal system	triclinic	
Space group	$P\bar{1}$ (no. 2)	
Lattice parameters / Å, °	$a = 6.7785(14)$	$\alpha = 91.92(3)$
	$b = 7.7528(16)$	$\beta = 91.61(3)$
	$c = 12.182(2)$	$\gamma = 112.26(3)$
Volume / Å ³	591.6(2)	
Z	2	
Diffractometer	IPDS	
Radiation, monochromator	Mo-K α ($\lambda = 71.073$ pm), graphite	
Temperature / K	140	
Structure solution	SHELXS-97 ^[101] (direct methods)	
Structure refinement	SHELXL-97 ^[101] (full-matrix least-squares on F^2)	
Corrections applied	Lorentz, polarization, absorption	
Data / restraints / parameters	3144 / 19 / 228	
R-indices	$R1 = 0.0587$ all data	
	$R1 = 0.0516 F_o^2 > 2\sigma(F_o^2)$ (reflections)	
	$wR2 = 0.1436$ all data	
	$wR2 = 0.1398 F_o^2 > 2\sigma(F_o^2)$	
Goof	1.000 (0.997 for 19 restraints)	
Weighting scheme	$w^{-1} = \sigma^2(F_o^2) + (0.1153P)^2$	
	where $P = (F_o^2 + 2F_c^2) / 3$	
Largest peak deepest hole / e Å ⁻³	-0.497 / 0.355	

$C_6N_{11}H_{10}Cl \cdot 0.5NH_4Cl$ crystallizes in the triclinic space group $P\bar{1}$. The unit cell is found to be identical with the one reported by *Jürgens* (obtained by indexing the PXRD diagram).^[107] The asymmetric unit contains one single-protonated melamium ion of formula $C_6N_{11}H_{10}^+$, its respective chloride counter ion and one half equivalent of ammonium chloride. The NH_4^+ ion displays disordered proton positions. This problem arises since the central atom (N12) of the tetrahedral (and thus non-centrosymmetric) ammonium ion is located on an inversion center. It has not been possible to resolve this disorder by reducing symmetry and no indications for a possible superstructure or a wrong choice of the unit cell were found. The ammonium ion can best be explained as two overlapping tetrahedra and was refined as such. This is resulting in a cube-like arrangement of 8 hydrogen atoms of occupancy 0.5 around the central nitrogen atom. Restraints were used to limit the geometry of the disordered ion to reasonable parameters. All possible proton positions are part of H-bonds supporting the plausibility of this structural description.

[n] The incompleteness of the data is mainly due to the fact that the software allowing data separation was only available on the IPDS diffractometer. Thus the triclinic crystal had to be measured using ϕ -scans only. The actual data separation only caused a minor loss of data, as the other individuals were rather weak.

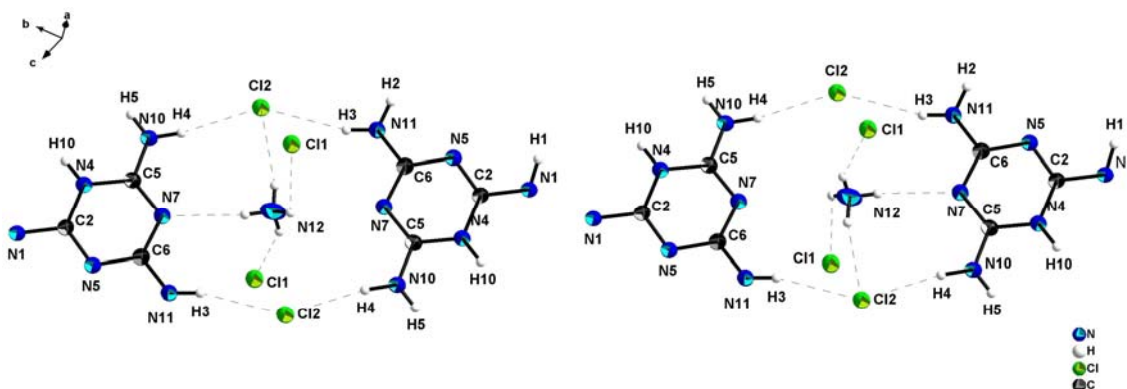


Figure 26. Two possible orientations of the disordered ammonium ion in $C_6N_{11}H_{10}Cl \cdot 0.5NH_4Cl$. Each orientation is equally probable as the tetrahedra are equivalent by symmetry. All possible hydrogen locations allow H-bonding interactions. Ellipsoids for non-hydrogen atoms are drawn at the 50 % probability level.

Structural investigations of melamium salts grown from solution have already been described in the literature.^[34,108] Whereas disorder involving the proton positions was observed there, the melamium ion found in $C_6N_{11}H_{10}Cl \cdot 0.5NH_4Cl$ allows undoubted proton localization. The structure of this ion is thus of value for the discussion of the

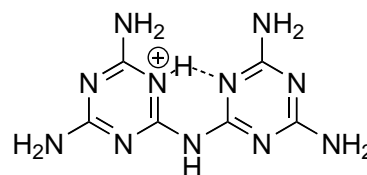
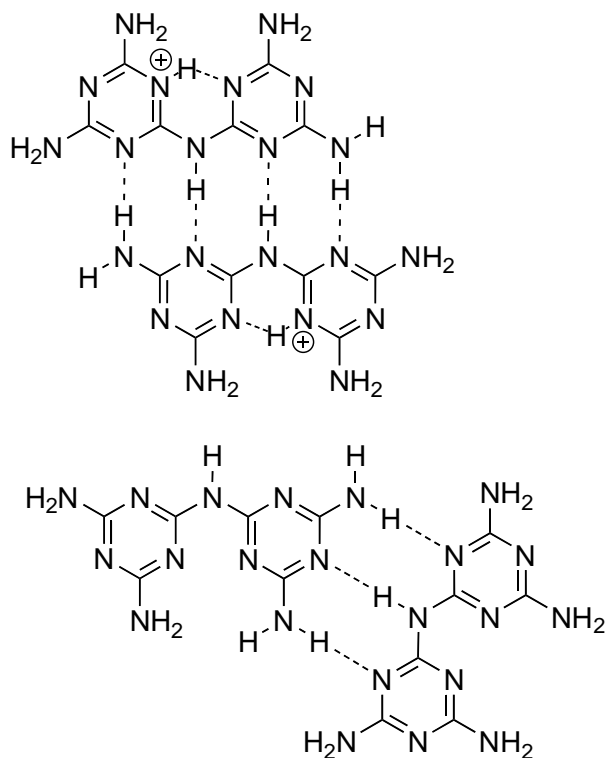


Figure 25. Molecular structure of the $C_6N_{11}H_{10}^+$ ion.

structure and the acid-base properties of melamium ions in general. The molecular structure of melam is built up of two amino-substituted triazine rings connected by an NH bridge (cf. Figure 24). The protonation site is located between the two rings allowing the formation of the intra-molecular and inter-annular H-bridge $N4-H10 \cdots N3$. Thus the planes defined by the



Scheme 18. H-bonding motifs observed in melamium adduct phases (top) and in pure melam^[34] (bottom).

two triazine rings are no longer tilted against each other, as is the case in pure melam,^[34] but are found to be coplanar for the $C_6N_{11}H_{10}^+$ ion (Figure 25, Figure 27). Two melamium ions are connected to each other by a total of four H-bonds resulting in a very stable dimer-like motif (cf. Scheme 18). As this H-bonding motif incorporates a total of four H-bonds it can be expected to possess a notable stability.^[125] In melam, however, another H-bonding motif is observed^[34] (cf. Scheme 18). It seems plausible, that the tilting of the NH group found in this case renders the four H-bond motif less favorable in this case.

4.1 The Melamium Adduct $C_6N_{11}H_{10}Cl \cdot 0.5NH_4Cl$

Table 6. Selected distances and angles (in Å and °) for $C_6N_{11}H_{10}Cl \cdot 0.5NH_4Cl$. Standard deviations in parentheses.

Distances					
N10-C5	1.3206(19)	N1-C2	1.359(2)	N4-C2	1.3533(19)
N9-C4	1.327(2)	N1-C1	1.387(2)	N4-C5	1.366(2)
N5-C2	1.314(2)	N6-C4	1.340(2)	N2-C1	1.330(2)
N5-C6	1.366(2)	N6-C3	1.3464(19)	N2-C3	1.351(2)
N7-C5	1.327(2)	N8-C3	1.328(2)	N3-C1	1.3293(19)
N7-C6	1.350(2)	N11-C6	1.317(2)	N3-C4	1.362(2)
Angles					
C2-N5-C6	114.50(14)	N11-C6-N7	118.01(16)	N6-C3-N2	124.70(15)
C5-N7-C6	115.77(14)	N11-C6-N5	115.95(14)	N5-C2-N4	123.07(15)
C2-N1-C1	127.97(13)	N7-C6-N5	126.04(15)	N5-C2-N1	117.72(14)
C4-N6-C3	115.43(15)	C1-N3-C4	113.64(14)	N4-C2-N1	119.21(15)
C2-N4-C5	118.78(15)	N3-C1-N2	127.53(16)	N9-C4-N6	118.70(15)
C1-N2-C3	114.00(13)	N3-C1-N1	119.05(14)	N9-C4-N3	116.62(15)
N10-C5-N7	121.26(16)	N2-C1-N1	113.42(14)	N6-C4-N3	124.68(14)
N10-C5-N4	117.60(16)	N8-C3-N6	117.62(15)		
N7-C5-N4	121.14(14)	N8-C3-N2	117.68(14)		

Bond lengths and angles within the melamium ion, $C_6N_{11}H_{10}^+$, are within a range expected for melam and other triazine-based molecules (cf. Table 6). Bonds within both $[C_3N_3]$ nuclei are found at lengths ranging between the expectations for double (C=N) and single bonds (C-N). The triazine rings are slightly distorted and thus deviate from their idealized symmetry. This is in accordance to observations made for the majority of triazine-based compounds. The protonation at N4 causes a small elongation of adjacent bonds.

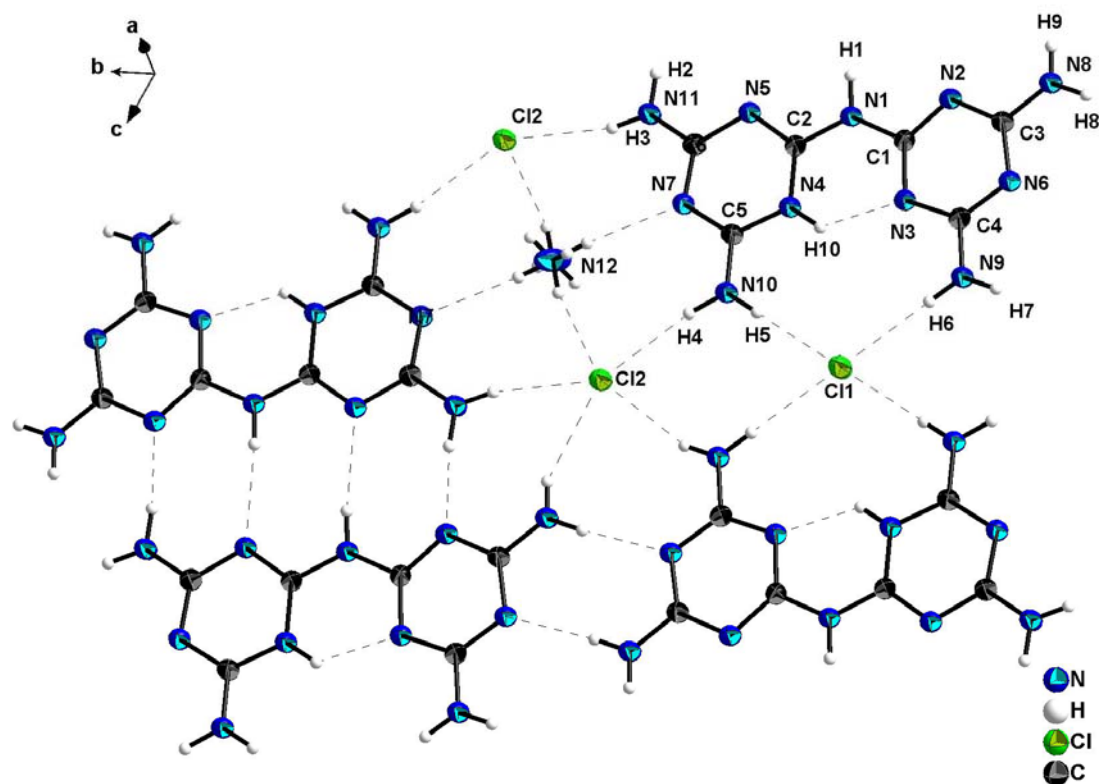


Figure 27. H-bonding interactions observed for $C_6N_{11}H_{10}Cl \cdot 0.5NH_4Cl$. Ellipsoids for non-hydrogen atoms are drawn at the 50 % probability level.

The melamium ions, as well as the chloride and ammonium ions are found to be almost in plane resulting in a layer-like arrangement. While a dense H-bonding network is found within one such layer, inter-layer interactions apparently are rather weak. The inter-layer stacking distance is about 3.4 Å. It is thus comparably large but in the same range as found for most heptazine or triazine compounds.

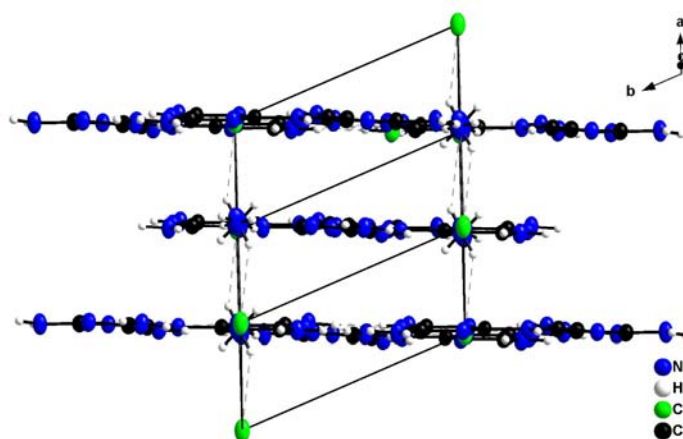


Figure 28. Layer-like structure of $C_6N_{11}H_{10}Cl \cdot 0.5NH_4Cl$.

4.2 The Melamium Melamine Adduct $C_6N_{11}H_{10}SCN \cdot 2C_3N_3(NH_2)_3$

Thiourea was used as a novel precursor for C/N/H compounds. The pyrolysis of this compound at 300 °C in sealed glass ampoules yielded a new melamine melam adduct phase of formula $C_6N_{11}H_{10}SCN \cdot 2C_3N_3(NH_2)_3$. Detailed experimental conditions are offered in Section 12.1.7. The compound was yielded in crystalline form allowing structural investigations. $C_6N_{11}H_{10}SCN \cdot 2C_3N_3(NH_2)_3$ crystallizes in the triclinic space group $P\bar{1}$. The structure of this compound could be solved by single-crystal XRD (cf. Table 7).

Table 7. Crystallographic data and details of the structure refinement for $C_6N_{11}H_{10}SCN \cdot 2C_3N_3(NH_2)_3$.

Formula	$C_6N_{11}H_{10}SCN \cdot 2C_3N_3(NH_2)_3$	
Formula weight	546.61	
Crystal system	triclinic	
Space group	$P\bar{1}$ (no. 2)	
Lattice parameters / Å, °	$a = 7.8625(16)$	$\alpha = 98.94(3)$
	$b = 10.237(2)$	$\beta = 103.23(3)$
	$c = 14.519(3)$	$\gamma = 93.33(3)$
Volume / Å ³	1118.4(4)	
Z	2	
Diffractometer	Kappa-CCD	
Radiation, monochromator	Mo-K α ($\lambda = 71.073$ pm), graphite	
Temperature / K	200 K	
Structure solution	SHELXS-97 ^[101] (direct methods)	
Structure refinement	SHELXL-97 ^[101] (full-matrix least-squares on F^2)	
Corrections applied	Lorentz, polarization, SCALEPACK, ^[96] extinction	
Data / restraints / parameters	4134 / 0 / 411	
R-indices	$R1 = 0.0840$ all data	
	$R1 = 0.0528$ $F_o^2 > 2\sigma(F_o^2)$ (reflections)	
	$wR2 = 0.1356$ all data	
	$wR2 = 0.1227$ $F_o^2 > 2\sigma(F_o^2)$	
Goof	0.995	
Weighting scheme	$w^{-1} = \sigma^2(F_o^2) + (0.0707P)^2$	
	where $P = (F_o^2 + 2F_c^2) / 3$	
Largest peak deepest hole / e Å ⁻³	-0.326 / 0.349	

The asymmetric unit comprises the melamium ion $C_6N_{11}H_{10}^+$, a thiocyanate ion and two neutral melamine molecules. The molecular structure of the melamium ion resembles the one already observed for the adduct $C_6N_{11}H_{10}Cl \cdot 0.5NH_4Cl$ (cf. Section 4.1) to a large extent. The two triazine rings are coplanar and an intra-molecular H-bridge is found. The melamine molecules only show minor deviations from their idealized structure (mainly torsions of the ammino groups against the cyanuric nucleus). The thiocyanate ion is of its expected linear form. Bond lengths and angles are in good agreement to other melam compounds (cf. Table 8).

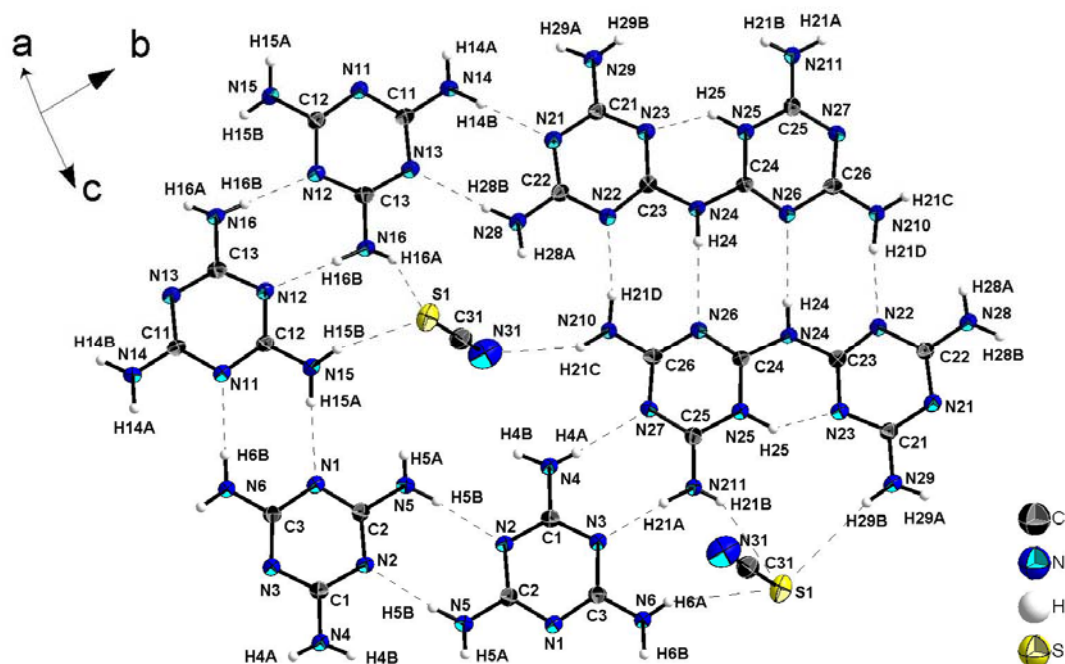


Figure 29. H-bonding interactions for $C_6N_{11}H_{10}SCN \cdot 2C_3N_3(NH_2)_3$. Ellipsoids for non-hydrogen atoms are drawn at the 50 % probability level.

The molecules are connected by a dense H-bonding network (cf. Figure 29). Rosette-like motifs, built up of melamium ions and melamine molecules, are present (cf. Figure 30). Two different types of these rosettes can be found. One type of rosettes is almost circular, while the other ones are elongated due to the incorporation of larger melamium ions. Both motifs display a central void that is filled with thiocyanate anions. The SCN^- ions are connected to the amino groups of melamine or melam by H-bonds. They are pointing towards the central voids acting as H-bond donors. The nitrogen atoms of the thiocyanate ions all point towards the smaller circular voids while the sulfur atoms point towards the elongated voids (cf. Figure 30).

4.2 The Melamium Melamine Adduct $C_6N_{11}H_{10}SCN \cdot 2C_3N_3(NH_2)_3$

Table 8. Selected distances and angles (in Å and °) for $C_6N_{11}H_{10}SCN \cdot 2C_3N_3(NH_2)_3$. Standard deviations in parentheses.

Distances					
C1-N4	1.329(3)	C12-N12	1.350(3)	C24-N25	1.347(3)
C1-N2	1.349(3)	C13-N13	1.338(3)	C24-N24	1.366(3)
C1-N3	1.349(3)	C13-N12	1.345(3)	C25-N211	1.313(3)
C2-N5	1.336(3)	C13-N16	1.357(3)	C25-N27	1.325(3)
C2-N1	1.339(3)	N14-H14A	0.84(3)	C25-N25	1.366(3)
C2-N2	1.348(3)	N14-H14B	0.89(3)	C26-N210	1.317(3)
C3-N6	1.324(3)	N15-H15A	0.89(3)	C26-N27	1.350(3)
C3-N3	1.346(3)	N15-H15B	0.82(2)	C26-N26	1.370(3)
C3-N1	1.350(3)	N16-H16A	0.78(3)	N24-H24	0.85(2)
N4-H4A	0.80(3)	N16-H16B	0.86(3)	N25-H25	0.95(3)
N4-H4B	0.86(3)	C21-N21	1.328(3)	N28-H28A	0.81(2)
N5-H5A	0.77(3)	C21-N29	1.331(3)	N28-H28B	0.88(3)
N5-H5B	0.89(3)	C21-N23	1.354(3)	N29-H29A	0.86(3)
N6-H6A	0.81(3)	C22-N28	1.322(3)	N29-H29B	0.82(2)
N6-H6B	0.87(3)	C22-N22	1.351(3)	N210-H21C	0.87(2)
C11-N14	1.331(3)	C22-N21	1.354(3)	N210-H21D	0.90(3)
C11-N11	1.343(3)	C23-N22	1.329(3)	N211-H21A	0.90(3)
C11-N13	1.352(3)	C23-N23	1.336(3)	N211-H21B	0.77(3)
C12-N15	1.334(3)	C23-N24	1.389(3)	S1-C31	1.644(3)
C12-N11	1.339(3)	C24-N26	1.312(3)	C31-N31	1.151(3)
Angles					
N4-C1-N2	118.0(2)	N13-C13-N16	117.6(2)	N27-C25-N25	120.92(19)
N4-C1-N3	117.0(2)	N12-C13-N16	115.7(2)	N210-C26-N27	116.77(19)
N2-C1-N3	125.00(19)	C12-N11-C11	114.94(18)	N210-C26-N26	117.48(19)
N5-C2-N1	118.0(2)	C13-N12-C12	114.03(18)	N27-C26-N26	125.74(19)
N5-C2-N2	116.3(2)	C13-N13-C11	113.44(19)	C21-N21-C22	115.30(18)
N1-C2-N2	125.7(2)	C11-N14-H14A	119.0(17)	C23-N22-C22	114.41(18)
N6-C3-N3	118.2(2)	C11-N14-H14B	122.3(15)	C23-N23-C21	114.49(18)
N6-C3-N1	116.7(2)	H14A-N14-H14B	119(2)	C24-N24-C23	127.35(19)
N3-C3-N1	125.1(2)	C12-N15-H15A	116.7(16)	C24-N24-H24	114.3(16)
C2-N1-C3	114.68(18)	C12-N15-H15B	117.4(18)	C23-N24-H24	118.0(16)
C2-N2-C1	114.57(19)	H15A-N15-H15B	126(2)	C24-N25-C25	119.24(19)
C3-N3-C1	114.94(18)	C13-N16-H16A	113.4(18)	C24-N25-H25	116.4(15)
C1-N4-H4A	116.0(19)	C13-N16-H16B	112.5(17)	C25-N25-H25	124.3(15)
C1-N4-H4B	113.3(16)	H16A-N16-H16B	119(3)	C24-N26-C26	114.54(18)
H4A-N4-H4B	129(3)	N21-C21-N29	118.6(2)	C25-N27-C26	116.19(18)
C2-N5-H5A	118.3(19)	N21-C21-N23	124.89(19)	C22-N28-H28A	116.2(18)
C2-N5-H5B	122.2(16)	N29-C21-N23	116.5(2)	C22-N28-H28B	121.4(15)
H5A-N5-H5B	120(3)	N28-C22-N22	118.6(2)	H28A-N28-H28B	122(2)
C3-N6-H6A	115.8(18)	N28-C22-N21	116.8(2)	C21-N29-H29A	114.2(16)
C3-N6-H6B	121.8(17)	N22-C22-N21	124.57(19)	C21-N29-H29B	121.1(18)
H6A-N6-H6B	122(3)	N22-C23-N23	126.3(2)	H29A-N29-H29B	124(2)
N14-C11-N11	117.6(2)	N22-C23-N24	115.31(18)	C26-N210-H21C	117.3(16)
N14-C11-N13	116.6(2)	N23-C23-N24	118.36(19)	C26-N210-H21D	116.0(15)
N11-C11-N13	125.7(2)	N26-C24-N25	123.3(2)	H21C-N210-H21D	126(2)
N15-C12-N11	117.2(2)	N26-C24-N24	119.16(18)	C25-N211-H21A	118.1(15)
N15-C12-N12	117.6(2)	N25-C24-N24	117.58(19)	C25-N211-H21B	115.7(18)
N11-C12-N12	125.1(2)	N211-C25-N27	120.7(2)	H21A-N211-H21B	126(2)
N13-C13-N12	126.7(2)	N211-C25-N25	118.4(2)	N31-C31-S1	178.3(3)

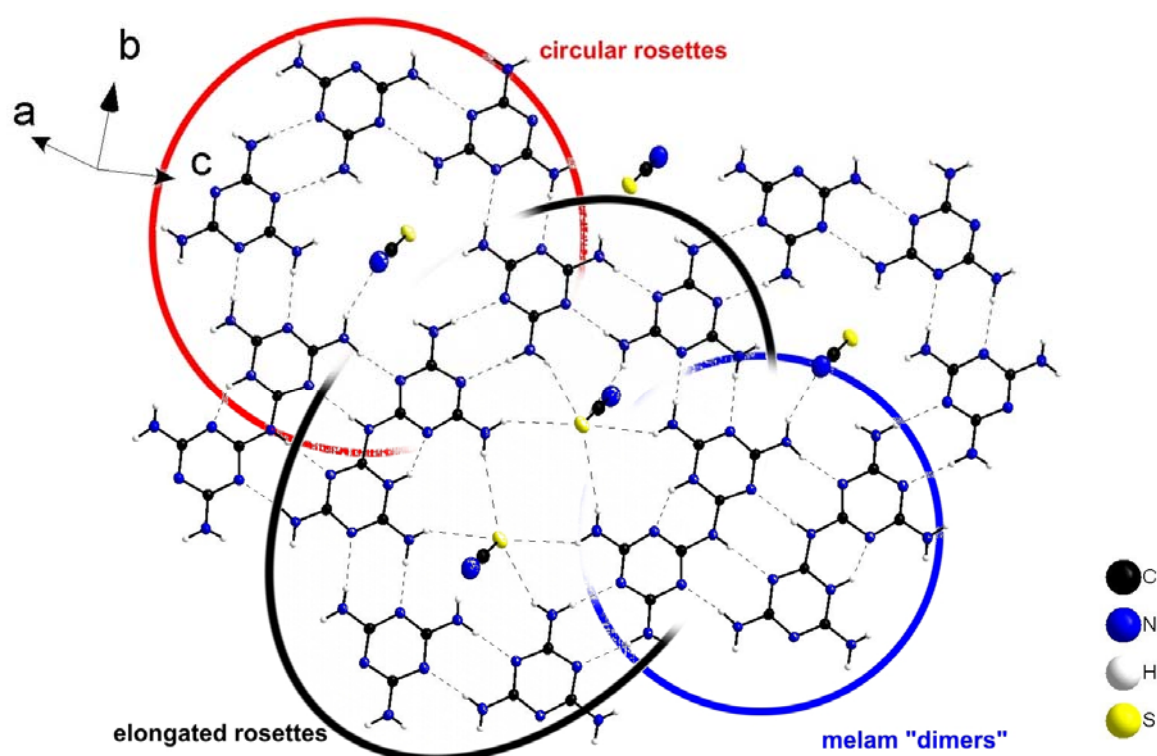


Figure 30. Structural motifs observed for $C_6N_{11}H_{10}SCN \cdot 2C_3N_3(NH_2)_3$.

The different layers are only inter-connected by SCN^- ions as no H-bonding occurs between melamine or melam molecules of different layers. This layer-like assembly is slightly corrugated with SCN^- ions acting like pillars. The inter-layer distance is around 3.0 to 3.2 Å and thus rather small in comparison to most other C/N/H compounds. This can possibly be explained since the thiocyanate ion (length = 2.79 Å) acts as a fixed length connector, dragging the layers into close proximity.

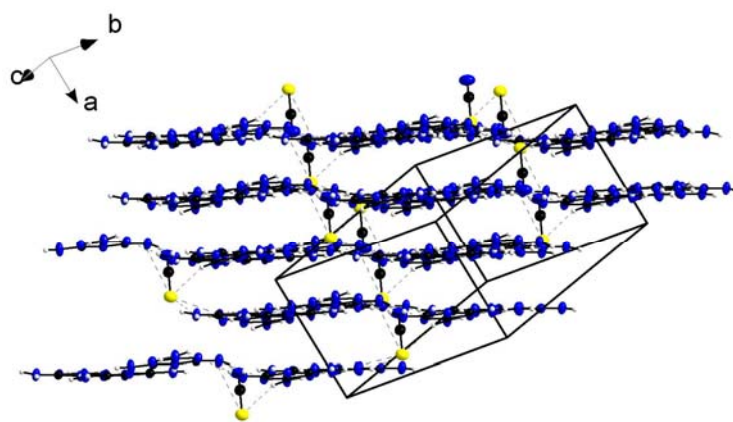


Figure 31. Layer-like arrangement of $C_6N_{11}H_{10}SCN \cdot 2C_3N_3(NH_2)_3$.

The finding that only melam and not melamine is protonated in this compound once more proves that melam is more basic than melamine (and thus also more basic than melem) and that its formation can be promoted by Brønsted acids. This acid was NH_4Cl for $C_6N_{11}H_{10}Cl \cdot 0.5NH_4Cl$ (Section 4.1). In the case of $C_6N_{11}H_{10}SCN \cdot 2C_3N_3(NH_2)_3$ the respective acid is HSCN. The formation of HSCN can be explained by degradation of the thiourea used as starting material (cf. Section 4.3 for more details). $C_6N_{11}H_{10}SCN \cdot 2C_3N_3(NH_2)_3$ is the first example of a melamium melamine adduct receiving structural investigation. This shows that, as was already expected on studying the melamine melam adducts (cf. Chapter 3), there is a vast potential for additional adduct phases involving various C/N/H molecules.

4.3 On the Potential of Thiourea as a Carbon Nitride Precursor

Sulfur-containing carbon nitride precursors have not been of primary concern for most research groups, lately. However, the introduction (cf. Section 1.2) has already covered the widespread use of ammonium thiocyanate as a precursor for several C/N/H compounds.^[74,75,81] Especially melam and melon have to be mentioned in this respect. Ammonium thiocyanate has also been reported to form guanidine thiocyanate at temperatures around 180 °C.^[126] In the melt, ammonium thiocyanate transforms into thiourea (Figure 32). This conversion is somewhat comparable to *Wöhler's* synthesis of urea from ammonium cyanate, but constitutes a true equilibrium reaction. The ration of thiourea to ammonium thiocyanate in a fully equilibrated melt has been reported as 1 : 3.^[127] The fraction of thiourea present in the melt is dependent on temperature and pressure, with high pressures and low temperatures shifting the equilibrium towards thiourea. Several works have covered this dependencies in detail.^[128]



Figure 32. Equilibrium reaction between thiourea and ammonium thiocyanate.

Thus it is not possible to clearly distinguish the thermal reactivity of both compounds as they can easily transform into each other. Several experiments were conducted in order to verify this assumption, showing only minimal differences for pyrolysis products obtained from thiourea or NH_4SCN . The pyrolysis of thiourea between 182 and 240 °C has been reported to yield CS_2 and NH_3 as main gaseous products by other investigations.^[129] The use of thiourea over ammonium thiocyanate is to be highly recommended for several practical reasons.

- Ammonium thiocyanate undergoes typical dissociation of ammonium salts and generates a notable amount of gases (HSCN and NH_3) when heated. As a consequence the initial pressure during a pyrolysis of NH_4SCN is often significantly higher than the one at the actual pyrolysis temperature after much of the NH_4SCN has been consumed by the reaction. Thus, in comparison to thiourea, the use of ammonium thiocyanate can destroy closed reaction vessels or cause lower yields due to product loss by sublimation in open systems.
- In contrast to thiourea, ammonium thiocyanate is very hygroscopic and thus more problematic concerning storage and purification if pure products are targeted.

Judging from the observations of this work thiourea can be considered a suitable precursor for carbon nitride materials. If working under equilibrium conditions is preferred, substitution of ammonium thiocyanate with thiourea can be widely recommended especially for accessing phases containing melam or for other compounds as well.

5. Melemium Salts

5.1 Introduction

Some adducts and salts containing melem, $C_6N_7(NH_2)_3$, have already been described preceding this thesis, namely the perchlorate salt $HC_6N_7(NH_2)_3ClO_4 \cdot H_2O$, the sulfate salt $H_2C_6N_7(NH_2)_3SO_4 \cdot 2H_2O$ and the phosphoric acid adduct $C_6N_7(NH_2)_3 \cdot H_3PO_4$.^[36,111] All these compounds have been synthesized from aqueous solutions of the respective acids, thus showing that melem is rather insensitive to hydrolysis in acidic solutions. In alkaline solutions, however, hydrolysis to cyameluric acid is observed comparably fast (cf. Chapter 7). Melemium salts are usually well defined and well crystalline compounds which are readily available. Thus they are valuable for gaining a comprehensive set of structural data for heptazine-based compounds. Furthermore, they are also possible precursors for carbon nitride materials or offer a way to increase the otherwise marginal solubility of melem in most solvents. Some additional compounds were thus prepared as part of this thesis and are presented in the following sections.

5.2 Melemium Melem Perchlorate

The contents of Section 5.2 are also dealt with in a publication preceding this thesis.^[37] Though the melemium melem perchlorate, $HC_6N_7(NH_2)_3ClO_4 \cdot C_6N_7(NH_2)_3$, has been synthesized from aqueous solution (cf. Section 12.1.8 for experimental details) it turned out to be anhydrous. According to single-crystal X-ray diffraction analysis (cf. Table 9) it crystallizes in the triclinic space group $P\bar{1}$ containing one melemium cation, a neutral melem molecule and a perchlorate ion in the asymmetric unit. Thus the compound can be understood as a melem adduct of solvate-free melemium perchlorate.

The molecular structures of both the melem molecule and the melemium cation as well as the labeling of the atoms as used in this work are displayed in Figure 33. In both entities the heptazine cores exhibit their usual structure and deviate only slightly from planarity. The hydrogen atoms of the amino groups are located in this plane as well. However, some of them are twisted by an angle of up to 8° thus enabling stronger hydrogen-bonds. The melemium ion is protonated at an N(c) atom of the heptazine core and not at one of the NH_2 groups. This finding is in accordance with the structural features of all other melemium salts described so far.^[36,111] The $[H(C_6N_7)(NH_2)_3]^+$ ion resembles the one found in $H(C_6N_7)(NH_2)_3ClO_4 \cdot H_2O$, with the protonation of an N(c) atom of the heptazine core effecting likewise to bond lengths of neighboring C-N bonds.^[36] The structural parameters of the melem molecule in the title compound are very similar to the ones reported for pure $C_6N_7(NH_2)_3$.^[35] The perchlorate ion exhibits its usual tetrahedral shape.

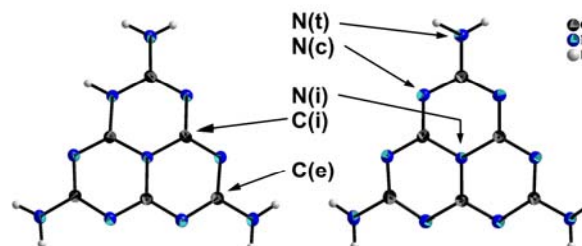


Figure 33. Molecular structure of the melem molecule and the melemium cation in melemium melem perchlorate. Labeling of crystallographically and chemically equivalent atoms. Ellipsoids for non-hydrogen atoms are drawn at the 50 % probability level.

5.2 Melemium Melem Perchlorate

Table 9. Crystallographic data and details of the refinement procedures for $\text{HC}_6\text{N}_7(\text{NH}_2)_3\text{ClO}_4 \cdot \text{C}_6\text{N}_7(\text{NH}_2)_3$.

Formula	$\text{HC}_6\text{N}_7(\text{NH}_2)_3\text{ClO}_4 \cdot \text{C}_6\text{N}_7(\text{NH}_2)_3$	
Formula weight / g mol^{-1}	536.87	
Crystal system	triclinic	
Space group	$P\bar{1}$ (no. 2)	
Lattice parameters / $\text{\AA}, ^\circ$	$a = 8.921(2)$ $b = 9.927(2)$ $c = 1.2015(2)$	$\alpha = 112.30(3)$ $\beta = 96.96(3)$ $\gamma = 95.38(3)$
Volume / \AA^3	965.8(4)	
Z	2	
Absorption coefficient / mm^{-1}	0.279	
Diffractometer	Kappa-CCD	
Radiation, monochromator	Mo- K_α ($\lambda = 71.73$ pm), graphite	
Temperature / K	200	
Structure solution	SHELXS-97 ^[101] (direct methods)	
Structure refinement	SHELXL-97 ^[101] (full-matrix least-squares on F^2)	
Corrections	extinction, Lorentz, polarization, SCALEPACK ^[96]	
Calculated density / g cm^{-3}	1.846	
Extinction coefficient	0.009(2)	
Data / restraints / parameters	4340 / 0 / 387	
R-indices	$R1 = 0.0387 F_o > 4\sigma(F_o)$ $R1 = 0.0519$ all data $wR2 = 0.0976 F_o > 4\sigma(F_o)$ $wR2 = 0.1057$ all data	
GooF	1.038	
Weighting scheme	$w^{-1} = \sigma^2(F_o^2) + (0.0525P)^2 + 0.2880P$ where $P = (F_o^2) + 2 F_c^2) / 3$	
Largest peak deepest hole / $e \text{\AA}^{-3}$	0.36 / -0.52	

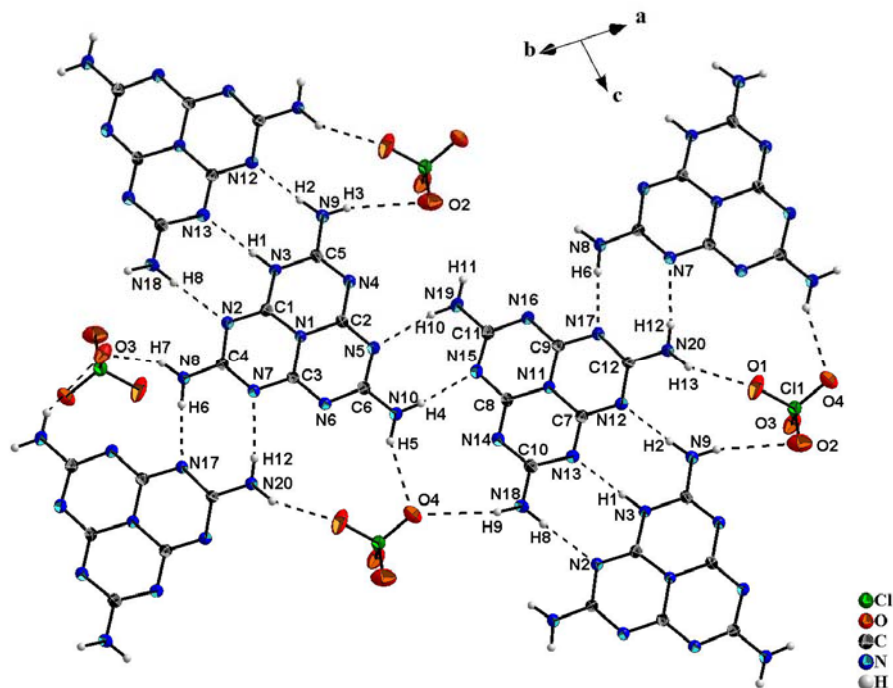


Figure 34. Hydrogen-bonding interactions for melemium melem perchlorate. View along [110]. Ellipsoids for non-hydrogen atoms are drawn at the 50 % probability level.

In analogy with many other mineral acid compounds of melem (cf. other sections of this chapter),^[36] $\text{HC}_6\text{N}_7(\text{NH}_2)_3\text{ClO}_4 \cdot \text{C}_6\text{N}_7(\text{NH}_2)_3$ is made up of planar layers of heptazine moieties which are stabilized by a network of hydrogen-bonds. While the hydrogen-bonds inter-connecting the heptazine cores are rather strong, those linking the perchlorate ions to the heptazines are relatively weak (cf. Figure 34 and Table 10). The ClO_4^- ions are significantly displaced out of the layer plane, while three oxygen atoms being acceptors of hydrogen-bonds to one layer and the other oxygen atom establishes a hydrogen-bond to the next layer (cf. Figure 35). The ClO_4^- ions of this next layer point towards the first plane and thus a double-layer structure is established. Apparently, the most stabilizing bonds between these double-layers derive from π -stacking of the aromatic heptazine cores (cf. Figure 35). However, this double-layer-like structure only has minimal impact on the average inter-layer distance that is roughly 3.3 Å in either case.

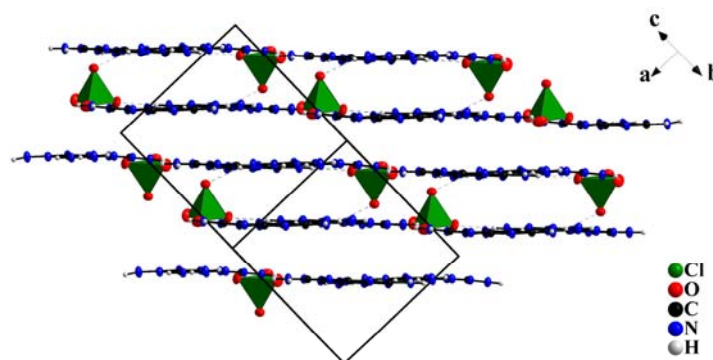


Figure 35. The layer-like structure of melemium melem perchlorate. View along [011].

Table 10. Hydrogen-bonds (in ° and Å) for $\text{HC}_6\text{N}_7(\text{NH}_2)_3\text{ClO}_4 \cdot \text{C}_6\text{N}_7(\text{NH}_2)_3$ (D = donor, H = hydrogen, A = acceptor).

D-H...A	$\angle \text{D-H}\cdots\text{A}$	D...A	$\angle \text{D-H}\cdots\text{A}$	H...A	D-H...A
N3-H1...N13	176.94	2.924	N8-H6...N16	128.87	3.309
N9-H2...N12	176.76	2.872	N8-H7...O3	153.12	2.963
N9-H3...O1	134.18	3.130	N18-H8...N2	176.25	3.061
N10-H4...N15	173.62	2.948	N19-H10...N5	165.53	3.056
N10-H5...O4	149.90	3.254	N20-H12...N7	172.39	2.974
N8-H6...N17	175.19	2.885	N20-H13...O1	156.22	3.055

The FTIR and Raman spectra (cf. Figure 36) exhibit characteristic vibrations of heptazines at 1665, 1451 and 790 cm^{-1} , respectively.^[130] The stretching vibration of the Cl-O bond is detected at 1051 cm^{-1} . The vibrational spectroscopic data are in complete agreement with the results of the X-ray structure determination.

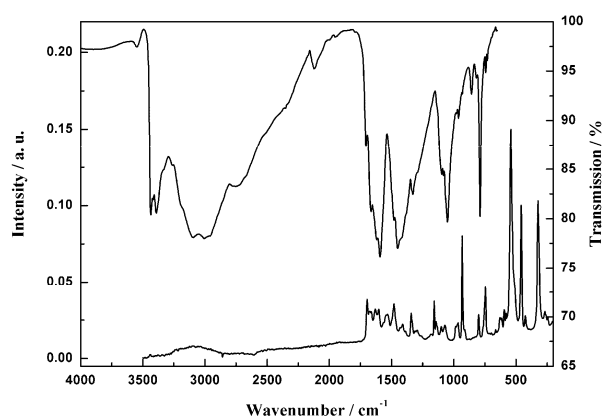


Figure 36. FTIR and Raman spectra for melemium melem perchlorate.

5.2 Melemium Melem Perchlorate

Table 11. Selected distances and angles (in Å and °) for $\text{HC}_6\text{N}_7(\text{NH}_2)_3\text{ClO}_4 \cdot \text{C}_6\text{N}_7(\text{NH}_2)_3$, standard deviations in parentheses.

Distances					
C11-O4	1.4239(14)	C5-N3	1.383(2)	C9-N17	1.322(2)
C11-O2	1.4321(16)	C6-N10	1.315(2)	C9-N11	1.404(2)
C11-O3	1.4336(13)	C6-N6	1.349(2)	C10-N18	1.326(2)
C11-O1	1.4404(14)	C6-N5	1.373(2)	C10-N14	1.345(2)
C1-N2	1.300(2)	N3-H1	0.90(2)	C10-N13	1.369(2)
C1-N3	1.349(2)	N8-H6	0.87(2)	C11-N19	1.320(2)
C1-N1	1.379(2)	N8-H7	0.88(2)	C11-N16	1.356(2)
C2-N5	1.310(2)	N9-H2	0.89(2)	C11-N15	1.359(2)
C2-N4	1.332(2)	N9-H3	0.81(2)	C12-N20	1.313(2)
C2-N1	1.405(2)	N10-H4	0.87(2)	C12-N17	1.350(2)
C3-N6	1.319(2)	N10-H5	0.89(2)	C12-N12	1.362(2)
C3-N7	1.322(2)	C7-N12	1.328(2)	N18-H8	0.89(2)
C3-N1	1.406(2)	C7-N13	1.329(2)	N18-H9	0.80(2)
C4-N8	1.304(2)	C7-N11	1.397(2)	N19-H10	0.88(2)
C4-N7	1.349(2)	C8-N15	1.318(2)	N19-H11	0.86(2)
C4-N2	1.379(2)	C8-N14	1.322(2)	N20-H12	0.82(2)
C5-N9	1.309(2)	C8-N11	1.403(2)	N20-H13	0.86(2)
C5-N4	1.327(2)	C9-N16	1.317(2)		
Angles					
O4-C11-O2	110.07(10)	C1-N2-C4	115.54(14)	N18-C10-N13	116.50(15)
O4-C11-O3	110.55(9)	C1-N3-C5	120.99(14)	N14-C10-N13	126.52(15)
O2-C11-O3	109.59(9)	C1-N3-H1	115.3(14)	N19-C11-N16	117.03(15)
O4-C11-O1	108.88(9)	C5-N3-H1	123.5(13)	N19-C11-N15	117.17(15)
O2-C11-O1	107.83(10)	C5-N4-C2	118.20(14)	N16-C11-N15	125.79(14)
O3-C11-O1	109.88(8)	C2-N5-C6	117.19(13)	N20-C12-N17	116.57(15)
N2-C1-N3	120.80(14)	C3-N6-C6	116.93(13)	N20-C12-N12	118.35(15)
N2-C1-N1	123.26(14)	C3-N7-C4	118.23(14)	N17-C12-N12	125.08(14)
N3-C1-N1	115.91(14)	C4-N8-H6	115.4(14)	C7-N11-C8	120.30(13)
N5-C2-N4	120.09(14)	C4-N8-H7	121.5(15)	C7-N11-C9	120.02(13)
N5-C2-N1	119.78(14)	H6-N8-H7	122(2)	C8-N11-C9	119.67(13)
N4-C2-N1	120.13(14)	C5-N9-H2	118.7(13)	C7-N12-C12	117.53(14)
N6-C3-N7	120.44(14)	C5-N9-H3	114.8(16)	C7-N13-C10	116.59(14)
N6-C3-N1	120.11(14)	H2-N9-H3	126(2)	C8-N14-C10	117.10(14)
N7-C3-N1	119.42(13)	C6-N10-H4	116.4(14)	C8-N15-C11	117.73(14)
N8-C4-N7	117.23(15)	C6-N10-H5	116.8(14)	C9-N16-C11	116.82(14)
N8-C4-N2	117.75(14)	H4-N10-H5	127(2)	C9-N17-C12	118.19(14)
N7-C4-N2	125.01(14)	N12-C7-N13	120.69(14)	C10-N18-H8	117.6(15)
N9-C5-N4	120.01(15)	N12-C7-N11	119.66(14)	C10-N18-H9	116.0(15)
N9-C5-N3	117.13(15)	N13-C7-N11	119.64(14)	H8-N18-H9	126(2)
N4-C5-N3	122.84(14)	N15-C8-N14	120.71(14)	C11-N19-H10	116.3(14)
N10-C6-N6	117.92(14)	N15-C8-N11	119.44(14)	C11-N19-H11	119.5(14)
N10-C6-N5	115.96(14)	N14-C8-N11	119.85(14)	H10-N19-H11	124(2)
N6-C6-N5	126.11(14)	N16-C9-N17	120.10(14)	C12-N20-H12	115.8(15)
C1-N1-C2	121.68(13)	N16-C9-N11	120.44(14)	C12-N20-H13	120.7(13)
C1-N1-C3	118.46(13)	N17-C9-N11	119.46(14)	H12-N20-H13	123(2)
C2-N1-C3	119.82(13)	N18-C10-N14	116.97(15)		

$\text{HC}_6\text{N}_7(\text{NH}_2)_3\text{ClO}_4 \cdot \text{C}_6\text{N}_7(\text{NH}_2)_3$ was obtained from an aqueous solution (8 %) of perchloric acid whereas $\text{H}(\text{C}_6\text{N}_7)(\text{NH}_2)_3\text{ClO}_4 \cdot \text{H}_2\text{O}$ ^[36,111] has been synthesized from a 15 % solu-

tion. Consequently, it seems reasonable that the degree of protonation of melem is lower for $\text{HC}_6\text{N}_7(\text{NH}_2)_3\text{ClO}_4 \cdot \text{C}_6\text{N}_7(\text{NH}_2)_3$. Contrary to the other known melemium salts^[36,111] the protonated nitrogen atom of the heptazine core is not part of a hydrogen-bond to the mineral acid or its anion. Apparently, there is a rather complete transfer of the proton from the perchloric acid to the melem molecule in the case of $\text{HC}_6\text{N}_7(\text{NH}_2)_3\text{ClO}_4 \cdot \text{C}_6\text{N}_7(\text{NH}_2)_3$ constituting one borderline case of the gradual proton transfer from the acid to the heptazine as discussed for $\text{C}_6\text{N}_7(\text{NH}_2)_3 \cdot \text{H}_3\text{PO}_4$, $(\text{H}_2\text{C}_6\text{N}_7(\text{NH}_2)_3)\text{SO}_4 \cdot 2\text{H}_2\text{O}$ and $\text{C}_6\text{N}_7(\text{NH}_2)_3 \cdot \text{H}_3\text{PO}_4$.^[36]

The fact that two different protonation levels of melem entities are stabilized alongside each other in the solid state might seem surprising at first glance. However, similar observations have been made for comparable systems like dimelaminium melamine tricyanomelamine dihydrate^[131] were both unprotonated melamine molecules and melaminium cations $\text{HC}_3\text{N}_3(\text{NH}_2)^+$ are found. Other compounds expressing comparable features are presented in the subsequent sections of this chapter and are also in line with this observation.

5.3 Melemium Diperchlorate Sesquihydrate

The preceding section has shown, that the new melemium perchlorate salt $\text{HC}_6\text{N}_7(\text{NH}_2)_3\text{ClO}_4 \cdot \text{C}_6\text{N}_7(\text{NH}_2)_3$ was obtainable at lower HClO_4 concentrations (8 %) compared to the ones used for the synthesis of $\text{HC}_6\text{N}_7(\text{NH}_2)_3\text{ClO}_4 \cdot \text{H}_2\text{O}$ (18 %).^[36] Accordingly the existence of additional perchlorate salts presented itself quite obviously. Thus, another new salt was yielded from an aqueous solution of HClO_4 at higher concentrations (40 % HClO_4). Experimental details are presented in Section 12.1.9. The structure of $\text{H}_2\text{C}_6\text{N}_7(\text{NH}_2)_3(\text{ClO}_4)_2 \cdot 1.5\text{H}_2\text{O}$ was solved by single-crystal XRD (cf. Table 12). For further data please refer to the tables presented in Section 12.6.3.

Table 12. Crystallographic data and details of the refinement procedures for $\text{H}_2\text{C}_6\text{N}_7(\text{NH}_2)_3(\text{ClO}_4)_2 \cdot 1.5\text{H}_2\text{O}$.

Formula	$\text{H}_2\text{C}_6\text{N}_7(\text{NH}_2)_3(\text{ClO}_4)_2 \cdot 1.5\text{H}_2\text{O}$	
Formula weight / g mol^{-1}	446.12	
Crystal system	triclinic	
Space group	$C\bar{1}$ (no. 2)	
Lattice parameters / $\text{Å}, ^\circ$	$a = 34.140(7)$ $b = 7.608(2)$ $c = 13.211(3)$	$\alpha = 90.000$ $\beta = 105.14(3)$ $\gamma = 90.000$
Volume / Å^3	3312.3(13)	
Z	8	
Absorption coefficient / mm^{-1}	0.468	
Diffractometer	IPDS	
Radiation, monochromator	Mo-K $_{\alpha}$ ($\lambda = 71.073$ pm), graphite	
Temperature / K	293	
Structure solution	SIR2004 ^[102] (direct methods)	
Structure refinement	SHELXL-97 ^[101] (full-matrix least-squares on F^2)	
BASF	0.476	
Corrections	Lorentz, polarization	
Absorption coefficient / mm^{-1}	0.468	
Calculated density / g cm^{-3}	1.789	
Data / restraints / parameters	5454 / 0 / 499	
R-indices	$R1 = 0.0713$ $F_o > 4\sigma(F_o)$ (3272 reflections) $R1 = 0.10039$ all data $wR2 = 0.1905$ $F_o > 4\sigma(F_o)$ $wR2 = 0.2094$ all data	
Goof	0.972	
Weighting scheme	$w^{-1} = \sigma^2(F_o^2) + (0.1400P)^2$ where $P = (F_o^2) + 2 F_c^2) / 3$	
Largest peak / deepest hole / $e \text{ Å}^{-3}$	0672 / -0.454	

The uncommon symmetry setting chosen for the refinement (space group $C\bar{1}$) is a result of the twinning observed for this compound. At first glance, the crystal appeared to be monoclinic, but a sufficient structure description was not possible in any monoclinic space group. Assuming a triclinic unit cell with $\alpha = \gamma = 90.000^\circ$ solved this issue. The symmetry was reintroduced via a twin law describing a twofold rota-

$$\begin{pmatrix} 0 & 0 & -1 \\ 0 & 1 & 0 \\ -1 & 0 & 0 \end{pmatrix}$$

Figure 37. Twin matrix used for the refinement of $\text{H}_2\text{C}_6\text{N}_7(\text{NH}_2)_3(\text{ClO}_4)_2 \cdot 1.5\text{H}_2\text{O}$.

tion around b (cf. Figure 37). As the resulting structural model, however, is not completely satisfactory, the symmetry setting was not transformed to the standard setting $P\bar{1}$.

$\text{H}_2\text{C}_6\text{N}_7(\text{NH}_2)_3(\text{ClO}_4)_2 \cdot 1.5\text{H}_2\text{O}$ crystallizes with 8 formula units per unit cell. Double-protonated melemium ions, perchlorate ions and crystal water molecules are found. The perchlorate ions and the solvate display large displacement ellipsoids (mainly involving oxygen atoms) and the protons of H_2O could not be localized (cf. Figure 38). This can be explained by assuming, that there is either additional disorder involved, or the description of symmetry and twinning is not entirely correct, as yet. Librational disorder involving the perchlorate ions suggests itself as an explanation for the large displacement ellipsoids in the current structural description. The melemium ions are very similar to the ones already observed in $\text{H}_2\text{C}_6\text{N}_7(\text{NH}_2)_3\text{SO}_4 \cdot 2\text{H}_2\text{O}$.^[36] Hydrogen positions for the melemium ions could be resolved from difference Fourier syntheses, but as proton refinement tended to be rather unstable they were fixed using geometrical constraints. Although not all proton positions could be localized, there is clear evidence for a quite dense H-bonding network (cf. Figure 38).

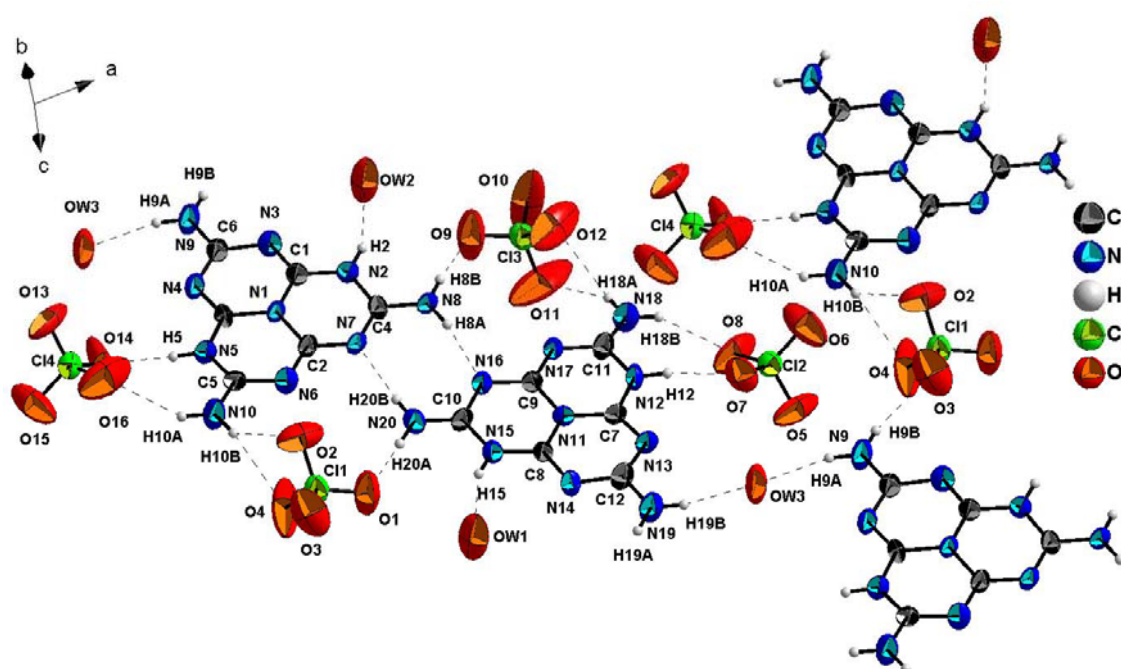


Figure 38. H-bonding interactions for $\text{H}_2\text{C}_6\text{N}_7(\text{NH}_2)_3(\text{ClO}_4)_2 \cdot 1.5\text{H}_2\text{O}$. The large displacement parameters of the perchlorate ions indicate librational disorder. Ellipsoids for non-hydrogen atoms are drawn at the 50 % probability level.

Only two melemium ions are connected to each other via H-bonding interactions. These “dimer-like” units are surrounded by a layer of perchlorate and crystal water. Once again a layer-like arrangement is observed. With the vast majority of H-bonds located in one layer, inter-layer connectivity is probably rather weak. The layers are stacked at a distance of roughly 3.8 Å which is the largest stacking distance observed for melemium salts so far. This finding can most likely be explained by the fact, that the perchlorate ions are centered within the layers in this compound. Thus, closer stacking is not possible due to the steric demands of the perchlorate ions.

5.3 Melemium Diperchlorate Sesquihydrate

Unlike observations made for most melemium salts, the perchlorate tetrahedra in $\text{H}_2\text{C}_6\text{N}_7(\text{NH}_2)_3(\text{ClO}_4)_2 \cdot 1.5\text{H}_2\text{O}$ are centered within one layer and accordingly not offering much potential for interconnections via H-bonds. This finding is different to the situation found for the perchlorate salts $\text{HC}_6\text{N}_7(\text{NH}_2)_3\text{ClO}_4 \cdot \text{C}_6\text{N}_7(\text{NH}_2)_3$ (cf. Section 5.2) and $\text{HC}_6\text{N}_7(\text{NH}_2)_3\text{ClO}_4 \cdot \text{H}_2\text{O}$.^[36]

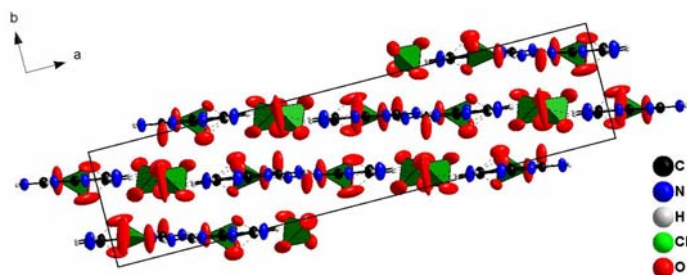


Figure 39. Layer-like arrangement of $\text{H}_2\text{C}_6\text{N}_7(\text{NH}_2)_3(\text{ClO}_4)_2 \cdot 1.5\text{H}_2\text{O}$.

5.3 Melemium Methylsulfonates

Contents of this section have already been published in advance to this thesis.^[38] Studying the behavior of melem in solutions of methylsulfonic acid some novel melemium methylsulfonate salts were identified. Two of them were yielded in crystalline form and could be investigated by single-crystal XRD. $\text{H}_2\text{C}_6\text{N}_7(\text{NH}_2)_3(\text{ClO}_4)_2 \cdot 1.5\text{H}_2\text{O}$ and $\text{H}_2\text{C}_6\text{N}_7(\text{NH}_2)_3(\text{SO}_3\text{Me})_2 \cdot \text{H}_2\text{O}$ can be crystallized from aqueous solutions of methylsulfonic acid (cf. Sections 12.1.10 – 12.1.11 for experimental details). Crystals of both salts were grown by slow cooling of hot saturated solutions. The most important factor directing the formation of one specific salt is the concentration of the acid. As $\text{HC}_6\text{N}_7(\text{NH}_2)_3\text{H}_2\text{C}_6\text{N}_7(\text{NH}_2)_3(\text{SO}_3\text{Me})_3 \cdot \text{H}_2\text{O}$ displays a lower overall protonation of melem it is yielded from less concentrated solutions. Increasing the concentration of methylsulfonic acid in solution, thus results in the formation of the higher protonated salt, $\text{H}_2\text{C}_6\text{N}_7(\text{NH}_2)_3(\text{SO}_3\text{Me})_2 \cdot \text{H}_2\text{O}$. The structures of both compounds could be solved using single-crystal XRD (cf. Table 13).

Table 13. Crystallographic data and details of the structure refinement for $\text{HC}_6\text{N}_7(\text{NH}_2)_3\text{H}_2\text{C}_6\text{N}_7(\text{NH}_2)_3(\text{SO}_3\text{Me})_3 \cdot \text{H}_2\text{O}$ and $\text{H}_2\text{C}_6\text{N}_7(\text{NH}_2)_3(\text{SO}_3\text{Me})_2 \cdot \text{H}_2\text{O}$.

Formula	$\text{HC}_6\text{N}_7(\text{NH}_2)_3\text{H}_2\text{C}_6\text{N}_7(\text{NH}_2)_3(\text{SO}_3\text{Me})_3 \cdot \text{H}_2\text{O}$	$\text{H}_2\text{C}_6\text{N}_7(\text{NH}_2)_3(\text{SO}_3\text{Me})_2 \cdot \text{H}_2\text{O}$
Formula weight / g mol ⁻¹	742.74	428.43
Crystal system	triclinic	monoclinic
Space group	$P\bar{1}$ (no. 2)	$P2_1/n$ (no. 14)
Lattice parameters / Å, °	$a = 10.096(2)$ $b = 12.865(3)$ $c = 13.369(3)$ $\alpha = 63.28(3)$ $\beta = 81.19(3)$ $\gamma = 72.92(3)$	$a = 8.0757(16)$ $b = 7.6937(15)$ $c = 27.540(6)$ $\beta = 92.03(3)$
Volume / Å ³	1461.4(7)	1710.6(6)
Z	2	4
Diffractometer	Kappa-CCD	
Radiation, monochromator	Mo-K α ($\lambda = 71.073$ pm), graphite	
Temperature / K	200	
Structure solution	SHELXS-97 ^[101] (direct methods)	
Structure refinement	SHELXL-97 ^[101] (full-matrix least-squares on F ²)	
Corrections applied	Lorentz, polarization, extinction, SCALEPACK ^[96]	
Extinction coefficient	0.0054(9)	0.0026(7)
Absorption coefficient / mm ⁻¹	0.342	0.372
Calculated density / g cm ⁻³	1.688	1.664
Data / restraints / parameters	5343 / 0 / 525	3786 / 2 / 301
R-indices	$R1 = 0.0572$ all data $R1 = 0.0381$ $F_o^2 > 2\sigma(F_o^2)$ (4141 reflections) $wR2 = 0.1028$ all data $wR2 = 0.0986$ $F_o^2 > 2\sigma(F_o^2)$	$R1 = 0.0988$ all data $R1 = 0.0467$ $F_o^2 > 2\sigma(F_o^2)$ (2432 reflections) $wR2 = 0.1071$ all data $wR2 = 0.0988$ $F_o^2 > 2\sigma(F_o^2)$
GooF	1.028	1.055
Weighting scheme	$w^{-1} = \sigma^2(F_o^2) + (0.0465P)^2 + 0.3351P$ where $P = (F_o^2 + 2F_c^2) / 3$	$w^{-1} = \sigma^2(F_o^2) + (0.0504P)^2 + 0.0322P$ where $P = (F_o^2 + 2F_c^2) / 3$
Largest peak / deepest hole / e Å ⁻³	0.282 / -0.395	0.366 / -0.352

The salt $\text{HC}_6\text{N}_7(\text{NH}_2)_3\text{H}_2\text{C}_6\text{N}_7(\text{NH}_2)_3(\text{SO}_3\text{Me})_3 \cdot \text{H}_2\text{O}$ crystallizes in the triclinic space group $P\bar{1}$ (no. 2). Additionally to the respective three methylsulfonate ions and one crystal water molecule, the asymmetric unit comprises both a melemium ion with single and double protonation. The melemium ions exhibit the usual molecular structure of melem, consisting of a heptazine nucleus and three amino moieties (cf. Figure 40).

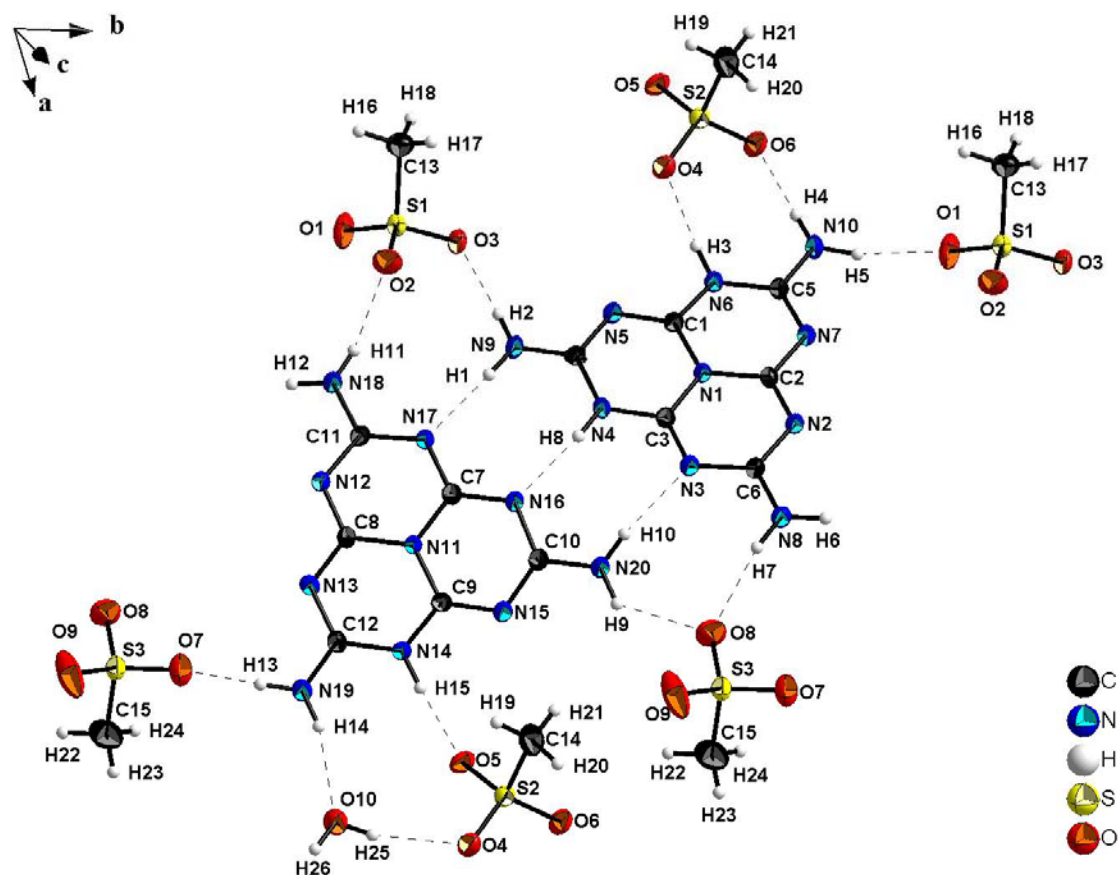


Figure 40. Molecular structure and H-bonding interactions for $\text{HC}_6\text{N}_7(\text{NH}_2)_3\text{H}_2\text{C}_6\text{N}_7(\text{NH}_2)_3(\text{SO}_3\text{Me})_3 \cdot \text{H}_2\text{O}$. Ellipsoids for non-hydrogen atoms are drawn at the 50 % probability level.

As expected from the findings for other melemium salts, melem is protonated at nitrogen atoms of the heptazine core. In comparison to non-protonated melem, elongation of C-N bonds neighboring a protonation site and shortening of the next bonds adjacent to the elongated bonds is also observed. Additionally a slight bending of bond angles at protonation sites can be found. This is observed for the other melemium salts as well (cf. other sections of this chapter).^[36,111] The C-N bonds at the terminal amino groups, however, are unaffected by proximity to protonation sites and show a general reduction in bond length by about 2 pm (in comparison to melem) instead. This applies to all respective bonds in all ions. The methylsulfonate ions do not display any unusual structural features. Both melemium cations are almost planar and deviation from planarity is mainly caused by H atoms in order to allow a more favorable H-bonding pattern, by increasing the D-H \cdots A angles.

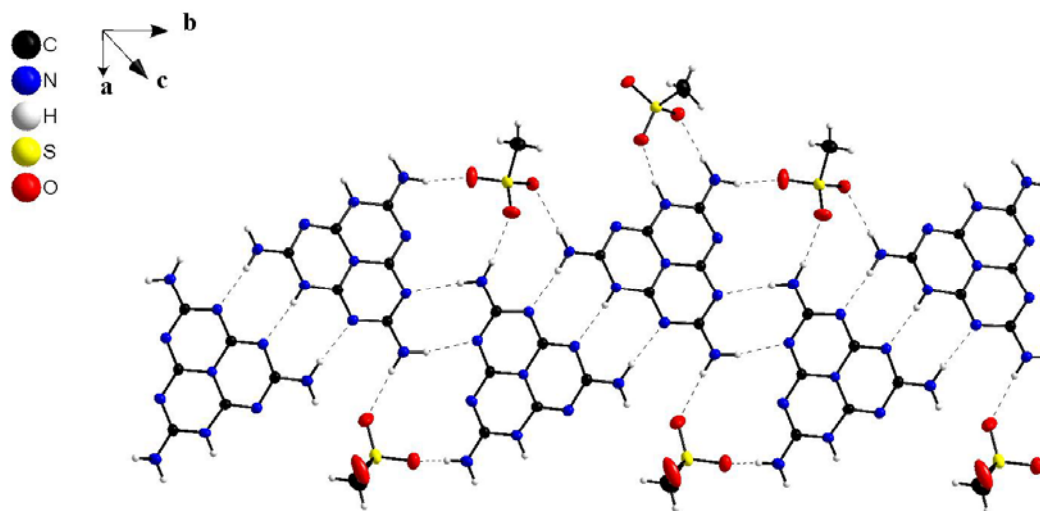


Figure 41. Hydrogen-bonded strands of melemium ions found in $\text{HC}_6\text{N}_7(\text{NH}_2)_3\text{H}_2\text{C}_6\text{N}_7(\text{NH}_2)_3(\text{SO}_3\text{Me})_3 \cdot \text{H}_2\text{O}$. Ellipsoids for non-hydrogen atoms are drawn at the 50 % probability level.

The melemium ions are arranged in hydrogen-bonded strands with one $\text{HC}_6\text{N}_7(\text{NH}_2)_3^+$ ion being connected to two $\text{H}_2\text{C}_6\text{N}_7(\text{NH}_2)_3^{2+}$ ions and vice versa (cf. Figure 41). Bridged by methylsulfonate ions and crystal water a corrugated, layer-like motif is assembled (cf. Figure 42). Layers of melemium ions are running parallel to the plane defined by b and the face diagonal of the ac plane (cf. Figure 42). The CH_3 groups of the methylsulfonate ions all point into the space between the layers. As proximity of the non-polar groups is favorable, only every second inter-layer space is filled with CH_3 groups.

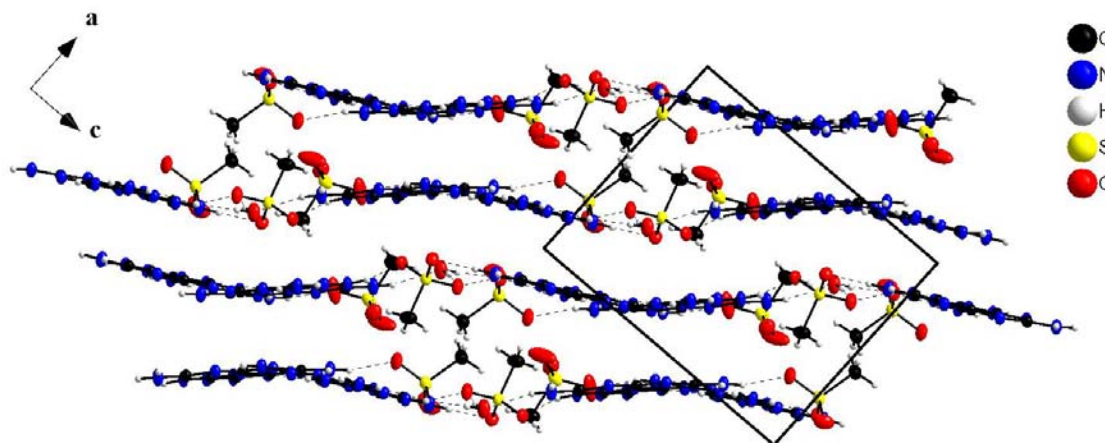


Figure 42. Layer-like structure of $\text{HC}_6\text{N}_7(\text{NH}_2)_3\text{H}_2\text{C}_6\text{N}_7(\text{NH}_2)_3(\text{SO}_3\text{Me})_3 \cdot \text{H}_2\text{O}$. View along b .

The second methylsulfonate salt, $\text{H}_2\text{C}_6\text{N}_7(\text{NH}_2)_3(\text{SO}_3\text{Me})_2 \cdot \text{H}_2\text{O}$ crystallizes in the monoclinic space group $P2_1/n$. One $\text{H}_2\text{C}_6\text{N}_7(\text{NH}_2)_3^{2+}$ ion, two methylsulfonate anions and a crystal water molecule constitute the asymmetric unit. Taking the molecular structure of melem and other melemium salts as a reference once again the usual structural features found for these compounds are also observed here. Thus bond lengths and angles are affected in the same manner as has been stated for $\text{HC}_6\text{N}_7(\text{NH}_2)_3\text{H}_2\text{C}_6\text{N}_7(\text{NH}_2)_3(\text{SO}_3\text{Me})_3 \cdot \text{H}_2\text{O}$. The melemium ions in $\text{H}_2\text{C}_6\text{N}_7(\text{NH}_2)_3(\text{SO}_3\text{Me})_2 \cdot \text{H}_2\text{O}$ are, unlike the findings for lower protonation grades, not linked to other melemium ions via hydrogen-bonding.

5.3 Melemium Methylsulfonates

Table 14. Selected distances (in Å) and angles (in °) for the melemium methylsulfonate salts $\text{HC}_6\text{N}_7(\text{NH}_2)_3$, $\text{H}_2\text{C}_6\text{N}_7(\text{NH}_2)_3(\text{SO}_3\text{Me})_3 \cdot \text{H}_2\text{O}$ and $\text{H}_2\text{C}_6\text{N}_7(\text{NH}_2)_3(\text{SO}_3\text{Me})_2 \cdot \text{H}_2\text{O}$. Standard deviations in parentheses.

$\text{HC}_6\text{N}_7(\text{NH}_2)_3\text{H}_2\text{C}_6\text{N}_7(\text{NH}_2)_3(\text{SO}_3\text{Me})_3 \cdot \text{H}_2\text{O}$									
C1-N5	1.298(3)	C9-N15	1.297(3)	N5-C1-N6	120.5(2)	C1-N5-C4	116.74(18)	C8-N12-C11	117.48(18)
C1-N6	1.345(3)	C9-N14	1.347(3)	N5-C1-N1	124.13(19)	C1-N6-C5	121.78(19)	C8-N13-C12	118.41(19)
C1-N1	1.378(3)	C9-N11	1.371(3)	N6-C1-N1	115.33(18)	C2-N7-C5	118.23(18)	C9-N14-C12	122.0(2)
C2-N2	1.314(3)	C10-N20	1.303(3)	N2-C2-N7	119.91(19)	N17-C7-N16	120.77(19)	C9-N15-C10	115.55(19)
C2-N7	1.319(3)	C10-N15	1.360(3)	N2-C2-N1	119.56(19)	N17-C7-N11	119.59(18)	C7-N16-C10	117.22(18)
C2-N1	1.404(3)	C10-N16	1.366(3)	N7-C2-N1	120.53(19)	N16-C7-N11	119.64(19)	C7-N17-C11	116.78(18)
C3-N3	1.293(3)	C11-N18	1.311(3)	N3-C3-N4	121.3(2)	N12-C8-N13	120.15(19)	O1-S1-O2	113.75(12)
C3-N4	1.353(3)	C11-N12	1.359(3)	N3-C3-N1	122.83(19)	N12-C8-N11	119.21(19)	O1-S1-O3	111.05(11)
C3-N1	1.372(3)	C11-N17	1.363(3)	N4-C3-N1	115.87(19)	N13-C8-N11	120.64(19)	O2-S1-O3	110.99(10)
C4-N9	1.296(3)	C12-N19	1.304(3)	N9-C4-N5	119.6(2)	N15-C9-N14	120.5(2)	O1-S1-C13	106.13(13)
C4-N5	1.345(3)	C12-N13	1.334(3)	N9-C4-N4	118.9(2)	N15-C9-N11	123.48(19)	O2-S1-C13	107.04(14)
C4-N4	1.371(3)	C12-N14	1.371(3)	N5-C4-N4	121.53(18)	N14-C9-N11	116.06(19)	O3-S1-C13	107.49(12)
C5-N10	1.308(3)	S1-O1	1.4475(18)	N10-C5-N7	119.99(19)	N20-C10-N15	116.4(2)	O6-S2-O5	112.38(10)
C5-N7	1.329(3)	S1-O2	1.4523(18)	N10-C5-N6	117.6(2)	N20-C10-N16	118.2(2)	O6-S2-O4	111.86(10)
C5-N6	1.376(3)	S1-O3	1.4683(17)	N7-C5-N6	122.36(19)	N15-C10-N16	125.39(19)	O5-S2-O4	110.01(10)
C6-N8	1.305(3)	S1-C13	1.750(3)	N8-C6-N2	117.50(19)	N18-C11-N12	115.90(19)	O6-S2-C14	107.75(12)
C6-N2	1.348(3)	S2-O6	1.4534(17)	N8-C6-N3	117.8(2)	N18-C11-N17	118.0(2)	O5-S2-C14	107.15(14)
C6-N3	1.376(3)	S2-O5	1.4571(16)	N2-C6-N3	124.74(19)	N12-C11-N17	126.08(19)	O4-S2-C14	107.43(14)
C7-N17	1.324(3)	S2-O4	1.4665(18)	C3-N1-C1	119.74(18)	N19-C12-N13	119.7(2)	O9-S3-O8	113.15(16)
C7-N16	1.325(3)	S2-C14	1.745(3)	C3-N1-C2	118.64(17)	N19-C12-N14	118.4(2)	O9-S3-O7	112.26(13)
C7-N11	1.400(3)	S3-O9	1.434(2)	C1-N1-C2	121.50(18)	N13-C12-N14	121.9(2)	O8-S3-O7	111.04(12)
C8-N12	1.313(3)	S3-O8	1.443(2)	C2-N2-C6	117.97(18)	C9-N11-C7	118.50(17)	O9-S3-C15	106.42(16)
C8-N13	1.323(3)	S3-O7	1.4462(17)	C3-N3-C6	115.94(19)	C9-N11-C8	120.92(18)	O8-S3-C15	106.60(17)
C8-N11	1.409(3)	S3-C15	1.747(3)	C3-N4-C4	121.85(19)	C7-N11-C8	120.54(18)	O7-S3-C15	106.89(16)
$\text{H}_2\text{C}_6\text{N}_7(\text{NH}_2)_3(\text{SO}_3\text{Me})_2 \cdot \text{H}_2\text{O}$									
C1-N2	1.297(3)	C5-N2	1.358(3)	N2-C1-N7	121.2(2)	N2-C5-N3	125.2(2)	C1-N1-C2	116.47(19)
C1-N7	1.344(3)	C5-N3	1.366(3)	N2-C1-N1	123.2(2)	N9-C6-N5	119.1(2)	C1-N1-C3	121.6(2)
C1-N1	1.379(3)	C6-N9	1.305(3)	N7-C1-N1	115.5(2)	N9-C6-N4	118.2(2)	O1-S1-O3	113.07(11)
C2-N3	1.297(3)	C6-N5	1.332(3)	N3-C2-N4	121.1(2)	C2-N1-C3	121.89(19)	O2-S1-O3	111.11(11)
C2-N4	1.349(3)	C6-N4	1.371(3)	N3-C2-N1	123.5(2)	C1-N2-C5	115.9(2)	O1-S1-C7	107.11(15)
C2-N1	1.381(3)	S1-O1	1.4503(19)	N4-C2-N1	115.4(2)	C2-N3-C5	115.5(2)	O2-S1-C7	107.32(15)
C3-N5	1.316(3)	S1-O2	1.458(2)	N5-C3-N6	119.8(2)	C2-N4-C6	121.4(2)	O3-S1-C7	106.44(14)
C3-N6	1.323(3)	S1-O3	1.4643(18)	N5-C3-N1	120.0(2)	C2-N4-H3	120.8(17)	O5-S2-O6	112.25(12)
C3-N1	1.406(3)	S1-C7	1.747(3)	N6-C3-N1	120.2(2)	C6-N4-H3	117.8(17)	O5-S2-O4	110.89(14)
C4-N10	1.306(3)	S2-O5	1.449(2)	N10-C4-N6	119.9(2)	C3-N5-C6	118.6(2)	O6-S2-O4	111.54(12)
C4-N6	1.336(3)	S2-O6	1.4520(18)	N10-C4-N7	117.4(2)	C3-N6-C4	118.0(2)	O5-S2-C8	106.68(15)
C4-N7	1.367(3)	S2-O4	1.459(2)	N6-C4-N7	122.7(2)	C1-N7-C4	121.7(2)	O6-S2-C8	109.05(14)
C5-N8	1.301(3)	S2-C8	1.743(3)	N8-C5-N2	117.4(2)	O1-S1-O2	111.42(13)	O4-S2-C8	106.10(16)
				N8-C5-N3	117.4(2)	N5-C6-N4	122.7(2)		

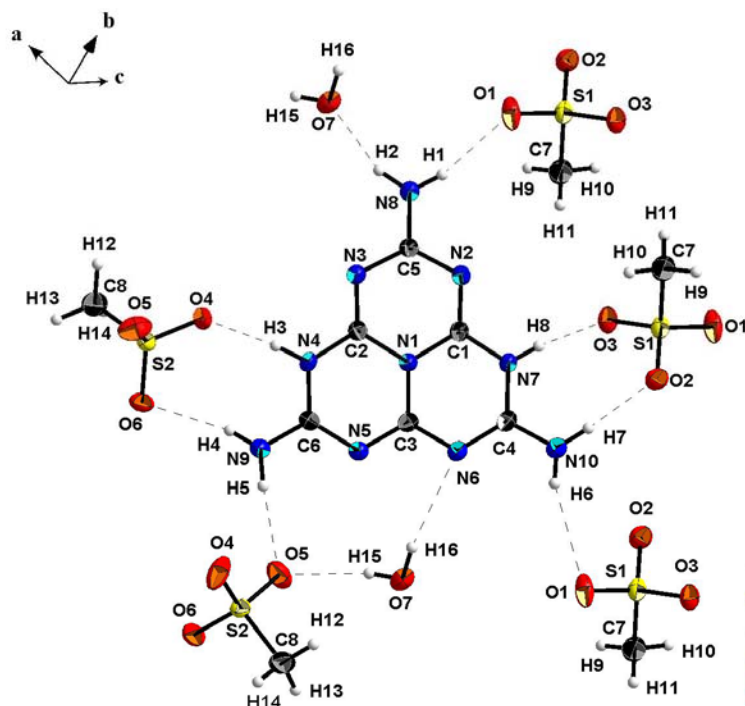


Figure 43. Molecular structure of the melemium ion and H-bonding interactions for $\text{H}_2\text{C}_6\text{N}_7(\text{NH}_2)_3(\text{SO}_3\text{Me})_2 \cdot \text{H}_2\text{O}$. Ellipsoids for non-hydrogen atoms are drawn at the 50 % probability level.

This corresponds to the situation observed for the $\text{H}_2\text{C}_6\text{N}_7(\text{NH}_2)_3^{2+}$ ions found in $\text{H}_2\text{C}_6\text{N}_7(\text{NH}_2)_3\text{SO}_4 \cdot 2\text{H}_2\text{O}$.^[36,111] The molecular structure of the methylsulfonyl ions is as expected. The three-dimensional arrangement is mainly governed by hydrogen-bonding interactions. The resulting structure comprises strand-like motifs alternating in an A A' B B' stacking pattern (cf. Figure 44).

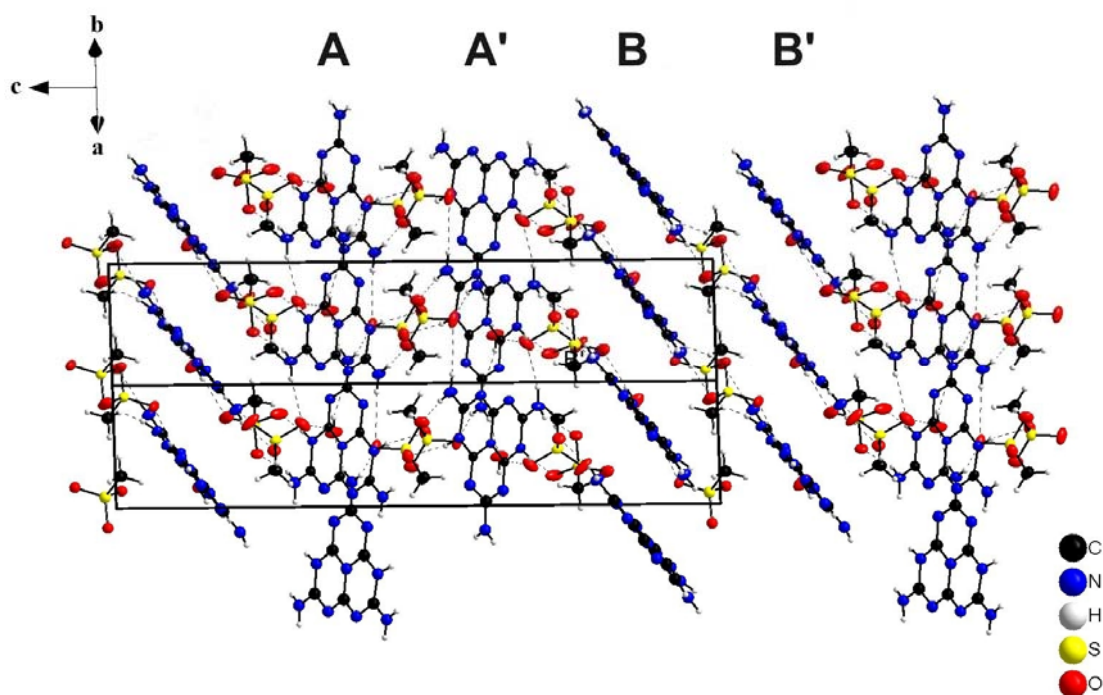


Figure 44. Stacking pattern of melemium ions in $\text{H}_2\text{C}_6\text{N}_7(\text{NH}_2)_3(\text{SO}_3\text{Me})_2 \cdot \text{H}_2\text{O}$.

At first glance, projections along the a or b axis might suggest H-bonded layers to be dominant (cf. Figure 44 - Figure 46). However, the actual structure is much more complicated, consisting of a complex three-dimensional H-bonding network. Distinct layer-like structures, found for other melemium salts, cannot be observed in this case.

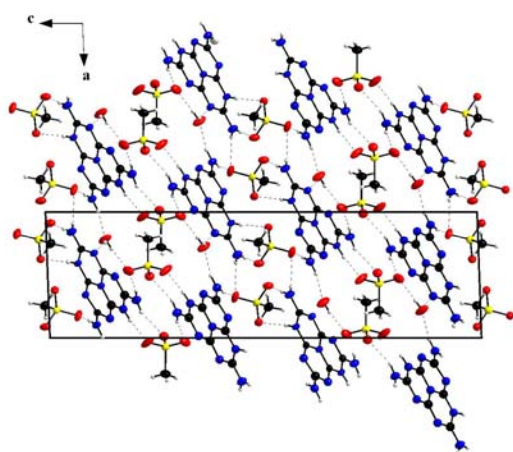


Figure 45. Crystal structure of $\text{H}_2\text{C}_6\text{N}_7(\text{NH}_2)_3(\text{SO}_3\text{Me})_2 \cdot \text{H}_2\text{O}$. View along b . Ellipsoids for non-hydrogen atoms are drawn at the 50 % probability level.

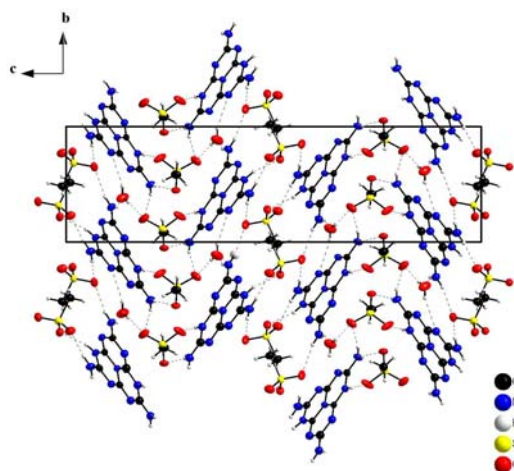
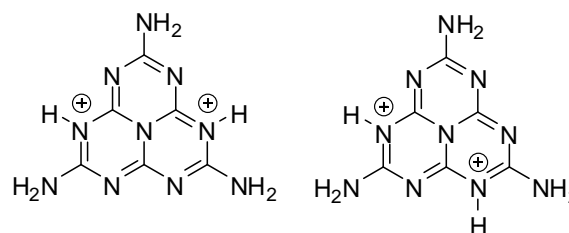


Figure 46 Crystal structure of $\text{H}_2\text{C}_6\text{N}_7(\text{NH}_2)_3(\text{SO}_3\text{Me})_2 \cdot \text{H}_2\text{O}$. View along a . Ellipsoids for non-hydrogen atoms are drawn at the 50 % probability level.

The molecular structure of the $\text{H}_2\text{C}_6\text{N}_7(\text{NH}_2)_3^{2+}$ ion found in $\text{HC}_6\text{N}_7(\text{NH}_2)_3\text{H}_2\text{C}_6\text{N}_7(\text{NH}_2)_3(\text{SO}_3\text{Me})_3 \cdot \text{H}_2\text{O}$ exhibits different protonation positions than the ions found in $\text{H}_2\text{C}_6\text{N}_7(\text{NH}_2)_3(\text{SO}_3\text{Me})_2 \cdot \text{H}_2\text{O}$ and $\text{H}_2\text{C}_6\text{N}_7(\text{NH}_2)_3\text{SO}_4 \cdot 2\text{H}_2\text{O}$.^[36] The two different tautomers of the diprotonated melemium ion found in melemium salts show different symmetry (cf. Scheme 19). The one realized in $\text{H}_2\text{C}_6\text{N}_7(\text{NH}_2)_3\text{SO}_4 \cdot 2\text{H}_2\text{O}$ ^[36] and in $\text{H}_2\text{C}_6\text{N}_7(\text{NH}_2)_3(\text{SO}_3\text{Me})_2 \cdot \text{H}_2\text{O}$ has C_{2v} symmetry (for the idealized molecule). The other tautomer found in $\text{HC}_6\text{N}_7(\text{NH}_2)_3\text{H}_2\text{C}_6\text{N}_7(\text{NH}_2)_3(\text{SO}_3\text{Me})_3 \cdot \text{H}_2\text{O}$ displays idealized C_s symmetry. Energetic differences between the two tautomeric forms of the cation seem to be low, allowing other effects like H-bonding to determine the realization of one tautomer. A similar situation can be discussed for the tautomers of the dihydrogencyamelurate anion as will be shown in subsequent sections of this thesis (cf. Chapter 7).



Scheme 19. Tautomers found for the $\text{H}_2\text{C}_6\text{N}_7(\text{NH}_2)_3^{2+}$ ion. The higher symmetric ion (left) found in $\text{H}_2\text{C}_6\text{N}_7(\text{NH}_2)_3\text{SO}_4 \cdot 2\text{H}_2\text{O}$ and in $\text{H}_2\text{C}_6\text{N}_7(\text{NH}_2)_3(\text{SO}_3\text{Me})_2 \cdot \text{H}_2\text{O}$ is of C_{2v} symmetry, while the lower symmetric one in $\text{HC}_6\text{N}_7(\text{NH}_2)_3\text{H}_2\text{C}_6\text{N}_7(\text{NH}_2)_3(\text{SO}_3\text{Me})_3 \cdot \text{H}_2\text{O}$ (right) expresses C_s symmetry.

Rather short contacts between the S=O groups of methylsulfonate ions and certain atoms (mostly carbon atoms) of the cyameluric nucleus were observed for the melemium methylsulfonate salts.^[o] Although further investigations concerning this point were not conducted, it seems reasonable to attribute this finding primarily to electrostatic interactions of

[o] These contacts range from 2.82 to 2.95 Å for $\text{HC}_6\text{N}_7(\text{NH}_2)_3\text{H}_2\text{C}_6\text{N}_7(\text{NH}_2)_3(\text{SO}_3\text{Me})_3 \cdot \text{H}_2\text{O}$ and from 2.93 to 2.96 Å for $\text{H}_2\text{C}_6\text{N}_7(\text{NH}_2)_3(\text{SO}_3\text{Me})_2 \cdot \text{H}_2\text{O}$.

the cyameluric nucleus with the S=O groups. Even shorter distances have been observed for $\text{H}_3\text{C}_6\text{N}_7(\text{NH}_2)_3(\text{HSO}_4)_3$ (cf. Section 5.4). Please refer to the discussion there for further details concerning such interactions.

Phase pure samples of the salt $\text{H}_2\text{C}_6\text{N}_7(\text{NH}_2)_3(\text{SO}_3\text{Me})_2 \cdot \text{H}_2\text{O}$ were readily available as can be seen by comparison of measured PXRD data with XRD pattern simulated from single-crystal data (cf. Figure 47 compound 2). For lower concentrations of methylsulfonic acid, however, the existence ranges of a multitude of phases overlap. A pure bulk sample of the methylsulfonate salt $\text{HC}_6\text{N}_7(\text{NH}_2)_3\text{H}_2\text{C}_6\text{N}_7(\text{NH}_2)_3(\text{SO}_3\text{Me})_3 \cdot \text{H}_2\text{O}$ could not be prepared. Impurities either are $\text{H}_2\text{C}_6\text{N}_7(\text{NH}_2)_3(\text{SO}_3\text{Me})_2 \cdot \text{H}_2\text{O}$ (cf. Figure 47 compound 1) or other salts presumably expressing lower overall protonation than is the case in $\text{HC}_6\text{N}_7(\text{NH}_2)_3\text{H}_2\text{C}_6\text{N}_7(\text{NH}_2)_3(\text{SO}_3\text{Me})_3 \cdot \text{H}_2\text{O}$. These species could, however not be structurally characterized so far.

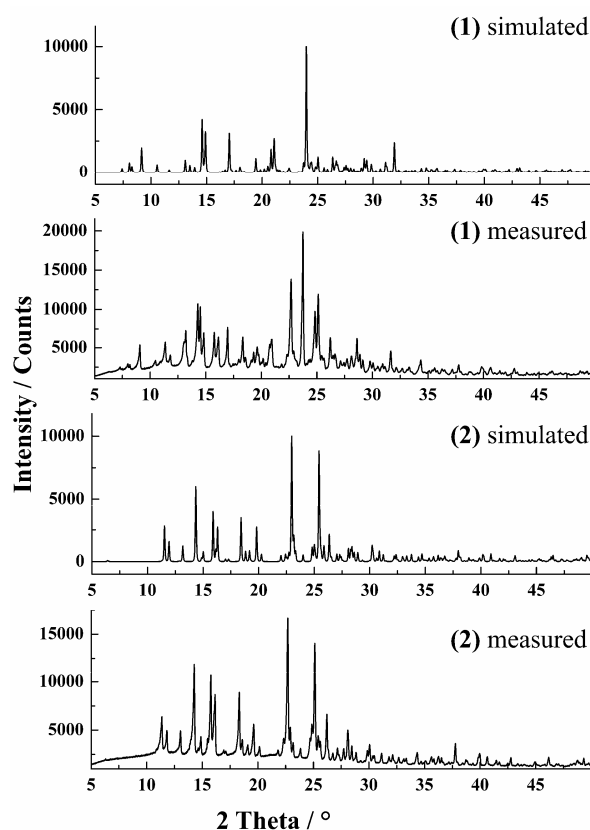


Figure 47. Comparison of measured and calculated PXRD patterns (Cu- $\text{K}\alpha_1$ radiation) for the melemium methylsulfonates and $\text{H}_2\text{C}_6\text{N}_7(\text{NH}_2)_3(\text{SO}_3\text{Me})_2 \cdot \text{H}_2\text{O}$, compound (1), and $\text{HC}_6\text{N}_7(\text{NH}_2)_3\text{H}_2\text{C}_6\text{N}_7(\text{NH}_2)_3(\text{SO}_3\text{Me})_3 \cdot \text{H}_2\text{O}$ compound (2)

5.4 The Melemium Hydrogensulfate $\text{H}_3\text{C}_6\text{N}_7(\text{NH}_2)_3(\text{HSO}_4)_3$

In order to provide a better overview the observation, that melem is capable of forming several different salts when subjected to sulfuric acid needs to be addressed. Which compound is formed is primarily dependant on the respective concentration of the acid. This finding is not very surprising as a tendency towards displaying different melemium salts has already been observed for perchloric and methylsulfonic acid (cf. respective sections). The salt $\text{H}_2\text{C}_6\text{N}_7(\text{NH}_2)_3(\text{SO}_4) \cdot 2\text{H}_2\text{O}$ was already characterized during prior works.^[36] A comprehensive study of the formation of melemium sulfate salts produced the following results (cf. Table 15).

Table 15. Existence ranges of different melemium salts in relation to the concentration of sulfuric acid as found in this work.

conc. / wt.%	<	7.8	40	44	48	53	58	>69
c / g mol ⁻¹	<	0.8	5.0	5.6	6.3	7.2	8.0	>10
compound observed ^[a]	melem hydrate	$\text{H}_2\text{C}_6\text{N}_7(\text{NH}_2)_3(\text{SO}_4) \cdot 2\text{H}_2\text{O}$		new salt A		new salt B		$\text{H}_3\text{C}_6\text{N}_7(\text{NH}_2)_3(\text{HSO}_4)_3$

[a] Determined by XRD methods.

It is necessary to add that the above-mentioned data only applies as long as reasonable ratios of melem to the volume of the solution are maintained. Values between 1 and 10 mg per mL of solution are suitable for lower sulfuric acid concentrations, while higher concentrations allow more melem to be used.

Starting from the concentrations known to produce $\text{H}_2\text{C}_6\text{N}_7(\text{NH}_2)_3(\text{SO}_4) \cdot 2\text{H}_2\text{O}$ three new salts obtainable at higher concentrations of sulfuric acid were identified. There, however, seem to be no additional salts that can be yielded at lower sulfuric acid concentrations. Instead only melem hydrate was found for very dilute solutions. Two of the three new salts discovered that way could unfortunately not be structurally studied due to crystal growth problems. The third compound, however, was yielded well-crystalline and could be investigated by single-crystal XRD (cf. Section 12.1.12). The formula was found to be $\text{H}_3\text{C}_6\text{N}_7(\text{NH}_2)_3(\text{HSO}_4)_3$, thus the compound is a triple-protonated melemium hydrogensulfate.

The pK_s value for HSO_4^- is given as 1.92.^[132] One might assume that the acidity of the $\text{H}_3\text{C}_6\text{N}_7(\text{NH}_2)_3^{3+}$ is higher than the one of HSO_4^- . Such speculations are quite problematic, since solid-state and solution acidities vary and the presence of HSO_4^- ions in the salt could only be due to the abundance of H_2SO_4 . In fact the existence of the two other salts A and B suggests that triple-protonation of melem might be possible at lower H_2SO_4 concentrations as well.

$\text{H}_3\text{C}_6\text{N}_7(\text{NH}_2)_3(\text{HSO}_4)_3$ is an extremely hygroscopic compound. Crystals decay within split-seconds when subjected to moist air, thus the compound needs to be handled in inert gas atmosphere. By reaction with moisture the compound is transformed into another melemium salt that, judging from PXRD, is not identical with either one of the salts accessible from solution (cf. Table 15). Taking this properties into account, $\text{H}_3\text{C}_6\text{N}_7(\text{NH}_2)_3(\text{HSO}_4)_3$ might be used as desiccant or moisture sensor.

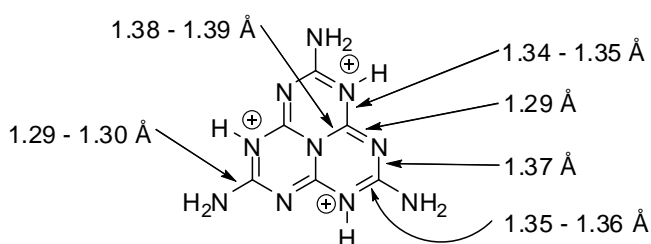
As was already mentioned, the structure of melemium hydrogensulfate was solved by single-crystal XRD (cf. Table 16). $\text{H}_3\text{C}_6\text{N}_7(\text{NH}_2)_3(\text{HSO}_4)_3$ crystallizes in the monoclinic space group $P2_1/n$ with 4 formula units per unit cell. The asymmetric unit comprises one

$\text{H}_3\text{C}_6\text{N}_7(\text{NH}_2)_3^{3+}$ ion and three hydrogensulfate ions. No solvate molecules are integrated into the compound. Please refer to Section 12.6.4 for additional tables.

Table 16. Crystallographic data and details of the structure refinement for $\text{H}_3\text{C}_6\text{N}_7(\text{NH}_2)_3(\text{HSO}_4)_3$.

Formula	$\text{H}_3\text{C}_6\text{N}_7(\text{NH}_2)_3(\text{HSO}_4)_3$
Formula weight / g mol^{-1}	512.44
Crystal system	monoclinic
Space group	$P2_1/n$ (no. 14)
Lattice parameters / $\text{\AA}, ^\circ$	$a = 10.277(2)$ $b = 14.921(3)$ $\beta = 99.24(3)$ $c = 11.771(2)$
Volume / \AA^3	1781.5(6)
Z	4
Diffractometer	IPDS
Radiation, monochromator	Mo- K_α ($\lambda = 71.073$ pm), graphite
Temperature / K	293
Structure solution	SHELXS-97 ^[101] (direct methods)
Structure refinement	SHELXL-97 ^[101] (full-matrix least-squares on F^2)
Corrections applied	Lorentz, polarization
Absorption coefficient / mm^{-1}	0.507
Calculated density / g cm^{-3}	1.911
Data / restraints / parameters	4087 / 0 / 328
R-indices	$R1 = 0.0614$ all data $R1 = 0.0371$ $F_o^2 > 2\sigma(F_o^2)$ (2894 reflections) $wR2 = 0.0904$ all data $wR2 = 0.0851$ $F_o^2 > 2\sigma(F_o^2)$
GooF	0.947
Weighting scheme	$w^{-1} = \sigma^2(F_o^2) + (0.0510P)^2$ where $P = (F_o^2 + 2F_c^2) / 3$
Largest peak / deepest hole / $e \text{\AA}^{-3}$	0.367 / -0.393

The $\text{H}_3\text{C}_6\text{N}_7(\text{NH}_2)_3^{3+}$ ions display three protonation sites at the cyameluric nucleus. As expected the protons avoid close proximity, resulting in an arrangement of C_{3h} symmetry (cf. Scheme 20, Figure 48). The bond lengths within the heptazine core are notably affected by protonation (cf. Table 17), as has already been observed for other melemium salts.^[36] Bonds are influenced in a way that can be visualized by assuming a slight preference for the resonance structure presented in Scheme 20. The C-N bonds to the amino groups are 2-3 pm shorter than the respective bonds in melem.



Scheme 20. Bond lengths observed for the melemium ions found in $\text{H}_3\text{C}_6\text{N}_7(\text{NH}_2)_3(\text{HSO}_4)_3$.

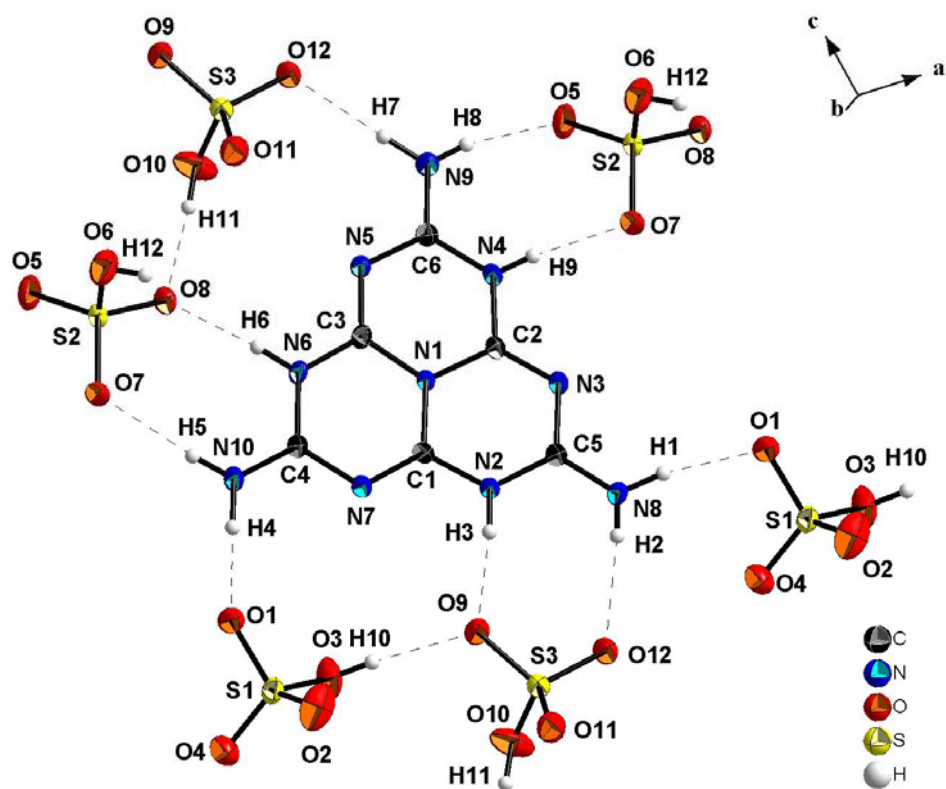


Figure 48. Molecular structure, H-bonding interactions and assignment of atom labels for $\text{H}_3\text{C}_6\text{N}_7(\text{NH}_2)_3(\text{HSO}_4)_3$. Ellipsoids for non-hydrogen atoms are drawn at the 50 % probability level.

The structure is stabilized by a multitude of H-bonding interactions. All possible NH and OH donors are involved in these interactions. $\text{H}_3\text{C}_6\text{N}_7(\text{NH}_2)_3^{3+}$ ions are not linked to each other (cf. Figure 48, Figure 49) by H-bonding interactions due to steric and electrostatic reasons. The presence of three protonation sites at the cyameluric nucleus greatly limits the possibilities to establish favorable H-bonding motifs involving several bonds and H-bonding would require close proximity of two ions with a high positive charge.

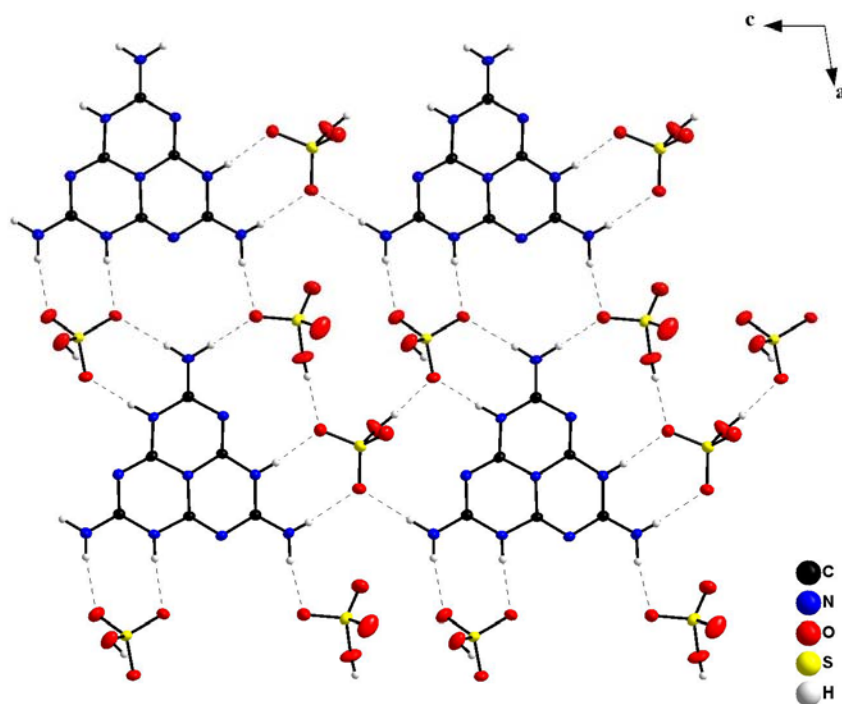


Figure 49. A H-bonded layer of melemium ions found in $\text{H}_3\text{C}_6\text{N}_7(\text{NH}_2)_3(\text{HSO}_4)_3$. View along b . Ellipsoids for non-hydrogen atoms are drawn at the 50 % probability level.

Layer-like H-bonded structures running perpendicular to b are assembled (cf. Figure 49) this way. The vast majority of H-bonds are located within the layers. Only some H-bonds are connecting two layers to each other forming a double-layer-like motif (cf. Figure 50.).

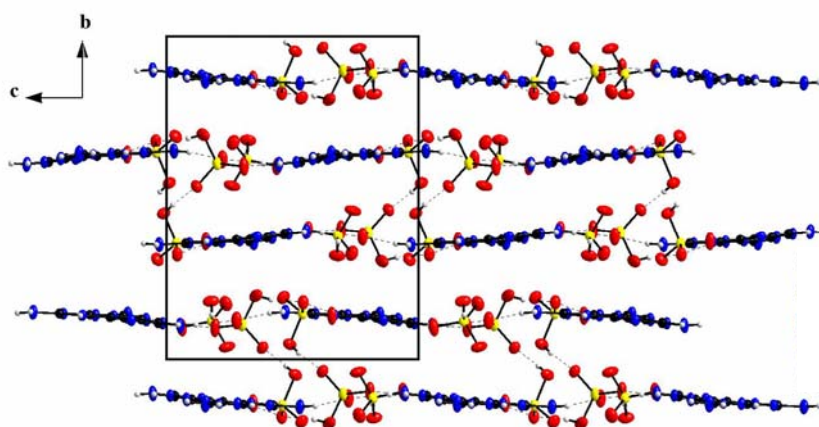


Figure 50. Double-layer-like stacking motif of melemium layers found in $\text{H}_3\text{C}_6\text{N}_7(\text{NH}_2)_3(\text{HSO}_4)_3$. View along a . Ellipsoids for non-hydrogen atoms are drawn at the 50 % probability level.

H-bonds in $\text{H}_3\text{C}_6\text{N}_7(\text{NH}_2)_3(\text{HSO}_4)_3$ have $\text{D}\cdots\text{A}$ distances ranging from 2.62 to 2.98 Å and $\text{D-H}\cdots\text{A}$ angles between 154 and 175°. Thus the average distances are notably shorter than the ones found for other melemium salts so far,^[36] allowing the conclusion that they also are comparably strong.

5.4 The Melemium Hydrogensulfate $\text{H}_3\text{C}_6\text{N}_7(\text{NH}_2)_3(\text{HSO}_4)_3$

Table 17. Selected distances (in Å) and angles (in °) for $\text{H}_3\text{C}_6\text{N}_7(\text{NH}_2)_3(\text{HSO}_4)_3$. Standard deviations in parentheses.

Distances				Angles			
C1-N7	1.294(3)	O1-S1	1.4629(18)	N7-C1-N2	120.6(2)	C1-N7-C4	117.08(19)
C1-N2	1.341(3)	O2-S1	1.425(2)	N7-C1-N1	123.48(19)	C5-N8-H1	121.5(18)
C1-N1	1.384(3)	O3-S1	1.5759(18)	N2-C1-N1	115.90(18)	C5-N8-H2	122(2)
C2-N3	1.290(3)	O3-H10	0.93(5)	N3-C2-N4	121.02(19)	H1-N8-H2	116(3)
C2-N4	1.350(3)	O4-S1	1.439(2)	N3-C2-N1	123.84(19)	C6-N9-H7	119.0(17)
C2-N1	1.391(3)	O5-S2	1.4322(17)	N4-C2-N1	115.14(18)	C6-N9-H8	120(2)
C3-N5	1.291(3)	O6-S2	1.536(2)	N5-C3-N6	120.93(18)	H7-N9-H8	120(3)
C3-N6	1.342(3)	O6-H12	0.81(4)	N5-C3-N1	123.56(19)	C4-N10-H4	121(2)
C3-N1	1.384(3)	O7-S2	1.4555(18)	N6-C3-N1	115.51(18)	C4-N10-H5	122.4(19)
C4-N10	1.299(3)	O8-S2	1.4673(17)	N10-C4-N7	118.9(2)	H4-N10-H5	116(3)
C4-N7	1.356(3)	O9-S3	1.4640(18)	N10-C4-N6	119.9(2)	S1-O3-H10	101(3)
C4-N6	1.367(3)	O10-S3	1.548(2)	N7-C4-N6	121.11(19)	S2-O6-H12	107(3)
C5-N8	1.291(3)	O10-H11	0.83(4)	N8-C5-N3	119.6(2)	S3-O10-H11	109(3)
C5-N3	1.353(3)	O11-S3	1.4450(19)	N8-C5-N2	119.1(2)	O2-S1-O4	115.87(14)
C5-N2	1.369(3)	O12-S3	1.4518(18)	N3-C5-N2	121.33(19)	O2-S1-O1	111.72(13)
C6-N9	1.302(3)	N8-H1	0.92(3)	N9-C6-N5	118.4(2)	O4-S1-O1	111.45(11)
C6-N5	1.350(3)	N8-H2	0.77(3)	N9-C6-N4	119.9(2)	O2-S1-O3	106.28(12)
C6-N4	1.369(3)	N9-H7	0.93(3)	N5-C6-N4	121.72(19)	O4-S1-O3	104.29(12)
N2-H3	0.81(3)	N9-H8	0.80(3)	C3-N1-C1	119.76(17)	O1-S1-O3	106.36(11)
N4-H9	0.81(3)	N10-H4	0.91(3)	C3-N1-C2	119.98(17)	O5-S2-O7	113.24(11)
N6-H6	0.86(3)	N10-H5	0.84(3)	C1-N1-C2	119.28(17)	O5-S2-O8	113.44(11)
				C1-N2-C5	122.38(19)	O7-S2-O8	109.77(10)
				C1-N2-H3	118(2)	O5-S2-O6	105.00(11)
				C5-N2-H3	120(2)	O7-S2-O6	107.56(13)
				C2-N3-C5	117.02(18)	O8-S2-O6	107.40(11)
				C2-N4-C6	122.18(18)	O11-S3-O12	114.24(11)
				C2-N4-H9	115(2)	O11-S3-O9	112.04(12)
				C6-N4-H9	123(2)	O12-S3-O9	111.43(11)
				C3-N5-C6	117.14(18)	O11-S3-O10	107.63(11)
				C3-N6-C4	122.54(18)	O12-S3-O10	105.18(13)
				C3-N6-H6	116.9(19)	O9-S3-O10	105.64(13)
				C4-N6-H6	120.4(19)		

Like it has already been the case in $\text{HC}_6\text{N}_7(\text{NH}_2)_3\text{H}_2\text{C}_6\text{N}_7(\text{NH}_2)_3(\text{SO}_3\text{Me})_3 \cdot \text{H}_2\text{O}$ and $\text{H}_2\text{C}_6\text{N}_7(\text{NH}_2)_3(\text{SO}_3\text{Me})$ (cf. Section 5.3) short distances between S=O moieties and carbon or nitrogen atoms within the cyameluric nucleus also were observed in $\text{H}_3\text{C}_6\text{N}_7(\text{NH}_2)_3(\text{HSO}_4)_3$. Especially the distances of the oxygen atom O2 to the atoms N1 (2.67 Å) and C2 (2.69 Å) are remarkably short (cf. Figure 48 for assignment). As could be shown by databank research such distances are, however, not unheard of.^[p] Some examples even display notably shorter atomic distances. Although comparable contacts were observed elsewhere (cf. Section 5.3), $\text{H}_3\text{C}_6\text{N}_7(\text{NH}_2)_3(\text{HSO}_4)_3$ shows the shortest such contacts yet found for melemium salts. The reason for this might be the that the $\text{H}_3\text{C}_6\text{N}_7(\text{NH}_2)_3^{3+}$ displays a higher positive charge, thus favoring interactions with negatively polarized oxygen atoms of sulfate.

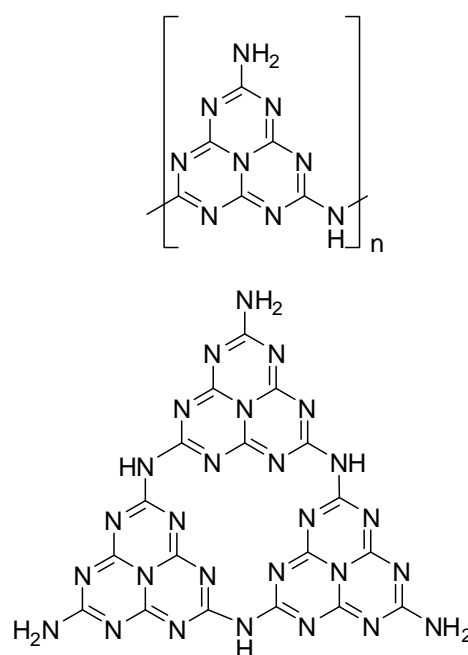
[p] Other compounds displaying short contacts between an S=O oxygen atom and a C-N bond could be identified. Examples are: CCDC 608134, CCDC 100391, CCDC 146348, CCDC 141245 and CSD 57371. Data was found using CCDC ConQuest v.1.11.

6. Melon

6.1 Introduction

The polymer melon has seen a long history of speculation concerning its composition, structure and properties (cf. Section 1.2). Some propositions are depicted in Scheme 21. Reliable in depth structural investigations have been conducted not before very recently. The 1D polymeric structure, $(C_6N_7(NH)(NH_2))_n$, of melon has been established by electron diffraction in conjunction with theoretical calculations and solid-state NMR.^[39] This structure is thus well established. The existence of polyheptazine imide,^[17] another compound found in addition to melon, however, shows that the 1D polymer is not the only structure possibly formed by condensed heptazines. Electron diffraction data has also shown the existence of several other crystalline phases in various samples of melon, which are yet to be elucidated.^[133] Thus, most samples of melon can barely be considered pure compounds but multi-component mixtures. Cyclic structures (cf. Scheme 21) have also been proposed, but remain unconfirmed as of now.

The paramount problem arising while investigating the structure(s) of melon hence is the ambiguity of most data gathered by standard-issue analytical methods. IR, PXRD, elemental analysis and routine MAS solid-state NMR often cannot distinguish between different structures. It is thus also most complicated to judge the number of different phases in a given sample of melon. The whole situation is rendered even more confusing by some other factors like the one that there are reports about different synthetic procedures for melon in the literature. Accordingly, various compounds have found use as starting material for the synthesis of melon so far. Many modern articles also refer to samples showing significant residual amounts of hydrogen (and thus most likely incorporating NH or NH₂ moieties) as g-C₃N₄ and not as melon. Such materials, however, usually show typical features of melon, like notable hydrogen content and N-H vibrations in IR, and can hence barely be considered binary compounds. In this work the expression melon will primarily be used for heptazine-based compounds of formula $C_6N_7(NH)(NH_2)$. Samples denoted as “melon” in the literature, however, will also be referred to as such for the sake of comparability. In such cases quotation marks will be used to indicate that the accordingly denoted substance is most likely not identical to the reported polymer $C_6N_7(NH)(NH_2)$ or that no reliable characterization is yet available.



Scheme 21. Two structural propositions for melon. The 1D heptazine-based polymer (top) has been identified by electron diffraction while cyclic structures (bottom) have not been validly established. Both depicted structures are consistent with the formula $C_6N_7(NH)(NH_2)$.

6.1 Introduction

Melon is an invaluable starting material allowing access to a wide range of heptazines (cf. Section 1.1). The following sections will describe synthetic and analytic aspects concerning melon as studied in this work. Special emphasis is placed on the comparison of the different synthesis procedures reported for melon and the analysis of products resulting from these conversions.

6.2 Synthesis by Condensation of Melamine



Figure 51. A typical sample of raw melon.

490 °C with a reaction time of several days. In accordance with other sources,^[74-78,108,153] melon is yielded as a yellow solid (cf. Figure 51). The compound is insoluble in any solvent. Solubility observed under very harsh condition like prolonged treatment with hot acids or bases is always due to decomposition (cf. Chapters 7, 9). Raw melon displays high thermal stability and can temporarily withstand temperatures up to 600 °C. No traces of melting or phase transitions could be detected prior to the decomposition by DTA/TG experiments (cf. Figure 52). This thermal stability is, however, only observed for limited durations of heat exposure. In open systems, preparative amounts of melon decompose after several weeks at temperatures of 500 °C or higher.

Elemental analysis of samples of raw melon shows good agreement with the composition of the idealized polymer. It has not been possible to significantly increase the condensation grade by heating at higher temperatures and/or prolonged reaction times (cf. Table 18). An increasing tendency towards total decomposition is observed instead. This decomposition, however, takes place rather slowly as was already mentioned in the preceding section.

In recent literature the condensation of melamine has probably become the most important synthetic route for accessing melon. For much of the synthetic work conducted as part of this thesis a substance which will, as follows, be referred to as “raw melon” was used. This is, however, not meant to say that “raw melon” discussed in this section is chemically identical with “raw” or “crude” melon mentioned elsewhere in the literature.^[q] Raw melon was usually prepared by heating melamine in a crucible loosely covered by a lid (cf. Section 12.1.13 for experimental details). The reaction was typically conducted at a temperature of

490 °C with a reaction time of several days. In accordance with other sources,^[74-78,108,153] melon is yielded as a yellow solid (cf. Figure 51). The compound is insoluble in any solvent. Solubility observed under very harsh condition like prolonged treatment with hot acids or bases is always due to decomposition (cf. Chapters 7, 9). Raw melon displays high thermal stability and can temporarily withstand temperatures up to 600 °C. No traces of melting or phase transitions could be detected prior to the decomposition by DTA/TG experiments (cf. Figure 52). This thermal stability is, however, only observed for limited durations of heat exposure. In open systems, preparative amounts of melon decompose after several weeks at temperatures of 500 °C or higher.

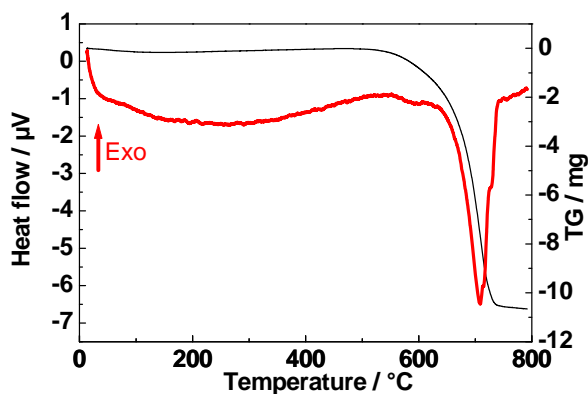


Figure 52. Thermal stability of a typical sample of raw melon measured by DTA/TG. Heat flow is drawn in red TG is drawn in black. Initial weight = 11.57 mg, scanning rate = 5 °C min⁻¹.

[q] Similar expressions are often found in the literature but refer to compounds prepared differently. *J. v. Liebig* has e.g. termed the residue of the calcination of ammonium thiocyanate “rohes Mellon” which would translate into “raw melon. The spelling “mellon” instead of melon was very common at that time.

6.2 Synthesis by Condensation of Melamine

Table 18. Elemental analysis (combustion) for typical samples of raw melon prepared by condensation of melamine.

	C / wt. %	N / wt. %	H / wt. /
melon prepared at 490 °C ^[a]	33.22	62.67	1.83
melon prepared at 550 °C ^[b]	33.55	62.44	1.85
calcd. for (C ₆ N ₇)NHNH ₂	35.83	62.67	1.50

- [a] Heated for 4 d;
[b] Heated for 6.5 d.

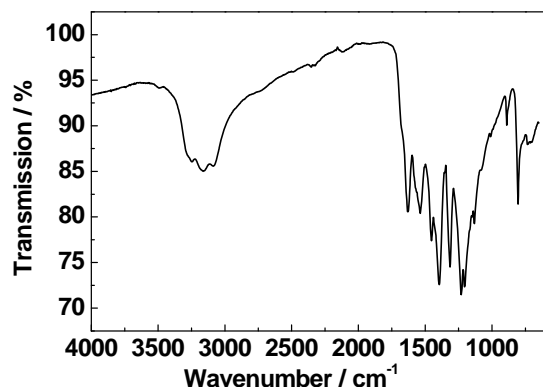


Figure 53. FTIR spectrum (ATR) of a typical sample of raw melon.

comparable experiments starting from pure melamine promoting the condensation at lower reaction temperatures. Typical reaction conditions involve heating to 490 °C for about one to two days (cf. Section 12.1.14).

FTIR spectroscopy was regularly conducted for samples of melon. The spectra display the typical absorption bands of melon in most cases (cf. Figure 53). Rather broad absorption bands corresponding to the N-H stretching vibrations are found between 3300 and 3000 cm⁻¹. A large variety of C-N vibrations are found between 1700 and 1100 cm⁻¹ and the characteristic vibration for C₃N₃ / C₆N₇ rings is observed around 810 cm⁻¹. Raw melon (cf. Figure 53) shows a spectrum identical to the ones of samples that had been annealed in the presence of NH₄Cl / melamine. In consequence, the method unfortunately is not capable of resolving any sort of fine structural differences as the spectra of all samples of melon prepared are virtually not discernable. The existing structural and chemical differences for different samples of melon prepared from melamine in this work hence are hardly substantial by nature.

The highly crystalline melon samples used for the structure elucidation of the polymer in the literature were prepared at reaction temperatures of up to 620 °C.^[39] Some experiments aiming to accomplish comparable crystallinity at lower reaction temperatures were conducted as part of this thesis. Very long reaction times were chosen based on the observations made for the melamine melem adduct phases (cf. Section 3.1). Raw melon was mixed with small amounts of melamine and/or NH₄Cl as to provide a certain ammonia pressure upon heating. Thus a certain amount of reversibility of the condensation reaction was assured favoring good crystal growth. The NH₃ pressure was, however much lower than for com-

Raw melon displays low overall crystallinity. Only a very broad reflection around $2\theta = 28^\circ$ can be observed. For the depicted sample of raw melon a value of 27.4° corresponding to a distance of 3.3 \AA was found. This can be used as a first rough estimation of the inter-layer distance. Upon heating with melamine / NH_4Cl the peak position has slightly shifted to 27.8° which is corresponding to an inter-layer distance of 3.2 \AA . This distance is identical to the one reported for melon prepared at higher temperatures.^[39,108] More importantly, however, the reflection is also significantly narrowed. The treatment of raw melon in glass ampoules can thus be definitively associated with the formation of a much more defined product and a notable increase in crystallinity. Nevertheless, high-temperature samples prepared from melamine have shown higher crystallinity than comparable samples prepared by annealing raw melon.

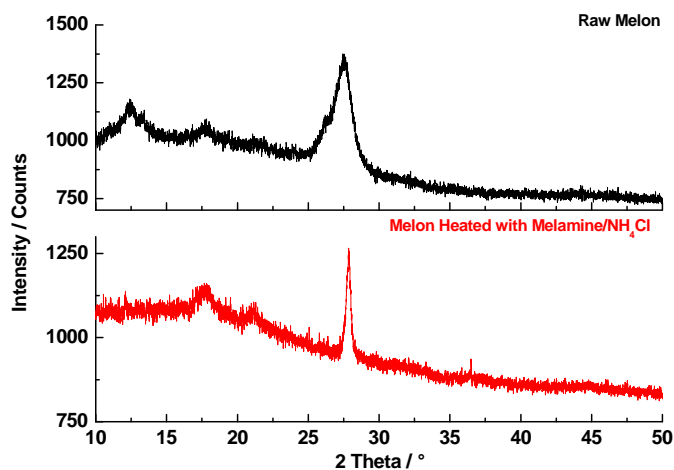


Figure 54. PXR D pattern (Cu-K_α radiation) of a typical sample of raw melon (black, top) in comparison to a fraction of raw melon subsequently heated with small amounts of melamine and ammonium chloride (bottom, red). A drastic decrease in FWHM of the reflection around 28° is observed.

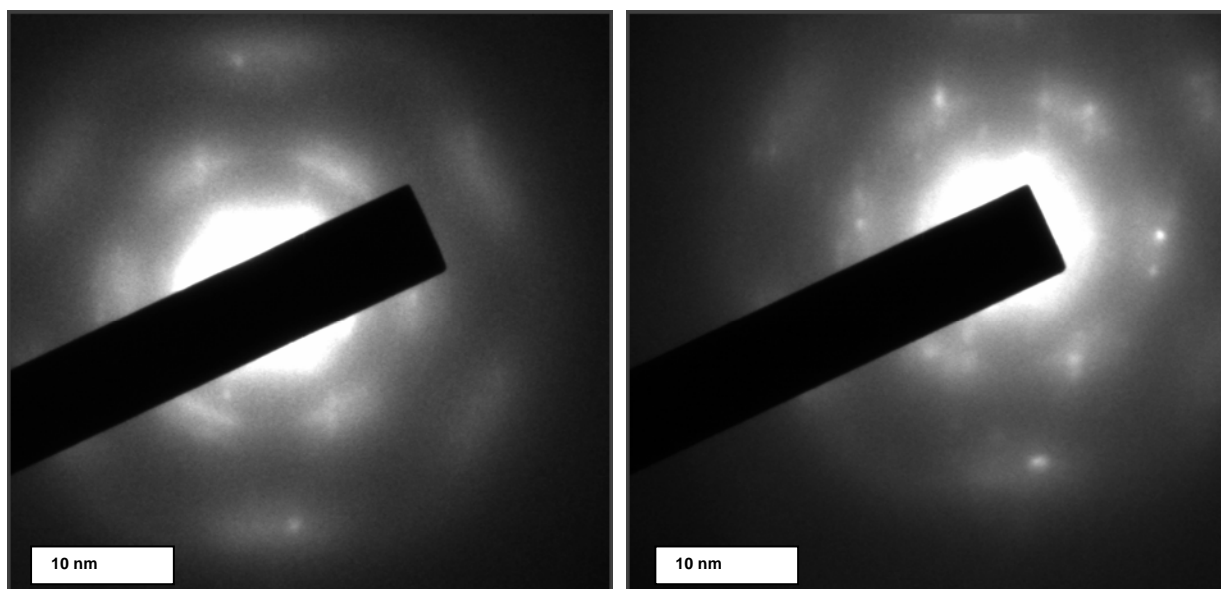


Figure 55. Typical electron diffraction patterns (200 kV) exhibiting a significant degree of disorder as observed for raw melon.

Electron crystallography has been proven as an invaluable instrument during structural investigations of melon^[39,108] and PHI.^[17] Electron diffraction and TEM investigations were employed to analyze samples of both raw and annealed melon. All samples of melon were

prepared in accordance to the statements made in the preceding paragraphs and in Sections 12.1.13 – 12.1.14. The measurements were conducted by Dr. *M. Döblinger* (LMU München). The data are compared in reference to the abovementioned preliminary investigations.^[17,39,108]

The ED experiments conducted for raw melon do not show a significant degree of well-crystalline material (cf. Figure 55). This is not surprising since a low overall crystallinity has also been found in powder XRD as is described above. A large amount of disordered regions are found (cf. Figure 55). A pseudo hexagonal pattern was usually observed in these cases. From a structural point of view, raw melon certainly is no pure compound. Amorphous regions are also regularly found. Good crystals displaying a non-disordered diffraction pattern are extremely rare but were sometimes observed nevertheless. Small amounts of a new well crystalline side phase were observed (cf. Figure 56). No definite statements concerning the nature of this compound can be made apart from not being identical with crystalline melon as reported in the literature

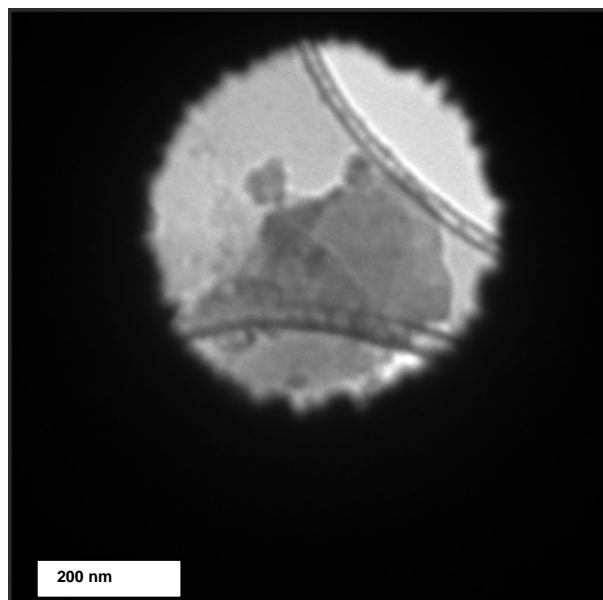
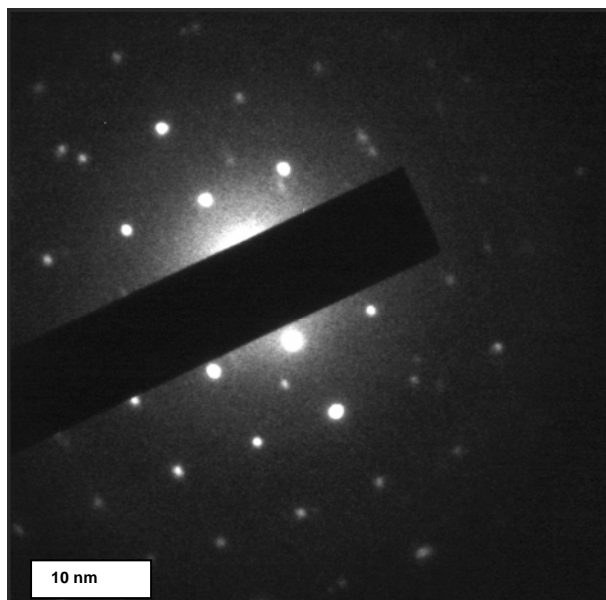


Figure 56. Typical electron diffraction pattern (200 kV) of an unknown crystalline side phase observed in a sample of raw melon.

Figure 57. TEM image of raw melon after preparation for electron diffraction (copper grid).

TEM images (cf. Figure 57) reveal some hints at crystalline structures as well as some resemblance to the platelets already observed for melon in the literature.^[39,108] This finding is, however, not sufficient in order to draw further structural conclusions. The annealed melon sample showed a much more defined morphology and platelet-like structures are typically observed (cf. Figure 58).

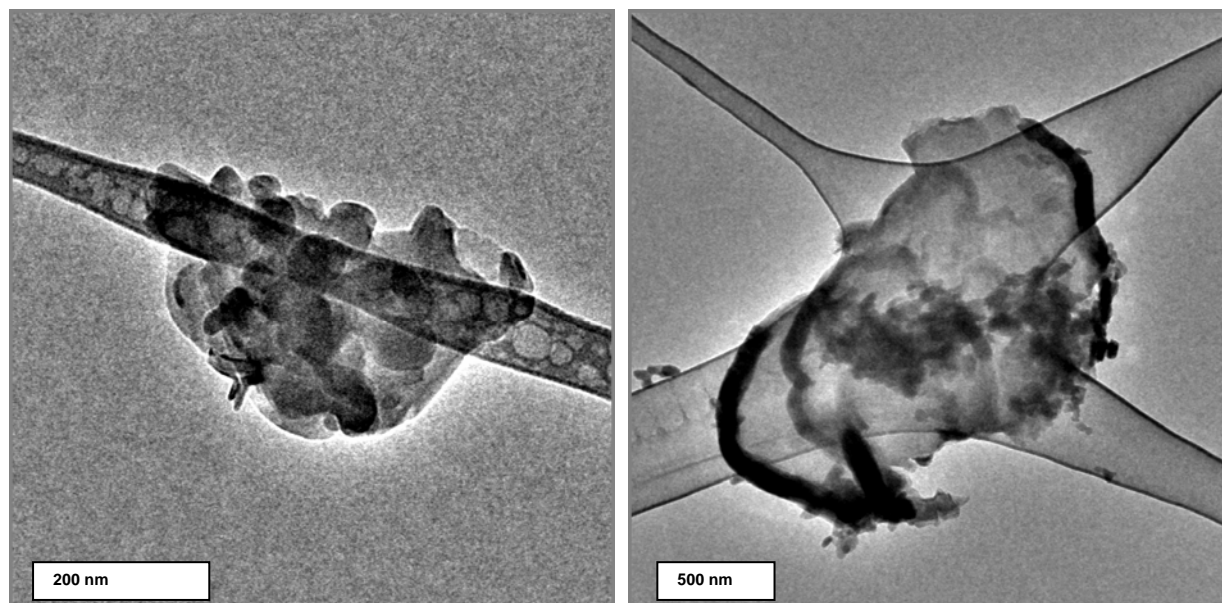


Figure 58. TEM images of a sample of melon after preparation for electron diffraction (copper grid). Platelet-like nanostructures can be observed.

Electron diffraction patterns (cf. Figure 59) usually match the expectations for the reported structure of melon. Various degrees of disorder could be observed for the studied sample, revealing amorphous as well as crystalline regions. In agreement to the results already obtained by powder XRD the overall crystallinity of the sample is, however significantly higher than is the one of raw melon. No hints at the new side phase previously observed during the study of raw melon were found in the annealed sample. Poly heptazine imide (PHI) was also not observed. Thus it can be rationalized that a low temperature synthesis of PHI from mixtures of melamine and raw melon is probably not a very promising approach. Improved synthetic procedures for this compound thus still remain to be devised.

Judging from its chemical reactivity and simple spectroscopic properties raw melon certainly is a heptazine-based polymer showing some resemblance with reported crystalline melon. Raw melon must be considered a highly disordered version of the melon reported by *Lotsch et al.*^[39,108] Especially turbostratic disorder of the H-bonded layers can probably be expected. This is consistent with the findings from powder XRD, indicating a slight increase in inter-layer distance, and the fact that the IR spectrum remains virtually identical for all different forms of melon. A significant change in H-bonding interactions would presumably have resulted in a noticeable effect on some absorption bands, the presence of similar H-bonded layers seems plausible. The highly crystalline melon prepared by annealing raw melon with melamine and / or NH_4Cl is structurally identical to the melon reported in the literature as could be shown by ED. The behavior of raw melon upon annealing shows that the linear polymer melon, displaying its reported structure,^[39,108] probably is another favorable thermodynamic sink. This can in a way be considered similar to the findings concerning melamine or melem, which are also regularly favored under equilibrium conditions. Another interesting finding is, that the annealed melon samples usually only show a slight yellow color, actually much less intense than the one observed for raw melon. Thus the coloring of melon probably is owed to defect sites and beginning carbonization to a much higher degree than it is to the properties of the actual (idealized) polymer itself.

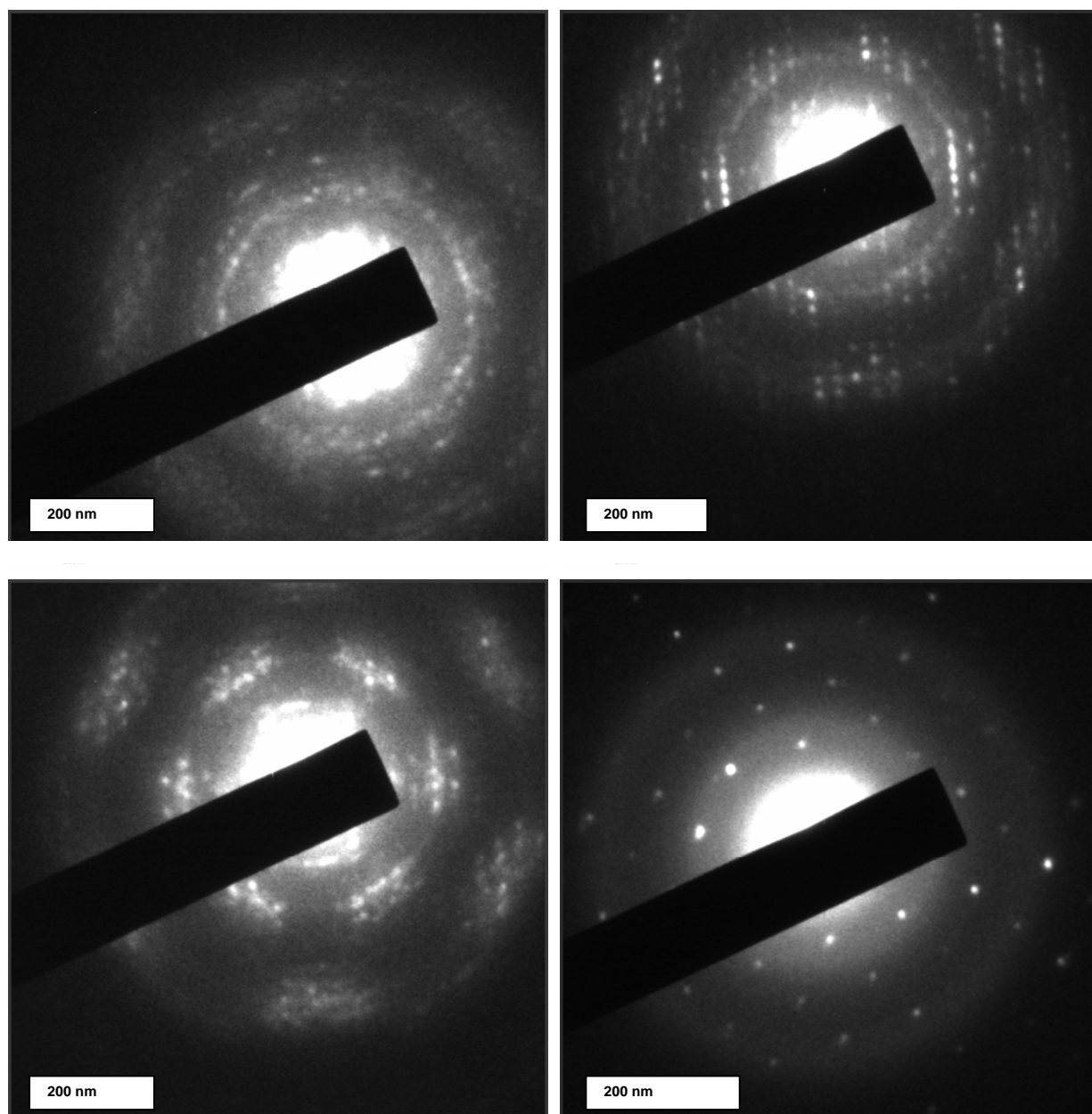
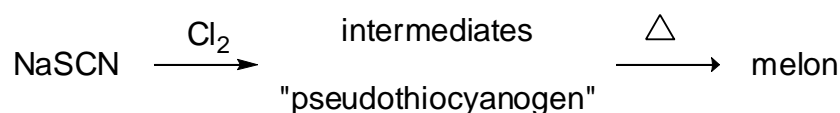


Figure 59. Exemplary ED patterns (200 kV) observed for a sample of melon heated with melamine / NH_4Cl .

6.3 Synthesis by Reaction of NaSCN with Chlorine

If chlorine gas is passed through an aqueous solution of sodium thiocyanate, a large amount of a voluminous precipitate is formed. The pyrolysis of this compound has been reported a source of melon. The first descriptions of this reaction route dates back well to the mid 19th century.^[80] It was particularly valuable during the 19th and early 20th century, before cheap melamine was commonly available. However, it is still used as a source of melon in contemporary works as well. Melon thus yielded is usually used for the preparation of other, heptazine-containing molecules like cyameluric acid. Due to the frequent employment of this reaction it is beyond doubt that a heptazine containing polymer is actually yielded by this reaction. In order to allow a comparison of this product with the raw melon described in the preceding section and other types of melon reported elsewhere the reaction was reproduced in accordance to literature procedures.^[148] Usually the reaction is explained by assuming that the precipitate initially yielded is the actual precursor. It is isolated from the solution, dried and transformed into melon upon further heating.



Scheme 22. The transformation of sodium thiocyanate into melon.

While repeating the reaction (cf. Section 12.1.15 for experimental details) the following observations were made. The color of the resulting precipitate gradually changes during the course of the reaction. Initially it is of a dark orange color (cf. Figure 60) which gradually shifts toward a bright yellow, observed for the last fractions of precipitate. The resulting product is insoluble in water and not notably affected by exposure to air. It must be well dried since it incorporates significant amounts of residual moisture.

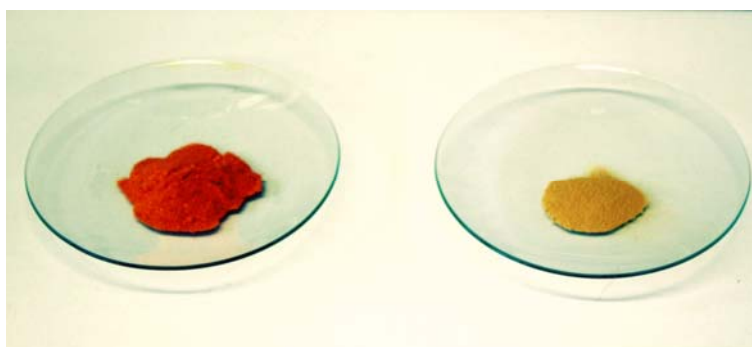


Figure 60. So-called “pseudothiocyanogen” (left) and “melon” prepared by pyrolysis of this compound (right).

The precipitate (often referred to as “pseudothiocyanogen” in the literature) is probably no pure compound. It is described as a “crude mixture composed of isoperthiocyanic acid, kanarine and various polymers of isoperthiocyanic acid”.^[148] This claim was, however, not supported by any form of analysis or further references.

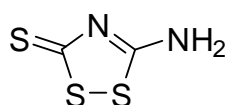


Figure 61. Molecular structure of isoperthiocyanic acid.

Isoperthiocyanic acid was first mentioned by *Wöhler* in the early 18th century,^[134] the correct molecular structure, a five-membered heterocyclic compound (cf. Figure 61), was assigned no sooner than in the 1960s.^[135] Kanarine was mentioned in some early 19th century literature as a compound of formula

6.2 Synthesis by Condensation of Melamine

$C_8H_6ON_8S_7$.^[136] No recent literature is found for the compound nor is there any established molecular formula or structure. The compound was not found in the CAS database. Thus this assumption on the nature of the precipitate has to be regarded with some reservation.

Table 19. Elemental analysis (combustion) for the precipitate yielded by the reaction of NaSCN with chlorine.

	C / wt. %	H / wt. %	N / wt. %	S / wt. %
found (sample 1)	19.99	0.80	24.78	52.15
found (sample 2)	19.86	0.96	24.79	53.21
calcd. for $C_2H_2NS_3$ ^[a]	15.99	1.34	18.65	64.03
calcd. for $C_8H_6ON_8S_7$ ^[b]	21.13	1.33	24.65	49.37

[a] Isoperthiocyanic acid;

[b] Kanarine.

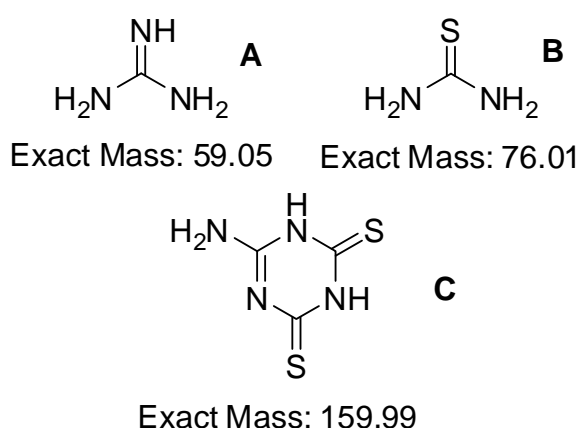


Figure 62. Molecular formula and exact mass of guanidine (upper left, A), thiourea (upper right, B) and dithioammeline (bottom, C).

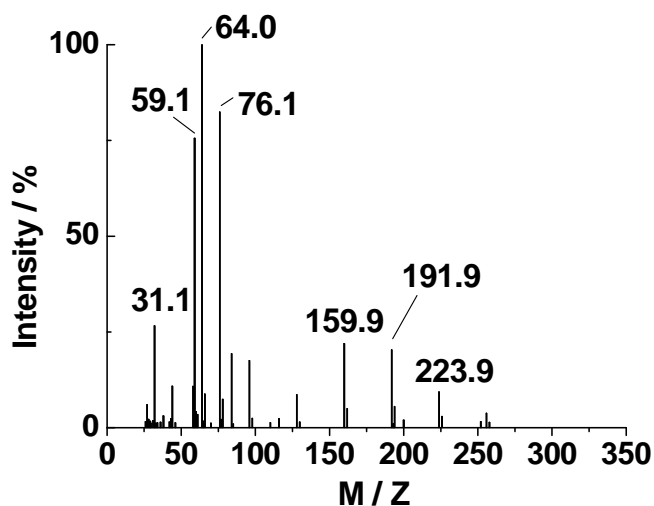


Figure 63. Mass spectrum (DEI⁺) of a sample of the precipitate yielded by the reaction of NaSCN with chlorine.

The elemental analysis (C/H/N/S, cf. Table 19) of the precipitate shows some slight resemblance to the formula of claimed kanarine. However, since the very existence of this compound must be subject to doubt and the reported formula was not unequivocally established, the mentioned similarities can accordingly not be considered very meaningful. The results reveal that the composition of the precipitate is well reproducible and that significant amounts of sulfur are still present. Small impurities of Na, O or Cl are probably incorporated as well. The sum of weights for the CHNS analysis is around 98 %, thus any substantial presence of these elements is rather unlikely. As to further investigate the presence of the reported molecules, mass spectrometric investigations were conducted. These experiments have found no indication supporting the presence of either isoperthiocyanic acid ($M/Z = 149.9$) as well as a molecule matching the formula of claimed kanarine ($M/Z = 453.9$). The occurrence of these compounds in the precipitate in molecular form can resultantly be considered most

unlikely. Some sort of polymeric species might, however, be possible. A large variety of signals was found. No reasonable assignment for most of the observed intensities was possible,

as yet, without resorting to speculation. The most plausible fragments are guanidine ($M/Z = 59.1$) and thiourea ($M/Z = 76.1$). Another signal at $M/Z = 159.9$ is probably best explained by dithioammelid (cf. Figure 62, Figure 63 and Table 20 for assignments). The remainder of peaks could not be identified. Most, if not all, peaks must be considered fragments originating from the beginning (thermal) decomposition of the precipitate. This is since especially the small fragments assigned cannot be part of the initial precipitate. Because of their comparably good solubility they would certainly have been removed during washing if they had precipitated at all.

Table 20. Select intensities from the mass spectrum (DEI^+) of a sample of the precipitate yielded by the reaction of NaSCN with chlorine.

M / Z	normalized intensity	assignment	M / Z	normalized intensity	assignment
32.0	27		96.0	18	
59.1	76	guanidine	159.9	22	dithioammelid
64.0	100		191.9	20	
76.0	82	thiourea	223.9	9	
84.0	19		255.8	4	

Neither the initial precipitate nor the resulting “melon” was yielded in crystalline form. Powder XRD of “pseudothiocyanogen” only shows a very broad reflection at $2\theta = 25.7^\circ$ and some small reflections originating from residual NaCl. The pyrolysis product appears totally amorphous. The reflection around $2\theta = 28^\circ$ observed for samples of melon prepared from melamine was not found in the pyrolysis product hence proving that the two products, though both referred to as melon, are definitively not identical.

Elemental analysis (cf. Table 21) shows the pyrolysis product still containing significant amounts of sulfur. It was not possible to produce sulfur-free “melon” samples from “pseudothiocyanogen”. Whether the sulfur is due to impurities or incorporated into the possible heptazine network remains to be resolved.

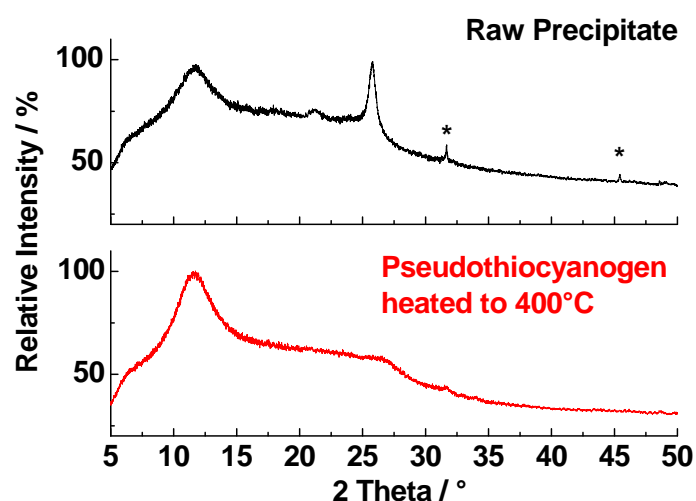


Figure 64. PXRD patterns ($Cu-K_{\alpha 1}$ radiation) for the precipitate of so-called “pseudothiocyanogen” (top, black) and its pyrolysis product at $400^\circ C$ (bottom, red). Side-phase reflections originating from NaCl are marked with *.

6.2 Synthesis by Condensation of Melamine

Table 21. Elemental analysis (combustion) for “melon” prepared by pyrolysis of “pseudothiocyanogen”.

	C / wt. %	H / wt. %	N / wt. %	S / wt. %
found sample heated to 400 °C	28.36	2.37	50.69	10.56
calcd. for C ₆ N ₇ NHNH ₂ ^[a]	35.83	1.50	62.67	0

[a] Formula of melon.

The IR spectrum of the precipitate (cf. Figure 65) is dominated by an intense absorption at 1216 cm⁻¹. Several other signals are also observed. There is a very broad peak at 3050 cm⁻¹ probably related to stretching vibrations involving hydrogen. Many absorption bands are not well resolved supporting the assumption that “pseudothiocyanogen” is not a pure molecular compound but either polymeric or a mixture of several compounds.

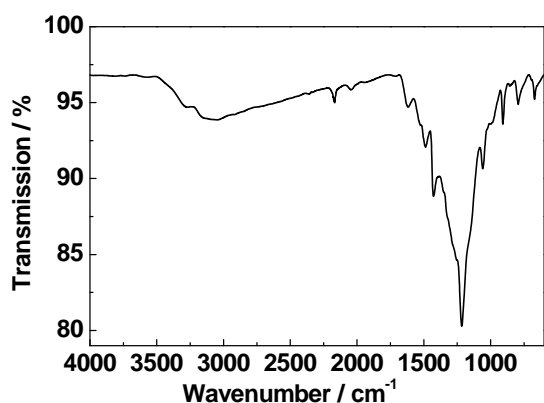


Figure 65. FTIR spectrum (ATR) of the precipitate formed by reaction of NaSCN with chlorine (so-called “pseudothiocyanogen”).

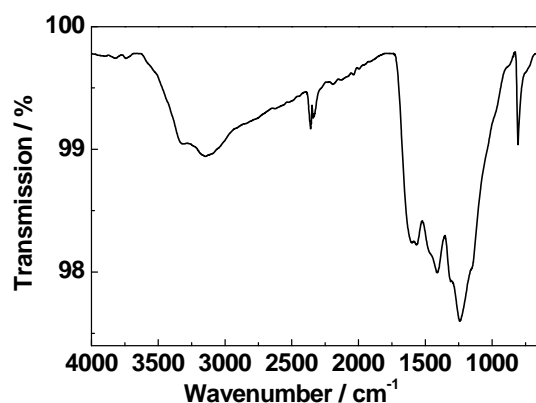


Figure 66. FTIR spectrum (ATR) of “melon” as yielded by the pyrolysis of the precipitate.

Upon heating of the precipitate (cf. Figure 67) a significant weight loss beginning around 200 °C is observed. A plateau is reached between 400 and 500 °C. At higher temperatures total decomposition occurs. The samples show less thermal stability than does melon prepared by thermal decomposition of melamine (cf. Figure 52). This finding is analog with observations made while heating bulk samples of the precipitate. A weight loss of approximately 60 % was observed after 2 h at 400 °C. The resulting solid product had the color of yellow ochre. The pyrolysis product (cf. Figure 66) is apparently not identical with melon prepared from melamine as has been discussed in Section 6.2 (cf. Figure 53). There, however, are some similarities. The broad signals observed between 1600 and 1200 cm⁻¹ (1567, 1411 and 1245 cm⁻¹) are within a typical range for C/N networks. The sharp absorption band at 805 cm⁻¹ is usually observed for systems featuring C₃N₃ motifs like heptazines or triazines. The two signals found at 2359 and 2340 cm⁻¹ might perhaps be related to C≡N triple-bonds.

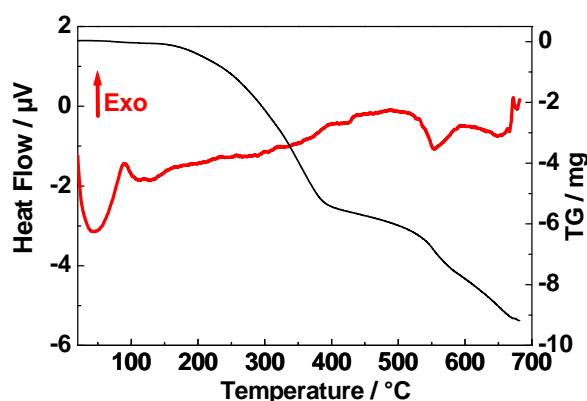


Figure 67. DTA/TG diagram for the precipitate yielded by the reaction of NaSCN with chlorine. Heat flow is drawn in red, TG is drawn in black. Thermogram was measured at a scanning rate of 10 °C min⁻¹; initial weight = 9.8 mg.

The observed notable differences regarding properties indicate that “melon”, as prepared in this section, is not completely identical to melon prepared from melamine. Its reported chemical reactivity in conjugation with the undeniably analytic similarities, however, give prove for a description as some form of mostly analog network structure. The best explanation at the moment seems to be the one as a less defined form of melon probably featuring more defect sites, disorder etc. in comparison to melon prepared from melamine.

6.4 The Pharaoh's Serpents – “Melon“ by Pyrolysis of $\text{Hg}(\text{SCN})_2$

Upon heating mercury(II) thiocyanate voluminous serpent-like structures are formed (cf. Figure 68). This bizarre pyrolysis constituted the first reported synthesis of melon (cf. Chapter 1). Although this finding is widely known very little effort was placed in the investigation of the reactivity of such mercury-containing carbon nitride precursor compounds. A central question in this context is whether or not melon is really yielded by this reaction. Many older (19th century) publications mention that $\text{Hg}(\text{SCN})_2$ yields rather impure melon. Accordingly, this method for preparing melon was of subordinate preparative interest during the 19th century and was virtually never exercised for this purpose during the 20th century.^[r] Hence a reinvestigation of the material of the Pharaoh's serpents, taking current results into account and utilizing modern analytical methods is definitively worthwhile. Recent investigations have revealed several different C/N polymers. Due to the analytic limitations of the time such differences in structure could well have been overlooked during preliminary works.



Figure 68. The Pharaoh's serpents as yielded after ignition of $\text{Hg}(\text{SCN})_2$ (left) and the ground and purified serpents (right).

Experimental details are given in Section 12.1.16. Once initiated, the obviously exothermic thermal decomposition proceeds until all $\text{Hg}(\text{SCN})_2$ is consumed. Small residual amounts of unreacted $\text{Hg}(\text{SCN})_2$ are however regularly observed in the raw product. The “serpents” appear yellow on the outside while their interior is black. Analysis by powder XRD shows that the black color is due to the presence of substantial amounts of black HgS (metacinnabar). The evaporation of large amounts of Hg metal often claimed to occur for the reaction was not observed in experiments conducted as part of this thesis. Respective observations can most likely be related to the common use of impure (i.e. initially containing significant amounts of elemental Hg) mercury thiocyanate samples for 19th century presentations.

Usually melon was considered the yellow part of the serpents that could be liberated from HgS by heating. No thermal analysis could be conducted due to the deteriorating effect of mercury-containing compounds on the DTA rod. Thus, only observations made upon heating samples of the “serpents” to select temperatures can be reported.

[r] The widespread use of this experiment for entertainment is no contradiction to this. Since little to no real interest into the chemical nature of the resulting product(s) was usually associated with these experiments they did not provide any real scientific advances. Most later experiments have also found some sort of less toxic substitute for $\text{Hg}(\text{SCN})_2$ and are thus based on totally different reactions.

The PXRD pattern of the initial pyrolysis products (cf. Figure 69) displays only the reflections expected for metacinnabar.^[137] Heating to temperatures up to 300 °C did not show any noticeable alteration of the product even after days of treatment. Prolonged (12 h or more) heating at 400 °C under air in open reaction vessels resulted in a significant loss of substance. The residual yellow solid optically resembles samples of melon prepared from melamine. The product is of extremely low density and easily dispersed by even the slightest air draft. Hence it was not possible to give any exact numbers on the weight loss as the loss by the actual reaction cannot be separated

from weight loss caused by convection flows, opening the crucible, transferring the product to the balance etc. However, more than 90 % of the weight is probably lost during the course of the reaction to give a rough estimate. Powder XRD (cf. Figure 69) shows the product is definitely is not identical with the usually observed form of melon (cf. Figure 54, Section 6.2). A truly crystalline product is formed although pyrolysis conditions in this open system are not reversible and thus anything but ideal for crystallization. The observed reflections were not present in the initial “serpents” nor could they be related to some common decomposition / conversion product of black HgS like red HgS (cinnabar) or HgO. It is thus evident that the pyrolysis of the “Pharaoh’s serpents” is more than a purification step that is merely removing HgS in a roasting reaction (cf. Equations 6.1, 6.2). Although the depicted reactivity probably also takes place in addition to other reactions.

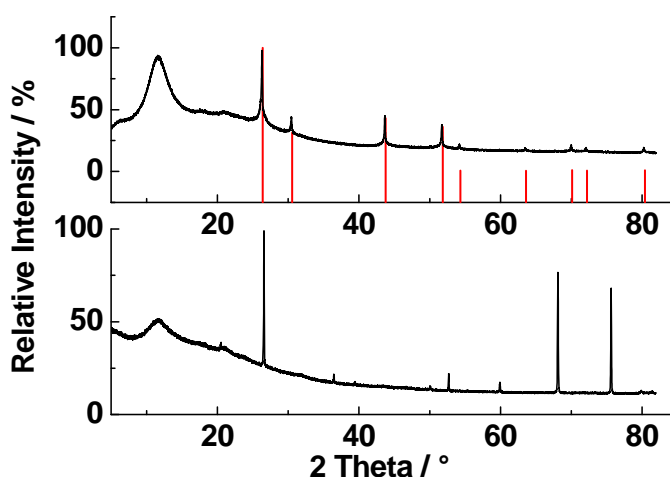
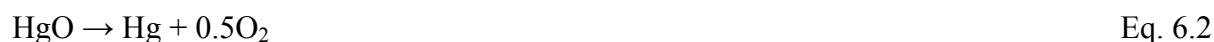


Figure 69. PXRD patterns (Cu-K α_1 radiation) for the “Pharaoh’s serpents” as yielded by the pyrolysis of Hg(SCN)₂ (bottom) as well as for the yellow product formed upon heating of the raw “serpents” (top). Red columns indicate lit. values for metacinnabar.



FTIR spectroscopy of the samples was conducted. Vibrational spectroscopy (cf. Figure 70) shows that the initial residue is almost free of vibrations involving hydrogen (like N-H vibrations). $\text{Hg}(\text{SCN})_2$ does not contain hydrogen, so finding shows that the product does not significantly react with moisture. Washing with water also does not alter the observed spectrum. Between 1600 and 1200 cm^{-1} several signals are observed and another absorption band is found at 797 cm^{-1} . This is altogether consistent with the expectations for a C/N network.

FTIR spectroscopy of the yellow residue (cf. Figure 71) shows some slight resemblance to melon (cf. Figure 53) or other C/N/H polymers. However, the product shows distinct and characteristic differences and certainly is not identical with melon as discussed in Section 6.2. Most interestingly the spectrum of “melon” prepared from $\text{Hg}(\text{SCN})_2$ is almost identical to one of melon prepared from heating the so-called “pseudothiocyanogen” (cf. Figure 66, Section 6.3). There clearly is intensity in the range expected for N-H vibrations indicating that some degree of uptake of hydrogen has taken place. The reaction with air moisture offers the most plausible explanation for this finding. Absorption bands at 2358 and 2337 cm^{-1} might point towards the presence of $\text{C}\equiv\text{N}$ bonds in the product. The three bands observed at 1612, 1429 and 1325 cm^{-1} in conjunction to the one found of 796 cm^{-1} are within typical ranges for C/N networks. Although the observed spectra of the initial serpents (cf. Figure 70) and the “melon” prepared by pyrolysis of them (cf. Figure 71) are rather similar there also are distinct differences.

Elemental analysis for mercury and sulfur contents was carried out by ICP-AES for all samples (cf. Table 22). As mercury-containing samples could not be analyzed by the available elemental analyzer, only the final (mercury-free) pyrolysis product was studied by C/N/H analysis.

Table 22. Elemental analysis for various samples associated with the pyrolysis of $\text{Hg}(\text{SCN})_2$.

	ICP-AES		Combustion		
	Hg / wt. %	S / wt. %	C / wt. %	N / wt. %	H / wt. %
raw “serpents”	64	12.5			
washed and dried product	61	12.5		not analyzed ^[a]	
heated to 400 °C	0.3	0.9 ^[b]	45.40	27.19	3.12

[a] Impossible due to device specifications;

[b] Combustion analysis offered a sulfur content of 2.48 %.

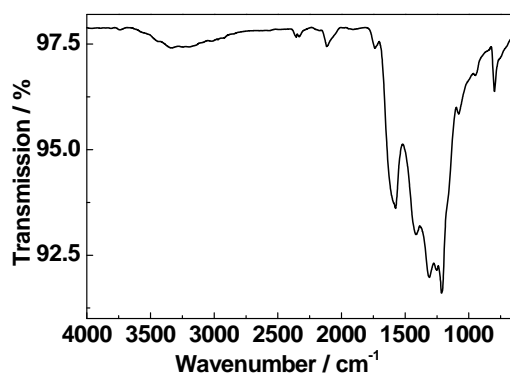


Figure 70. FTIR spectrum (ATR) of the Pharaoh's serpents as yielded after the ignition of $\text{Hg}(\text{SCN})_2$.

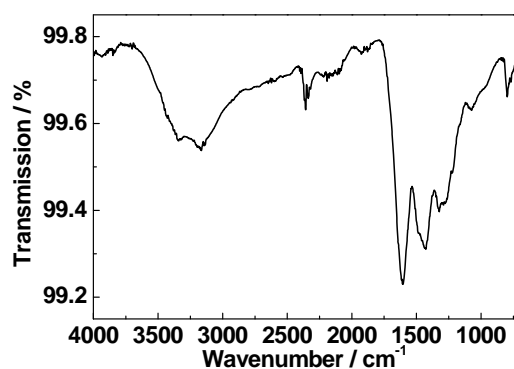


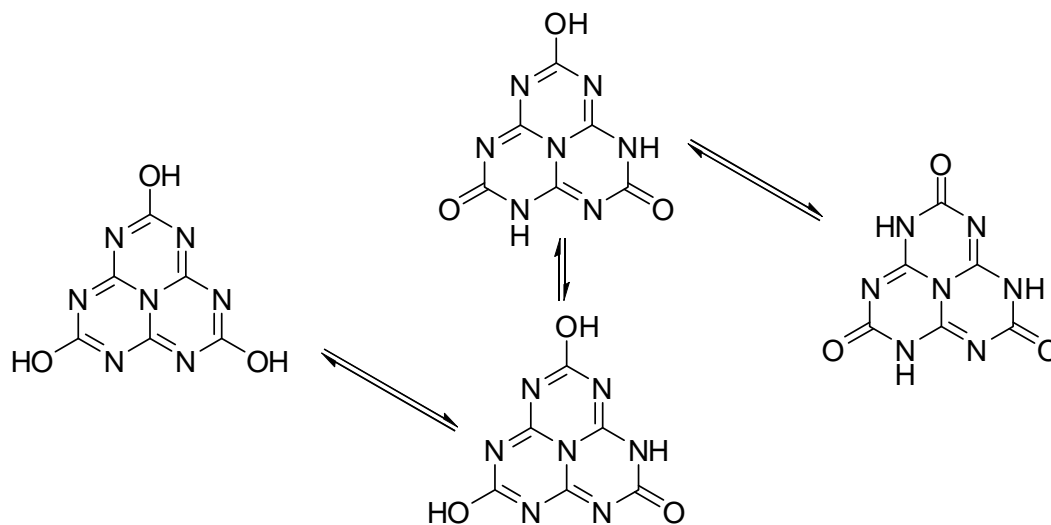
Figure 71. FTIR spectrum (ATR) of the pyrolysis product of $\text{Hg}(\text{SCN})_2$ at 400 °C.

In agreement to the XRD investigations (cf. Figure 69), the initial heterogeneous residue remaining after ignition of $\text{Hg}(\text{SCN})_2$ contains substantial amounts of mercury and sulfur. The mercury content in relation to the sulfur content is slightly higher than would be expected for only assuming the presence of HgS . Some sort of Hg-containing C/N network could possibly explain this discrepancy. The final yellow reaction product does not show any notable mercury content (the measured values are in a region no longer allowing reliable detection of Hg and are thus insignificant). Notable amounts of iron (5 %) and sodium (2 %) were also detected in the pyrolysis product. This might be explained by the accumulation of small temperature stable impurities due to the large weight loss. Notable amounts of sulfur also retain in the product. The sum of all percentages measured only accounts for 85 % hence a significant amount of oxygen is probably also present in the product.

7. Cyameluric Acid and its Salts

7.1 Introduction

Cyameluric acid, $C_6N_7O_3H_3$, a key molecule for heptazine chemistry referring to which *Pauling* coined the expression cyameluric nucleus,^[9] will be addressed in detail in the following. Although the compound has initially been described in the 19th century, complete structural characterization was not achieved before 2006 (cf. Section 1.2). Especially the questions concerning proton localization remained unclear even long after the basic structure of the cyameluric nucleus had been correctly proposed.^[9] The formula presented in the introduction (cf. Scheme 7) has anticipated the results presented in this section. One can assume several possible tautomeres for cyameluric acid. However, not all of them can be considered equally feasible. Especially the ones featuring an accumulation of protonation sites at close proximity do not seem very likely to occur. The tautomerism of cyameluric acid can be regarded as a variant of the common keto–enol tautomerism. The two most plausible variants are depicted in Scheme 23.



Scheme 23. Tautomerism of cyameluric acid. Hydroxy form (left) and keto form (right) are depicted. Some possible mixed intermediates are displayed (middle). Other conceivable tautomeres are omitted for clarity.

The paper by *Pauling* et al. presenting the concept of the cyameluric nucleus depicts cyameluric acid as a triol (left) without discussing the relative stability of different tautomers.^[9] The question which tautomer is actually realized for cyameluric acid was first brought up by *Finkel'shtein* et al., who proposed an all hydroxy structure based primarily on their spectroscopic investigations.^[89] Cyanuric acid was studied by single-crystal XRD comparably early showing a preference for the keto tautomer.^[138,139] Simply stressing the analogies existing for both compounds, however, does not provide sufficient argumentative value as to justify further claims. The basicity of heptazines is significantly lower than the one of triazines thus rendering a protonation of the cyameluric nucleus less favorable than one of the cyanuric nucleus. As structural investigations by single-crystal XRD could provide clarity in this issue cyameluric acid and some of its salts were investigated as will be shown in the following. Preliminary to the presented works only alkali metal cyamelurates (Li – Cs) had been thor-

oughly characterized.^[42] Respectively there was much room for investigations regarding the actual structure of cyameluric acid and its salts.

It should be added, that the investigations of cyameluric acid^[41,43] and some other cyameluric acid derivatives^[42,44,54] carried out almost simultaneously to the present work by *Kroke* et al. are in line with the data presented in the following.

7.2 Cyameluric Acid Trihydrate $\text{H}_3\text{C}_6\text{N}_7\text{O}_3 \cdot 3\text{H}_2\text{O}$

7.2.1 General Aspects and Synthesis

The contents of Section 7.2 have been published in advance to this thesis.^[40] The labeling of atoms is in accordance to the statements made in the general introduction. Nomenclature used for chemically equivalent atoms is depicted in Figure 72. Cyameluric acid used in all this work was usually prepared by hydrolysis of the polymer melon with aqueous sodium hydroxide. The resulting sodium cyamelurate was transferred into cyameluric acid by acidification with HCl. Exemplary reaction conditions are shown in Scheme 24. Further details are given in Section 12.1.17. The synthesis of well crystalline samples suitable for XRD on the one hand and bulk material have different requirements. Thus different reaction protocols are given in the respective section. Alternatively, cyameluric acid can be prepared by hydrolysis starting from melon or melonate salts in a comparable fashion. These reactions can be conducted with slightly reduced reaction times but do not show any significant synthetic advantage otherwise. Since the synthesis of melon or even melonates requires additional purification / reaction steps, such reaction routes were not usually chosen during this thesis.

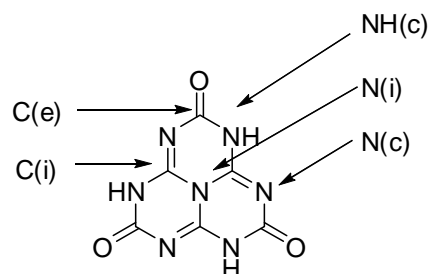
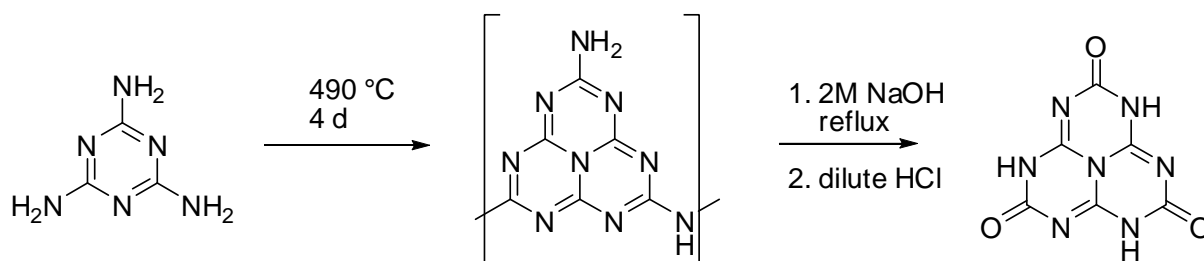


Figure 72. Formula and labeling of chemically equivalent atoms for cyameluric acid.



Scheme 24. Typical synthesis conditions for cyameluric acid. Reaction is starting from melamine.

7.2.2 Crystal Structure of $\text{H}_3\text{C}_6\text{N}_7\text{O}_3 \cdot 3\text{H}_2\text{O}$

Cyameluric acid crystallized from a slightly acidic aqueous solution forming a tri-hydrate of formula $\text{H}_3(\text{C}_6\text{N}_7\text{O}_3) \cdot 3\text{H}_2\text{O}$ (cf. Section 12.1.17 for experimental details). The structure of this compound could be solved and refined using the monoclinic space group *Cc* (cf. Table 23).

Table 23. Crystallographic data and details for the structure refinement of $\text{H}_3(\text{C}_6\text{N}_7\text{O}_3) \cdot 3\text{H}_2\text{O}$.

Formula	$\text{H}_3(\text{C}_6\text{N}_7\text{O}_3) \cdot 3\text{H}_2\text{O}$
Formula weight / g mol^{-1}	275.20
Crystal system	monoclinic
Space group	<i>Cc</i> (no. 9)
Lattice parameters / $\text{Å}, ^\circ$	$a = 15.5221(2)$ $b = 20.1089(3)$ $\beta = 102.1066(8)$ $c = 13.8533(2)$
Volume / Å^3	4227.89(10)
Z	16
Diffractometer	Kappa-CCD
Radiation, monochromator	Mo-K α ($\lambda = 71.073$ pm), graphite
Temperature	200(2)
Structure solution	SIR97 ^[102] (direct methods)
Structure refinement	SHELXL-97 ^[101] (full-matrix least-squares on F^2)
Corrections	SCALEPACK, ^[96] extinction, Lorentz, polarization
Extinction coefficient	0.0019(2)
Calcd. Density / g cm^{-3}	1.729
Flack-parameter	0.3(6)
Data / restraints / parameters	9224 / 26 / 818
R-indices	$R1 = 0.0396$ ($F_o > 4\sigma(F_o)$) $R1 = 0.0582$ (all Data) $wR2 = 0.0853$ ($F_o > 4\sigma(F_o)$) $wR2 = 0.0934$ (all data)
GooF	1.028 (1.030 for 26 restraints)
Weighting scheme	$w^{-1} = \sigma^2(F_o^2) + (0.0538P)^2$ where $P = (F_o^2) + 2 F_c^2) / 3$
Largest peak / deepest hole / $e \text{ Å}^{-3}$	0.300 and -0.293

The asymmetric unit comprises four cyameluric acid molecules and twelve crystal water molecules. All four crystallographically independent molecules were found displaying the keto tautomer. Distances and angles between chemically equivalent but crystallographically non-equivalent atoms are virtually identical within the given margin of error. This is the case for bonds and angles within one cyameluric acid molecule as well as between different molecules of the asymmetric unit (cf. Table 24 and Table 25). Thus, the following discussion will mostly refer to averaged data as presented in Table 26. The nomenclature of these atoms is in accordance to the statements of the preceding section (cf. Figure 72).

7.2 Cyameluric Acid Trihydrate $\text{H}_3\text{C}_6\text{N}_7\text{O}_3 \cdot 3\text{H}_2\text{O}$ **Table 24.** Selected distances (in Å) for $\text{H}_3(\text{C}_6\text{N}_7)\text{O}_3 \cdot 3\text{H}_2\text{O}$. Standard deviations in parentheses.

N(i)-C(i)		N-H		C(e) – O	
N1-C2	1.387(2)	N2-H1	1.00(3)	O1-C4	1.232(3)
N1-C3	1.388(3)	N4-H2	0.89(3)	O2-C5	1.228(3)
N1-C1	1.396(3)	N6-H3	0.92(3)	O3-C6	1.224(3)
N8-C8	1.383(3)	N9-H4	0.93(3)	O4-C10	1.224(3)
N8-C9	1.384(3)	N11-H5	0.82(2)	O5-C11	1.227(3)
N8-C7	1.389(3)	N13-H6	0.97(3)	O6-C12	1.233(3)
N15-C15	1.384(3)	N16-H7	0.87(3)	O7-C16	1.231(3)
N15-C13	1.392(3)	N18-H8	0.98(3)	O8-C17	1.232(3)
N15-C14	1.392(3)	N20-H9	0.88(3)	O9-C18	1.230(3)
N22-C19	1.388(3)	N23-H10	0.87(3)	O12-C24	1.232(3)
N22-C21	1.388(3)	N25-H11	0.93(3)	O11-C23	1.228(3)
N22-C20	1.393(3)	N27-H12	0.84(3)	O10-C22	1.226(3)
N(c)-C(i)		NH(c)-C(i)		N(c)-C(e)	
N3-C1	1.292(3)	N2-C1	1.342(3)	N3-C5	1.364(3)
N5-C2	1.293(3)	N4-C2	1.337(3)	N5-C6	1.367(3)
N7-C3	1.293(3)	N6-C3	1.342(3)	N7-C4	1.364(3)
N10-C8	1.303(3)	N9-C7	1.346(3)	N10-C10	1.367(3)
N12-C9	1.296(3)	N11-C8	1.337(3)	N12-C11	1.368(3)
N14-C7	1.292(3)	N13-C9	1.352(3)	N14-C12	1.373(3)
N17-C14	1.291(3)	N16-C13	1.343(3)	N17-C16	1.367(3)
N19-C15	1.298(3)	N18-C14	1.347(3)	N19-C17	1.374(3)
N21-C13	1.292(3)	N20-C15	1.347(3)	N21-C18	1.365(3)
N24-C20	1.294(3)	N23-C19	1.344(3)	N24-C22	1.374(3)
N26-C21	1.298(3)	N25-C20	1.351(3)	N26-C23	1.361(3)
N28-C19	1.295(3)	N27-C21	1.339(3)	N28-C24	1.369(3)
NH(c)-C(e)					
N2-C4	1.386(3)	N11-C11	1.382(3)	N20-C18	1.383(3)
N4-C5	1.388(3)	N13-C12	1.382(3)	N23-C22	1.386(3)
N6-C6	1.391(3)	N16-C16	1.380(3)	N25-C23	1.381(3)
N9-C10	1.388(3)	N18-C17	1.381(3)	N27-C24	1.380(3)

Table 25. Selected angles (in °) in $\text{H}_3(\text{C}_6\text{N}_7)\text{O}_3 \cdot 3\text{H}_2\text{O}$. Standard deviations in parentheses.

C(i)-N(i)-C(i)		C(i)-NH(c)-C(e)		C(i)-N(c)-C(e)	
C2-N1-C3	120.10(17)	C1-N2-C4	124.47(18)	C1-N3-C5	118.00(19)
C2-N1-C1	119.74(17)	C7-N9-C10	124.98(19)	C8-N10-C10	117.88(18)
C3-N1-C1	119.64(16)	C13-N16-C16	124.6(2)	C14-N17-C16	117.82(19)
C8-N8-C9	119.66(17)	C19-N23-C22	124.2(2)	C20-N24-C22	117.46(19)
C8-N8-C7	120.33(17)	C2-N4-C5	124.66(19)	C2-N5-C6	118.22(19)
C9-N8-C7	120.01(17)	C8-N11-C11	124.4(2)	C9-N12-C11	117.33(19)
C15-N15-C13	120.06(17)	C14-N18-C17	124.15(19)	C15-N19-C17	117.36(19)
C15-N15-C14	120.26(17)	C20-N25-C23	124.8(2)	C21-N26-C23	118.05(19)
C13-N15-C14	119.63(17)	C3-N6-C6	124.56(19)	C3-N7-C4	117.66(19)
C19-N22-C21	120.07(17)	C9-N13-C12	123.5(2)	C7-N14-C12	117.05(18)
C19-N22-C20	120.07(17)	C15-N20-C18	124.7(2)	C13-N21-C18	117.82(19)
C21-N22-C20	119.86(18)	C21-N27-C24	124.66(19)	C19-N28-C24	117.64(18)

N(c)-C(i)-N(i)		NH(c)-C(i)-N(i)		N(c)-C(i)-NH(c)	
N3-C1-N1	123.84(19)	N2-C1-N1	114.49(18)	N3-C1-N2	121.67(19)
N14-C7-N8	124.41(19)	N9-C7-N8	114.28(18)	N14-C7-N9	121.3(2)
N21-C13-N15	124.05(19)	N16-C13-N15	114.66(18)	N17-C14-N18	121.25(19)
N28-C19-N22	123.92(19)	N23-C19-N22	114.81(19)	N28-C19-N23	121.3(2)
N5-C2-N1	123.82(19)	N4-C2-N1	114.76(18)	N7-C3-N6	121.06(19)
N10-C8-N8	123.94(18)	N11-C8-N8	115.05(18)	N12-C9-N13	120.56(19)
N17-C14-N15	124.09(19)	N18-C14-N15	114.66(18)	N21-C13-N16	121.3(2)
N24-C20-N22	124.1(2)	N25-C20-N22	114.30(18)	N26-C21-N27	121.30(19)
N7-C3-N1	124.37(19)	N6-C3-N1	114.57(17)	N5-C2-N4	121.42(19)
N12-C9-N8	124.4(2)	N13-C9-N8	115.00(18)	N10-C8-N11	121.00(19)
N19-C15-N15	124.04(19)	N20-C15-N15	114.35(19)	N19-C15-N20	121.6(2)
N26-C21-N22	124.06(19)	N27-C21-N22	114.64(18)	N24-C20-N25	121.6(2)
O-C(e)-N(c)		O-C(e)-NH(c)		N(c)-C(e)-NH(c)	
O1-C4-N7	122.1(2)	O1-C4-N2	118.7(2)	N7-C4-N2	119.18(18)
O4-C10-N10	122.06(19)	O4-C10-N9	119.36(19)	N10-C10-N9	118.57(19)
O7-C16-N17	122.28(19)	O7-C16-N16	118.8(2)	N21-C18-N20	118.93(19)
O10-C22-N24	121.5(2)	O10-C22-N23	119.1(2)	N24-C22-N23	119.32(18)
O2-C5-N3	122.1(2)	O2-C5-N4	119.10(19)	N5-C6-N6	118.5(2)
O5-C11-N12	122.0(2)	O5-C11-N11	118.9(2)	N14-C12-N13	119.9(2)
O8-C17-N19	121.5(2)	O8-C17-N18	119.0(2)	N19-C17-N18	119.48(19)
O11-C23-N26	121.8(2)	O11-C23-N25	119.3(2)	N28-C24-N27	119.06(18)
O3-C6-N5	122.6(2)	O3-C6-N6	118.9(2)	N3-C5-N4	118.80(19)
O6-C12-N14	121.6(2)	O6-C12-N13	118.5(2)	N12-C11-N11	119.06(19)
O9-C18-N21	121.5(2)	O9-C18-N20	119.5(2)	N17-C16-N16	118.91(19)
O12-C24-N28	121.66(19)	O12-C24-N27	119.27(18)	N26-C23-N25	118.9(2)
C-N(c)-H					
C1-N2-H1	115.2(16)	C2-N4-H2	120(2)	C3-N6-H3	123.4(16)
C4-N2-H1	120.0(16)	C5-N4-H2	114(2)	C6-N6-H3	111.9(16)
C7-N9-H4	118.5(17)	C8-N11-H5	117.1(16)	C9-N13-H6	114.4(17)
C10-N9-H4	116.5(17)	C11-N11-H5	118.1(16)	C12-N13-H6	122.1(17)
C13-N16-H7	115.9(16)	C14-N18-H8	115.6(16)	C15-N20-H9	116.1(15)
C16-N16-H7	119.6(16)	C17-N18-H8	120.1(16)	C18-N20-H9	119.2(15)
C19-N23-H10	114.9(17)	C20-N25-H11	116.2(17)	C21-N27-H12	118(2)
C22-N23-H10	120.5(17)	C23-N25-H11	118.6(17)	C24-N27-H12	117(2)

Table 26. Distances and angles (in Å and °) for $H_3(C_6N_7)O_3 \cdot 3H_2O$. Data averaged over chemically equivalent atoms.

Distances					
N(i)-C(i)	1.38	N-H	0.91	C(e) - O	1.229
N(c)-C(i)	1.295	NH(c)-C(i)	1.344	N(c)-C(e)	1.368
NH(c)-C(e)	1.384				
Angles					
C(i)-N(i)-C(i)	119.95	C(i)-NH(c)-C(e)	124.47	C(i)-N(c)-C(e)	117.69
N(c)-C(i)-N(i)	124.09	NH(c)-C(i)-N(i)	114.63	N(c)-C(i)-NH(c)	121.28
O-C(e)-N(c)	121.89	O-C(e)-NH(c)	119.04	N(c)-C(e)-NH(c)	119.05
C-N(c)-H	117.6				

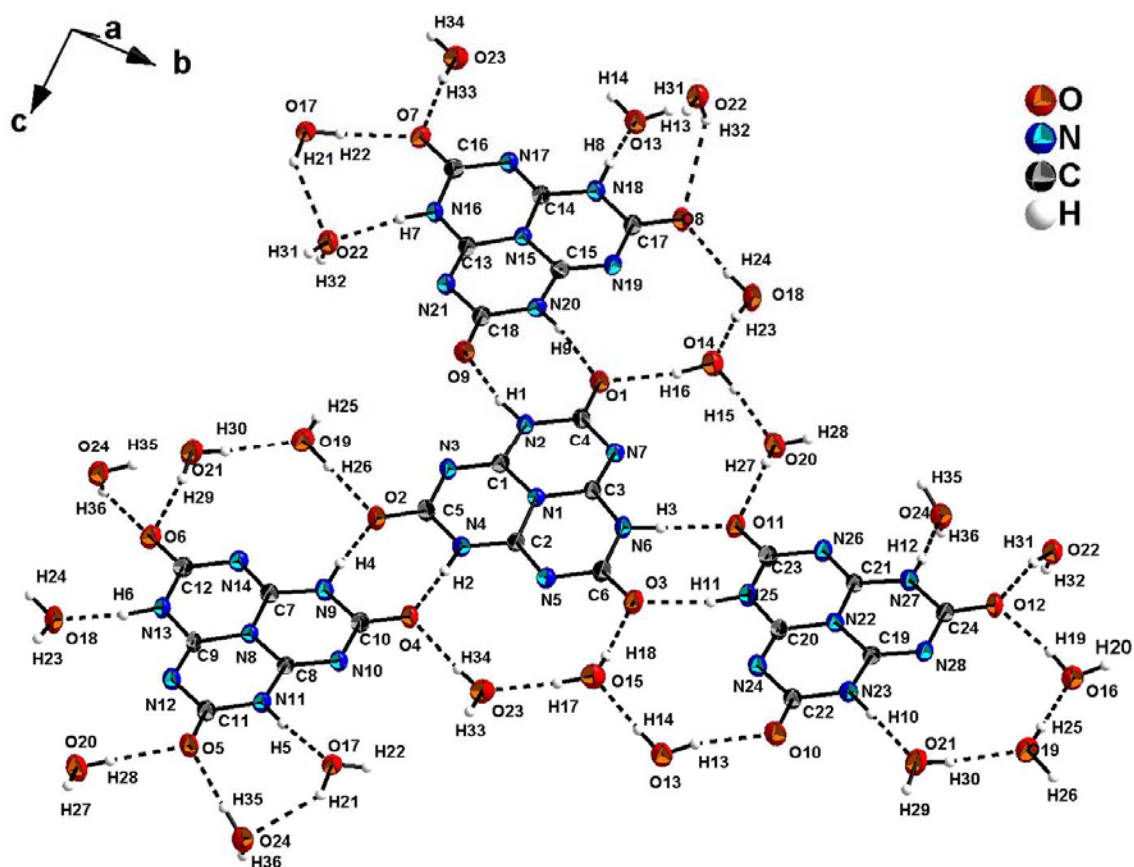


Figure 73. H-bonding interactions found for $\text{H}_3(\text{C}_6\text{N}_7)\text{O}_3 \cdot 3\text{H}_2\text{O}$. Ellipsoids for non-hydrogen atoms are drawn at the 50 % probability level.

Bond lengths are conclusive with the expectations arising from the formula depicted. The C-O distances display values typical for double-bonds. The average distances C(i)-N(c) which are found at 129.5 pm are corresponding to a C=N double-bond. The C(i)-NH(c) distances, however, are significantly longer (with an average of 134.4 pm) and thus already within the range expected for C-N single-bonds. The other C-N bonds are even longer and are thus also to be considered single-bonds. The angles within the cyameluric nucleus are close to the ideal value of 120° . Angles around the C(i) atoms, however, show a significant deviation. The angles N(c)-C(i)-N(i) assume an averaged value of 124.1° that is notably higher than the average for the adjacent NH(c)-C(i)-N(i) angles. Distances and angles for the whole cyameluric nucleus are thus in approximate agreement to the values expected for the present tautomer.

Table 27. H-bonding interactions (in Å and °) for H₃(C₆N₇)O₃ · 3H₂O (D = donor, H = hydrogen, A = acceptor).

D-H...A	∠ D- H...A	D...A	D-H...A	∠ D- H...A	D...A	D-H...A	∠ D- H...A	D...A
N2-H1...O9	171.48	2.731	O13-H13...O10	168.26	2.829	O19-H25...O16	178.00	2.731
N4-H2...O4	174.83	2.763	O13-H14...O15	177.20	2.699	O19-H26...O2	171.07	2.849
N6-H3...O11	176.05	2.760	O14-H15...O20	174.48	2.730	O20-H27...O11	159.51	2.864
N9-H4...O2	172.17	2.788	O14-H16...O1	166.46	2.812	O20-H28...O5	174.85	2.799
N11-H5...O17	172.08	2.726	O15-H17...O23	171.68	2.728	O21-H29...O6	170.84	2.785
N13-H6...O18	173.05	2.660	O15-H18...O3	165.39	2.819	O21-H30...O19	168.89	2.731
N16-H7...O22	170.18	2.712	O16-H19...O12	170.84	2.824	O22-H31...O12	164.99	2.782
N18-H8...O13	173.38	2.643	O16-H20...O9	161.75	2.874	O22-H32...O10	128.08	3.041
N20-H9...O1	170.56	2.806	O17-H21...O24	140.15	2.856	O22-H32...O8	125.49	3.103
N23-H10...O21	176.35	2.645	O17-H21...O22	135.76	2.906	O23-H33...O7	166.82	2.797
N25-H11...O3	169.79	2.795	O17-H22...O7	165.49	2.815	O23-H34...O4	167.61	2.835
N27-H12...O24	170.25	2.734	O18-H23...O14	170.36	2.716	O24-H35...O5	168.93	2.783
			O18-H24...O8	172.21	2.834	O24-H36...O6	153.14	2.848

The cyameluric acid molecules are part of a H-bonding network also comprising the crystal water molecules (cf. Figure 73, Table 27). The H-bonds found are of medium strength in average. Most bonds only show slight deviations from linearity. The H-bonding network comprises all H atoms found in the crystal. The cyameluric acid molecules are arranged in a layer-like pattern (cf. Figure 74), with intra-layer H-bonding being significantly more numerous than inter-layer interactions.

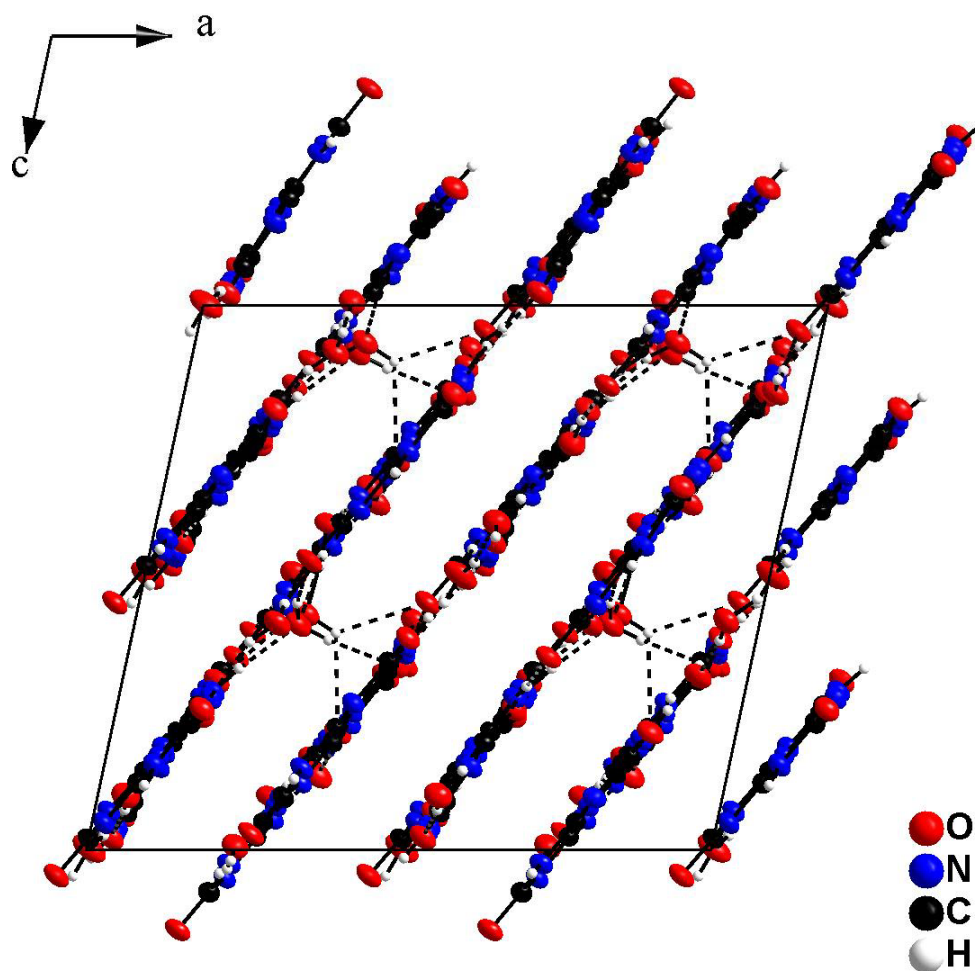


Figure 74. Layer-like structure of $\text{H}_3(\text{C}_6\text{N}_7)\text{O}_3 \cdot 3\text{H}_2\text{O}$. View along *b*. Ellipsoids for non-hydrogen atoms are drawn at the 50 % probability level.

7.2.3 Properties

The ^{13}C -NMR spectrum of cyameluric acid displays two distinct signals. The resonance observed at 156.6 ppm was assigned to the C(e) atoms, while the C(i) atoms correspond to the signal at 150.6 ppm. The ^1H resonances of crystal water are found as a broad signal at 4.9 ppm, the more acidic protons of the cyameluric acid molecule are found at a shift of 13.2 ppm. Two signals were detected in the ^{15}N CP spectrum under the measurement conditions chosen. The respective resonances were observed at -242.7 and -245.9 ppm. These chemical shift values are in line with protonated N atoms of the cyameluric nucleus. The other nitrogen atoms probably could not be resolved by the CP experiment as they are not directly bound to protons.

FTIR- and Raman spectroscopy of cyameluric acid trihydrate were conducted. The respective data is displayed in Figure 75. Most of the signals are in good accordance to literature values. The vibration that was reported at 1668 cm^{-1} by *Finkel'shtein* and *Spiridonova*^[89] was instead observed at 1583 cm^{-1} in this work. The following signals were observed. (FTIR, reflection, $25\text{ }^{\circ}\text{C}$, cm^{-1}) 3483, 3427, 3328, 3200, 2984, 2851, 2779, 1583, 1470, 1393, 1306, 1167, 932, 823, 784. (Raman, cm^{-1}) 1705, 1560, 1475, 1403, 1327, 1102, 965, 737, 550, 450, 360 247, 105.

The elemental analysis results are in good accordance to theoretical expectations. Data is listed as follows. Elemental analysis for $\text{H}_3(\text{C}_6\text{N}_7)\text{O}_3 \cdot 3\text{H}_2\text{O}$ (wt.%) N: 36.07 (calcd. 35.63) C: 26.26 (calcd. 26.19) H: 3.06 (calcd. 3.30).

Cyameluric acid trihydrate successively decomposes upon heating. Endothermic desolvation leading to anhydrous cyameluric acid is found onseting at $88\text{ }^{\circ}\text{C}$. Beginning at $409\text{ }^{\circ}\text{C}$ another endothermic event accompanied by a weight loss of about 30 % is observed. This can probably be assigned to a condensation reaction of some sort. Total decomposition of the sample was observed beyond $648\text{ }^{\circ}\text{C}$.

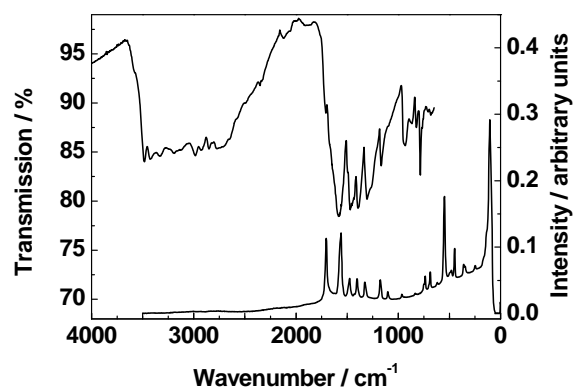


Figure 75. FTIR- (ATR) and Raman spectrum for $\text{H}_3(\text{C}_6\text{N}_7)\text{O}_3 \cdot 3\text{H}_2\text{O}$.

7.2 Sodium Dihydrogencyamelurate Tetrahydrate - $\text{NaH}_2\text{C}_6\text{N}_7\text{O}_3 \cdot 4\text{H}_2\text{O}$

The contents of the proceeding section have been published in advance to this thesis.^[140] Cyameluric acid trihydrate was yielded from an acidic solution (cf. Section 7.1). If a solution containing cyamelurate anions is only neutralized to $\text{pH} = 7$ dihydrogencyamelurate salts can be crystallized. Sodium dihydrogencyamelurate tetrahydrate, $\text{NaH}_2\text{C}_6\text{N}_7\text{O}_3 \cdot 4\text{H}_2\text{O}$, was crystallized by slow evaporation of a respective solution. Experimental details are presented in Section 12.1.18.

Table 28. Crystallographic data and details for the structure refinement of $\text{NaH}_2(\text{C}_6\text{N}_7)\text{O}_3 \cdot 4\text{H}_2\text{O}$.

Formula	$\text{NaH}_2\text{C}_6\text{N}_7\text{O}_3 \cdot 4\text{H}_2\text{O}$	
Formula weight / g mol^{-1}	315.20	
Crystal system	triclinic	
Space group	$P\bar{1}$ (no. 2)	
Lattice parameters / $\text{Å}, ^\circ$	$a = 6.6345(13)$	$\alpha = 68.96(3)$
	$b = 8.7107(17)$	$\beta = 87.57(3)$
	$c = 11.632(2)$	$\gamma = 68.24(3)$
Volume / Å^3	579.5(3)	
Z	2	
Diffractometer	Kappa-CCD	
Radiation, monochromator	Mo-K α ($\lambda = 71.073$ pm), graphite	
Temperature	273(2)	
Structure solution	SHELXS-97 ^[101] (direct methods)	
Structure refinement	SHELXL-97 ^[101] (full-matrix least-squares on F^2)	
Corrections	SCALEPACK, ^[96] Lorentz, polarization	
Data / restraints / parameters	2634 / 4 / 230	
R-indices	$R1 = 0.0415$ ($F_o > 4\sigma(F_o)$)	
	$R1 = 0.0535$ (all data)	
	$wR2 = 0.1184$ ($F_o > 4\sigma(F_o)$)	
	$wR2 = 0.1251$ (all data)	
Goof	1.083 (1.084 for 4 restraints)	
Weighting scheme	$w^{-1} = \sigma^2(F_o^2) + (0.0705P)^2 + 0.0372P$ where $P = (F_o^2) + 2 F_c^2 / 3$	
Largest peak / deepest hole / $e \text{ Å}^{-3}$	0.247 and -0.307	

The structure of $\text{NaH}_2(\text{C}_6\text{N}_7)\text{O}_3 \cdot 4\text{H}_2\text{O}$ was solved by single-crystal XRD (cf. Table 28). Hydrogen atoms were located by difference Fourier synthesis and refined with isotropic thermal displacement parameters. The compound crystallizes in the triclinic space group $P\bar{1}$ (no. 2). Details for the refinement are given in Table 28. Sodium dihydrogencyamelurate crystallizes from aqueous solution forming a tetrahydrate. The unit cell comprises two formula units.

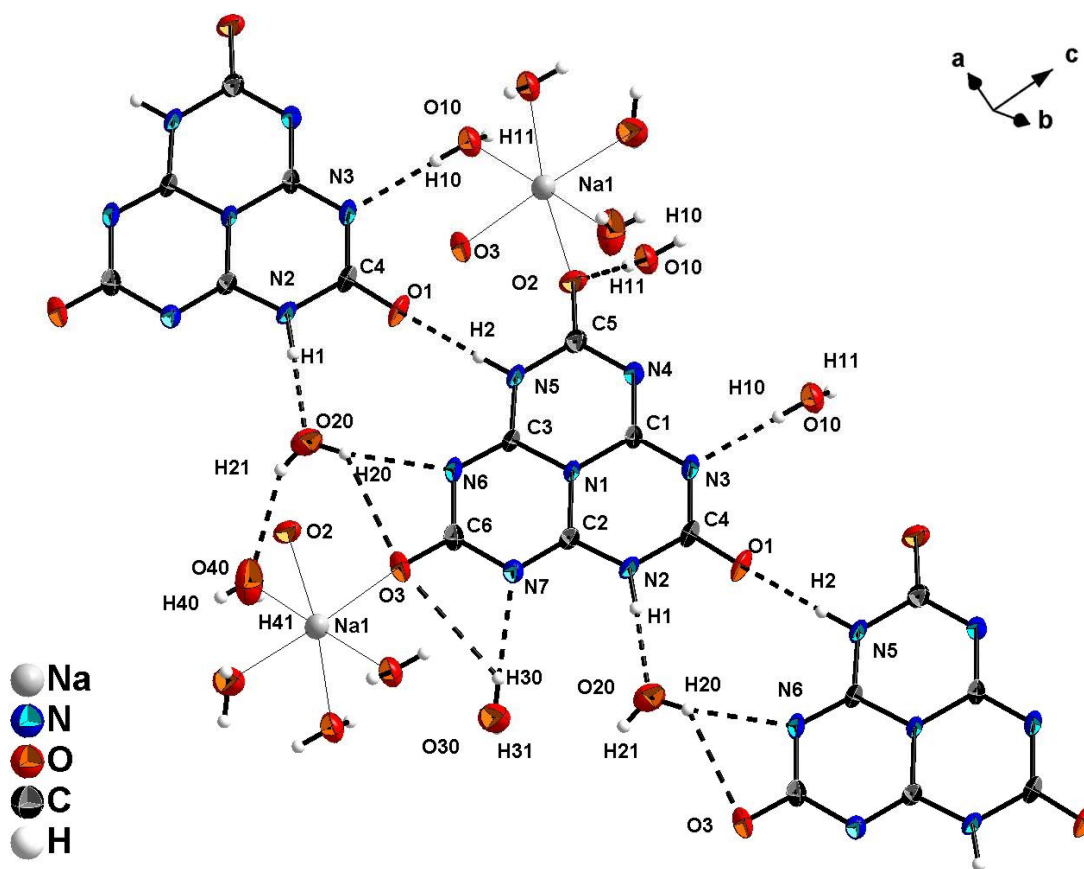


Figure 76. H-bonding interactions for $\text{NaH}_2(\text{C}_6\text{N}_7)\text{O}_3 \cdot 4\text{H}_2\text{O}$. Ellipsoids for non-hydrogen atoms are drawn at the 50 % probability level.

The crystal structure displays planar $\text{H}_2(\text{C}_6\text{N}_7)\text{O}_3^-$ ions and Na^+ ions octahedrally coordinated by O. Bond lengths and angles are well consistent with other heptazine systems and especially with values reported for alkali metal cyamelurates of formula $\text{M}_3[\text{C}_6\text{N}_7\text{O}_3] \cdot x\text{H}_2\text{O}$ ($\text{M} = \text{Li}, \text{Na}, \text{K}, \text{Rb}, \text{Cs}$).^[42] The H atoms are bound to N atoms of the cyameluric nucleus. Equal to the findings for cyameluric acid described in the preceding section, there is no indication for OH groups. The C-O bonds are average 1.228 Å in length which is typical for C=O double-bonds. The two protons of the $\text{H}_2(\text{C}_6\text{N}_7)\text{O}_3^-$ ions assume maximum distance. They thus arrange themselves in a similar way as found for $\text{H}_2(\text{C}_6\text{N}_7)(\text{NH}_2)_3^{2+}$ ions in the melemium salt

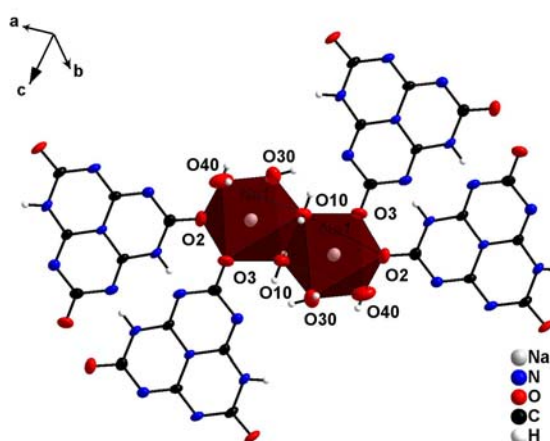


Figure 77. Coordination spheres of the Na^+ ions in $\text{NaH}_2(\text{C}_6\text{N}_7)\text{O}_3 \cdot 4\text{H}_2\text{O}$. Ellipsoids for non-hydrogen atoms are drawn at the 50 % probability level.

7.2 Sodium Dihydrogencyamelurate Tetrahydrate - NaH₂C₆N₇O₃ · 4H₂O

H₂(C₆N₇)(NH₂)₃SO₄ · 2H₂O.^[36] Na⁺ is coordinated by O atoms of both dihydrogencyamelurate ions and crystal water, forming a slightly distorted octahedron (cf. Figure 77). Two neighboring octahedrons are connected by a shared edge.

The structure shows a dense H-bonding network of varying strength. The H₂(C₆N₇)O₃⁻ ions and one crystal water molecule are arranged in strands stabilized by the H-bonds N5-H2...O1, N2-H1...O20 and the forked H-bridge O20-H20...N6 (main component) and O20-H20...O3.

Table 29. Selected distances (in Å), angles (in °) and H-bonding interactions (in ° and Å) for NaH₂(C₆N₇)O₃ · 4H₂O (D = donor, H = hydrogen, A = acceptor).

Distances					
Na1-O2	2.4221(15)	N2-C2	1.3416(19)	N5-H2	0.85(2)
Na1-O3	2.3565(14)	N2-C4	1.391(2)	N6-C3	1.2968(19)
Na1-O10	2.3860(15)	N2-H1	0.84(2)	N6-C6	1.388(2)
Na1-O10	2.4104(16)	N3-C1	1.3210(19)	N7-C2	1.3015(19)
Na1-O30	2.3737(16)	N3-C4	1.354(2)	N7-C6	1.386(2)
Na1-O40	2.4384(18)	N4-C1	1.319(2)	O1-C4	1.2261(19)
N1-C3	1.3823(18)	N4-C5	1.352(2)	O2-C5	1.2298(19)
N1-C2	1.3850(19)	N5-C3	1.3413(19)	O3-C6	1.2268(18)
N1-C1	1.4196(18)	N5-C5	1.3913(19)		
Angles					
C3-N1-C2	116.73(12)	C3-N6-C6	117.79(12)	O1-C4-N3	122.63(14)
C3-N1-C1	121.74(12)	C2-N7-C6	118.41(13)	O1-C4-N2	117.81(14)
C2-N1-C1	121.53(12)	N7-C2-N2	121.91(13)	N3-C4-N2	119.57(12)
C2-N2-C4	123.40(13)	N7-C2-N1	122.51(13)	O2-C5-N4	122.85(14)
C2-N2-H1	126.9(15)	N2-C2-N1	115.57(13)	O2-C5-N5	117.92(14)
C4-N2-H1	109.7(15)	N4-C1-N3	120.58(13)	N4-C5-N5	119.23(13)
C1-N3-C4	120.21(13)	N4-C1-N1	119.77(12)	O3-C6-N7	119.82(14)
C1-N4-C5	120.22(12)	N3-C1-N1	119.65(13)	O3-C6-N6	119.03(14)
C3-N5-C5	123.97(13)	N6-C3-N5	121.58(12)	N7-C6-N6	121.14(13)
C3-N5-H2	116.6(13)	N6-C3-N1	123.39(13)		
C5-N5-H2	119.4(13)	N5-C3-N1	115.03(12)		
H-bonds					
	∠D-H...A	D...A		∠D-H...A	D...A
N2-H1...O20	172(3)	2.774(3)	O20-H21...O40	154(2)	3.033(3)
N5-H2...O1	173(3)	2.784(2)	O30-H30...N7	178(3)	2.956(3)
O10-H10...N3	171(2)	2.887(3)	O40-H40...O40	120(3)	3.038(3)
O10-H11...O2	174(3)	2.893(3)	O40-H40...N4	139(2)	3.173(3)
O20-H20...N6	171(3)	3.018(3)	O40-H41...N4	158(4)	3.203(3)
O20-H20...O3	133(3)	3.252(3)			

Each Na⁺ is coordinated by two H₂(C₆N₇)O₃⁻ ions of differed strands. The coordination spheres of the Na⁺ ions thus crosslink the H-bonded strands resulting in double-layer-like arrangement (cf. Figure 78).

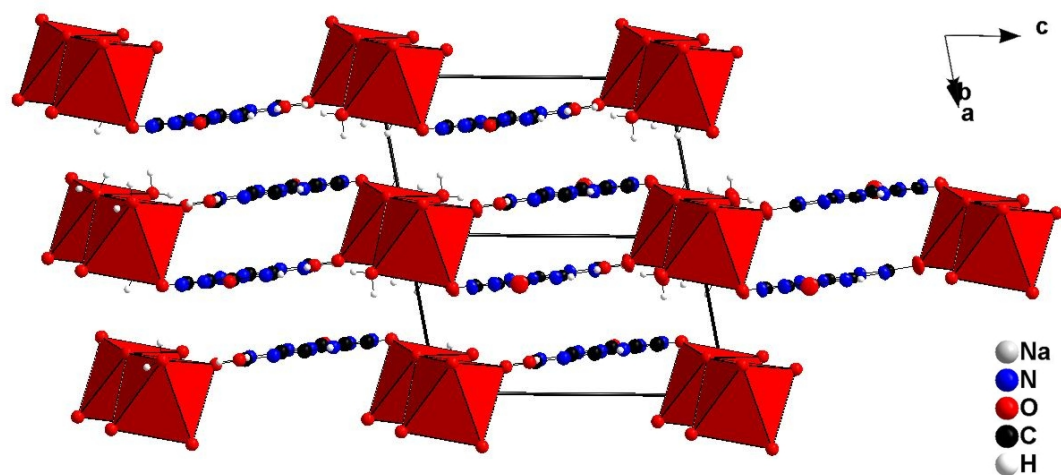


Figure 78. Layer-like arrangement for $\text{NaH}_2(\text{C}_6\text{N}_7)\text{O}_3 \cdot 4\text{H}_2\text{O}$. Ellipsoids for non-hydrogen atoms are drawn at the 50 % probability level.

7.3 Metal(II) Cyamelurates

The contents of this section have already been published in advance to this thesis.^[141] Some work on cyamelurate salts of polyvalent metals can be found in the literature.^[142,143] These compounds have, however, not been sufficiently characterized, making further investigations in this direction desirable. The claim of a copper ammonium salt of cyameluric acid ($\text{CuNH}_4\text{C}_6\text{N}_7\text{O}_3 \cdot \text{NH}_3$)^[143] likely showing special properties concerning the structure of the anion drew additional interest towards those compounds.

The compounds presented in this section were prepared with structural investigations by single-crystal XRD in mind. Hence, the cyamelurate salts had to be prepared under terms allowing good crystal growth. A simple emulsion of the synthetic procedure used for alkali metal cyamelurates was barely applicable for metal ions forming insoluble hydroxides. By using Cu(II) and Zn(II) salts the work was focused on ions allowing an increase in solubility by complexation. New structures were identified by doing so. Not surprisingly, NH_3 ligands or NH_4^+ ions have been incorporated into the products in addition to the targeted metal ions. Metal ammonium salts of cyameluric acid can also be obtained by using other metal ions, e.g. Ca^{2+} . An important drive behind the ambition in preparing these compounds was their possible thermal reactivity. An appropriate compound might be employed to device a reaction leading from a metal cyamelurate of an oxophilic metal to the respective oxide and a carbon nitride network. A synthesis of a condensed heptazine-based phase has already been described starting from a copper melonate $\text{Cu}_3(\text{C}_6\text{N}_7(\text{NCN})_3)_2$.^[19b] This illustrates that heptazine-based metal salts have some potential use as precursor compounds. For a detailed investigation of such reactivity it is of course essential not only to establish a good access to suitable metal salts but also to gather structural data.

The synthesis of the calcium salt is quite remarkable since this compound can already be obtained when minimal amounts of Ca^{2+} are present in solution. In fact a good way to yield single-crystals of $\text{CaNH}_4(\text{H}_2\text{C}_6\text{N}_7\text{O}_3)(\text{HC}_6\text{N}_7\text{O}_3) \cdot 6\text{H}_2\text{O}$ is to grow them from hard tap water treated with ammonia. Water of a hardness of 15.8 °dH (which equals 281 ppm CaCO_3) was used for this purpose. Unfortunately, this approach is not suitable for preparation of phase pure material, since of course ammonium cyamelurate is the major product. It should, however, be pointed out that, considering this finding, cyameluric acid or cyamelurates might be useful for deionization purposes, like removing water hardness.

It has to be noted that by variation of reaction conditions a variety of different metal cyamelurate species could be identified using powder XRD for the metal species investigated. Preparing phase pure samples and growing good single-crystals is, however, quite challenging in most cases, due to the existence of a multitude of different products. Detailed synthesis conditions for the respective compounds are given in Sections 12.1.19 to 12.1.21.

Table 30. Crystallographic data and details of the structure refinement for $[\text{Cu}(\text{NH}_3)_2]_3(\text{C}_6\text{N}_7\text{O}_3)_2 \cdot 2\text{H}_2\text{O}$, $(\text{NH}_4)_2[\text{Zn}(\text{H}_2\text{O})_6](\text{HC}_6\text{N}_7\text{O}_3)_2 \cdot 2\text{H}_2\text{O}$ and $\text{CaNH}_4(\text{H}_2\text{C}_6\text{N}_7\text{O}_3)(\text{HC}_6\text{N}_7\text{O}_3) \cdot 6\text{H}_2\text{O}$.

Formula	$[\text{Cu}(\text{NH}_3)_2]_3(\text{C}_6\text{N}_7\text{O}_3)_2 \cdot 2\text{H}_2\text{O}$	$(\text{NH}_4)_2[\text{Zn}(\text{H}_2\text{O})_6](\text{HC}_6\text{N}_7\text{O}_3)_2 \cdot 2\text{H}_2\text{O}$	$\text{CaNH}_4(\text{H}_2\text{C}_6\text{N}_7\text{O}_3)(\text{HC}_6\text{N}_7\text{O}_3) \cdot 6\text{H}_2\text{O}$
Formula weight / g mol ⁻¹	765.12	683.86	605.50
Crystal system	triclinic	triclinic	triclinic
Space group	$P\bar{1}$ (no. 2)	$P\bar{1}$ (no. 2)	$P\bar{1}$ (no. 2)
Lattice parameters / Å, °	$a = 7.1732(14)$ $b = 9.2338(18)$ $c = 9.994(2)$ $\alpha = 94.15(3)$ $\beta = 106.13(3)$ $\gamma = 106.28(3)$	$a = 6.7568(14)$ $b = 8.7252(17)$ $c = 10.505(2)$ $\alpha = 77.03(3)$ $\beta = 77.08(3)$ $\gamma = 82.95(3)$	$a = 6.6428(13)$ $b = 8.7159(17)$ $c = 19.245(4)$ $\alpha = 92.52(3)$ $\beta = 92.22(3)$ $\gamma = 106.95(3)$
Volume / Å ³	602.3(3)	586.5(2)	1063.3(4)
Z	1	1	2
Diffractometer	Kappa-CCD		
Radiation, monochromator	Mo-K α ($\lambda = 71.073$ pm), graphite		
Temperature / K	200		
Structure solution	SHELXS-97 ^[101] (direct methods)		
Structure refinement	SHELXL-97 ^[101] (full-matrix least-squares on F ²)		
Corrections applied	Lorentz, polarization, SCALEPACK ^[96]		
Absorption coefficient / mm ⁻¹	2.714	1.156	0.400
Calculated density / g cm ⁻³	2.110	1.936	1.891
Data / restraints / parameters	2738 / 11 / 233	2695 / 13 / 248	4293 / 16 / 428
R-indices	$R1 = 0.0428$ all data $R1 = 0.0344$ $F_o^2 > 2\sigma(F_o^2)$ (1494 reflections) $wR2 = 0.0874$ all data $wR2 = 0.0829$ $F_o^2 > 2\sigma(F_o^2)$	$R1 = 0.0483$ all data $R1 = 0.0401$ $F_o^2 > 2\sigma(F_o^2)$ (2365 reflections) $wR2 = 0.1213$ all data $wR2 = 0.1159$ $F_o^2 > 2\sigma(F_o^2)$	$R1 = 0.1088$ all data $R1 = 0.0545$ $F_o^2 > 2\sigma(F_o^2)$ (2669 reflections) $wR2 = 0.1291$ all data $wR2 = 0.1144$ $F_o^2 > 2\sigma(F_o^2)$
Goof	1.082 1.084 for 11 restraints	1.088 1.088 for 13 restraints	0.980 0.979 for 16 restraints
Weighting scheme	$w^{-1} = \sigma^2(F_o^2) + (0.0347)^2 + 0.9416P$ where $P = (F_o^2 + 2F_c^2) / 3$	$w^{-1} = \sigma^2(F_o^2) + (0.0626)^2 + 0.6616P$ where $P = (F_o^2 + 2F_c^2) / 3$	$w^{-1} = \sigma^2(F_o^2) + (0.0635)^2$ where $P = (F_o^2 + 2F_c^2) / 3$
Largest peak / deepest hole / e Å ⁻³	0.81 / -0.49	0.49 / -0.70	0.38 / -0.38

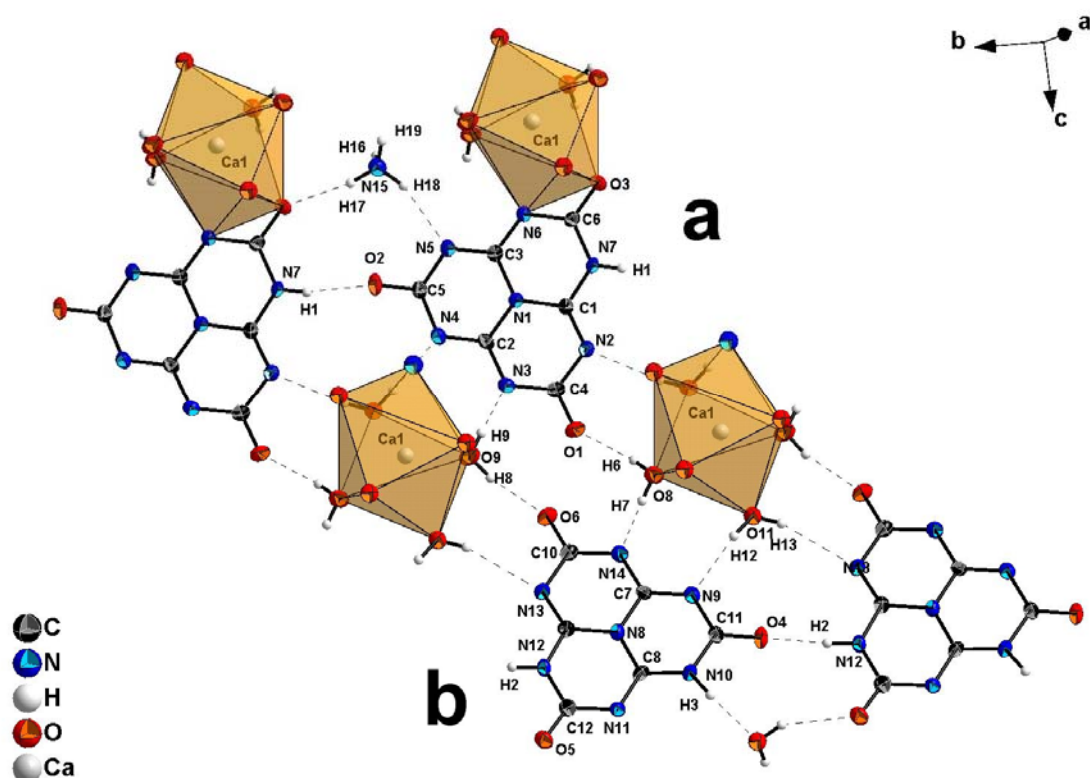


Figure 79. Hydrogen-bonding interactions and coordination of Ca^{2+} -ions for $\text{CaNH}_4(\text{H}_2\text{C}_6\text{N}_7\text{O}_3)(\text{HC}_6\text{N}_7\text{O}_3) \cdot 6\text{H}_2\text{O}$. The strand labeled **a** consists of $\text{HC}_6\text{N}_7\text{O}_3^{2-}$ ions while strand **b** consists of $\text{H}_2\text{C}_6\text{N}_7\text{O}_3^-$ ions. Ellipsoids for non-hydrogen atoms are drawn at the 50 % probability level.

$\text{CaNH}_4(\text{H}_2\text{C}_6\text{N}_7\text{O}_3)(\text{HC}_6\text{N}_7\text{O}_3) \cdot 6\text{H}_2\text{O}$ crystallizes in the triclinic space group $P\bar{1}$ (no. 2). There are one hydrogencyamelurate ion, one dihydrogencyamelurate ion as well as one Ca^{2+} and one NH_4^+ ion within the asymmetric unit. Ca^{2+} is coordinated by one hydrogencyamelurate ion and six crystal water molecules forming a square anti-prism. With $\text{HC}_6\text{N}_7\text{O}_3^{2-}$ acting as a bidentate ligand coordinating with both N6 and O3, a distortion of the coordinating polyhedron is achieved. Hydrogen-bonded strands of hydrogencyamelurate and dihydrogencyamelurate units are found running along *b*. Each strand is either composed of $\text{HC}_6\text{N}_7\text{O}_3^{2-}$ or of $\text{H}_2\text{C}_6\text{N}_7\text{O}_3^-$ ions, exclusively. The two different types of strands are alternating (cf. Figure 79). The strands are tilted against each other and connected via hydrogen-bonding interactions. As a result, a double-layer-like structure is generated (cf. Figure 80).

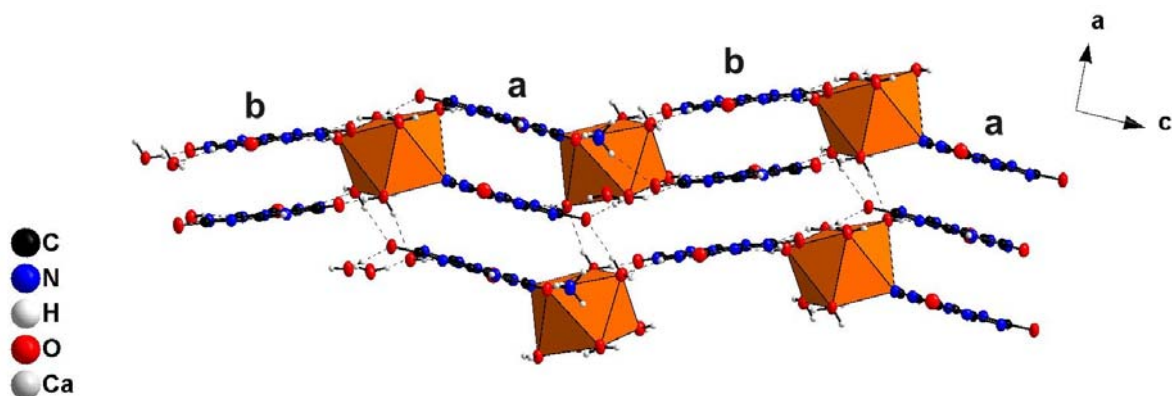
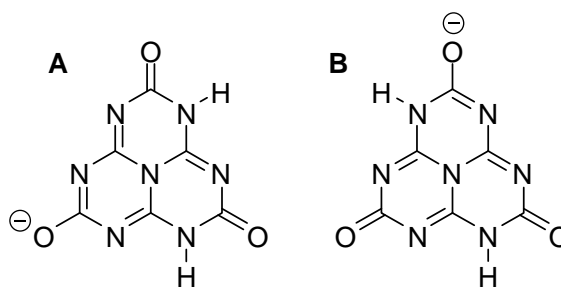


Figure 80. Layer-like structure for $\text{CaNH}_4(\text{H}_2\text{C}_6\text{N}_7\text{O}_3)(\text{HC}_6\text{N}_7\text{O}_3) \cdot 6\text{H}_2\text{O}$. Strands are running perpendicularly to the image plane. Strands labeled **a** consist of $\text{HC}_6\text{N}_7\text{O}_3^{2-}$ ions while strands **b** consist of $\text{H}_2\text{C}_6\text{N}_7\text{O}_3^-$ ions.

In this regard the fact that two tautomeric forms of the $\text{H}_2\text{C}_6\text{N}_7\text{O}_3^-$ ion exist in the solid should be pointed out (cf. Scheme 25). However, this observation has not been much regarded so far. The molecular structure **A** (left) is found in $\text{NH}_4\text{Ca}(\text{HC}_6\text{N}_7\text{O}_3)(\text{H}_2\text{C}_6\text{N}_7\text{O}_3) \cdot 6\text{H}_2\text{O}$ and in $\text{K}(\text{C}_6\text{N}_7\text{O}_3\text{H}_2) \cdot 2\text{H}_2\text{O}$ ^[54] while structure **B** (right) is found in $\text{Na}[\text{H}_2(\text{C}_6\text{N}_7)\text{O}_3] \cdot 4\text{H}_2\text{O}$ (cf. Section 7.2). None of these compounds shows any special structural features, responsible for the predominance of one tautomer. Energetic differences between the tautomers thus seem to be rather low.



Scheme 25 The two tautomeric forms of the dihydrogencyamelurate ion.

$(\text{NH}_4)_2[\text{Zn}(\text{H}_2\text{O})_6](\text{HC}_6\text{N}_7\text{O}_3)_2 \cdot 2\text{H}_2\text{O}$ crystallizes in the triclinic space group $P\bar{1}$. Zn^{2+} is surrounded by crystal water in an almost regular octahedral coordination. The hydrogencyamelurate ion is essentially identical with the one found in the potassium salt.^[54] The anions are arranged in hydrogen-bonded strands running along b (cf. Figure 81). There is no direct coordinative interaction between Zn^{2+} and the hydrogencyamelurate anion. The $[\text{Zn}(\text{H}_2\text{O})_6]^{2+}$ ion is connected to several different strands via hydrogen-bonding interactions (cf. Figure 82).

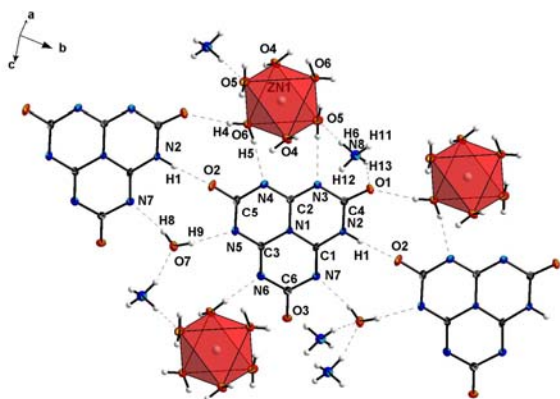


Figure 81. Hydrogen-bonding interactions for $(\text{NH}_4)_2[\text{Zn}(\text{H}_2\text{O})_6](\text{HC}_6\text{N}_7\text{O}_3)_2 \cdot 2\text{H}_2\text{O}$. Ellipsoids for non-hydrogen atoms are drawn at the 50 % probability level.

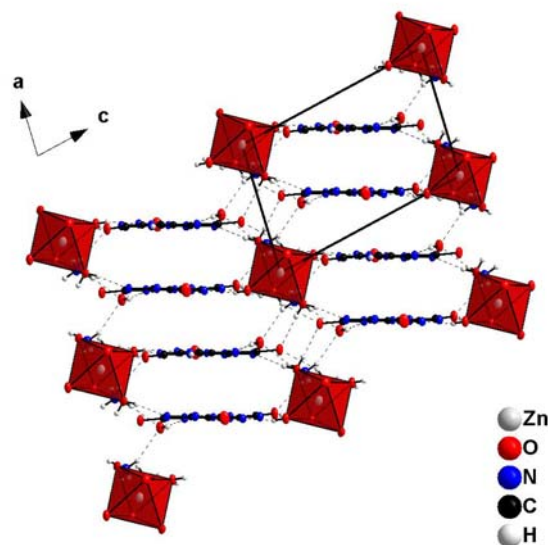


Figure 82. Layer-like structure for $(\text{NH}_4)_2[\text{Zn}(\text{H}_2\text{O})_6](\text{HC}_6\text{N}_7\text{O}_3)_2 \cdot 2\text{H}_2\text{O}$. Ellipsoids for non-hydrogen atoms are drawn at the 50 % probability level.

The copper salt $[\text{Cu}(\text{NH}_3)_2]_3(\text{C}_6\text{N}_7\text{O}_3)_2 \cdot 2\text{H}_2\text{O}$ crystallizes in the triclinic space group $P\bar{1}$. There are two different crystallographic Cu^{2+} positions both of which show square planar coordination of the central atom. Cu1 is surrounded solely by nitrogen atoms of two amine ligands and two fully deprotonated cyamelurate ions ($\text{C}_6\text{N}_7\text{O}_3^{3-}$), while Cu2 is also coordinated by an oxygen atom (O3), a heptazine nitrogen atom and two NH_3 molecules (cf. Figure 83). Cu1 is located on an inversion center and thus planarity of its coordination sphere is achieved. Although this is not the case for Cu2 the sum of angles around Cu2 amounts 359.8° and thus coordination is nearly planar within the accuracy of the measurement. Cop-

per-ligand distances are found to range between 1.961 and 2.004 Å for all ligands. Each Cu^{2+} is coordinated by two NH_3 and two different cyamelurate ions thus forming a one-dimensional coordination polymer (cf. Figure 83). This building motif is cross-linked by hydrogen-bonds between the NH_3 ligands and the anions resulting in a layer-like arrangement of the cyamelurate units (cf. Figure 84). The crystal water molecules are also found participating in these H-bonds. Furthermore, the $\text{Cu}2$ atoms are stacked at a distance of 4.3 Å.

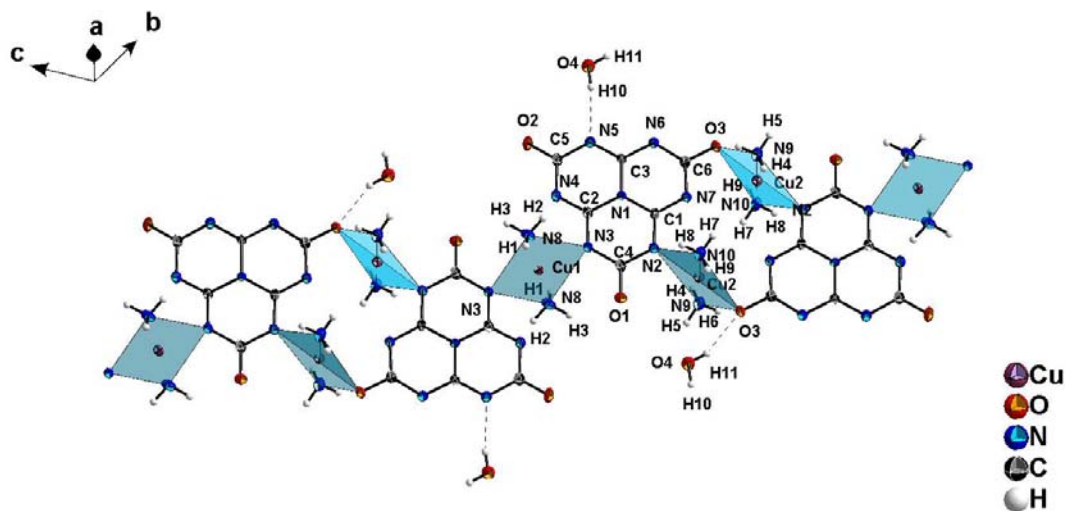


Figure 83. Copper bonded cyamelurate strands found in $[\text{Cu}(\text{NH}_3)_2]_3(\text{C}_6\text{N}_7\text{O}_3)_2 \cdot 2\text{H}_2\text{O}$. Ellipsoids for non-hydrogen atoms are drawn at the 50 % probability level.

Cu-O coordination has a significant effect on bond lengths within the cyamelurate ion as the respective O3-C6 bond is elongated by about 30 pm while the neighboring C-N bonds are about 20 pm shorter. Cu^{2+} coordination to heptazine N atoms on the other hand does not result in a notable distortion of the heptazine core, as does Ca^{2+} coordination to a cyamelurate anion in $\text{CaNH}_4(\text{H}_2\text{C}_6\text{N}_7\text{O}_3) \cdot 6\text{H}_2\text{O}$.

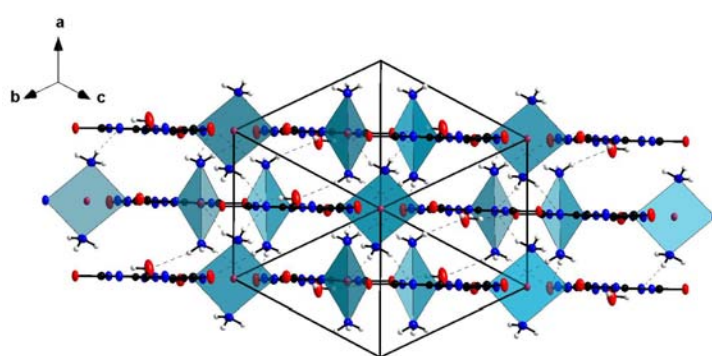


Figure 84. Layer-like structure for $[\text{Cu}(\text{NH}_3)_2]_3(\text{C}_6\text{N}_7\text{O}_3)_2 \cdot 2\text{H}_2\text{O}$.

The reported procedure for the synthesis of claimed $\text{CuNH}_4(\text{C}_6\text{N}_7\text{O}_3) \cdot \text{NH}_3$ ^[143] is not exactly identical with the one used for crystal growth in this work. Claimed $\text{CuNH}_4(\text{C}_6\text{N}_7\text{O}_3) \cdot \text{NH}_3$ must be considered identical with $[\text{Cu}(\text{NH}_3)_2]_3(\text{C}_6\text{N}_7\text{O}_3)_2 \cdot 2\text{H}_2\text{O}$ by comparison of color, reported properties and most importantly due to the powder XRD patterns found for “ $\text{CuNH}_4(\text{C}_6\text{N}_7\text{O}_3) \cdot \text{NH}_3$ ” prepared in analogy to literature procedures being identical with the ones simulated from the presented crystal structure.

Table 31 Selected bond lengths (in Å) for $(\text{NH}_4)_2[\text{Zn}(\text{H}_2\text{O})_6](\text{HC}_6\text{N}_7\text{O}_3)_2 \cdot 2\text{H}_2\text{O}$, $[\text{Cu}(\text{NH}_3)_2]_3(\text{C}_6\text{N}_7\text{O}_3)_2 \cdot 2\text{H}_2\text{O}$ and $\text{CaNH}_4(\text{H}_2\text{C}_6\text{N}_7\text{O}_3)(\text{HC}_6\text{N}_7\text{O}_3) \cdot 6\text{H}_2\text{O}$. Standard deviations in parentheses.

$(\text{NH}_4)_2[\text{Zn}(\text{H}_2\text{O})_6](\text{HC}_6\text{N}_7\text{O}_3)_2 \cdot 2\text{H}_2\text{O}$							
Zn1-O6	2.063(2)	N7-C6	1.384(3)	N5-C3	1.319(3)	N2-C1	1.344(3)
Zn1-O5	2.141(2)	N7-C1	1.303(3)	N4-C5	1.377(4)	N1-C3	1.403(3)
Zn1-O4	2.063(2)	N6-C6	1.362(3)	N3-C4	1.356(3)	N1-C2	1.405(3)
O3-C6	1.249(3)	N6-C3	1.324(3)	N3-C2	1.331(3)	N1-C1	1.378(3)
O2-C5	1.246(3)	N5-C5	1.365(3)	N2-C4	1.389(3)	C2-N4	1.317(3)
O1-C4	1.237(3)						
$[\text{Cu}(\text{NH}_3)_2]_3(\text{C}_6\text{N}_7\text{O}_3)_2 \cdot 2\text{H}_2\text{O}$							
Cu1-N8	1.977(3)	O1-C4	1.239(4)	N4-C2	1.308(4)	N5-C3	1.310(4)
Cu1-N3	2.003(2)	O2-C5	1.232(4)	N4-C5	1.380(4)	N5-C5	1.384(4)
Cu2-N10	1.961(3)	O3-C6	1.275(3)	N2-C1	1.325(4)	N6-C3	1.330(4)
Cu2-N9	1.961(3)	N1-C2	1.391(4)	N2-C4	1.377(4)	N6-C6	1.347(4)
Cu2-N2	2.004(2)	N1-C1	1.399(4)	N3-C2	1.341(4)	N7-C1	1.318(4)
Cu2-O3	2.020(2)	N1-C3	1.408(4)	N3-C4	1.372(4)	N7-C6	1.365(4)
$\text{CaNH}_4(\text{H}_2\text{C}_6\text{N}_7\text{O}_3)(\text{HC}_6\text{N}_7\text{O}_3) \cdot 6\text{H}_2\text{O}$							
C9- N13	1.290(4)	N14- C7	1.315(4)	C4- N2	1.400(4)	Ca1- O9	2.328(3)
C9- N12	1.358(4)	C1- N2	1.299(4)	C5- O2	1.245(4)	Ca1- O10	2.391(3)
C9- N8	1.391(4)	C1- N7	1.345(4)	C5- N4	1.370(4)	Ca1- O11	2.461(3)
C10- O6	1.223(4)	C1- N1	1.380(4)	C5- N5	1.379(4)	Ca1- O12	2.615(3)
C10- N14	1.381(4)	C2- N4	1.323(4)	C6- O3	1.236(4)	C7- N9	1.323(4)
C10- N13	1.398(4)	C2- N3	1.325(4)	C6- N6	1.344(4)	C7- N8	1.414(4)
C11- O4	1.227(4)	C2- N1	1.404(4)	C6- N7	1.377(4)	C8- N11	1.298(4)
C11- N9	1.356(4)	C3- N5	1.308(4)	Ca1- N6	2.560(3)	C8- N10	1.340(4)
C11- N10	1.391(4)	C3- N6	1.334(4)	N7- H1	0.81(3)	C8- N8	1.387(4)
C12- O5	1.221(4)	C3- N1	1.409(4)	Ca1- O3	2.571(2)	N10- H3	0.89(4)
C12- N11	1.372(4)	C4- O1	1.239(4)	Ca1- O7	2.666(3)	N12- H2	0.88(4)
C12- N12	1.379(4)	C4- N3	1.359(4)	Ca1- O8	2.328(3)		

Table 32 Selected angles (in °) for $(\text{NH}_4)_2[\text{Zn}(\text{H}_2\text{O})_6](\text{HC}_6\text{N}_7\text{O}_3)_2 \cdot 2\text{H}_2\text{O}$, $[\text{Cu}(\text{NH}_3)_2]_3(\text{C}_6\text{N}_7\text{O}_3)_2 \cdot 2\text{H}_2\text{O}$ and $\text{CaNH}_4(\text{H}_2\text{C}_6\text{N}_7\text{O}_3)(\text{HC}_6\text{N}_7\text{O}_3) \cdot 6\text{H}_2\text{O}$. Standard deviations in parentheses.

$(\text{NH}_4)_2[\text{Zn}(\text{H}_2\text{O})_6](\text{HC}_6\text{N}_7\text{O}_3)_2 \cdot 2\text{H}_2\text{O}$					
O6-Zn1-O6	180	C1-N7-C6	117.5(2)	N2-C1-N1	115.9(2)
O6-Zn1-O4	88.42(9)	C3-N5-C5	118.6(2)	C3-N6-C6	119.6(2)
O6-Zn1-O4	91.58(9)	C1-N1-C3	118.3(2)	H8-O7-H9	111(4)
O6-Zn1-O4	91.58(9)	C1-N1-C2	121.3(2)	N5-C3-N6	120.8(2)
O6-Zn1-O4	88.42(9)	C3-N1-C2	120.5(2)	N5-C3-N1	119.6(2)
O4-Zn1-O4	180	C2-N3-C4	119.7(2)	N6-C3-N1	119.6(2)
O6-Zn1-O5	87.72(8)	C1-N2-C4	123.5(2)	O1-C4-N3	122.4(2)
O6-Zn1-O5	92.28(8)	C1-N2-H1	119(3)	O1-C4-N2	118.5(2)
O4-Zn1-O5	87.45(9)	C4-N2-H1	117(3)	N3-C4-N2	119.1(2)
O4-Zn1-O5	92.55(9)	N4-C2-N3	120.9(2)	O2-C5-N5	119.0(2)
O6-Zn1-O5	92.28(8)	N4-C2-N1	118.8(2)	O2-C5-N4	117.7(2)
O6-Zn1-O5	87.72(8)	N3-C2-N1	120.3(2)	N5-C5-N4	123.2(2)
O4-Zn1-O5	92.55(9)	C2-N4-C5	119.2(2)	O3-C6-N6	119.5(2)
O4-Zn1-O5	87.45(9)	N7-C1-N2	121.3(2)	O3-C6-N7	118.5(2)
O5-Zn1-O5	180	N7-C1-N1	122.8(2)	N6-C6-N7	122.0(2)

7.3 Metal(II) Cyamelurates

[Cu(NH₃)₂]₃(C₆N₇O₃)₂ · 2H₂O					
N8-Cu1-N8	180	C1-N2-C4	120.4(3)	N4-C2-N1	122.0(3)
N8-Cu1-N3	92.63(11)	C1-N2-Cu2	123.7(2)	N3-C2-N1	117.9(3)
N8-Cu1-N3	87.37(11)	C4-N2-Cu2	115.77(19)	N5-C3-N6	121.4(3)
N8-Cu1-N3	87.37(11)	C2-N3-C4	121.0(2)	N5-C3-N1	119.8(2)
N8-Cu1-N3	92.63(11)	C2-N3-Cu1	115.73(19)	N6-C3-N1	118.8(3)
N3-Cu1-N3	180	C4-N3-Cu1	123.28(19)	O1-C4-N3	120.4(3)
N10-Cu2-N9	176.31(12)	C2-N4-C5	118.1(3)	O1-C4-N2	119.1(3)
N10-Cu2-N2	90.83(11)	C3-N5-C5	119.7(3)	N3-C4-N2	120.5(3)
N9-Cu2-N2	92.18(11)	C3-N6-C6	118.2(2)	O2-C5-N4	118.9(3)
N10-Cu2-O3	89.41(11)	C1-N7-C6	117.4(2)	O2-C5-N5	119.2(3)
N9-Cu2-O3	87.33(11)	N7-C1-N2	121.1(3)	N4-C5-N5	121.8(3)
N2-Cu2-O3	172.78(9)	N7-C1-N1	120.1(3)	O3-C6-N6	118.3(3)
C2-N1-C1	121.3(2)	N2-C1-N1	118.9(2)	O3-C6-N7	116.3(3)
C2-N1-C3	118.5(2)	N4-C2-N3	120.1(3)	N6-C6-N7	125.4(3)
C1-N1-C3	120.2(2)				
CaNH₄(H₂C₆N₇O₃)(HC₆N₇O₃) · 6H₂O					
N13-C9-N12	121.5(3)	N6-C6-N7	119.8(3)	O8-Ca1-O12	79.26(9)
N13-C9-N8	124.0(3)	O3-C6-Ca1	60.56(17)	O9-Ca1-O12	146.66(9)
N12-C9-N8	114.5(3)	N6-C6-Ca1	60.37(17)	O10-Ca1-O12	74.35(9)
O6-C10-N14	119.4(3)	O3-C6-N6	119.9(3)	O11-Ca1-O12	75.40(9)
O6-C10-N13	118.9(3)	N7-C6-Ca1	168.5(2)	N6-Ca1-O12	107.11(9)
N14-C10-N13	121.7(3)	C1-N1-C2	118.6(3)	O3-Ca1-O12	75.85(8)
O4-C11-N9	122.4(3)	C1-N1-C3	121.7(3)	O8-Ca1-O7	71.14(9)
O4-C11-N10	118.2(3)	C2-N1-C3	119.6(3)	O9-Ca1-O7	72.75(9)
N9-C11-N10	119.4(3)	C1-N2-C4	117.3(3)	O10-Ca1-O7	137.61(9)
O5-C12-N11	122.4(3)	C2-N3-C4	119.9(3)	O11-Ca1-O7	124.55(9)
O5-C12-N12	119.8(3)	C2-N4-C5	118.6(3)	N6-Ca1-O7	72.24(9)
N11-C12-N12	117.8(3)	C3-N5-C5	118.7(3)	O3-Ca1-O7	72.32(8)
C9-N13-C10	116.8(3)	C3-N6-C6	120.5(3)	O12-Ca1-O7	138.53(8)
C7-N14-C10	120.4(3)	C1-N7-C6	123.2(3)	N14-C7-N9	121.1(3)
N2-C1-N7	121.3(3)	C6-O3-Ca1	94.70(18)	N14-C7-N8	119.0(3)
N2-C1-N1	122.9(3)	O8-Ca1-O9	110.01(11)	N9-C7-N8	119.9(3)
N7-C1-N1	115.8(3)	O8-Ca1-O10	151.09(10)	N11-C8-N10	121.7(3)
N4-C2-N3	121.0(3)	O9-Ca1-O10	86.79(10)	N11-C8-N8	123.1(3)
N4-C2-N1	119.7(3)	O8-Ca1-O11	79.21(9)	N10-C8-N8	115.2(3)
N3-C2-N1	119.3(3)	O9-Ca1-O11	75.17(10)	C8-N8-C9	120.3(3)
N5-C3-N6	121.0(3)	O10-Ca1-O11	82.88(9)	C8-N8-C7	121.7(3)
N5-C3-N1	120.1(3)	O8-Ca1-N6	128.27(9)	C9-N8-C7	118.0(3)
N6-C3-N1	119.0(3)	O9-Ca1-N6	92.24(10)	C7-N9-C11	119.9(3)
O1-C4-N3	120.1(3)	O10-Ca1-N6	71.93(9)	C8-N10-C11	123.9(3)
O1-C4-N2	118.0(3)	O11-Ca1-N6	152.51(8)	C8-N10-H3	126(2)
N3-C4-N2	121.9(3)	O8-Ca1-O3	82.95(9)	C11-N10-H3	110(2)
O2-C5-N4	119.1(3)	O9-Ca1-O3	135.86(9)	C8-N11-C12	119.3(3)
O2-C5-N5	117.7(3)	O10-Ca1-O3	101.56(9)	C9-N12-C12	124.9(3)
N4-C5-N5	123.2(3)	O11-Ca1-O3	148.45(8)	C9-N12-H2	118(2)
O3-C6-N7	120.3(3)	N6-Ca1-O3	51.61(8)	C12-N12-H2	117(2)

In order to investigate a possible magnetic interaction of the Cu^{2+} pairs (distance 4.3 Å) identified by single-crystal XRD magnetic measurements of $[\text{Cu}(\text{NH}_3)_2]_3(\text{C}_6\text{N}_7\text{O}_3)_2 \cdot 2\text{H}_2\text{O}$ were conducted (cf. Figure 85). The magnetic behavior can be described by application of the Curie-Weiss law for temperatures above 150 K resulting in $\Theta = -72.6 (\pm 0.9)$ K and $\mu_{\text{eff}} = 1.986 (\pm 0.003) \mu_{\text{B}}$. This indicates strong antiferromagnetic interactions. Although this finding cannot be directly attributed to the pairs of Cu2 atoms with the magnetic data at hand, such an explanation can be considered to be most likely. Although one would expect a μ_{eff} value of $1.73 \mu_{\text{B}}$ for Cu(II) the determined value is not surprising since experimental values for Cu(II) species are usually found ranging between 1.7 and $2.2 \mu_{\text{B}}$ ^[144] due to spin-orbit-coupling which is in full agreement with the observed data. A deviation from the Curie-Weiss behavior becomes increasingly evident at lower temperatures possibly hinting at a structural transition below 30 K. At temperatures below 9 K antiferromagnetic ordering is observed.

With the data at hand one can easily find certain preferred hydrogen-bonding motifs involving $\text{HC}_6\text{N}_7\text{O}_3^{2-}$ and $\text{H}_2\text{C}_6\text{N}_7\text{O}_3^-$ ions. The predominance of strand-like structures is rather obvious. The preferred arrangement drawn in Scheme 26 can be slightly altered in a way that some hydrogen-bonds are not expressed or by replacing H_2O molecules with NH_4^+ ions in some cases.

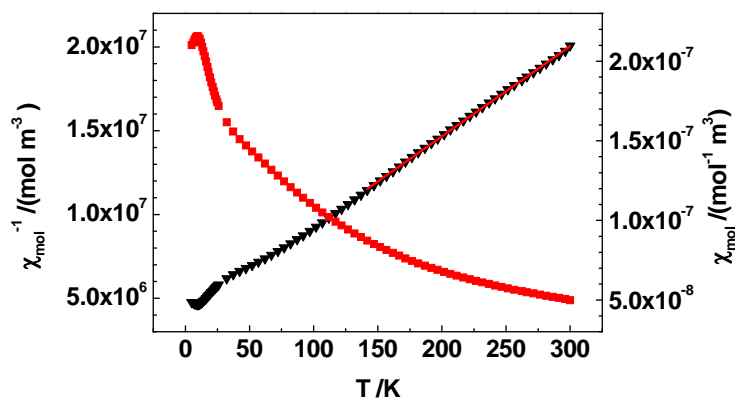
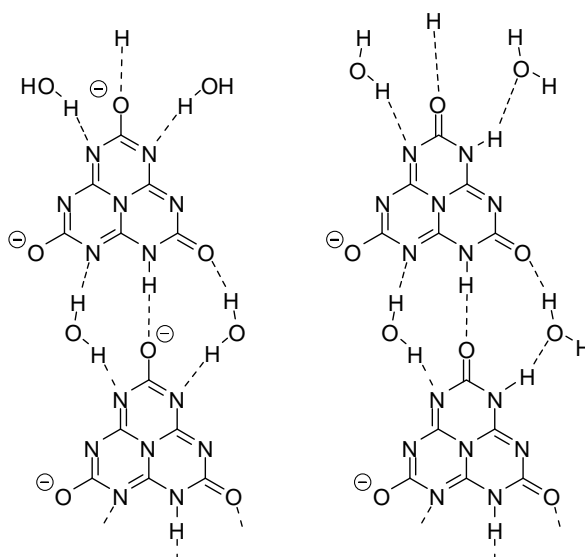


Figure 85. Magnetic properties of $[\text{Cu}(\text{NH}_3)_2]_3(\text{C}_6\text{N}_7\text{O}_3)_2 \cdot 2\text{H}_2\text{O}$. Molar susceptibility (red squares) and inverse molar susceptibility (black triangles) plotted against absolute temperature. Measurement conducted at a flux density of 1 T.

First experiments of using metal cyamelurates as precursors for carbon nitride networks were conducted due to the initial considerations made. After an initial loss of solvate the thermogram of the copper salt shows only a gradual weight loss without any characteristic steps being detectable. In the end only Cu_2O is obtained indicating that no simple condensation reaction has taken place. A reduction of Cu(II) was also observed for the pyrolysis of $\text{Cu}_3(\text{C}_6\text{N}_7(\text{NCN})_3)_2$ yielding metallic copper in this case.^[19b] The effects of these redox processes on the reactivity of cyamelurates remain to be eluded. However, the possibility of allowing more diversity in carbon nitride networks in such a manner seems promising. This clearly illustrates that a lot more work is needed to find suitable precursor species in metal cyamelurates.



Scheme 26. Predominant hydrogen-bonding motifs found for protonated cyamelurate ions. The right hand side displays a motif found for $\text{H}_2\text{C}_6\text{N}_7\text{O}_3^-$ ions while the left hand side shows the one for $\text{HC}_6\text{N}_7\text{O}_3^{2-}$ ions.

7.4 The Cyameluric Acid Adduct

$\text{H}_3\text{C}_6\text{N}_7\text{O}_3 \cdot \text{H}_2\text{NMe}_2\text{Cl} \cdot \text{H}_2\text{O}$

Contents of this section have already been published in advance to this thesis.^[145] The slow hydrolytic decomposition of a solution of cyameluric chloride, $\text{C}_6\text{N}_7\text{Cl}_3$, in DMF subjected to air produced a new compound (cf. Section 12.1.22 for experimental details). The adduct $\text{H}_3\text{C}_6\text{N}_7\text{O}_3 \cdot \text{H}_2\text{NMe}_2\text{Cl} \cdot \text{H}_2\text{O}$ was yielded in crystalline form and was studied by single-crystal XRD (cf. Table 33).

Table 33. Crystallographic data and details of the structure refinement for $\text{C}_6\text{N}_7\text{H}_3\text{O}_3 \cdot \text{H}_2\text{N}(\text{CH}_3)_2\text{Cl} \cdot \text{H}_2\text{O}$.

Formula	$\text{C}_6\text{N}_7\text{H}_3\text{O}_3 \cdot \text{H}_2\text{N}(\text{CH}_3)_2\text{Cl} \cdot \text{H}_2\text{O}$
Molecular weight / g mol^{-1}	320.71
Crystal system	monoclinic
Space group	$P 2_1 / c$ (no. 14)
Lattice parameters / $\text{Å}, ^\circ$	$a = 6.0908(12)$ $b = 22.710(5)$ $\beta = 105.63(3)$ $c = 9.821(2)$
Volume / Å^3	1308.2(5)
Z	4
Absorption coefficient / mm^{-1}	0.326
Density / g cm^{-3}	1.628
Diffractometer	IPDS
Radiation, monochromator	Mo-K $_{\alpha}$ ($\lambda = 71.073$ pm), graphite
Temperature / K	130
Structure solution	SHELXS-97 ^[101] (direct methods)
Structure refinement	SHELXL-97 ^[101] (full-matrix least-squares on F^2)
Corrections	Lorentz, polarisation, absorption
Data / restraints / parameters	2844 / 0 / 242
R-indices	$R1 = 0.0342$ $F_o > 4\sigma(F_o)$ $R1 = 0.0615$ all data $wR2 = 0.0719$ $F_o > 4\sigma(F_o)$ $wR2 = 0.0764$ all data
Goof	0.881
Weighting scheme	$w^{-1} = \sigma^2(F_o^2) + (0.0393P)^2$ with $P = (F_o^2 + 2 F_c^2) / 3$
Largest peak / deepest hole / $e \text{Å}^{-3}$	0.33 / -0.25

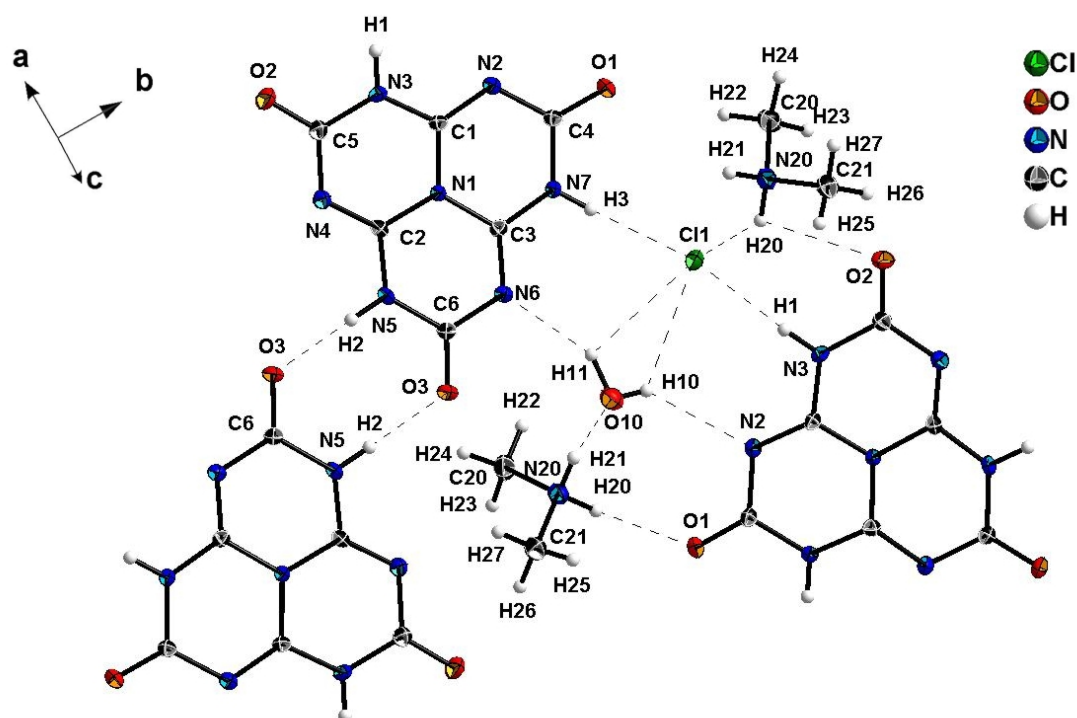


Figure 86. Hydrogen-bonding interactions in $\text{C}_6\text{N}_7\text{H}_3\text{O}_3 \cdot \text{H}_2\text{N}(\text{CH}_3)_2\text{Cl} \cdot \text{H}_2\text{O}$. Ellipsoids for non-hydrogen atoms are drawn at the 50 % probability level.

$\text{C}_6\text{N}_7\text{H}_3\text{O}_3 \cdot \text{H}_2\text{N}(\text{CH}_3)_2\text{Cl} \cdot \text{H}_2\text{O}$ crystallizes monoclinically (space group $P 2_1/c$). The asymmetric unit comprises one molecule of cyameluric acid, a dimethylammonium cation, a chloride anion and one crystal water molecule. With the protonation taking place at the nitrogen atoms of the C_6N_7 -nucleus, the cyameluric acid molecules nearly approach D_{3h} symmetry by slightly bending out of their molecular plane as can be seen in Figure 86 to Figure 88. Two molecules of cyameluric acid are each linked through hydrogen-bridging. These pairs of cyameluric acid molecules are coplanar and inter-connected by hydrogen-bonding to water and the chloride anion (cf. Figure 86), thus establishing a layer-like structure in which the said planes are slightly tilted against each other (cf. Figure 87). The dimethylammonium ions are located between two layers and are connected to these by the split hydrogen-bridge originating from N20-H20 and ending at Cl1 and O1 (cf. Table 34).

Table 34. Hydrogen-bonds ($^\circ$ and \AA) for $\text{C}_6\text{N}_7\text{H}_3\text{O}_3 \cdot \text{H}_2\text{N}(\text{CH}_3)_2\text{Cl} \cdot \text{H}_2\text{O}$ (D = donor, H = hydrogen, A = acceptor).

D-H...A	$\angle \text{D-H}\cdots\text{A}$	D...A	D-H...A	$\angle \text{D-H}\cdots\text{A}$	H...A
N3-H1...Cl1	173.45	3.105	O10-H11...N6	149.03	2.973
N5-H2...O3	177.35	2.870	O10-H11...Cl1	108.01	3.247
N7-H3...Cl1	177.78	3.141	N20-H20...O1	118.07	2.978
O10-H10...N2	139.66	3.051	N20-H20...Cl1	138.02	3.189
O10-H10...Cl1	124.67	3.247	N20-H21...O10	170.16	2.701

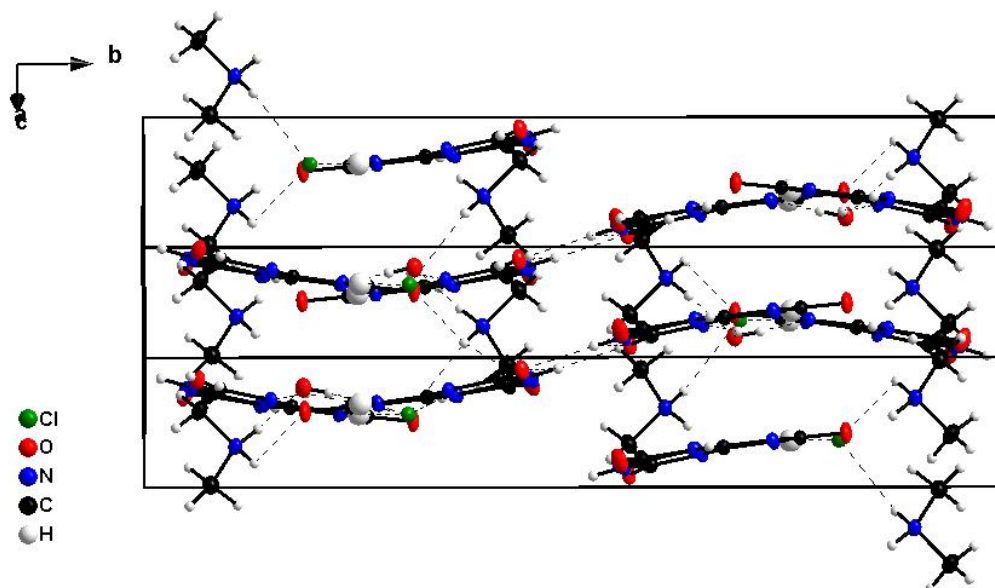


Figure 87. Layer-like arrangement of cyameluric acid molecules in $C_6N_7H_3O_3 \cdot H_2N(CH_3)_2Cl \cdot H_2O$, view along $[20\bar{1}]$.

There is no evidence for rotation of the methyl groups at the temperature of the measurement, thus allowing for an exact localization of the respective hydrogen atoms. The cyameluric nuclei are stacked at an inter-layer distance of approximately 3.2 Å. However with respect to minor overlap between two nuclei π -stacking interactions do not seem to be dominant. The variations of bond lengths within the cyameluric nucleus are in agreement with the proton positions determined. The localized double-bonds are significantly shorter as compared to the other C-N bonds (cf. Table 35). An overview is provided by Figure 88.

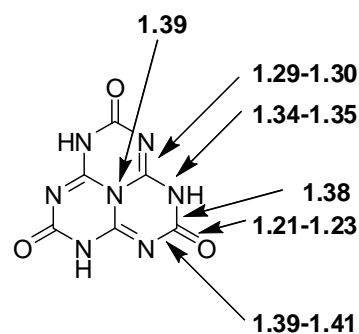


Figure 88. Bond lengths (in Å) for chemically equivalent bonds within the cyameluric acid molecule for $C_6N_7H_3O_3 \cdot H_2N(CH_3)_2Cl \cdot H_2O$.

Table 35. Selected distances (in Å) for $C_6N_7H_3O_3 \cdot H_2N(CH_3)_2Cl \cdot H_2O$, standard deviations in parentheses.

O1-C4	1.214(2)	N4-C2	1.291(3)	O10-H11	0.96(4)
O2-C5	1.218(3)	N4-C5	1.377(3)	N20-C20	1.48.1(3)
O3-C6	1.227(2)	N5-C2	1.350(3)	N20-C21	1.48.1(3)
N1-C3	1.392(2)	N5-C6	1.389(3)	N20-H20	0.97(2)
N1-C2	1.392(2)	N5-H2	0.87(3)	N20-H21	0.93(2)
N1-C1	1.392(2)	N6-C3	1.302(3)	C20-H22	1.01(3)
N2-C1	1.293(2)	N6-C6	1.375(2)	C20-H23	1.00(2)
N2-C4	1.384(2)	N7-C3	1.339(2)	C20-H24	1.03(3)
N3-C1	1.347(3)	N7-C4	1.405(3)	C21-H25	0.97(3)
N3-C5	1.399(2)	N7-H3	0.83(3)	C21-H26	0.96(3)
N3-H1	0.86(3)	O10-H10	0.71(4)	C21-H27	0.94(3)

Table 36. Selected angles (in $^\circ$) for $\text{C}_6\text{N}_7\text{H}_3\text{O}_3 \cdot \text{H}_2\text{N}(\text{CH}_3)_2\text{Cl} \cdot \text{H}_2\text{O}$, standard deviations in parentheses.

C3-N1-C2	119.97(17)	N4-C2-N5	120.91(17)	C20-N20-H20	109.5(14)
C3-N1-C1	119.78(15)	N4-C2-N1	124.40(18)	C21-N20-H20	108.6(15)
C2-N1-C1	119.57(16)	N5-C2-N1	114.69(17)	C20-N20-H21	107.5(15)
C1-N2-C4	118.20(17)	N6-C3-N7	121.31(18)	C21-N20-H21	108.8(15)
C1-N3-C5	125.03(18)	N6-C3-N1	123.71(16)	H20-N20-H21	108.2(19)
C1-N3-H1	117.3(17)	N7-C3-N1	114.98(18)	N20-C20-H22	109.7(15)
C5-N3-H1	117.6(18)	O1-C4-N2	123.13(18)	N20-C20-H23	106.5(15)
C2-N4-C5	118.40(16)	O1-C4-N7	119.15(18)	H22-C20-H23	112(2)
C2-N5-C6	124.81(16)	N2-C4-N7	117.72(16)	N20-C20-H24	110.0(15)
C2-N5-H2	117.5(18)	O2-C5-N4	122.97(18)	H22-C20-H24	108(2)
C6-N5-H2	117.4(18)	O2-C5-N3	119.33(19)	H23-C20-H24	110.4(19)
C3-N6-C6	118.24(17)	N4-C5-N3	117.69(18)	N20-C21-H25	107.2(16)
C3-N7-C4	124.88(18)	O3-C6-N6	122.58(18)	N20-C21-H26	110.3(16)
C3-N7-H3	117.0(19)	O3-C6-N5	119.04(17)	H25-C21-H26	113(2)
C4-N7-H3	118.1(19)	N6-C6-N5	118.36(17)	N20-C21-H27	107.6(17)
N2-C1-N3	121.09(18)	H10-O10-H11	101(3)	H25-C21-H27	112(2)
N2-C1-N1	124.31(18)	C20-N20-C21	114.06(17)	H26-C21-H27	107(2)
N3-C1-N1	114.60(16)				

$\text{C}_6\text{N}_7\text{H}_3\text{O}_3 \cdot \text{H}_2\text{N}(\text{CH}_3)_2\text{Cl} \cdot \text{H}_2\text{O}$ has been synthesized from slightly hydrous DMF solutions. It has also been found that the low solubility of the cyameluric acid trihydrate rendered all efforts of preparing the title compound from aqueous solution unsuccessful. Large crystals of the title compound were accessible by slow hydrolysis of cyameluric chloride by air moisture. The decomposition of DMF into carbon monoxide and dimethylamine is known to be catalyzed by acids and basis.^[146] Thus, the presence of dimethylammonium chloride in solution is due to the prolonged exposure of the solvent to hydrochloric acid.

Upon heating to 800 $^\circ\text{C}$ (cf. Figure 89) $\text{C}_6\text{N}_7\text{H}_3\text{O}_3 \cdot \text{H}_2\text{N}(\text{CH}_3)_2\text{Cl} \cdot \text{H}_2\text{O}$ showed several endothermic decomposition / condensation steps. At 106 $^\circ\text{C}$ the compound releases crystal water (measured weight loss 5.3 %, calc. 5.6 %). This dehydration is followed by three subsequent endothermic effects at 217, 284 and 388 $^\circ\text{C}$, respectively, which altogether account for a weight loss of 44 %. At higher temperatures the compound gradually loses weight until it undergoes total decomposition onsetting at 649 $^\circ\text{C}$.

The FTIR spectrum shows characteristic vibrations^[89] for the constituting molecular entities found in the crystal structure.

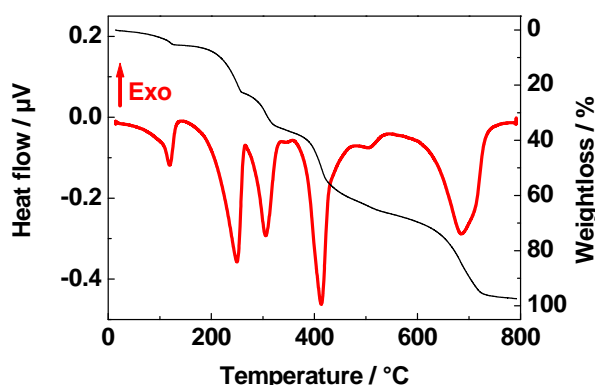


Figure 89. DTA/TG diagram for $\text{C}_6\text{N}_7\text{H}_3\text{O}_3 \cdot \text{H}_2\text{N}(\text{CH}_3)_2\text{Cl} \cdot \text{H}_2\text{O}$. Measurement conducted at a scanning rate of 5 K min^{-1} ; initial weight = 17.41 mg.

Comparison of the structural data of hydrogen-containing cyameluric acid derivatives known so far indicates some general trends. Typically, hydrogen localization has an evident effect on the bond length distribution within the cyameluric nucleus, which is in accordance with the determined tautomer. Therefore, inaccurate proton localization would be conspicuous. The increasing number of examples in the literature suggest that cyameluric acid in particular and perhaps heptazines in general disfavor OH groups as substituents and respective compounds are not likely accessible in the solid-state. However, in the title compound and in several other comparable cases the hydrogen atoms are located in hydrogen bridges. Therein, a double-minimum potential could allow the transition of the keto into the enol-like tautomer (cf. Figure 90).

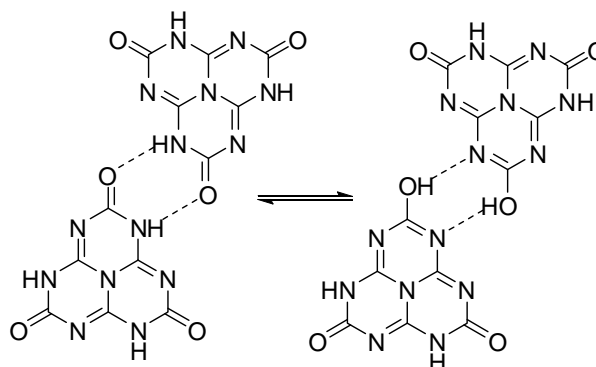


Figure 90. Possible isomerization through double-minimum hydrogen-bonds for cyameluric acid molecules.

Another feature of $C_6N_7H_3O_3 \cdot H_2N(CH_3)_2Cl \cdot H_2O$ is the fact that it is a multi-component adduct. Apparently, heptazines (e.g. cyameluric acid, melam) have a certain tendency for the formation of such adducts due to their inflexible structure and their multiple hydrogen-bonding acceptor and donor positions in one molecule. The rigidity of the molecule hinders the formation of saturated hydrogen-bonding networks in which the molecules are packed in a more space-filling manner. Accordingly, additional components can be incorporated to participate in H-bonds or fill gaps in the structures thus accomplishing a favorable packing. This consideration points towards the existence of other adduct phases incorporating substances capable of building hydrogen-bonding interactions.

7.5 A New Sodium Cyamelurate

A new cyamelurate salt, presumably another sodium melonate was found crystallizing from aqueous solution. The compound was first discovered as a hydrolysis product yielded by the reaction of melon with NaOH. Synthesis of this compound, however, was poorly reproducible under such conditions. The salt $\text{Na}_3\text{C}_6\text{N}_7\text{O}_3 \cdot 4.5\text{H}_2\text{O}$, first described by *Kroke et al.*,^[42] is usually found instead. The new salt was also found under other conditions. Especially solutions containing sodium cyamelurate and additional small amounts of other metal ions (especially Al^{3+} and Zn^{2+}) have shown to yield the compound (cf. Section 12.1.31 for experimental details). The compound was repeatedly yielded in crystalline form as a side product obtained from solutions prepared during the investigations of metal(II) cyamelurates (cf. Section 7.3). Unfortunately crystallographic problems have impeded a satisfactory structural elucidation of the compound. Thus not all structural details could be resolved.

The sodium cyamelurate salt presented in the following definitively crystallizes in a novel structure and is not identical with reported $\text{Na}_3\text{C}_6\text{N}_7\text{O}_3 \cdot 4.5\text{H}_2\text{O}$.^[42] The PXRD diagrams (cf. Figure 91) of the two compounds display vastly different diffraction patterns. Hence the salt actually is a new compound and not merely owed to a misinterpretation of a crystallographic problem or effect randomly occurring for $\text{Na}_3\text{C}_6\text{N}_7\text{O}_3 \cdot 4.5\text{H}_2\text{O}$. The newly identified salt could be prepared in bulk quantities, however, the observed reflections do not exactly match the simulation for single-crystal data. If this is due to impurities or flaws in the current structural models remains unresolved.

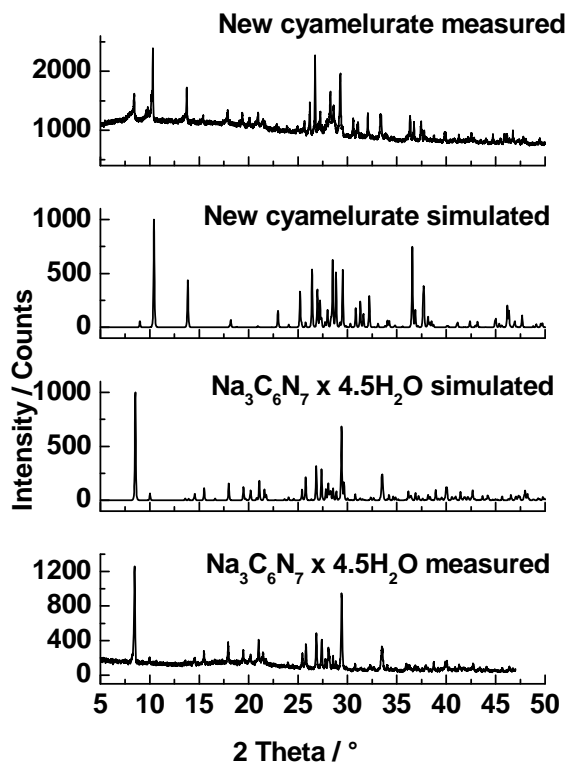


Figure 91. Comparison of measured and simulated (from single-crystal XRD) PXRD patterns ($\text{Cu-K}_{\alpha 1}$ radiation) for the new cyamelurate salt of supposed formula $\text{Na}_3\text{C}_6\text{N}_7\text{O}_3 \cdot 4\text{H}_2\text{O}$ and reported $\text{Na}_3\text{C}_6\text{N}_7\text{O}_3 \cdot 4.5\text{H}_2\text{O}$.

Table 37. Crystallographic data and details for the structure refinement of the new cyamelurate salt of supposed formula $\text{Na}_3\text{C}_6\text{N}_7\text{O}_3 \cdot 4\text{H}_2\text{O}$.

Formula	$\text{Na}_3(\text{C}_6\text{N}_7\text{O}_3) \cdot 4\text{H}_2\text{O}$
Formula weight / g mol^{-1}	359.17
Crystal system	orthorhombic
Space group	<i>Pnma</i> (no. 62)
Lattice parameters / $\text{Å}, ^\circ$	$a = 19.641(4)$ $b = 16.835(3)$ $c = 3.5886(7)$
Volume / Å^3	1186.6(4)
Z	4
Diffractometer	Kappa-CCD
Radiation, monochromator	Mo-K α ($\lambda = 71.073$ pm), graphite
Temperature / K	200
Structure solution	SHELXS-97 ^[101] (direct methods)
Structure refinement	SHELXL-97 ^[101] (full-matrix least-squares on F^2)
Corrections applied	Lorentz, polarization, SCALEPACK ^[96]
Absorption coefficient / mm^{-1}	0.265
Calculated density / g cm^{-3}	2.010
Data / restraints / parameters	1216 / 5 / 128
R-indices	$R1 = 0.0802$ all data $R1 = 0.0655 F_o^2 > 2\sigma(F_o^2)$ (949 reflections) $wR2 = 0.2091$ all data $wR2 = 0.1937 F_o^2 > 2\sigma(F_o^2)$
GooF	1.098 1.099 for 5 restraints
Weighting scheme	$w^{-1} = \sigma^2(F_o^2) + (0.0347)^2 + 0.9416P$ where $P = (F_o^2 + 2F_c^2) / 3$
Largest peak / deepest hole / $e \text{ Å}^{-3}$	0.81 / -0.49

The compound was studied by single-crystal XRD suggesting the formula $\text{Na}_3\text{C}_6\text{N}_7\text{O}_3 \cdot 4\text{H}_2\text{O}$. The structure model presented in the following (cf. Table 37) was solved and refined in the orthorhombic space group *Pnma* (no. 62). The model incorporates some disorder which will subsequently be addressed in more detail. It has not been possible to satisfactorily resolve the disorder by any other means like twinning or different space groups as of now. Due to the observed disorder some minor discrepancies concerning the formula of the compound might be possible.

The structure of the cyamelurate anion (cf. Figure 92) was found identical with other cyamelurate ions presented in the preliminary sections of this chapter as well as in the literature^[41] within the given margin of error. The planar heptazine core is substituted by three oxygen atoms. Bond lengths and angles are observed within normal ranges (cf. Table 38). The oxygen atoms of the crystal water molecules coordinate sodium atoms while the respective H atoms are involved in H-bonding interactions. The N and O atoms of cyamelurate ions are acting as acceptors for the H-bonds. Hydrogen localization for crystal water could not be conducted very precisely. Details for the H-bonding interactions thus have to be regarded with some reservation.

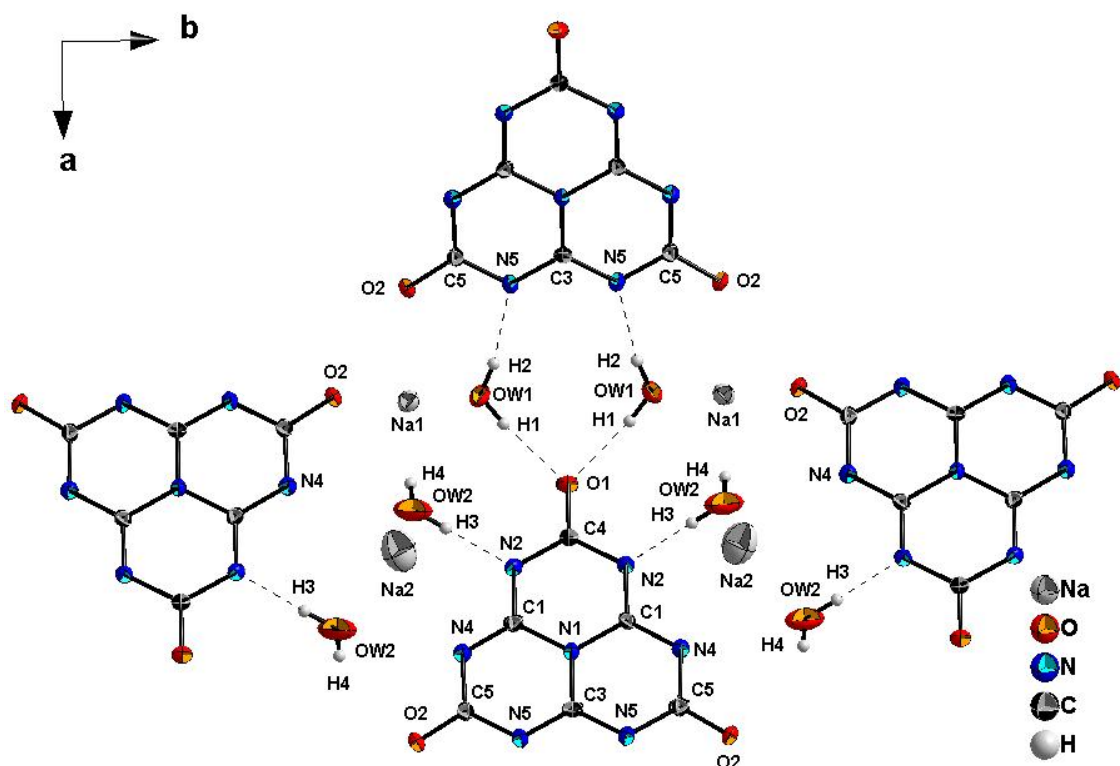


Figure 92. Labeling of atoms and H-bonding interactions for the new cyamelurate salt of supposed formula $\text{Na}_3\text{C}_6\text{N}_7\text{O}_3 \cdot 4\text{H}_2\text{O}$. Ellipsoids for non-hydrogen atoms are drawn at the 50 % probability level

The sodium ion Na1 is octahedrally coordinated by oxygen atoms of crystal water as well as of the cyamelurate ions. The octahedra share common edges assembling an infinite double-band-like structure running along *c* (cf. Figure 93). In contrast to the perfectly ordered Na1 the sodium atom Na2 is found in disordered strands also running along *c*. Na2 is coordinated by three oxygen and three nitrogen atoms forming a distorted capped trigonal bipyramid. The occupancy of Na2 was fixed at 0.5 as is required due to charge neutrality. The closest Na2-Na2 distance is only 1.9 Å (cf. Table 38). Thus two Na2 atoms can never be neighbors. If every second sodium atom is removed two arrangements both featuring corner sharing polyhedra are possible (cf. Figure 94). The strands involving Na1 and Na2 are connected to each other resulting in a stacking of alternating sodium layers and cyamelurate anions.

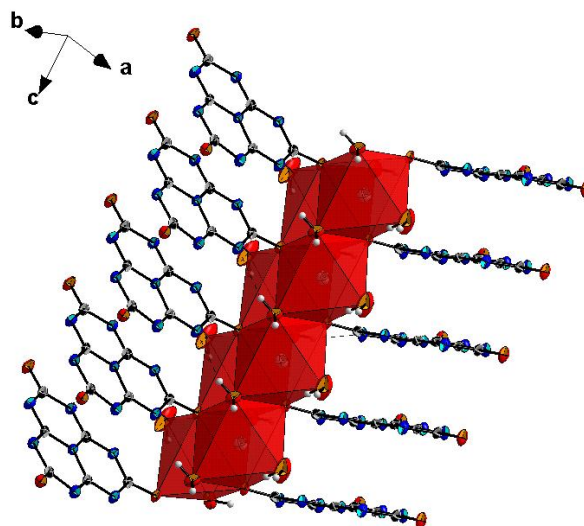


Figure 93. Coordination of atom Na1 as observed in the new cyamelurate salt of supposed formula $\text{Na}_3\text{C}_6\text{N}_7\text{O}_3 \cdot 4\text{H}_2\text{O}$. Ellipsoids for non-hydrogen atoms are drawn at the 50 % probability level

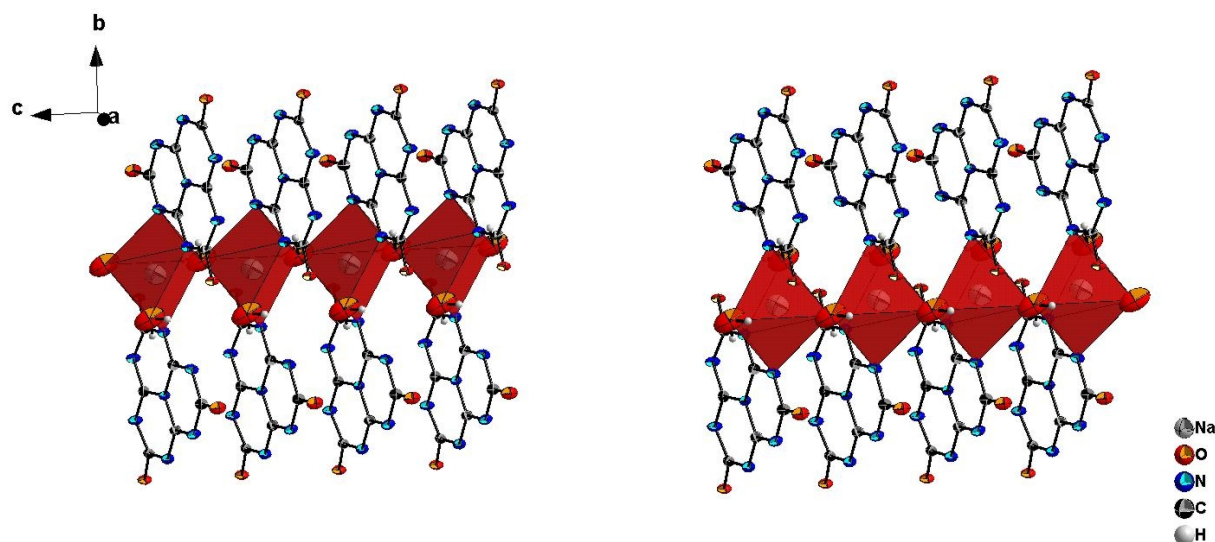


Figure 94. Possible coordination of atom Na2 as observed in the new cyamelurate salt of supposed formula $\text{Na}_3\text{C}_6\text{N}_7\text{O}_3 \cdot 4\text{H}_2\text{O}$. Only one strand-like arrangement (left or right) can be realized for every given strand.

The current model can only offer a tentative structure of the salt as the disorder cannot be sufficiently described or resolved. Additional investigations are required in order to unequivocally establish the structure and formula of this compound.

Table 38. Select distances and angles (in $^\circ$ and \AA) given for the new cyamelurate salt of supposed formula $\text{Na}_3\text{C}_6\text{N}_7\text{O}_3 \cdot 4\text{H}_2\text{O}$. Standard deviations in parentheses.

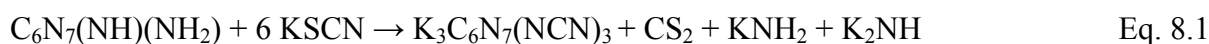
Distances					
Na1-OW1	2.364(3)	Na2-C1	3.031(6)	N1-C1	1.404(3)
Na1-OW1	2.378(3)	O1-C4	1.230(6)	N1-C1	1.404(3)
Na1-OW2	2.365(4)	O2-C5	1.254(4)	N2-C1	1.318(4)
Na1-O2	2.367(3)	O2-Na1	2.367(3)	N2-C4	1.382(3)
Na1-O2	2.446(3)	O2-Na1	2.446(3)	N2-Na2	2.509(6)
Na1-O2	2.478(3)	OW1-Na1	2.364(3)	N4-C1	1.329(4)
Na1-Na2	3.625(6)	OW1-H1	0.802(19)	N4-C5	1.363(4)
Na2-Na2	1.898(11)	OW1-H2	0.800(19)	N4-Na2	2.774(7)
Na2-OW2	1.993(8)	OW2-Na2	1.993(8)	N4-Na2	2.816(6)
Na2-OW2	2.044(8)	OW2-Na2	2.044(8)	N5-C3	1.330(3)
Na2-OW2	2.216(7)	OW2-Na2	2.216(7)	N5-C5	1.369(4)
Na2-N2	2.509(6)	OW2-H3	0.83(2)	C3-N5	1.330(3)
Na2-N4	2.774(7)	OW2-H4	0.82(2)	C4-N2	1.382(3)
Na2-N4	2.816(6)	N1-C3	1.386(6)	C5-N5	1.369(4)
Angles					
H1-OW1-H2	119(4)	C3-N5-C5	118.6(3)	O1-C4-N2	118.9(2)
H3-OW2-H4	105(3)	N2-C1-N4	120.7(3)	O1-C4-N2	118.9(2)
C3-N1-C1	120.06(18)	N2-C1-N1	119.9(3)	N2-C4-N2	122.2(4)
C3-N1-C1	120.06(18)	N4-C1-N1	119.4(3)	O2-C5-N4	118.9(3)
C1-N1-C1	119.9(4)	N5-C3-N5	120.5(4)	O2-C5-N5	118.1(3)
C1-N2-C4	119.1(3)	N5-C3-N1	119.7(2)	N4-C5-N5	123.0(3)
C1-N4-C5	118.8(3)	N5-C3-N1	119.7(2)		

8. Tricyanomelaminates and Melonates

8.1 Formation and Decomposition of Melonates in Salt Melts

8.1.1 General Aspects and Synthetic Procedures

The contents of Chapter 8 have been published in advance to this thesis.^[147] The most commonly used procedure for the preparation of $\text{K}_3\text{C}_6\text{N}_7(\text{NCN})_3$ was described by *Redemann et al.*,^[148] where melon has been successively added to molten KSCN. The reaction occurs upon heating with a Bunsen burner and carbon disulfide is evolved, which instantly ignites, since the reaction is carried out under air. It is difficult to balance a reaction equation by assuming the products to be no more than melonate, CS_2 and NH_3 (which is easily detectable by the alkaline reaction of the evolved gasses). Thus it is manifest that some additional reaction products, decomposition reactions or even some necessary starting materials must also be involved in order to explain the reactivity. Recent works have assumed a formula involving the reaction products KNH_2 and K_2NH (equation 8.1).^[44]



The formation of these products could however not be experimentally verified. This remains the only balanced reaction equation ever given for the title reaction. H_2S or sulfides possibly play a role as reaction products as well. A slight smell of H_2S can often be detected during the course of the reaction and many reaction procedures given in the literature include steps to purify the product from sulfides.

The interesting discovery that the method of preparing the thiocyanate melts using a Bunsen burner is actually a quite smart choice was made during the investigations. When the reaction mixtures are heated in a laboratory furnace oxidation of the thiocyanate forming the respective sulfate is a troublesome side reaction as long as the reaction is performed under air. This is however hardly observed when a Bunsen burner is used since the temperature gradient deriving from the use of this heat source seems to protect the melt from oxidation as the surface is significantly cooler than the lower part of the reaction vessel. The oxidation problem can also be avoided by using inert gas atmosphere or by conducting the reaction on a scale of 50 to 100 g (as is described in most literature procedures), thus reducing the proportion of surface to volume.

In order to broaden the applicability of the reaction the behavior of melon in cyanate melts was investigated. Such a reaction procedure would eliminate or mitigate some unfavorable aspects of the original setup like the evolution of CS_2 , sensitivity to oxidation by air or the corrosive behavior of the melt towards metals due to formation of the respective metal sulfides. Most fortunately the reaction protocol used for KSCN melts can be easily applied to KOCN melts as well. As it was possible to yield potassium melonate this way the reaction was studied in more detail in order to determine other possible alterations of the reaction

setup. The cation component of the melts was also altered by employing Na^+ . Upon addition of melon NaSCN melts show a behavior much alike the one of KSCN melts finally yielding sodium melonate. For NaOCN , however, the situation is somewhat more complicated as will be shown below. The formation of tricyanomelamine ions was observed in this case and for KOCN melts at higher temperatures as well. For experimental details please refer to Sections 12.1.23 – 12.1.27.

8.1.2. Thermal Analysis

A major weak point of most research provided on the synthesis of melonates so far is the lack of exact data on the reaction conditions and the progress of the reaction. Temperatures have only been given very roughly by referring to optical assessments of the reaction process, like presence or absence of red heat when observing the Bunsen burner heated reaction. Some more detailed temperatures are given by *Kroke et al.*,^[44] but do not cover all reaction conditions discussed in this work. Thus a series of thermoanalytical experiments was conducted in order to provide more detailed information on the course of the reaction. Thermograms of each salt were collected as a reference, in order to allow the distinction between the thermal events of the pure melt and the reactivity of the mixture. As can be seen the salts melt at their respective melting points which are in agreement with given literature values.^[149-151] Decomposition of the melts takes place commencing in the higher region of the temperature range studied (cf. Figure 95, Figure 96). The decomposition of the potassium (thio)cyanate melts has been shown to yield cyanides and elemental sulfur / oxygen (cf. equation 8.2-8.3),^[151b] while different decomposition routes have been reported for NaOCN (equation 8.4).^[151a]



Reaction mixtures with molar ratios of 4 ($\text{SCN}^-/\text{OCN}^-$) to 1 (melon) were used for all experiments. The molar mass of the idealized melon monomer was used for stoichiometric calculations in this regard. Small samples were chosen for mixtures containing SCN^- due to the deteriorating effect of the CS_2 evolved during the course of the reaction on the platinum parts of the DTA rod.

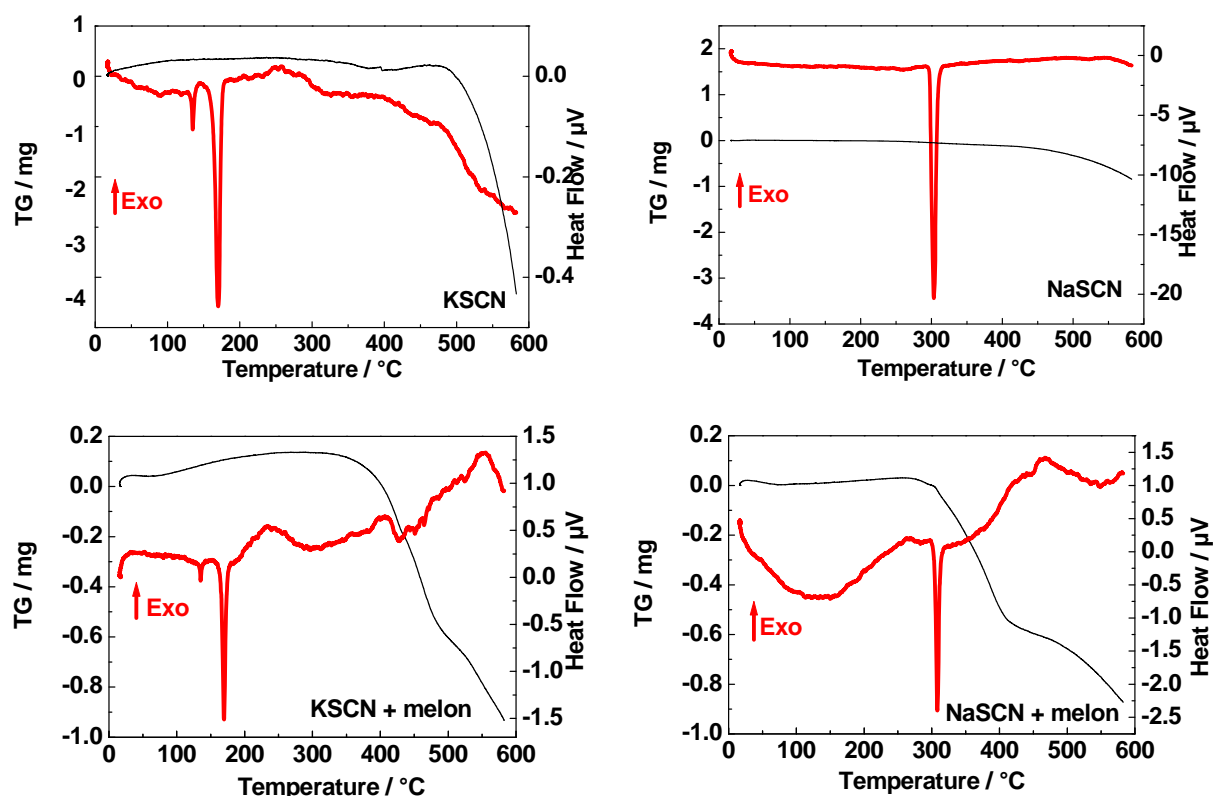


Figure 95. Thermograms for pure thiocyanate melts (top) and melon / thiocyanate mixtures (bottom). Heat flow curves are drawn in bold (red), TG curves are drawn in narrow (black). Thermograms were measured at a scanning rate of 10 °C min^{-1} . Initial weights are: KSCN = 13.9, NaSCN = 20.45, KSCN / melon = 5.5, NaSCN / melon = 5.0 mg.

The thermal behavior of both sodium and potassium thiocyanate / melon mixtures was studied first by using thermal analysis (cf. Figure 95). The principal course of the reaction is identical for both salts while temperatures vary. No reaction takes place below the melting point of the thiocyanates. The endothermic heat flow signal observed in reactions involving KSCN at ca. 133 °C (lit. values range between 140 and 146 °C)^[149b] has to be attributed to the order-disorder transition observed for this compound and is followed by melting at about 165 °C (lit. value = 173 °C)^[149]. The reaction itself onsets around 400 °C (calculated value based on the TG curve). Unfortunately, the heat flow signal could not be well resolved due to kinetic aspects (probably slow reaction rates) and limited sample sizes. No plateau is reached after this reaction and a slow weight loss is observable until decomposition of the melt itself commences at around 500 °C .

For NaSCN mixtures melting is observed at 304 °C (lit. values vary significantly and are reported between 287 ^[151] and 323 °C)^[149]. Unlike the observations for KSCN melts reaction takes place almost immediately after the melt has formed (onset based on TG at 322 °C) and is concluded at around 420 °C . Decomposition of a pure NaSCN melt onsets earlier ($\approx 450\text{ °C}$) than is the case for KSCN.

After identification of reaction temperatures experiments were conducted for identical SCN^- / melon mixtures at these distinct temperatures using a muffle furnace. By these experiments, the initial weight loss could be clearly associated with the formation of the melonate salts. The nature of the decomposition reactions associated with the weight loss of the melonate-containing melts could however not be elucidated this way, due to the negative effect of oxidation reactions. An intense blue color was detectable for all melts containing SCN^-

during the course of the reaction. However, the blue intermediate could not be preserved and the melts lost color, even if they were rapidly quenched using liquid nitrogen.

Potassium melonate could be yielded by reaction of melon with molten potassium cyanate. As a result this reaction was studied in more detail using thermal analysis (cf. Figure 96). The potassium cyanate / melon mixtures show a melting signal of KOCN at 305 °C slightly lower than the pure salt due to melting point depression. At about 368 °C an endothermic reaction associated with weight loss occurs. The mixture gradually loses more weight upon heating. At above 650 °C the degradation of the melt itself commences thus further increasing the weight loss. Due to the slowness of the process no individual reactions could be resolved in the heat flow signal in this temperature range.

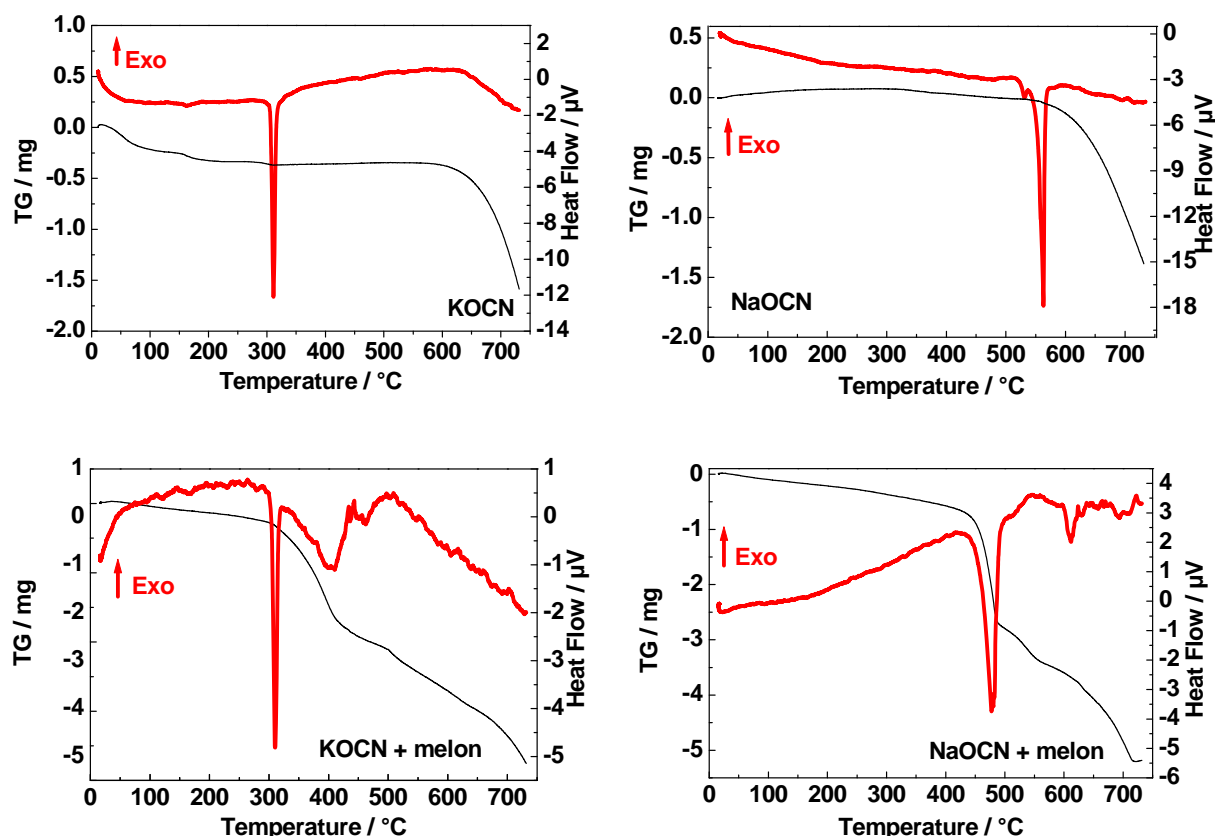


Figure 96. Thermograms for pure cyanate melts (top) and melon / cyanate mixtures (bottom). Heat flow curves are drawn in bold (red), TG curves are drawn in narrow (black). Thermograms were measured at a scanning rate of 10 °C min⁻¹. Initial weights are: KOCN = 9.45, NaOCN = 11.89, KOCN / melon = 11.46, NaOCN / melon = 10.55 mg.

Based on these findings a couple of reactions in a muffle furnace were conducted using identical mixtures of melon and KOCN at select temperatures. Thus optical assessment of the reaction mixture was allowed and the products of different reaction steps could be isolated. Taking all data into account the course of the reaction can be understood in some detail. A cyanate melt can only dissolve a very limited quantity of melon. At first no reaction is observed. A comparably fast reaction yielding potassium melonate is observed quite early. This reaction is accompanied by an evolution of gases noticeable by a temporarily foaming of the melt. This step is usually concluded in a matter of no more than a few minutes. If the melt is heated well beyond the initial reaction temperature and maintained at that temperature for a prolonged time no melonate can be observed any longer upon cooling to room temperature. However potassium tricyanomelaminates has formed instead. Since this conversion happens

quite slowly, this conversion should be assigned to the gradual weight loss found in the TG curve.

The situation is somewhat different when sodium cyanate is used in comparison to all other mixtures studied. The melting point of NaOCN is significantly higher than that of KOCN and thus well beyond the reaction temperatures observed for the formation of $K_3C_6N_7(NCN)_3$ in KOCN melts. A melting point of 549 °C was measured in the experiment, confirming literature values of 550 °C.^[150] A rather weak endothermic event (onset = 520 °C) overlapping with the melting signal was also detected. It was not possible to find any reference for this thermal event in the literature. This signal is probably related to a phase transition. For the reactive mixture an endothermic reaction associated with a notable weight loss is observed around 458 °C, thus much lower than the actual melting point of pure sodium cyanate. In a control experiment at the given temperature the sodium cyanate / melon mixture partially melts, yielding a product of rubber-like consistency (at the respective temperature). Evolution of gases is also easily detectable. This product solidifies again upon further heating and stays solid well beyond the melting point of pure NaOCN. No melting occurs below 601 °C. The melting of the mixture at that temperature is also associated with the degradation of the C/N species only leaving NaOCN after a prolonged time at this temperature. Sodium tricyanomelaminates is the only product that could be isolated from mixtures of NaOCN and melon so far. This can be rationalized by comparison to the experiments conducted for the potassium salt. Due to the high melting point of NaOCN a reaction can only occur at temperatures high enough to favor the degradation of melonates into tricyanomelaminates thus rendering sodium melonate not accessible by this reaction.

Current investigations have not dealt with sodium melonate. The compound was reported to crystallize from water forming a pentahydrate.^[82] The analytical results of hydrated sodium melonate yielded from NaSCN melts during this work are, however, more in line with a hexahydrate (cf. Table 39).

Table 39. Elemental analysis of sodium melonate.

	N / wt. %	C / wt. %	H / wt. %	Na / wt. %	drying loss / wt. % ^[a]
observed	38.69	22.70	2.75	14.36	23.6
$Na_3C_6N_7(NCN)_3 \cdot 5H_2O$	40.53	24.06	2.24	15.35	20.0
$Na_3C_6N_7(NCN)_3 \cdot 6H_2O$	38.97	23.13	2.59	14.76	23.1
$Na_3C_6N_7(NCN)_3 \cdot 7H_2O$	37.52	22.28	2.91	14.21	26.0

[a] Calculated for complete solvent loss and measured by DTA/TG.

The DTA/TG diagram of sodium melonate (cf. Figure 97) shows that the dehydrated compound is stable until about 640 °C; above this temperature it melts and decomposes.

8.1.3 Mechanistic Considerations

Detailed mechanistic considerations regarding the reaction of melon in thiocyanate melts have not been reported. With the data at hand, it is hardly possible to devise a mechanism explaining the described reactivity free of doubt or room for alternative assumptions. However, as some important discoveries have been made, reaction mechanisms should be discussed to a certain extent. In order to provide a basis for mechanistic considerations some possible explanations for the formation of melonate salts will be addressed as follows.

The reaction can tolerate a variety of educts. It is not necessary that the mechanism for OCN^- and SCN^- melts is similar. This assumption should, however, be made as a first hypothesis. In order to assess the plausibility of certain products, some experiments regarding the reactions of thiocyanate melts towards certain species considered likely to occur as intermediates in a reaction mechanism were made (cf. Section 12.1.28). All experiments were conducted under the same conditions used for the classic synthesis of potassium melonate since most data is available for this reaction.

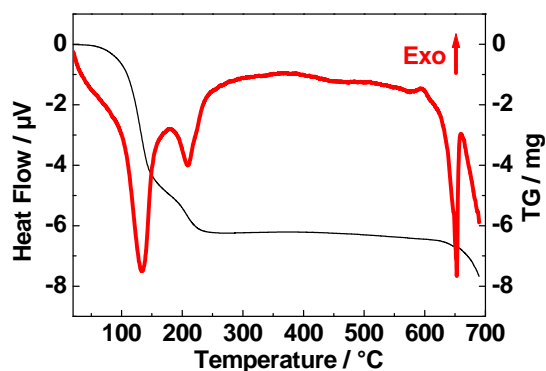
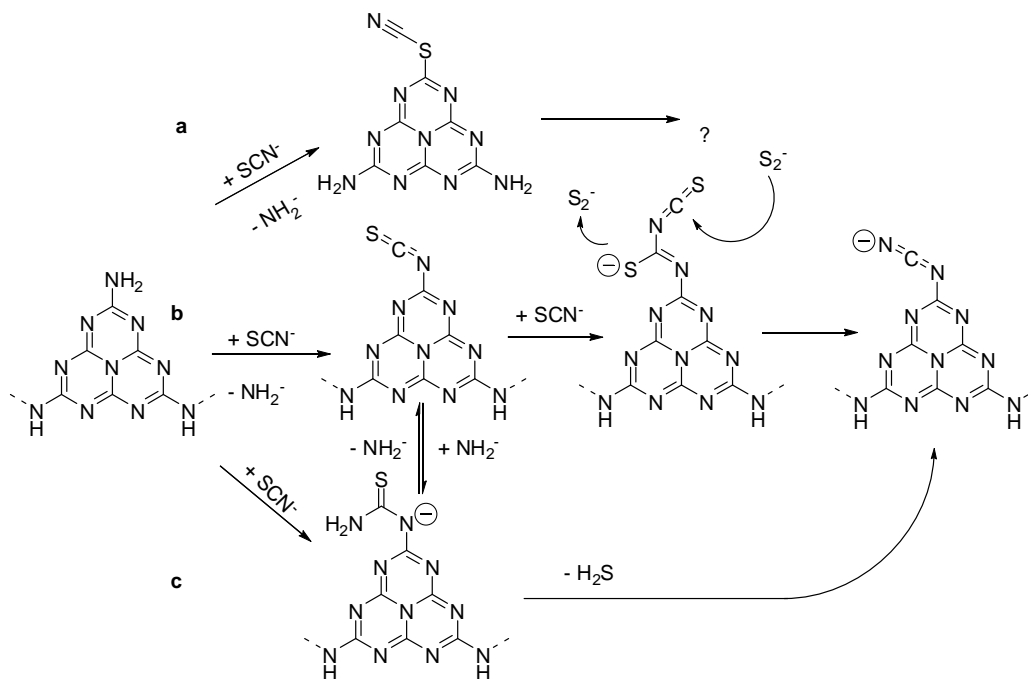


Figure 97. DTA / TG diagram for $\text{Na}_3\text{C}_6\text{N}_7(\text{NCN})_3 \cdot 6\text{H}_2\text{O}$. Heat flow curve is drawn in bold (red), TG curve is drawn in narrow (black). Thermogram was measured at a scanning rate of $5\text{ }^\circ\text{C min}^{-1}$; initial weight = 26.4 mg.

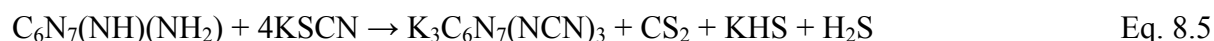


Scheme 27. Possible mechanisms for the observed reactivity of the thiocyanate anion towards melon. Mechanisms **b** and **c** are explaining the formation of cyanamide groups.

When discussing the following mechanisms one must be aware of the fact that they include two assumptions not to be confirmed at the moment. The first one is that the heptazine core is retained during the formation of melonates, and reactivity can thus be explained by cleavage of the polymer chain of melon and derivatization of the amino groups. The second hypothesis is that the reactive component is thiocyanate itself and not some other species formed by beginning decomposition of the melt or any other in-situ activation step. When one considers the possibilities of the SCN^- (or OCN^-) ion for attacking melon, some species seem likely to occur during the reaction (cf. Scheme 27). A nucleophilic substitution at the heptazine core could occur possibly yielding a (thio)cyanate (route **a**) or an iso(thio)cyanate species (route **b**). Any convenient explanation how the thiocyanate presented in route **a** could transform into a cyanamide group of a melonate anion can, however, not be offered. Thus such a mechanism cannot be considered a good explanation for the observed reactivity. It could however be an initial source of NH_2^- anions for other mechanistic routes.

The isothiocyanate (route **b**) could possibly react forming a cyanamide by first consuming a second equivalent of SCN^- and afterwards releasing CS_2 in the presence of sulfides. An addition of SCN^- to a NH_2 group forming a thiourea intermediate that could decompose into a NCN^- group and H_2S (route **c**) might also be possible.

Cleavage of the polymer chain of melon is most likely explained by a possible nucleophilic substitution of the NH groups, allowing a reaction comparable to route **b** in Scheme 27 to follow. This would probably result in the following reaction (Equation 8.5) taking place for route **c**.



The reaction equation offered by *Kroke* et al. (cf. equation 8.1) would result from reaction route **b** taking place.

The evolution of CS_2 needs to be explained by the mechanism since it is constantly observed for all reaction conditions involving thiocyanates no matter whether melon, melem or other C/N/H compounds (like melamine) are present. The fact that a SCN^- melt evolves CS_2 when treated with melem and not melon shows that route **c** cannot offer a complete description of the observed reactivity. Otherwise only H_2S should have been detected in such a case as cleavage of the polymeric melon could not result in other reactions possibly yielding CS_2 . As no evolution of CS_2 was detected upon adding a source of sulfides ($\text{Na}_2\text{S} \cdot \text{H}_2\text{O}$) to a KSCN melt under comparable conditions a reaction of the H_2S with the thiocyanate melt eventually evolving the CS_2 can be considered unlikely.

Route **b** also has its setbacks as the postulated NH_2^- (and NH^{2-} if one takes cleavage of the heptazine chain into account) species certainly are reactive towards melon and / or the melt and additional steps thus should be necessary to explain their further reactions. Also a source of the sulfide ions discussed in the mechanism needs to be explained to suggest the likelihood of such a reaction. A combination of both mechanisms could perhaps be possible. In such a case H_2S from route **c** could react with NH_2^- from route **b** yielding S^{2-} and NH_3 thus generating a sufficient amount of sulfides.

tricyanomelaminates in molten KOCN, which were conducted at 500 °C, the starting material is on the border of its thermal stability. It thus seems likely that melonate is initially broken down into smaller, probably acyclic ions like cyanamides, dicyanamides or dicyandiamides (or a mixture of such). These species can subsequently form tricyanomelaminates much alike the mixtures described above. It is possible to devise a balanced reaction equation for this decomposition involving no more starting materials than potassium melonate and potassium cyanate (cf. equation 8.9). It is, however, not possible to give further proof or mechanistic details for this equation.



The source of the blue color still remains to be determined. This intermediary coloring of the melt only occurs for SCN^- melts while OCN^- melts do not show this phenomenon. An intense blue color can also temporarily occur upon addition of several other compounds to a SCN^- melt.

Based on the thermal condensation leading from melamine to melem and melon one may believe that heptazine-based molecules are always favored over triazines when temperature is increased. The reactivity leading to tricyanomelaminates in cyanate melts shows that accepting this to be a general principle applicable under all circumstances, however, is a rash assumption. As the properties of salt melts are fundamentally different to those within a sealed glass ampoule used for condensation reactions, many conclusions previously drawn do not necessarily apply to reactions in a melt. Under the conditions studied in this work polymeric heptazines are broken down into molecular heptazine species and upon further heating into molecular triazine species. In some sense this is the inversion of the reactivity known to take place in sealed glass ampoules.

8.2 Anhydrous Potassium Melonate - $\text{K}_3\text{C}_6\text{N}_7(\text{NCN})_3$

When a hot, fully reacted melt containing potassium melonate in potassium thiocyanate is slowly cooled to room temperature, crystals of anhydrous potassium melonate have been obtained. This compound is moderately hygroscopic, forming the pentahydrate if subjected to air for a prolonged time. However, the formation of the hydrate is favored by the hygroscopic nature of the melt itself, thus the crystals quickly decay when not separated from the melt. As can be proved by powder XRD the crystals collected from the melt display the same structure as the anhydrous melonate prepared by drying of the pentahydrate. Experimental details are presented in Section 12.1.23.

Table 40. Crystallographic data and details of the refinement procedures for $\text{K}_3\text{C}_6\text{N}_7(\text{NCN})_3$.

Formula	$\text{K}_3\text{C}_6\text{N}_7(\text{NCN})_3$
Formula weight / g mol^{-1}	407.52
Crystal system	monoclinic
Space group	$P2_1/c$ (no. 14)
Lattice parameters / $\text{Å}, ^\circ$	$a = 1321.3(3)$ $b = 1755.6(4)$ $\beta = 114.17(3)$ $c = 1311.4(3)$
Crystal size / mm^3	0.03 x 0.08 x 0.31
Volume / Å^3	2775.4(13)
Z	8
Absorption coefficient / mm^{-1}	1.011
F(000)	1616
Diffraction, radiation	Kappa-CCD, Mo- K_α ($\lambda = 71.073$ pm), graphite monochromator
Temperature / K	200
Theta range / $^\circ$	3.31 to 27.49
Structure solution	SHELXS-97 ^[101] (direct methods)
Structure refinement	SHELXL-97 ^[101] (full-matrix least-squares on F^2)
Corrections	Lorentz, polarization, SCALEPACK ^[96]
Data / restraints / parameters	6355 / 0 / 451
R-indices	$R1 = 0.0384$ $F_o > 4\sigma(F_o)$ (4756 reflections) $R1 = 0.0612$ all data $wR2 = 0.0890$ $F_o > 4\sigma(F_o)$ $wR2 = 0.985$ all data
GooF	1.047
Largest peak deepest hole / $e \text{ Å}^{-3}$	0.714 / -0.610

Potassium melonate crystallizes in the monoclinic space group $P2_1/c$. Consisting of a cyameluric nucleus typical for all heptazines which is substituted by three cyanamide groups, the molecular structure of the melonate ion is as expected (cf. Figure 98). The asymmetric unit comprises two different melonate anions since two different rotamers of the $\text{C}_6\text{N}_7(\text{NCN})_3^{3-}$ ion are stabilized alongside each other in the solid state (cf. Figure 98). One of them is of slightly distorted C_{3h} symmetry, allowing the three $\text{N-C}\equiv\text{N}$ groups to maintain maximum distance from each other and essentially maintaining the planarity of the molecule. The other rotamer brings two cyanamide groups into closer proximity, thus deviating from planar geometry by tilting $\text{N}(21)\text{-C}(16)\equiv\text{N}(26)$ notably out of plane. This conformation thus only slightly resembles C_s - the symmetry the idealized planar molecule would exhibit. The occurrence of similar rotamers has also been reported for tricyanomelaminates. Examples are:

$(C_s)^{[22a]}$ and $(C_{3h})^{[22c]}$ No tricyanomelaminat expressing both rotamers of its anion side by side has been described so far. Hydrated potassium melonate crystallizes displaying the higher symmetric rotamer alone.^[44]

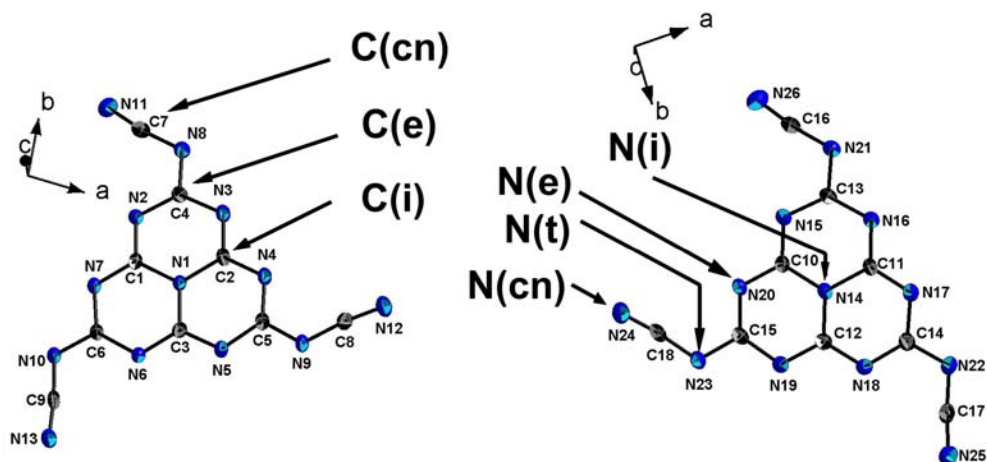


Figure 98. Molecular structure of the two rotamers of the melonate ion derived from single-crystal XRD. Ellipsoids for non-hydrogen atoms are drawn at 50 % probability level. Chemically equivalent atoms are labeled in accordance to the depicted formalism.

The data at hand show that for melonates the C_s conformation can be assumed and that since both conformations can exist alongside each other it is not significantly disfavored to the C_{3h} rotamer. The rotation of the cyanamide groups only seems to result in minor energetic preferences, thus allowing coordination and packing effects to determine the resulting molecular conformation.

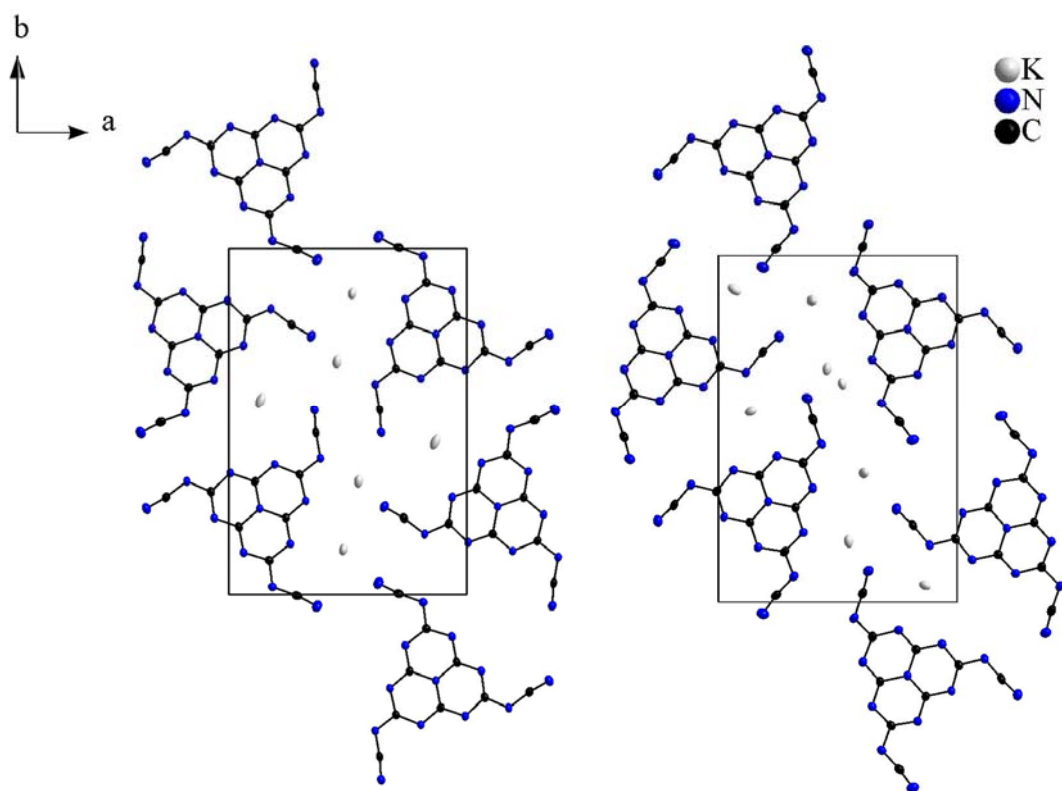


Figure 99. Two different layers of melonate anions in $K_3C_6N_7(NCN)_3$. Each layer contains only one rotamer of the anion. View along the c axis. Molecules in other layers are omitted for clarity.

Bond lengths and angles between chemically equivalent atoms are found to be almost identical. Unless noted otherwise only averaged values are used in the following discussion (cf. Table 41). The structure of the cyameluric nucleus resembles the geometry found in the pentahydrate and in other heptazines. It is almost planar, all angles are close to 120° . Similarly with other melonates the bond lengths between the central nitrogen atom and the neighboring carbon atoms are notably longer than the other bonds in the nucleus which have bond lengths between those expected for C-N single and double-bonds. The cyanamide residues are almost linear with an average angle of 173.4° at the central carbon atom. The average $\text{C}\equiv\text{N}$ bond length is 1.158 \AA . The melonate anions are stacked perpendicular to c at a distance of 3.28 \AA (one quarter of c). The K^+ ions are located between these stacks. This nicely illustrates that π -stacking becomes the predominant structure-directing interaction since hydrogen-bonding is impossible. Taking recent works on interactions between aromatic molecules^[152] into account, however, a significant energetic preference of melonate stacks is not to be expected. This finding is comparable to the situation reported for triazido heptazine^[49] whereas trichloro heptazine^[20,48] expresses short $\text{N}\cdots\text{Cl}$ contacts rather than π -stacks.

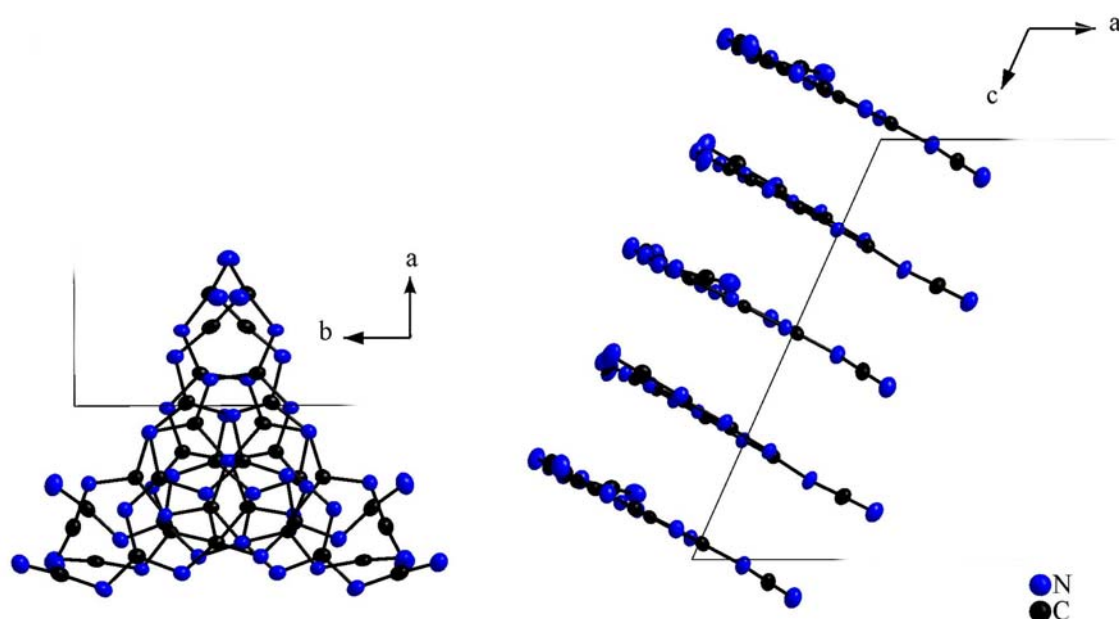


Figure 10. Stacking of melonate ions found in $\text{K}_3\text{C}_6\text{N}_7(\text{NCN})_3$. View along the c axis (left) and b axis (right). Only one stack is shown, other unit cell contents are omitted for clarity. Only a fraction of the unit cell is displayed.

The K^+ ions are coordinated by five to seven nitrogen atoms in asymmetric coordination spheres. All nitrogen positions, except the central atom of the cyameluric nucleus, take part in the coordination of potassium. Potassium-nitrogen distances are relatively long, ranging from 2.802 to 3.179 \AA .

8.2 Anhydrous Potassium Melonate - $K_3C_6N_7(NCN)_3$

Table 41. Distances and angles (in Å and °) between selected chemically equivalent atoms in $K_3C_9N_{13}$. For atom assignments please refer to Figure 98.

Distances		Angles	
N(i)-C(i)	1.393 - 1.407	C(i)-N(i)-C(i)	119.3 - 120.4
C(i)-N(c)	1.316 - 1.342	N(i)-C(i)-N(c)	119.2 - 120.3
N(c)-C(e)	1.349 - 1.368	N(c)-C(i)-N(c)	120.3 - 121.0
C(e)-N(e)	1.329 - 1.348	C(i)-N(c)-C(e)	116.8 - 118.1
N(e)-C(cn)	1.313 - 1.335	N(c)-C(e)-N(e)	124.8 - 125.2
C(cn)-N(cn)	1.155 - 1.163	C(e)-N(e)-C(cn)	116.3 - 118.9
		N(e)-C(cn)-N(cn)	172.3 - 175.2

9. Other Reactions of Heptazines

9.1 Cyameluric Chloride $C_6N_7Cl_3$

The introduction has already addressed cyameluric chloride (also known as trichloro heptazine, $C_6N_7Cl_3$) as a valuable reactive intermediate allowing a variety of reactions. Some synthetic approaches towards $C_6N_7Cl_3$ have been reported in the literature. Some of these reactions were reproduced and eventually altered in order to assess their use for obtaining $C_6N_7Cl_3$. A brief summary on the results of these experiments will be given in the following. For further experimental details cf. Section 12.1.32.

The reaction of the alkali metal cyamelurates $Na_3C_6N_7O_3$ and $K_3C_6N_7O_3$ with solid PCl_5 in closed reaction vessels is commonly reported.^[20,49,52] No specific reaction equations have been given by preliminary works, but a reaction according to the following equation can be expected.



Many protocols report a pressure buildup during the course of the reaction. If both starting materials as well as the reaction vessel were sufficiently dried no significant pressure buildup could be observed in this work. Otherwise HCl liberated by hydrolysis of PCl_5 could probably be responsible for a drastic increase in pressure. The resulting alkali chlorides and remaining phosphorous compounds could be removed by washing with ice water without noticeable decomposition if the washing step was conducted fast and the resulting product was dried in vacuo. However, incomplete reactions showing much residual cyamelurates could be observed when the starting materials were not sufficiently mixed. Judging from optical assessment of the progressing reaction $POCl_3$ (created in situ, cf. Eq. 9.1) served as a solvent and notably promoted the reaction. If cyameluric acid was used instead of its salts, no chloride salts are formed eliminating the need for a washing step.



The reaction can, however, hardly be handled in closed reaction vessels as significant amounts of hydrogen chloride are evolved (cf. Eq. 9.2).

The use of *o*-dichloro benzene as a solvent for the synthesis of $C_6N_7Cl_3$ has also been reported.^[153] This reaction can be easily performed starting from both cyameluric acid and its salts and yields cyameluric chloride in all cases. The product is, however often contaminated with a significant amount of impurities^[s] and complete removal of the solvent is very time consuming. Thus, this reaction setup cannot be recommended in most cases. Probably the best reaction procedure currently available for the chlorination of cyameluric acid is the applica-

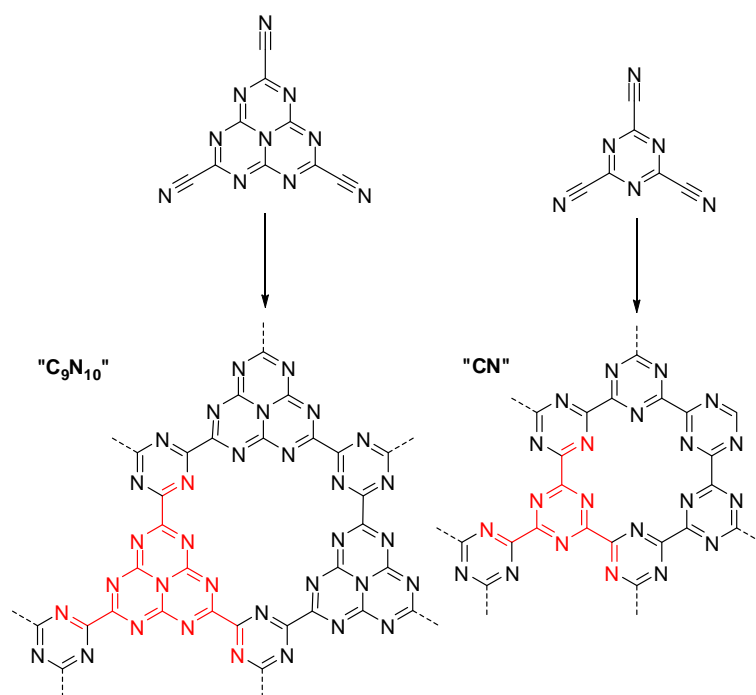
[s] Especially significant amounts of phthalic acid anhydride have been identified in the resulting products. The formation of this compound cannot be explained in detail at the moment. Some sort of decomposition of the solvent, however is the most plausible source of this impurity.

tion of PCl_5 as chlorination agent while using $POCl_3$ as a solvent. Such a course of reaction has been claimed in a patent application.^[154] The reaction tolerates cyameluric acid as well as (anhydrous) sodium or potassium cyamelurate. It is conducted under reflux conditions (boiling point of $POCl_3 = 105.3\text{ }^\circ\text{C}$).^[155] After removal of all volatiles in vacuo pure cyameluric chloride or a mixture of cyameluric chloride and $NaCl / KCl$ is yielded respectively. The cyameluric chloride thus prepared was usually synthetically pure without further purification. Other (weaker) chlorination agents than PCl_5 (like pure $POCl_3$) only resulted in a minimal inter-conversion of cyameluric acid and are thus not applicable for the preparation of cyameluric chloride. This also shows that $POCl_3$ formed by reaction of PCl_5 remains unreactive towards the starting materials and accordingly supports equations 9.1 and 9.2 by showing that $POCl_3$ can be considered a final reaction product. Reactions dealing with the formation of cyameluric chloride while not starting from cyameluric acid derivatives are rarely found. Only one reference describes pyrolysis of cyanogen chloride as a source of $C_6N_7Cl_3$.^[156] Small quantities of cyameluric chloride were also observed as pyrolysis product of cyanuric chloride.^[48]

Further purification of cyameluric chloride can be achieved by sublimation. This is, however, associated with a significant loss of product. An alternative method for removing salts, apart from the abovementioned washing with water, is Soxhlet extraction with aromatic solvents like toluene or benzene.

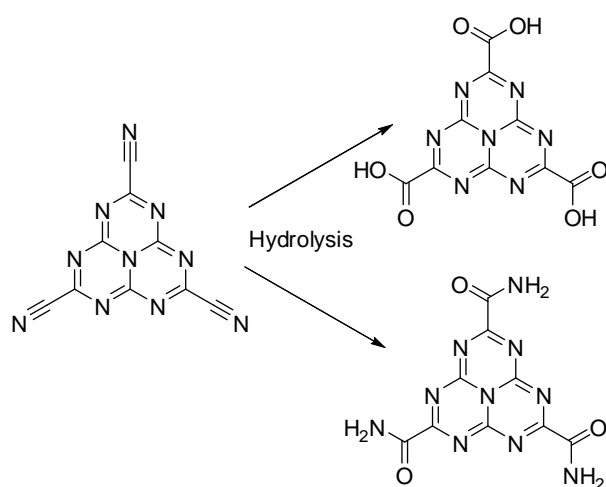
9.2 Synthetic Attempts towards Cyameluric Cyanide

The cyanided derivatives of *s*-triazine or *s*-heptazine also constitute promising precursor compounds. The molecules incorporate C-C bonds and thus have no reasonable potential as precursors for C_3N_4 due to the mismatch in oxidation states. This might be an explanation for the relative lack of interest into such compounds in comparison to the ammono-carbonic acids. The condensation of which is offering a straightforward condensation into C_3N_4 . Nitriles, however, offer alternative cross-linking reactions potentially leading to carbon nitrides. A range of promising structures can be regarded as products of poly $C\equiv N$ trimerization reactions (cf. Scheme 29). The depicted layered carbon nitrides are the supposable products of such a reaction. The composition of the respective polymerizations products would equal C_9N_{10} for networks made up of tricyano-*s*-heptazine and CN for networks made up of tricyano-*s*-triazine.



Scheme 29. Tricyano-*s*-heptazine (upper left) and tricyano-*s*-triazine (upper right) and their expected polymerization into layered network structures. The one initial molecule incorporated into the layer is marked in red in each case.

Apart from the possibility of forming carbon nitride layers the respective nitrides offer other promising ways for synthesis. If a selective hydrolysis were achieved carbon acids or carbon acid amides might be prepared in such a way (cf. Scheme 30). Especially melem carbon acids or the respective melem carboxylates would be new and promising building blocks for metal organic frameworks (MOFs) or other coordination polymers. Most coordination polymers incorporate linkers based on aromatic hydrocarbons. Differing properties for such compounds are to be expected due to the effect of the cyameluric nucleus.



Scheme 30. Possible synthesis routes of heptazine-based carbon acid or amide derivatives by hydrolysis of expected tricyano-*s*-heptazine.

The synthesis and reactivity of tricyano-*s*-triazine, $C_3N_3(CN)_3$, has already been described in the literature,^[157-159] whereas a tricyano-*s*-heptazine, $C_6N_7(CN)_3$, has not been mentioned as yet. A preferably reported synthesis of $C_3N_3(CN)_3$ is the reaction of cyanuric chloride, $C_3N_3Cl_3$, with al-

kali metal cyanides like KCN or NaCN (Eq. 9.3).^[159,160]



The reaction is typically conducted in suspensions of the starting materials. Typical solvents are acetonitrile or THF. Reaction occurs upon prolonged stirring at room temperature.

The emulation of the reaction protocol to cyameluric chloride (Eq. 9.4) has not been a successful one. Dry acetonitrile or DMF were used as solvents. The reactions were conducted under argon. No defined reaction product was yielded this way. Some sort of reaction, however, definitely took place since considerable amounts of the cyanide salt were consumed and KCl was found in the reaction product (studied by PXRD). An analogue reaction conducted using NaCN instead of KCN produced similar results.



The reaction of cyameluric chloride with trimethylsilyl cyanide (Eq. 9.5) was inspired by the comparable reaction used for obtaining triazido-*s*-heptazine (Eq. 9.6) reported by Gillan et al.^[49]



Due to the lower long term thermal stability of trimethylsilyl cyanide in comparison to the azide, a significant degree of decomposition occurred. Thus the reported reaction times of several hours (for $\text{C}_6\text{N}_7(\text{N}_3)_3$) had to be significantly shortened. Unreacted TMS-CN was removed in vacuo. The product was yielded as an amorphous, poorly defined solid, the color of which varied between a reddish brown and black. No CN functionalities were observed by IR or solution NMR spectroscopy. No reaction was observed for prolonged stirring at lower temperatures (RT to 40 °C).

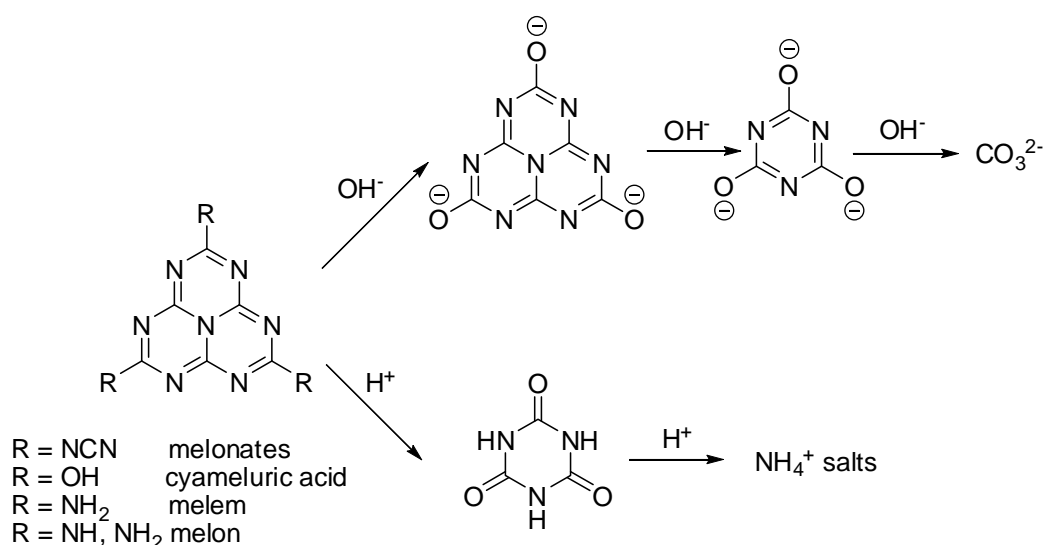
Palladium-catalyzed cyanation reactions^[161] of cyameluric chloride were also attempted but remained unsuccessful. The protocol attempted was the reaction of cyameluric chloride, $\text{C}_6\text{N}_7\text{Cl}_3$, with $\text{K}_4[\text{Fe}(\text{CN})_6]$ in the presence of catalytic amounts of $\text{Pd}(\text{OAc})_2$ (cf. Equation 9.7).^[162]



Unfortunately, the synthesis of cyameluric cyanide remained unsuccessful as yet. However, the potential of this molecule certainly justifies further investigations in this regard.

9.3 Decomposition of Heptazines in Aqueous Solution

The decomposition of melem, melon and melonates in alkaline aqueous solutions is known to produce cyamelurates (cf. Chapter 7). This can be regarded as a nucleophilic substitution reaction of the respective heptazine. Prolonged hydrolysis of the heptazine compounds will decompose the cyameluric nucleus thus producing cyanurates and finally carbonates (cf. Scheme 31 upper route).



Scheme 31. Decomposition of some heptazines in aqueous solution. Common intermediates are depicted several other intermediates are omitted for clarity or due to uncertainties concerning their nature.

Melem is unaffected by treatment with water at room temperature and is not notably affected by boiling in water for several days.^[111] Melon shows different properties in this regard. Raw melon prepared from melamine (cf. Section 6.2) was used for the investigations described in the following. Prolonged boiling of melon resulted in a notable loss of its yellow color. Total decomposition of melon at pH = 7 could, however, not be observed on a reasonable timescale (up to one day).

In acidic solution decomposition occurs much faster. Despite the usual poorly defined nature of most batches defined products are sometimes obtainable from the decomposition. Cyanuric acid is regularly found during such decompositions but other compounds were also found (cf. Section 9.4). The final reaction products after several days of boiling usually are ammonium salts (cf. Scheme 31 lower route). This observation has also been made during very early investigations.^[78,81] The observed decomposition is not surprising and reminiscent to the *Kjeldahl* method for nitrogen analysis.^[163] Other intermediary products were also observed in acidic solution. Selective decomposition reactions thus allow access to certain compounds that would otherwise require a complex multi-step synthesis as will be shown there. Understanding the acidic degradation of heptazines is far less straightforward than is the case for the alkaline hydrolysis. The stability towards acidic hydrolysis is vastly different depending on the chemical nature of the respective heptazines. While cyameluric acid, $\text{H}_3\text{C}_6\text{N}_7\text{O}_3$, and melonates, $\text{C}_6\text{N}_7(\text{NCN})_3^{3-}$, decompose with relative rapidity melon and especially melem require prolonged and harsh treatment.

The synthetic potential arising from this reaction offers a rewarding perspective for further investigations. The mechanism of the breakdown of the heptazine core remains unresolved as yet. During the investigations conducted as part of this thesis one new decomposi-

9.3 Decomposition of Heptazines in Aqueous Solution

tion intermediate could be identified and structurally investigated (N-guanylamelin dihydrochloride, $\text{H}_2(\text{C}_3\text{N}_3)=\text{O}(\text{NH}_2)\text{NHC}(\text{NH}_2)_2\text{Cl}_2$, cf. Section 9.4). Hence the existence of further defined intermediates seems likely. Another important question in this regard is whether or not the substitution of the respective heptazine compound might cause fundamentally different decomposition routes and not just differences in reaction times etc.

9.4 N-Guanyllammelin Dihydrochloride

The compound N-guanyllammelin dihydrochloride, $\text{H}_2(\text{C}_3\text{N}_3)=\text{O}(\text{NH}_2)\text{NH}-\text{C}(\text{NH}_2)_2\text{Cl}_2$ (cf. Figure 101), was yielded by the decomposition of cyameluric acid in hot, concentrated, aqueous HCl (cf. Section 12.1.29 for experimental details). This compound constitutes a new intermediate in the decomposition of cyameluric acid under acidic conditions. Cyameluric acid has already been reported to decompose into cyanuric acid and finally into ammonium salts. Especially the respective reaction with sulfuric acid has been described very early.^[78] The fact that ammonium ions are ultimately yielded upon prolonged treatment with an acid is hardly surprising and can be observed for almost all nitrogen-containing compounds (cf. preceding section). The finding that certain intermediates may selectively be prepared this way is a very interesting and helpful one. N-guanyllammelin and its salts have not been described in the literature, as yet. The observed decomposition reaction grants facile access to this novel heterocyclic compound and thus is of potential synthetic interest.

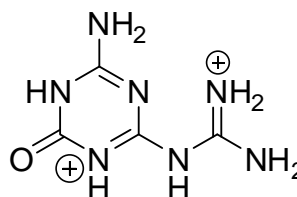


Figure 101. Formula of the guanyllammelinium dication as found in guanyllammelin dihydrochloride, $\text{H}_2(\text{C}_3\text{N}_3)=\text{O}(\text{NH}_2)\text{NH}-\text{C}(\text{NH}_2)_2\text{Cl}_2$. Only one select resonance structure is depicted.

Table 42. Crystallographic data and details of the refinement procedures for $\text{H}_2(\text{C}_3\text{N}_3)=\text{O}(\text{NH}_2)\text{NHC}(\text{NH}_2)_2\text{Cl}_2$.

Formula	$\text{H}_2(\text{C}_3\text{N}_3)=\text{O}(\text{NH}_2)\text{NHC}(\text{NH}_2)_2\text{Cl}_2$
Formula weight / g mol ⁻¹	242.08
Crystal system	monoclinic
Space group	<i>P2₁/c</i> (no. 14)
Lattice parameters / Å, °	<i>a</i> = 6.9305(14) <i>b</i> = 13.698(3) <i>β</i> = 106.67(3) <i>c</i> = 10.533(2)
Volume / Å ³	957.9(3)
Z	4
Absorption coefficient / mm ⁻¹	0.659
Calculated density / g cm ⁻³	1.679
F(000)	496
Diffractometer, radiation	IPDS, Mo-K _α (λ = 71.073 pm), graphite monochromator
Temperature / K	293
Theta range / °	3.41 to 30.53
Structure solution	SHELXS-97 ^[101] (direct methods)
Structure refinement	SHELXL-97 ^[101] (full-matrix least-squares on F ²)
Corrections	Lorentz, polarization
Data / restraints / parameters	2040 / 0 / 163
R-indices	R1 = 0.0437 Fo > 4σ(Fo) (1528 reflections) R1 = 0.0602 all data wR2 = 0.1154 Fo > 4σ(Fo) wR2 = 0.1271 all data
Goof	1.036
Largest peak deepest hole / e Å ⁻³	0.267 / -0.363

9.4 N-Guanyllammelin Dihydrochloride

Crystals of $\text{H}_2(\text{C}_3\text{N}_3)=\text{O}(\text{NH}_2)\text{NHC}(\text{NH}_2)_2\text{Cl}_2$ were collected and studied by single-crystal XRD. Due to immanent non-merohedral twinning, observed for all crystals studied, datasets for the two individuals were separated for the select crystal. Only non-overlapping reflections are used for the present refinement. Guanyllammelin dihydrochloride crystallizes in the monoclinic space group $P2_1/c$ with four formula units per unit cell. The observed $\text{H}_2(\text{C}_3\text{N}_3)=\text{O}(\text{NH}_2)\text{NHC}(\text{NH}_2)_2^{2+}$ ion is almost

perfectly planar, even the amino groups are not twisted out of plane to any significant degree. An internal H-bridge interaction ($\text{N6-H6}\cdots\text{N2}$) stabilizes the molecule and probably fosters coplanarity of the *s*-triazine ring and the guanyl group (cf. Figure 102). This is an interesting similarity to the melamium ions discussed in Chapter 4 in which planarity is also forced by an internal H-bridge. Bond lengths and angles range within expected parameters. The allocation of atom sorts chosen is in agreement with the observed bond lengths. The bond C1-O1 is notably shorter than the C-N bonds present. All hydrogen atoms were located by difference Fourier synthesis and could be refined with isotropic thermal displacement parameters. The proton localization chosen allows a maximum of H-bonding to occur and any other localization would have resulted in unlikely distances or bonding situations or would not have allowed overall electro neutrality. This gives further support for the presented model. Selected distances and angles are summarized in Table 43.

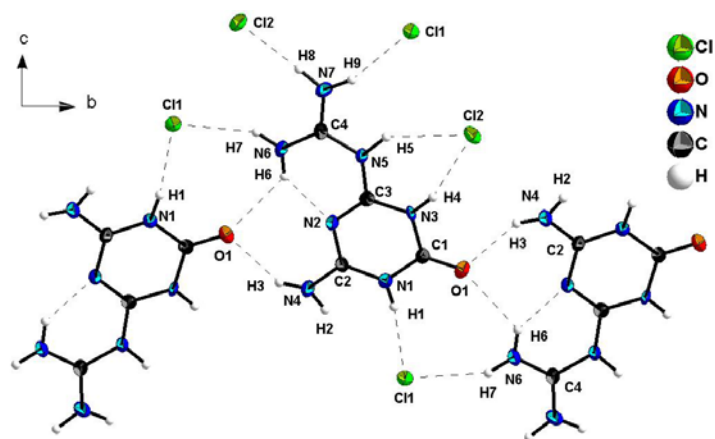


Figure 102. Molecular structure and labeling of atoms for $\text{H}_2(\text{C}_3\text{N}_3)=\text{O}(\text{NH}_2)\text{NHC}(\text{NH}_2)_2\text{Cl}_2$. Ellipsoids for non-hydrogen atoms are drawn at the 50 % probability level.

Table 43. Selected distances and angles (in Å and °) for $\text{H}_2(\text{C}_3\text{N}_3)=\text{O}(\text{NH}_2)\text{NHC}(\text{NH}_2)_2\text{Cl}_2$. Standard deviations in parentheses.

Distances					
O1-C1	1.221(3)	N3-C1	1.366(3)	N5-H5	0.81(4)
N1-C2	1.350(3)	N3-H4	1.03(4)	N6-C4	1.315(3)
N1-C1	1.365(3)	N4-C2	1.302(3)	N6-H6	0.90(4)
N1-H1	0.99(5)	N4-H2	0.90(6)	N6-H7	0.76(5)
N2-C3	1.304(3)	N4-H3	0.90(5)	N7-C4	1.307(3)
N2-C2	1.351(3)	N5-C3	1.360(3)	N7-H9	0.97(5)
N3-C3	1.349(3)	N5-C4	1.372(3)	N7-H8	0.95(4)
Angles					
C2-N1-C1	121.9(2)	C3-N5-H5	117(3)	N4-C2-N1	120.0(2)
C2-N1-H1	121(2)	C4-N5-H5	115(3)	N4-C2-N2	118.2(2)
C1-N1-H1	117(2)	C4-N6-H6	122(2)	N1-C2-N2	121.8(2)
C3-N2-C2	116.37(19)	C4-N6-H7	128(3)	N2-C3-N3	123.7(2)
C3-N3-C1	121.27(19)	H6-N6-H7	109(4)	N2-C3-N5	121.2(2)
C3-N3-H4	115(2)	C4-N7-H9	126(3)	N3-C3-N5	115.05(19)
C1-N3-H4	123(2)	C4-N7-H8	124(3)	N7-C4-N6	121.9(2)
C2-N4-H2	118(3)	H9-N7-H8	110(4)	N7-C4-N5	116.9(2)
C2-N4-H3	112(3)	O1-C1-N1	122.5(2)	N6-C4-N5	121.2(2)
H2-N4-H3	130(4)	O1-C1-N3	122.7(2)		
C3-N5-C4	127.63(19)	N1-C1-N3	114.81(19)		

The N-guanyllammelinium ions are arranged in as strand-like pattern connected by the H-bridges N6-H6...O1 and N4-H3...O1. Several other H-bridges are connecting the chloride anions and the $\text{H}_2(\text{C}_3\text{N}_3)=\text{O}(\text{NH}_2)\text{NHC}(\text{NH}_2)_2^{2+}$ ions establishing densely inter-connected layers (cf. Figure 103).

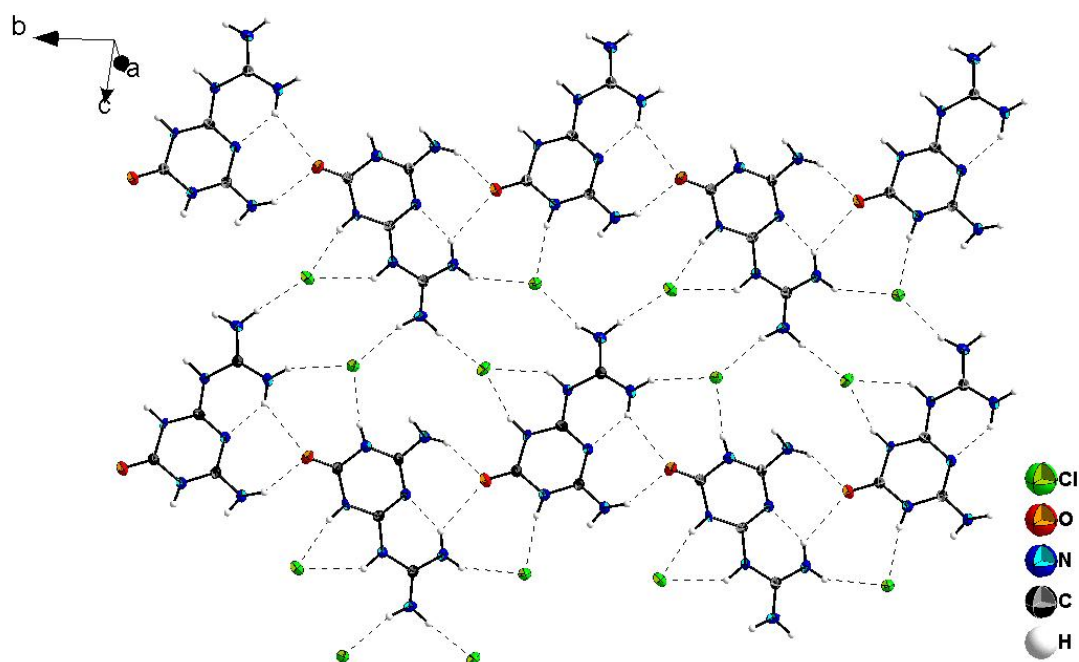


Figure 103. Hydrogen-bonding interactions found for $\text{H}_2(\text{C}_3\text{N}_3)=\text{O}(\text{NH}_2)\text{NHC}(\text{NH}_2)_2\text{Cl}_2$. Ellipsoids for non-hydrogen atoms are drawn at the 50 % probability level.

The slightly corrugated layers are stacked at a distance of 3.5 Å (cf. Figure 104). This is a rather long stacking distance making a significant influence of π -stacking very much unlikely. The layers are not inter-connected by H-bonding interactions.

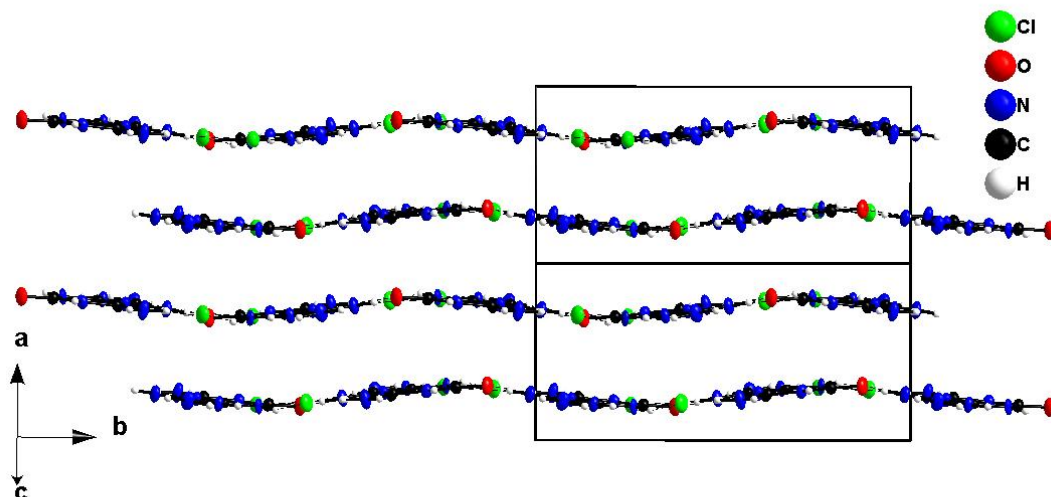
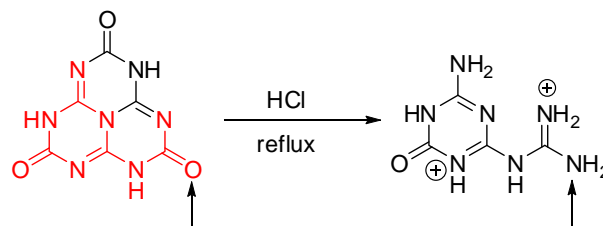
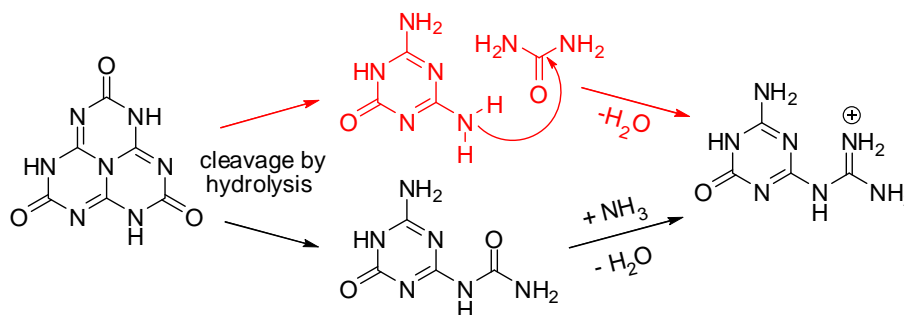


Figure 104. Layer-like arrangement for $\text{H}_2(\text{C}_3\text{N}_3)=\text{O}(\text{NH}_2)\text{NHC}(\text{NH}_2)_2\text{Cl}_2$.

Explaining the formation of the N-guanylammelinium ion starting from cyameluric acid is far from straightforward. It can easily be visualized, that the ion cannot be explained as a simple fragment obtainable by cleaving C-N bonds within one cyameluric acid molecule. This is since there is a mismatch in atom sorts as is shown in Scheme 32. Thus a mechanistic explanation is rather problematic. One could assume an initial degradation of cyameluric acid into ammelin followed by a subsequent condensation reaction of this molecule with other cleavage products like urea (cf. Scheme 33 top, red). Another possible approach would be proposing the decomposition of cyameluric acid into a urea derivative that is somehow transferred into the N-guanyl compound (cf. Scheme 33 black, bottom).



Scheme 32. Decomposition of cyameluric acid to form guanylammelin dihydrochloride. A part of the cyameluric acid molecule best suiting as a source of the resulting compound is marked in red. The differing atom sort (O/N) therein is marked with arrows in each formula.



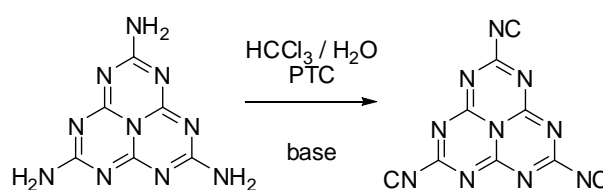
Scheme 33. Two possible mechanistic explanations for the observed formation of N-guanylammelin dihydrochloride.

Although the decomposition of heptazines in acidic aqueous solution is capable of providing defined reaction products it is not mechanistically understood how these compounds are formed. Further products might well be obtainable under alternative conditions (e.g. by further variation of acids, reaction times and concentrations). The finding that this decomposition allows a simple access to new triazine compounds provides an additional reason for subsequent investigations.

9.5 Additional Derivatization Reactions of Heptazines

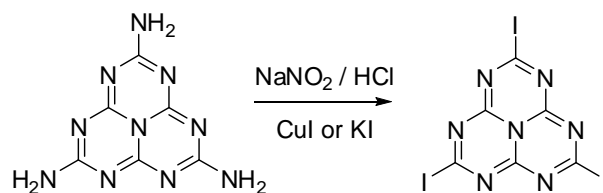
Apart from the previously mentioned attempts to prepare heptazine-based cyano compounds (cf. Section 9.2), several other derivatization reactions known for aromatic organic compounds were also attempted for heptazine-based molecules. A poor transferability for reaction protocols was generally observed. Apart from the obvious electronic distinctions of the cyameluric nucleus from an aromatic hydrocarbon the comparably low solubility of heptazines most likely also affects the reactivity. These fundamental differences have usually impeded advances in this direction. However, the observations made for some reactions will be presented as follows.

Heptazine isonitriles are isomers of the nitriles presented in Section 9.2. These pure carbon nitride molecules would constitute potential precursors for C/N networks. Synthesis was attempted in agreement to the usual isonitrile synthesis. Melem was subjected to aqueous base / chloroform under phase transfer catalysis (PTC) conditions (cf. Scheme 34). No hints at the formation of isonitriles were found by analytical results or observation of the reaction mixture.



Scheme 34. Possible synthesis of heptazine triisonitrile

Sandmeier reactions are another important derivatization of amino groups and were attempted for heptazine-based molecules as well. Additional heptazine halides, apart from the trichloride (cf. Section 9.1), might be regarded possible products of such a reaction. Especially triiodo heptazine would constitute an ideal compound for further cross-linking reactions like transition metal catalyzed cross-couplings. The formation of the desired product could not be observed under the given reaction conditions (cf. Scheme 35).

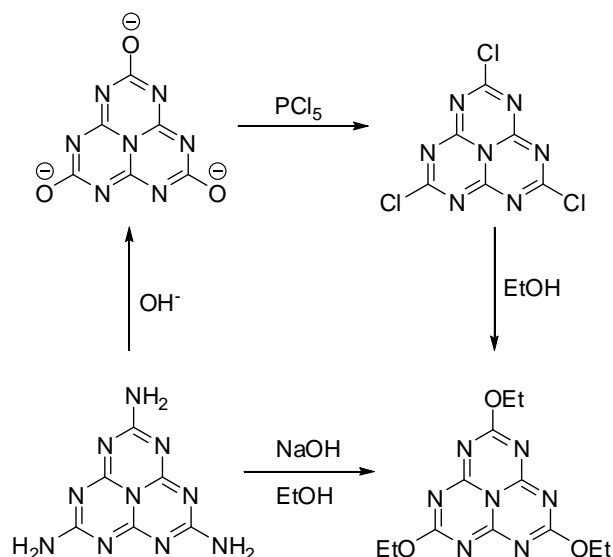


Scheme 35. Possible synthesis of triiodo heptazine.

Heptazine-based ligands are rarely reported. Based on some preliminary investigations of melem^[111] other heptazines were investigated in this work. Cyameluric chloride, $\text{C}_6\text{N}_7\text{Cl}_3$, shows a dramatically increased solubility in comparison to melem and might thus qualify as a possible ligand. Reactions with TiCl_4 (in pure TiCl_4) and $\text{Pd}(\text{OAc})_2$ (in acetonitrile) were attempted hoping to achieve observable complex formation. Unfortunately no reaction was observed for TiCl_4 ^[t] and for palladium salts results are inconclusive.

[t] $\text{C}_6\text{N}_7\text{Cl}_3$ is stable against TiCl_4 even after prolonged heating. It can even be recrystallized from TiCl_4 .

Heptazine-based alkoxy compounds like $C_6N_7(OEt)_3$ are usually prepared by reaction of cyameluric chloride with alcohols.^[52,55] Cyameluric chloride is prepared starting from melem or melon as has already been stated (cf. Section 9.1). Hence the whole procedure is rather time consuming as several preliminary reactions are required. A direct synthesis from melem by substitution with OEt^- was attempted in order to assess the potential for such a “shortcut” (cf. Scheme 36). No notable degree of product formation was observed. This finding can probably be associated with the low solubility of melem in alcohols.

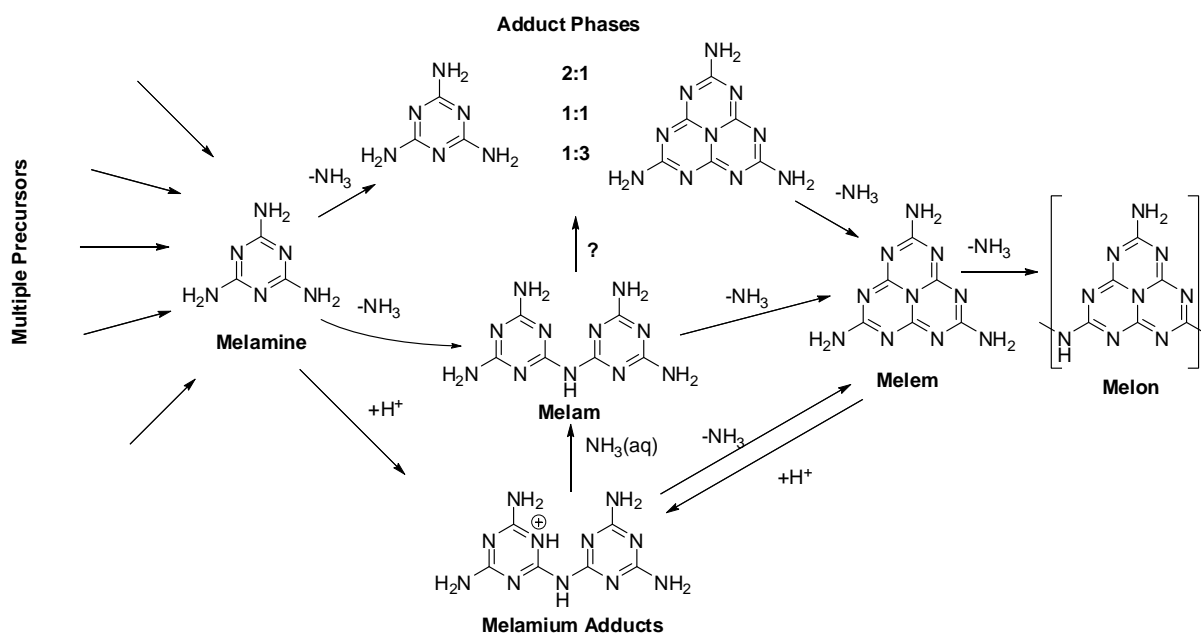


Scheme 36. A possible direct synthesis of triethoxy-*s*-heptazine.

10. Discussion and Outlook

10.1 Structuring and Understanding the Thermal Condensation of C/N/H Precursors

The experimental results achieved in this thesis allow a more in-depth understanding of the condensation of small C/N/H molecules like melamine. Some general assumptions should be made in order to structure the thermal condensation of these important carbon nitride precursors. One must distinguish between two separate types of reactions. The first of which is the actual condensation successively forming compounds like melam, melem and the polymer melon (cf. Scheme 37).



Scheme 37. Overview of possible condensation reactions involving C/N/H precursor compounds.

The other one is the organization of these species into a plethora of possible phases. The resulting compounds can either contain the pure molecules / polymers or may be, and regularly are, adduct phases incorporating at least two different molecular species. Retaining selected molecules as final condensation products is, however, very much dependent on fine-tuning reaction conditions and not always readily achieved. The most important factors in this regard are temperature and pressure. In addition to the usual (i.e. employed in prior contributions of our work group)^[34,35,107,108,111] closed reaction setup using sealed glass ampoules, condensation in what might best be termed a semi-closed setup, using covered crucibles, was also studied. Thus, much larger quantities of the reaction products could be obtained facilitating the study of subsequent derivatization and decomposition reactions. Melam has proven to be particularly challenging to prepare. Though it definitively occurs as an intermediate during the condensation of C/N/H precursors like melamine^[34] it can hardly ever be isolated in significant amount from such reactions. It can easily be rationalized, in accordance to the ammonocarbonic acid formalism (cf. Chapter 1), that melamine melem adduct phases (cf. Chapter 3) show similar, if not identical (in the case of the adduct 2melamine · melem), condensa-

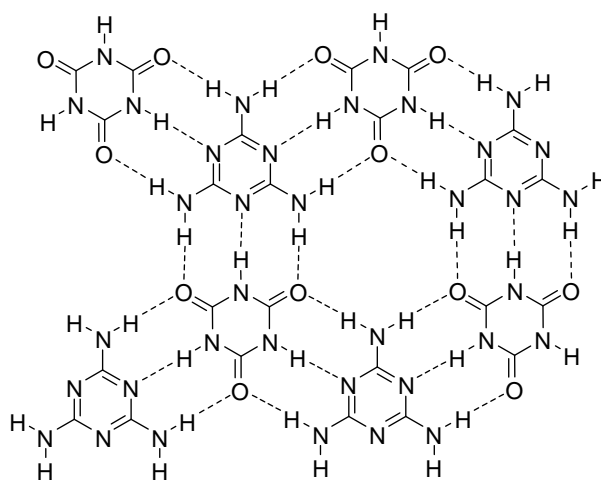
tion grades as does melam. There also is an energetic drive to establish the heptazine core [C₆N₇]. Thus, the formation of melam is thermodynamically disfavored for a wide range of reaction conditions. Since melam is more basic than is melem or melamine, its formation can be drastically promoted by addition (or in situ generation) of acidic compounds. Melamium adduct phases (cf. Chapter 4) are regularly yielded by this approach and melam can subsequently be liberated from such. It has been stated before, that the actual condensation of C/N/H precursors clearly is an equilibrium reaction influenced by temperature and pressure (in order of magnitude). The time need for this condensation to fully equilibrate within a sealed ampoule, however, can account for several days and, thus, seems to have been severely underestimated by previous works. This finding is a significant improvement to the synthesis of some compounds. Especially the possibilities for crystal growth, purity and accessibility of certain compounds have been advanced this way. Most work presented in Chapters 3 - 4 was made possible or at least significantly promoted by this approach.

10.2 The Importance of Adduct Phases Containing Carbon Nitride Precursors

Non-covalent organization of the molecules and / or networks is a reaction type frequently observed for C/N/H compounds. A variety of solid, molecular adducts could be identified. This reactivity is complementing the formation of certain molecular and polymeric species as has already been mentioned in the preceding paragraph. Preceding investigations have already pointed out certain aspects concerning some adduct phases obtainable by condensation of common precursor compounds. Exact characterizations, however, were not achieved and both the chemical nature and structure of the resulting phases remained mostly obfuscated.

Adduct phases incorporating melamine and cyanuric acid have aroused considerable interest. Crystalline samples of such phases are typically prepared under hydrothermal conditions. Especially the adducts melamine · cyanuric acid (commonly labeled CA·M)^[164] and the diprotonated melaminium cyanuric acid dichloride dihydrate, $\text{H}_2\text{C}_3\text{N}_3(\text{NH}_2)_3\text{Cl}_2 \cdot \text{H}_3\text{C}_3\text{N}_3\text{O}_3 \cdot 2\text{H}_2\text{O}$,^[165] (initially wrongly reported to be $\text{C}_3\text{N}_3(\text{NH}_2)_3 \cdot \text{H}_3\text{C}_3\text{N}_3\text{O}_3 \cdot 3\text{HCl}$, CA·M·3HCl)^[166] are to be mentioned in this respect. These systems are fine and prominent examples of non-covalent synthesis.^[167] The H-bonded rosettes expressed by CA·M (cf. Scheme 38) are a most interesting structural motif that has found considerable recognition. It is thus made clear, that as other densely hydrogen-bonded adducts hold an enormous potential for self organization and non-covalent synthesis, the molecules investigated in this work might do as well. In following, the adduct phases studied in the preceding chapters are once again regarded in order to fully assess this interesting potential. For the sake of clarity the adduct phases investigated are divided up into groups.

Melamine melem adducts (cf. Chapter 3) constitute the first such group. The adduct phases (2melamine · melem, melamine · melem and melamine · 3melem) are examples of heptazine-containing adducts. The compounds were prepared by thermal condensation of melamine in sealed glass ampoules. The effects of ammonia scavengers on the reaction (Eu metal) were studied in this regard. Structural (XRD) and solid-state NMR spectroscopic investigations have provided a detailed and consistent set of data regarding these compounds. Thus, knowledge of these compounds could be substantially amended and corrected wherever necessary. Phase separation yielding mixtures of adducts and / or the pure components, however, is a rather common phenomenon when melem and melamine are formed at unfavorable ratios or if temperature gradients occur. The advances made for these systems have brought up further interest in other, comparable systems. If the reaction conditions can be altered significantly, further adduct phases can possibly be found especially if the equilibrium can be shifted towards other molecular species.



Scheme 38. Rosette-like H-bonding motif found for the equimolar adduct of cyameluric acid and melamine (CA·M).

Thus, the existence of distinct adducts between melamine and melam or melem and melam seemed quite plausible judging from the existence of the melamine melem adducts. The central problem in this regard was preserving melam under equilibrium conditions within the ampoule. Melamium-containing adducts were actually prepared from mixtures of melamine and ammonium chloride or from thiourea. All these mixtures contained acids or produced such upon heating (HCl/NH_4^+ , HSCN) thus melam was stabilized by protonation. These compounds also allowed the first structural characterization of single-protonated melamium compounds clearly resolving hydrogen positions.

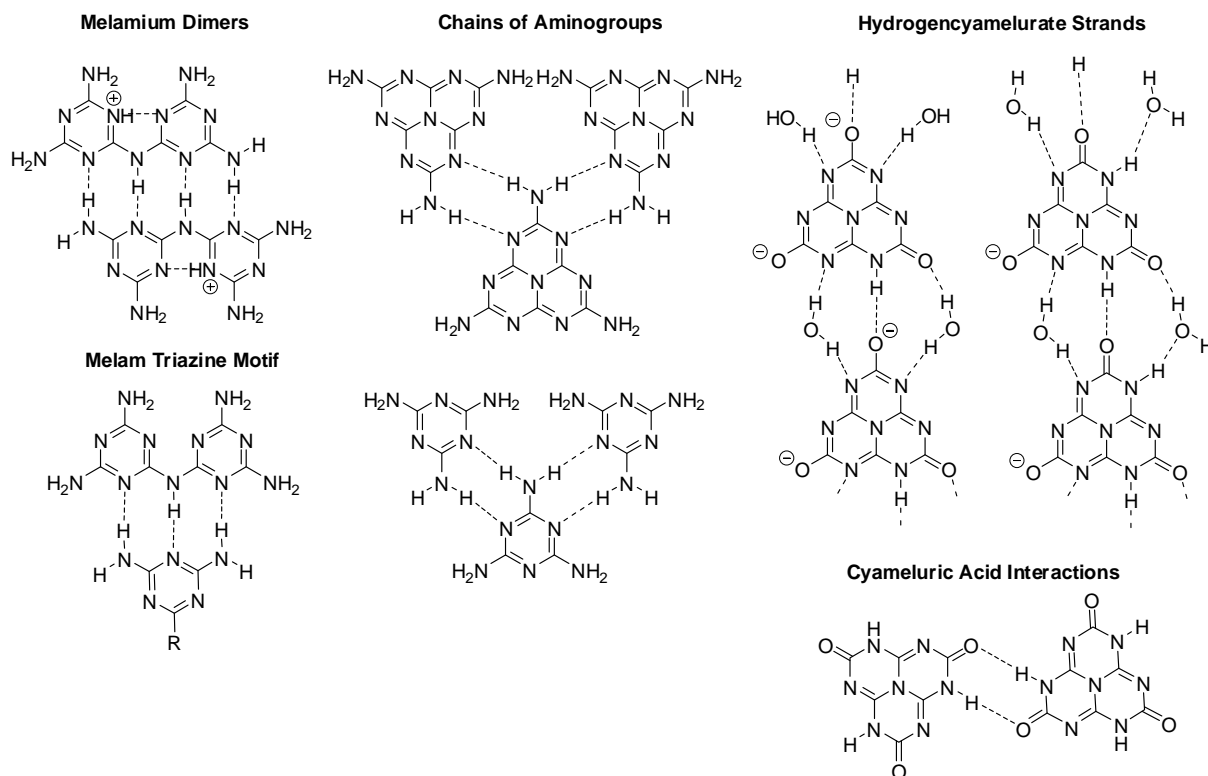
The third and last group contains adducts like $\text{C}_6\text{N}_7\text{H}_3\text{O}_3 \cdot \text{H}_2\text{N}(\text{CH}_3)_2\text{Cl} \cdot \text{H}_2\text{O}$. These compounds were not formed during the thermal condensation of precursors. As a difference to the other groups of adducts, such compounds can be prepared from solution. Salts of rather complex composition often observed (Chapter 5, Chapter 7) also fall into this category.

Other reported compounds like PHI^[17] must also be regarded to fully understand the potential of adduct phases. In this compound an adduct of melamine and a polyheptazine imide layer on the one hand allows the molecule melamine to endure well beyond its normal thermal stability and on the other hand a highly condensed layer can be established.

A true and comprehensive understanding of carbon nitrides essentially requires an in-depth understanding of possible adduct phases. Knowledge of such adduct phases and their properties thus holds a vast potential for truly controlling properties and reactivity of many heptazine and / or triazine-based compounds. The fact that such a large amount of adducts does exist for many C/N/H compounds can be understood by several factors. All molecules involved feature a significant potential for expressing H-bonding interactions. In most cases several donor and acceptor sites are combined in one molecule. Especially molecular heptazines, featuring the large $[\text{C}_6\text{N}_7]$ nucleus, cannot easily form complete H-bonding networks on their own due to steric hindrance. Other compounds show similar effects. A significant mismatch between the number of hydrogen donor and acceptor sites in many molecules also is a major drive towards adduct formation.

10.3 Comparison of Structural and Spectroscopic Data

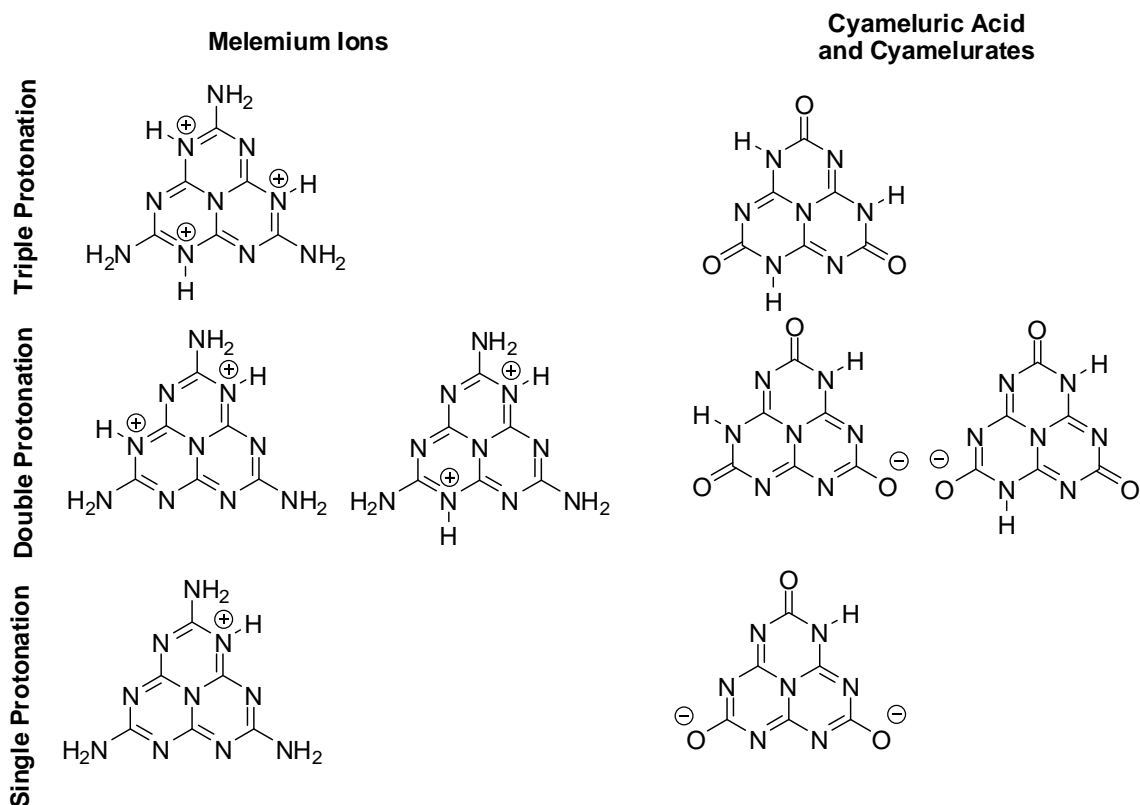
H-bonding interactions are a crucial factor directing and explaining the structural diversity observed for heptazines. Understanding and interpreting these interactions thus constitutes an important aspect of carbon nitride chemistry. It may often be misleading to deduce preferable motifs bases on to few structures. The amount structural data available has been significantly expanded during this work and thus allows a comprehensive revision of H-bonding motifs commonly realized for prominent heptazine-based molecules. Some favorable structural motifs observed are depicted in Scheme 39.



Scheme 39. Overview of some common H-bonding interactions observed for select triazine and heptazine-based compounds.

As can be seen, certain reoccurring motifs can easily be identified. The amount of H-bonding interactions incorporated in one motif (between two molecules) is very important for judging how often the respective motif is realized.^[125] Accordingly, motifs displaying many interactions between few molecules can be expected capable of directing structures to a large extent, while motifs build up of many molecules connected by few interactions cannot. For the compounds observed, most motifs only link two molecules with two H-bonds and are thus not exceptionally stable. These motifs, however do allow a notable amount of recognition. The structure and formation tendency of certain motifs might thus not be controllable to the same extent as has been reported of compounds imitating the cyameluric acid melamine motif (cf. Scheme 38).^[167] This, however, allows for more structural diversity possible for non-covalent synthesis of compounds incorporating molecules based on melam, melam or cyameluric acid. Especially when regarded in conjunction with the observed tendencies towards adduct formation discussed before (cf. Section 10.2).

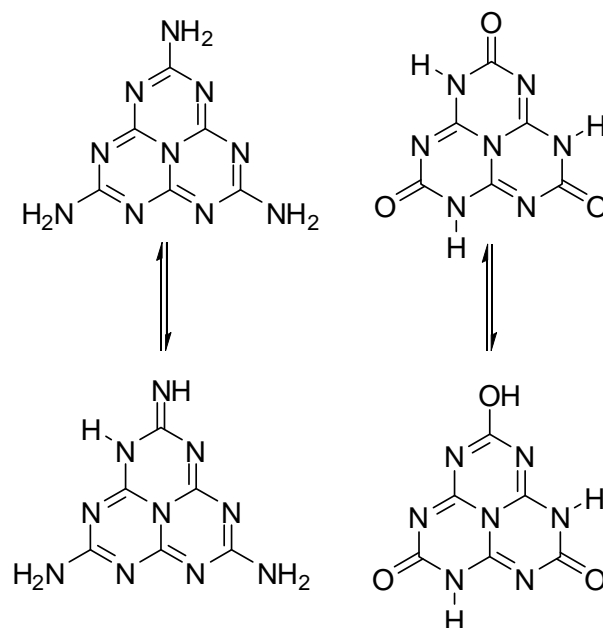
Uncertainties concerning the tautomerism of several C/N/H compounds could be resolved by structural investigations. Some structures of certain molecular species are given in Scheme 40.



Scheme 40. Compilation of observed tautomeres for melemium and cyamelurate ions. All depicted structures were observed as part of this thesis.

Certain protonation variants of melem and cyameluric acid are compared. Although data is mostly based on single-crystal XRD, the vast majority of structures offer very consistent and reliable datasets. Protonation causes a characteristic distortion of bond lengths and angles within the cyameluric nucleus that can be used for additional validation of proton positions. Wherever conducted spectroscopic investigations have fully supported the proton localization found in XRD. Only one tautomer of single-protonated melemium ion, $\text{HC}_6\text{N}_7(\text{NH}_2)_3^+$, and one kind of hydrogenocyanurate ion, $\text{HC}_6\text{N}_7\text{O}_3^{2-}$, have been observed. Protonation only occurs at the cyameluric nucleus. Compounds incorporating OH or NH_3^+ functionalities were not observed in any case. There are two variants of double-protonated melemium ions, $\text{H}_2\text{C}_6\text{N}_7(\text{NH}_2)_3^{2+}$, and dihydrogenocyanurate ions, $\text{H}_2\text{C}_6\text{N}_7\text{O}_3^-$, respectively. One tautomer is of C_{2v} symmetry the other one shows C_s symmetry. Each tautomer has been observed in more than one structure and no clear energetic preference can be concluded from the data at hand. The realization of one or the other ion thus is probably directed by comparably weak non-covalent interactions. No additional tautomers for diprotonated heptazine compounds have been observed so far. Three hydrogen atoms connected to the cyameluric nucleus ($\text{H}_3\text{C}_6\text{N}_7(\text{NH}_2)_3^{3+}$ and $\text{H}_3\text{C}_6\text{N}_7\text{O}_3$) avoid close proximity of protonation sites. This always results in an arrangement of C_{3h} symmetry. It must be added that the idealized point symmetry given is usually reduced by minor distortions observed for the actual compounds as found in the solid state.

The possibility for the occurrence of additional tautomeres is often being discussed for heptazine-based molecules. A tautomerism of melem or cyameluric acid forming imine or hydroxo molecules (cf. Scheme 41) was not observed and no hints pointing at respective structures were found for all structures investigated in this thesis. The structural investigation of cyameluric acid trihydrate by single-crystal XRD (cf. Chapter 7) settled the long lasting uncertainty concerning the proton localization in this compound. It could be shown, that only the keto-like tautomer is present in the solid. Structural investigations of other compounds containing cyameluric acid or cyamelurates fully support the observations made for the trihydrate. It might be added, that for cyameluric acid additional tautomeres can be observed in form of derivatives.^[54] For melem, however, no derivatives expressing any resemblance to the depicted tautomerism are established. This is well in line with the observations made by detailed solid-state NMR investigations of melem, which have proven the structure displaying only amino groups.^[35a] Accordingly it can most likely be ruled out that several tautomeres of melem or cyameluric acid can easily occur or even coexist in one compound under conditions investigated in this thesis.



Scheme 41. Possible tautomeres of melem (left) and cyameluric acid (right). Only the structures depicted at the top are observed. Bottom structures or variants thereof have not been observed.

Further Synthetic Advancements

Melemium salts of various acids have been prepared as part of the present work. Such salts are considered to be promising precursor compounds for the synthesis of carbon nitride materials. Their direct thermal reaction products as well as a conversion into compounds also containing C-N(H) anions, like the ones already known for triazines,^[168] via ion-exchange is subject to further investigation. A total of eight crystalline compounds have been identified so far (cf. Table 44). Thus melemium salts provide a considerable amount of usually well crystalline, defined and comparably soluble melem compounds. A significant amount of further melemium salts is to be expected as hints towards such compounds were frequently found by powder XRD and other methods. Due to the low basicity of melem only strong acids regularly yield salt-like structures upon reaction with melem. Usually several melemium salts of the same acid can be readily prepared by adjusting the respective concentration of the acid.

10. Discussion and Outlook

Table 44. Summary of observed melemium salts and melem acid adducts. Compounds prepared as part of this thesis are printed in bold.

Protonation of melem ^[a]	Sulfuric acid	Methylsulfonic acid	Perchloric acid	Phosphoric acid
0				$C_6N_7(NH_2)_3 \cdot H_3PO_4$
0.5			$HC_6N_7(NH_2)_3ClO_4 \cdot C_6N_7(NH_2)_3$	
1			$HC_6N_7(NH_2)_3ClO_4 \cdot H_2O$	
1.5		$HC_6N_7(NH_2)_3$ $H_2C_6N_7(NH_2)_3(SO_3Me)_3 \cdot H_2O$		
2	$H_2C_6N_7(NH_2)_3SO_4 \cdot 2H_2O$	$H_2C_6N_7(NH_2)_3(SO_3Me)_2 \cdot H_2O$	$H_2C_6N_7(NH_2)_3(ClO_4)_2 \cdot H_2O$	
3	$H_3C_6N_7(NH_2)_3(HSO_4)_3$			

[a] Numbers being fractions of one are caused by the coexistence of different protonation grades of melem.

Three compounds were already described in the literature.^[36,111] The following salts were prepared as part of this thesis (cf. Chapter 5): The melemium perchlorate salts melem melemium perchlorate and melemium diperchlorate hydrate have been synthesized and studied by single-crystal XRD. Melemium methylsulfonates have also been synthesized and structurally characterized. Knowledge of these compounds and their structure allows a better understanding of the structural features possible for melemium salts in general. $HC_6N_7(NH_2)_3$ $H_2C_6N_7(NH_2)_3(SO_3Me)_3 \cdot H_2O$ incorporates both $HC_6N_7(NH_2)_3^+$ and $H_2C_6N_7(NH_2)_3^{2+}$ ions. The melemium hydrogensulfate $H_3C_6N_7(NH_2)_3(HSO_4)_3$, also investigated by single-crystal XRD, is the first example of a triple-protonated melemium salt.

Cyamelic acid and cyamelurates (cf. Chapter 7) also have a vast potential for preparing salts and adducts. The structural investigation of cyameluric acid trihydrate proved the preference of a keto-like tautomer. Structural investigations of other compounds containing cyameluric acid or cyamelurates fully support the observations made for the trihydrate. Studying solutions of cyameluric acid in aqueous ammonia three salts were yielded. The structure of these compounds was solved using single-crystal XRD. The results shed light on the structural properties possible for cyamelurate ions. Especially the copper salt shows new coordination types involving this ion, since copper cyamelurate bonds are the first metal cyamelurate bonds notably affecting bond lengths within the cyamelurate itself. This is probably due to the rather soft Cu^{2+} ions' tendency to establish bonds with an increasingly covalent character also explaining the increasing affinity towards Cu-N bonds. Magnetic properties have been studied for this compound showing antiferromagnetic ordering at low temperatures (9 K). Hopefully these results will be helpful in order to establish an improved access to metal cyamelurate salts. This would allow for a better study of their properties as well as their potential use as precursors for carbon nitride-based networks

The work on melonates (cf. Chapter 8) illustrates some modifications usable for the synthesis of melonates from salt melts. The applicability of this reaction has been broadened, as it was able to show that apart from potassium thiocyanate melts potassium cyanate and sodium thiocyanate are usable for yielding melonates. Thus new and presumably more convenient reaction routes could be pointed out. The crystal structure of anhydrous potassium melonate, solved as part of these investigations, is one of few structural analyses conducted for a melonate salts so far. This XRD data also proves that melonates are already yielded in the melt as such and not affected or generated by further treatment of the melt (like contact with water).

hints and rough tendencies. A comprehensive, rational substitution or derivatization chemistry for heptazines still needs a significant amount of further research.

10.4 Additional Goals and Possible Applications

A lot of theoretical insight concerning the formation, properties and structure of carbon nitride precursors and their condensation products has been gathered in the course of this thesis as well as by preceding works from our workgroup and various contributions from other workgroups (cf. Chapter 1). A very important aspect is to use this knowledge in order to understand actual problems, be they related to synthesis or applications of carbon nitride materials. Understanding the different compounds / phases that can possibly be realized during the condensation of carbon nitride precursors is of great importance. Thus the knowledge of reactivity and synthesis of carbon nitrides and their molecular precursors can be significantly enhanced. A good example for this is the synthesis of melem from melamine. The very fact that this reaction can well be carried out in open or “semi-closed” (i.e. loosely covered) systems can only be understood by the knowledge of melamine melem adduct phases. The formation of such compounds on the one hand prevents melamine from almost completely sublimating thus allowing the reaction to take place at reasonable yields. The fact that adduct phases are formed, however, also explains that it is very hard to completely remove all melamine from the reaction mixture although temperatures are often significantly above the sublimation point of melamine. It could however be shown, that melamine can much easier be removed by extraction with solvents (cf. Chapter 3). This shows that understanding the formation of melamine melem adduct phases ultimately was of great help for improving the bulk synthesis of melem. Accordingly, achieving a full understanding of the thermal condensation process leading to carbon nitrides is not merely a matter of collecting data for its own sake. In depth understanding of basic reaction processes is an invaluable aid for further studies. Knowledge, reference data and mechanistic insight gathered this way will promote a comprehensive understanding of carbon nitride chemistry as a whole. Thus, a significantly more rational and planned synthesis can be established very much promoting further scientific efforts. Especially the conceivable progression of carbon nitride chemistry aiming to provide a certain control and tailoring of networks is only truly possible if the basics are well understood. Especially in the high-temperature range of the condensation a lot of principal questions still remain. Many species occurring after the formation of melem have either been proposed or already been proven but many phases occurring at temperature higher than 450 °C are still puzzling regarding their nature. The question if and how such phases can be intentionally prepared in pure form is especially important as it might yield many principal insights regarding the formation of carbon nitride networks in general.

11. Summary

The present thesis provides detailed considerations regarding structure, properties, reactivity and preparation of a variety of carbon nitride materials and their precursors. A brief summary concerning the different aspects of the present work is given in the following.

11.1 The Condensation of Carbon Nitride Precursors

Melem and its adducts (Chapter 3, The Formation of Melem, pp. 26)

Studying the thermal condensation of melamine three solid molecular adducts consisting of melamine $C_3N_3(NH_2)_3$ and melem $C_6N_7(NH_2)_3$ in differing molar ratios were identified. The crystal structure of $2C_3N_3(NH_2)_3 \cdot C_6N_7(NH_2)_3$ ($C2/c$ (no. 15), $Z = 4$, $a = 21.526(4)$, $b = 12.595(3)$, $c = 6.8483(14)$ Å, $\beta = 94.80(3)^\circ$, $V = 1850.2(7)$ Å³), $C_3N_3(NH_2)_3 \cdot C_6N_7(NH_2)_3$ ($Pcca$ (no. 54), $Z = 4$, $a = 7.3280(2)$, $b = 7.4842(2)$, $c = 24.9167(8)$ Å, $V = 1366.54(7)$ Å³) and $C_3N_3(NH_2)_3 \cdot 3C_6N_7(NH_2)_3$ ($C2/c$ (no. 15), $Z = 4$, $a = 14.370(3)$, $b = 25.809(5)$, $c = 8.1560(16)$ Å, $\beta = 94.62(3)^\circ$, $V = 3015.0(10)$ Å³) was solved using single-crystal XRD. All syntheses were carried out in sealed glass ampoules starting from melamine. By variation of the reaction conditions concerning temperature, pressure and presence of ammonia binding metals (europium) insight into the occurrence of the three adduct phases during the thermal condensation process of melamine leading to melem was advanced. A rational bulk synthesis allows controlling the formation of adduct phases as well as phase separation into melamine and melem under equilibrium conditions. A multi-nuclear solid-state NMR spectroscopic investigation of $2C_3N_3(NH_2)_3 \cdot C_6N_7(NH_2)_3$ was conducted, fully supporting and complementing the structural investigations.

The synthesis of melem on a bulk scale was enhanced. The reactivity of some precursor compounds (especially urea) was compared to the one of melamine.

Melamium adduct phases (Chapter 4, The Formation of Melam, pp. 43)

Two molecular adducts featuring mono-protonated melamium ions were prepared by pyrolysis of suitable precursor compounds. The adduct $C_6N_{11}H_{10}Cl \cdot 0.5NH_4Cl$ was obtained by the reaction of melamine with ammonium chloride. The structure of the compound was solved by single-crystal XRD ($P\bar{1}$ (no. 2), $Z = 2$, $a = 6.7785(14)$, $b = 7.7528(16)$, $c = 12.182(2)$ Å, $\alpha = 91.92(3)$, $\beta = 91.61(3)$, $\gamma = 112.26(3)^\circ$, $V = 591.6(2)$ Å³). The second adduct, $C_6N_{11}N_{10}SCN \cdot 2C_3N_3(NH_2)_3$, was prepared by pyrolysis of thiourea. Its structure was also solved by single-crystal XRD ($P\bar{1}$ (no. 2), $Z = 2$, $a = 7.8625(16)$, $b = 10.237(2)$, $c = 14.519(3)$ Å, $\alpha = 98.94(3)$, $\beta = 103.23(3)$, $\gamma = 93.33(3)^\circ$, $V = 1118.4(4)$ Å³).

The melamium adduct phases represent the first protonated melam species allowing unequivocal proton localization (i.e. without disorder). Thus, they provide valuable structural data. Characteristic H-bonding motifs were identified and new insight into the formation of melam was gained.

Melon (Chapter 6, Melon, pp. 73)

Melon prepared from melamine and so-called “melon” based on several differing synthesis protocols were compared. The characterizations conducted propose the formation of a condensed, probably heptazine-containing, solid in all cases. Thus, most sorts of “melon” are suitable as starting materials for further derivatization reactions. Notable differences for the respective products were, however, observed by several analytical methods. This hints at significant structural differences or the presence of impurities for the types of so-called “melon” prepared from other precursors instead of melamine. Additional characterizations were conducted for melon prepared by condensation of melamine. Investigations by electron microscopy and ED were conducted for raw condensation products as well as for highly crystalline samples prepared from such. The samples were compared to the structural data already reported for melon. A synopsis of all analytical data is indicating that raw melon, obtainable by condensation of melamine at 490 - 500 °C, probably is a highly disordered form of the melon reported in the literature.

11.2 Investigations of Heptazine-Based Compounds**Melemium perchlorates (Chapter 5, Section 5.2-5.3, pp. 53)**

A new perchlorate salt of melem, $C_6N_7(NH_2)_3$, was obtained from an aqueous solution of $HClO_4$ at lower concentrations than the ones reported for the synthesis of melemium perchlorate monohydrate $(HC_6N_7(NH_2)_3)ClO_4 \cdot H_2O$. The new salt was identified as melemium melem perchlorate $(HC_6N_7(NH_2)_3)ClO_4 \cdot C_6N_7(NH_2)_3$ representing a melem adduct of water-free melemium perchlorate. The crystal structure was solved by single-crystal X-ray methods ($P\bar{1}$ (no. 2), $Z = 2$, $a = 8.921(2)$, $b = 9.927(2)$, $c = 12.015(2)$ Å, $\alpha = 112.30(3)$, $\beta = 96.96(3)$, $\gamma = 95.38(3)^\circ$, $V = 965.8(4)$ Å³). Another new melemium salt was crystallized at higher concentrations of $HClO_4$. The structure of this compound of composition $H_2C_6N_7(NH_2)_3(ClO_4)_2 \cdot 1.5H_2O$ was also elucidated by single-crystal XRD: ($C\bar{1}$ (no.2), $Z = 8$, $a = 34.140(7)$, $b = 7.608(2)$, $c = 13.211(3)$, $\alpha = 90.000^\circ$, $\beta = 105.14(3)$, $\gamma = 90.000^\circ$, $V = 3312.3(13)$ Å³). Melemium melem perchlorate crystallizes in a layer-like structure containing both protonated $HC_6N_7(NH_2)_3^+$ and non-protonated $C_6N_7(NH_2)_3$ moieties in the coplanar layers as well as perchlorate ions between them all of which being inter-connected by hydrogen-bonds. Melemium diperchlorate sesquihydrate, $H_2C_6N_7(NH_2)_3(ClO_4)_2 \cdot 1.5H_2O$, also displays a layer-like structure which is, however, different from most melemium salts as the perchlorate tetrahedra are centered in plane with the melemium ions and not located between planes. Unfortunately, a complete resolution of the H-bonding network was impeded by twinning / disorder problems in this case. Spectroscopic investigations were also conducted.

Melemium methylsulfonates (Section 5.3 Melemium Methylsulfonates, pp. 61)

The reaction of melem with methylsulfonic acid was investigated. Two new melemium salts with formula $HC_6N_7(NH_2)_3H_2C_6N_7(NH_2)_3(SO_3Me)_3 \cdot H_2O$ and $H_2C_6N_7(NH_2)_3(SO_3Me)_2 \cdot H_2O$ were thus identified. The structure of the compounds was elucidated using single-crystal XRD, $HC_6N_7(NH_2)_3H_2C_6N_7(NH_2)_3(SO_3Me)_3 \cdot H_2O$: ($P\bar{1}$ (no. 2), $Z = 2$, $a = 10.096(2)$, $b = 12.865(3)$, $c = 13.369(3)$ Å, $\alpha = 63.28(3)$, $\beta = 81.19(3)$, $\gamma = 72.92(3)^\circ$, $V = 1461.4(7)$ Å³) $H_2C_6N_7(NH_2)_3(SO_3Me)_2 \cdot H_2O$: ($P2_1/n$ (no. 14), $Z = 4$, $a = 8.0757(16)$, $b = 7.6937(15)$, $c = 27.540(6)$ Å, $\beta = 92.03(3)^\circ$, $V = 1710.6(6)$ Å³). Both compounds are discussed in comparison to structural data from the literature of other melemium salts.

Melemium sulfates (Section 5.4, The Melemium Hydrogensulfate $\text{H}_3\text{C}_6\text{N}_7(\text{NH}_2)_3$, pp. 68)

The melemium sulfate $\text{H}_3\text{C}_6\text{N}_7(\text{NH}_2)_3(\text{HSO}_4)_3$ was synthesized by reaction of melem with concentrated sulfuric acid. The structure of this salt was elucidated by single-crystal XRD ($P2_1/n$ (no. 14), $Z = 4$, $a = 10.277(2)$, $b = 14.921(3)$, $c = 11.771(2)$ Å, $\beta = 99.24(3)^\circ$, $V = 1781.5(6)$ Å³). $\text{H}_3\text{C}_6\text{N}_7(\text{NH}_2)_3(\text{HSO}_4)_3$ is the first compound displaying a triple-protonation of melem. The formation of different melemium sulfates depending on the concentration of sulfuric acid was also investigated. Two additional melemium sulfates were thus identified.

Cyamelic acid (Chapter 7, pp. 90)

Cyamelic acid was synthesized starting from melamine via melon and sodium cyamelurate. Cyameluric acid crystallizes from dilute aqueous hydrochloric acid, forming a trihydrate $\text{H}_3(\text{C}_6\text{N}_7)\text{O}_3 \cdot 3\text{H}_2\text{O}$. The crystal-structure was solved by single-crystal X-ray diffraction (Cc (no. 9), $Z = 16$, $a = 15.5221(2)$, $b = 20.1089(3)$, $c = 13.8533(2)$ Å, $\beta = 102.1066(8)^\circ$, $V = 4227.89(10)$ Å³). There has been some unresolved discussion in the literature concerning the question which of the possible tautomeric forms of cyameluric acid is preferred in the solid state. The structural investigation presented provides proof that the keto-tautomer is favored. The IR, Raman and solid-state NMR-spectroscopic properties of cyameluric acid trihydrate were studied. The thermal behavior of the compound was investigated.

Salts and adducts of cyameluric acid (Chapter 7, Section 7.2 – 7.5, pp. 100)

A keto-like tautomer is found in sodium dihydrogencyamelurate tetrahydrate $\text{NaH}_2(\text{C}_6\text{N}_7)\text{O}_3 \cdot 4\text{H}_2\text{O}$ obtained by neutralization of an aqueous solution, previously prepared by hydrolysis of the polymer melon with sodium hydroxide. The crystal structure was solved by single-crystal X-ray diffraction ($P\bar{1}$ (no. 2), $Z = 2$, $a = 6.6345(13)$, $b = 8.7107(17)$, $c = 11.632(2)$ Å, $\alpha = 68.96(3)$, $\beta = 87.57(3)$, $\gamma = 68.24(3)^\circ$, $V = 579.5(2)$ Å³). The compound forms a layer-like structure with an extensive hydrogen-bonding network.

Three metal(II) salts of cyameluric acid, namely $\text{CaNH}_4(\text{H}_2\text{C}_6\text{N}_7\text{O}_3)(\text{HC}_6\text{N}_7\text{O}_3) \cdot 6\text{H}_2\text{O}$, $[\text{Cu}(\text{NH}_3)_2]_3(\text{C}_6\text{N}_7\text{O}_3)_2 \cdot 2\text{H}_2\text{O}$ and $(\text{NH}_4)_2[\text{Zn}(\text{H}_2\text{O})_6](\text{HC}_6\text{N}_7\text{O}_3)_2 \cdot 2\text{H}_2\text{O}$ were identified. All three compounds were prepared by crystallization from aqueous ammonia solutions containing the respective metal(II) ions. Apparently, the copper salt is identical with a compound claimed in the literature with formula $\text{CuNH}_4\text{C}_6\text{N}_7\text{O}_3 \cdot \text{NH}_3$. The structure of all three compounds was studied using single-crystal XRD ($\text{CaNH}_4(\text{H}_2\text{C}_6\text{N}_7\text{O}_3)(\text{HC}_6\text{N}_7\text{O}_3) \cdot 6\text{H}_2\text{O}$: $P\bar{1}$ (no. 2), $Z = 2$, $a = 6.6428(13)$, $b = 8.7159(17)$, $c = 19.245(4)$ Å, $\alpha = 92.52(3)$, $\beta = 92.22(3)$, $\gamma = 106.95(3)^\circ$, $V = 1063.3(4)$ Å³), ($[\text{Cu}(\text{NH}_3)_2]_3(\text{C}_6\text{N}_7\text{O}_3)_2 \cdot 2\text{H}_2\text{O}$: $P\bar{1}$ (no. 2), $Z = 1$, $a = 7.1732(14)$, $b = 9.2338(18)$, $c = 9.994(2)$ Å, $\alpha = 94.15(3)$, $\beta = 106.13(3)$, $\gamma = 106.28(3)^\circ$, $V = 602.3(3)$ Å³), ($(\text{NH}_4)_2[\text{Zn}(\text{H}_2\text{O})_6](\text{HC}_6\text{N}_7\text{O}_3)_2 \cdot 2\text{H}_2\text{O}$: $P\bar{1}$ (no. 2), $Z = 1$, $a = 6.7568(14)$, $b = 8.7252(17)$, $c = 10.505(2)$ Å, $\alpha = 77.03(3)$, $\beta = 77.08(3)$, $\gamma = 82.95(3)^\circ$, $V = 586.5(2)$ Å³). As part of this thesis the first structural investigation of cyamelurate salts containing divalent metal ions is being provided. The occurrence of special structural features which have been claimed for copper salts of cyameluric acid by earlier works was disproved. Some fundamental discoveries about the crystal growth in these systems are also reported. The copper compound was studied further, using magnetic measurements and thermal analysis.

The dimethylammonium chloride adduct of cyameluric acid, $\text{C}_6\text{N}_7\text{H}_3\text{O}_3 \cdot \text{H}_2\text{N}(\text{CH}_3)_2\text{Cl} \cdot \text{H}_2\text{O}$, was obtained by slow hydrolytic decomposition of cyameluric chloride dissolved in *N,N*-dimethylformamide (DMF). Cyameluric acid crystallizes forming a hydrated molecular adduct with dimethylammonium chloride, which is yielded by decomposition of the solvent.

$C_6N_7H_3O_3 \cdot H_2N(CH_3)_2Cl \cdot H_2O$ is inter-connected by an extensive hydrogen-bonding network. The structure was determined by single-crystal XRD ($P2_1/c$ (no. 14), $Z = 4$, $a = 6.0908(12)$, $b = 22.710(5)$, $c = 9.821(2)$ Å, $\beta = 105.63(3)^\circ$, $V = 1308.2(5)$ Å³). Only the all-keto tautomer of cyameluric acid is found in the course of the structural investigation. Vibrational and thermal properties of the compound were investigated.

11.3 Chemical Reactivity of Heptazines

Melonates (Chapter 8, Tricyanomelaminates and Melonates, pp. 122)

The synthesis of potassium melonate, $K_3C_6N_7(NCN)_3$, by reaction of a potassium thiocyanate melt with the polymer melon ($C_6N_7(NH)(NH_2)_n$) is an established, though poorly understood reaction. The original approach was modified by using salt melts containing Na^+ ions and / or cyanate ions thus yielding the respective melonate salts. These melonates, however, are not the final reaction products. When subjected to cyanate melts at higher temperatures and prolonged reaction times melonates decompose to form tricyanomelaminates. This is the first selective decomposition reaction leading from heptazines to triazines. The progress of the reactions was studied using thermal analysis thus allowing the exact determination of reaction temperatures and weight losses. With the data at hand a better insight into the formation and properties of alkali melonates was gained while establishing new synthetic routes to these compounds. Crystals of anhydrous potassium melonate were isolated directly from a thiocyanate melt. The structure of this compound was solved by single-crystal X-ray-diffraction ($P2_1/c$ (no. 14), $Z = 8$, $a = 13.213(3)$, $b = 17.556(4)$, $c = 13.114(3)$ Å, $\beta = 114.17(3)^\circ$, $V = 2775.4(13)$ Å³). The new reaction conditions involving cyanates on the one hand avoid the release of CS_2 and are no longer highly corrosive to most metallic reaction vessels and on the other hand pose a new cheap and convenient access to melonates and tricyanomelaminates.

Decomposition of C/N/H compounds by aqueous acids (Chapter 9, pp. 139)

The decomposition of melem and cyameluric acid in neutral and acidic aqueous solution was studied. N-guanylammelin dihydrochloride, $H_2(C_3N_3)=O(NH_2)NHC(NH_2)_2Cl_2$, was identified as a selective decomposition product of cyameluric acid in HCl. The structure of the compound was solved by single-crystal XRD ($P2_1/c$ (no. 14), $Z = 4$, $a = 6.9305(14)$, $b = 13.698(3)$, $c = 10.533(2)$ Å, $\beta = 106.67(3)^\circ$, $V = 957.9(3)$ Å³). The reported decomposition reaction is the first synthesis of this novel molecule.

Derivatizations of heptazines (Chapter 9, pp. 135)

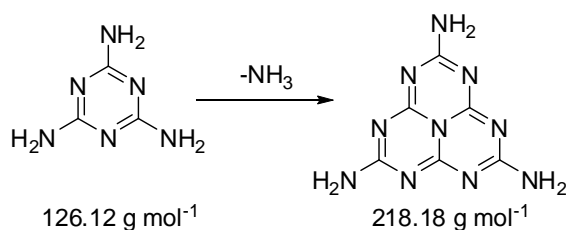
Several ways to prepare additional derivatives involving the heptazine core were investigated. Special interest was placed in improving the synthesis of the reactive intermediate cyameluric chloride, $C_6N_7Cl_3$, as well and in the preparation of cyameluric cyanide $C_6N_7(CN)_3$.

12. Appendix

12.1 Synthesis

The synthesis procedures and experimental details which have not been dealt with in the respective chapters are presented in the following. Analytical data for the products is given wherever appropriate. For additional data concerning the employed commercially available chemicals please refer to Section 12.2.

12.1.1 C₆N₇(NH₂)₃



Small amounts (less than 1 g)

A dried Duran[®] glass ampoule ($\varnothing_{\text{ext}} = 16$ mm, $\varnothing_{\text{int}} = 12$ mm) was loaded with melamine (approximately 200 mg, 1.6 mmol). The ampoule was sealed under argon at a length of approximately 150 cm and heated to a temperature of 460 °C at a rate of 60 °C h⁻¹. After 12 h the ampoule was cooled to RT (cooling rate ≥ 60 °C h⁻¹). The product was yielded as colorless solid in the lower part of the ampoule (typical yield 60 %).

FTIR (reflection, 25 °C, cm⁻¹) 3488 s, 3428 s, 3330 - 3090 vbr, 3070 - 3020 br, 1606 s br, 1469 s br, 1677 m, 1304 m, 1259 w, 1196 w, 1154 w, 1103 w, 1078 w br, 938 w br, 802 s; **Raman** (cm⁻¹), 3190 vbr w, 3020 br w, 1657 w, 1582 w, 1521 w, 1457 m, 1403 w, 1153 m, 981 m, 744 w, 545 s, 456 m, 349 m.

Preparative amounts (more than 1 g)

Melamine (usually about 40 - 60 g, 31 - 47 mmol) was placed in a porcelain crucible covered with a lid and heated to 390 °C for 24 h using a muffle furnace. Slow heating rates should be avoided. The crucible is at best directly placed in the preheated furnace. The resulting impure condensation product, usually a mixture of melem and melamine melem adducts, was ground to a powder suspended in aqueous acetic acid (ca. 10 %, about 600 mL) and heated under reflux for at least 3 h. The product was collected by suction and washed with water until all acetic acid was removed. Prolonged drying at RT yielded melem hydrate, C₆N₇(NH₂)₃ · 1.5H₂O, as a white solid. Crystal water can be removed by drying at 100 - 150 °C for 12 h

FTIR (reflection, 25 °C, cm⁻¹) 3430 m br, 3274 m br, 3100 s br, 1619 s, 1465 s, 2785 w, 1505 w, 1483 m, 1309 w, 1152 m, 794 m, 708 w, 610 w.

12.1.2 $2\text{C}_3\text{N}_3(\text{NH}_2)_3 \cdot \text{C}_6\text{N}_7(\text{NH}_2)_3$

A dried Duran[®] glass ampoule ($\text{Ø}_{\text{ext}} = 10 \text{ mm}$, $\text{Ø}_{\text{int}} = 7 \text{ mm}$) was loaded with melamine (about 1 g, 7.8 mmol). The ampoule was sealed under vacuum (10^{-3} mbar) at a length of approximately 120 mm, placed in a tube furnace and heated to a reaction temperature of 360 °C at a rate of 20 °C h^{-1} . The temperature was maintained for 168 h and slowly reduced by 0.1 °C h^{-1} over the first 20 °C . Subsequently, the cooling rate was increased to 1 °C h^{-1} . The cooled ampoule was opened using a glass cutter and the product was collected. Possible impurities could mostly be mechanically separated from the desired product. The product was yielded as colorless solid.

FTIR (reflection, 25 °C , cm^{-1}) 3486 m, 3465 m, 3361 sh, 3307 sh, 3138 s br, 2991 s br, 2780 m br, 1634 s, 1591 s, 1555 s, 197 s, 1435 s, 1299 w, 1187 m, 1104 m, 1040 m br, 797 m, 711 w br, 681 w, 649 w br; **elemental analysis** for $2\text{C}_3\text{N}_3(\text{NH}_2)_3 \cdot \text{C}_6\text{N}_7(\text{NH}_2)_3$ (wt.%), N: 65.67 (calcd. 65.50), C: 30.60 (calcd. C 30.64), H: 3.95 (calcd. 3.86).

12.1.3 $\text{C}_3\text{N}_3(\text{NH}_2)_3 \cdot \text{C}_6\text{N}_7(\text{NH}_2)_3$

A dried Duran[®] glass ampoule ($\text{Ø}_{\text{ext}} = 10 \text{ mm}$, $\text{Ø}_{\text{int}} = 7 \text{ mm}$) was loaded with melamine (120 mg, 0.94 mmol), europium metal (70 mg, 0.46 mmol) and catalytic amounts of mercury. The ampoule was sealed under vacuum (10^{-3} mbar) at a length of approximately 120 mm, placed in a tube furnace and heated to a reaction temperature of 370 °C at a rate of 20 °C h^{-1} . The temperature was maintained for 168 h and then slowly reduced by 0.1 °C h^{-1} over the first 20 °C . Subsequently the cooling rate was increased to 1 °C h^{-1} . The cooled ampoule was opened using a glass cutter and the product was collected. Loading and opening of the ampoule was conducted using an Ar-filled glove-box. The product was mechanically separated from the Eu particles.

12.1.4 $\text{C}_3\text{N}_3(\text{NH}_2)_3 \cdot 3\text{C}_6\text{N}_7(\text{NH}_2)_3$

A dried Duran[®] glass ampoule ($\text{Ø}_{\text{ext}} = 10 \text{ mm}$, $\text{Ø}_{\text{int}} = 7 \text{ mm}$) was loaded with melamine (about 200 mg, 1.6 mmol). The ampoule was sealed under vacuum (10^{-3} mbar) at a length of approximately 120 mm, placed in a tube furnace and heated to a reaction temperature of 430 °C at a rate of 20 °C h^{-1} . The temperature was maintained for 168 h and slowly reduced by 0.1 °C h^{-1} over the first 20 °C . Subsequently, the cooling rate was increased to 1 °C h^{-1} . The cooled ampoule was opened using a glass cutter and the product was collected. Possible impurities could mostly be mechanically separated from the desired product. The product was yielded as colorless solid.

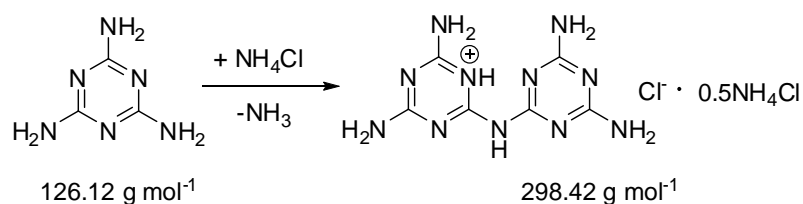
12.1.5 Attempts to Synthesize Adduct Phases from Solution

Mixtures of melem and melamine were prepared from melem (1 g) with the respective amount of melamine. The molar ratios (melamine to melem) of 2 : 1, 1 : 1 and 1 : 3 were prepared to match the known melamine melem adduct phases adducts. The mixtures were ground together carefully and used for all experiments in solution / suspension. The following reaction conditions were applied:

- A** 100 mg of each mixture was suspended in water (10 mL) and boiled under reflux for 5 minutes. The suspension was evaporated to dryness at a temperature of 75 °C.
- B** 100 mg of each mixture was suspended in DMSO (5 mL). The suspension was slowly evaporated to dryness at a temperature of 75 °C.
- C** 100 mg of each mixture was suspended in water (10 mL) and stirred at RT over night. The product was collected by filtration and dried at RT.

It was not successful to prepare one or more adduct phases as yielded in ampoules (cf. Section 12.1.2 – 12.1.4) by any of the abovementioned routes. The products were characterized by PXRD.

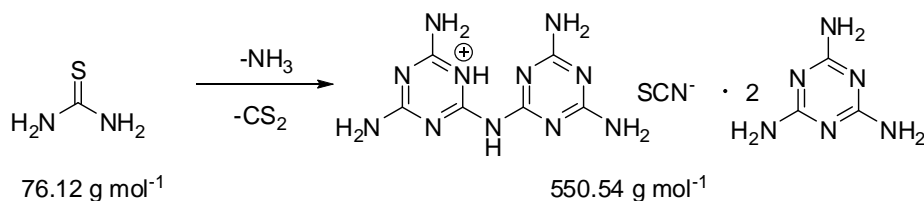
12.1.6 C₆N₁₁H₁₀Cl · 0.5NH₄Cl



Melamine (390 mg, 3.05 mmol) and ammonium chloride (110 mg 2.06 mmol) were placed in a dried Duran[®] ampoule ($\varnothing_{\text{ext}} = 10$ mm, $\varnothing_{\text{int}} = 7$ mm) under argon and sealed at atmospheric pressure at a length of approximately 150 mm. After heating to 450 °C the temperature was maintained for 125 h. After slow cooling to room temperature the ampoule was opened. The whole content of the ampoule was made up of the desired product as a colorless solid (combined yield 189.6 mg, 0.64 mmol).

FTIR (reflection, 25 °C, cm⁻¹) 3314 br s, 3118 br s, 2864 br s, 1672 m, 1634 s, 1597 s, 1508 m, 1472 m, 1418 s, 1375 m, 1326 m, 1272 m, 1185 m, 1153 m, 1107 m, 1063 m, 1026 m, 1006 m, 983 w, 815 w, 786 m, 768 w, 750 w, 704 m, 688 w.

12.1.7 $C_6N_{11}N_{10}SCN \cdot 2C_3N_3(NH_2)_3$



Thiourea (200 mg, 2.63 mmol) was placed in a pre-dried Duran[®] ampoule ($\varnothing_{\text{ext}} = 10 \text{ mm}$, $\varnothing_{\text{int}} = 7 \text{ mm}$) under argon and sealed at atmospheric pressure at a length of approximately 150 mm. After heating to 400 °C the temperature was maintained for 12 h. After slow cooling to room temperature the ampoule was opened. The lower parts of the ampoule contained $C_6N_{11}N_{10}SCN \cdot 2C_3N_3(NH_2)_3$ as a colorless solid (100.3 mg, 0.18 mmol).

12.1.8 $HC_6N_7(NH_2)_3ClO_4 \cdot C_6N_7(NH_2)_3$

Melemium melem perchlorate was synthesized by heating a stirred suspension of melem (250 mg, 1.15 mmol) in aqueous perchloric acid (57.5 mL, 8 %) under reflux. Upon cooling over night the title compound crystallized as colorless blocks which were collected by filtration over a Büchner funnel and dried in streaming air (130 mg, 0.24 mmol, 42 %).

FTIR (reflection, 25 °C, cm^{-1}) 3436 s, 3391 s, 3102 s br, 1705 w, 1665 s, 1592 s, 1451 s, 1329 m, 1051 s, 961 w, 858 w, 790 s, 743 w; **Raman** (cm^{-1}) 1696 m, 1631 w, 1603 w, 1533 w, 1480 w, 1342 w, 1157 m, 932 w, 800 w, 745 m, 541 s, 457 s, 323 s.

12.1.9 $H_2C_6N_7(NH_2)_3(ClO_4)_2 \cdot 1.5H_2O$

Melem (250 mg, 1.15 mmol) was suspended in a solution prepared by dilution of $HClO_4$ (60 %, 30 mL) with water (20 mL). After heating to 70 °C all melem had dissolved and the clear solution was cooled to 4 °C over night. The product was yielded as needle-shaped colorless crystals and collected by suction (140 mg, 0.31 mmol, 28 %)

12.1.10 $HC_6N_7(NH_2)_3H_2C_6N_7(NH_2)_3(SO_3Me)_3 \cdot H_2O$

Melem hydrate (400 mg, 1.63 mmol) was suspended in a solution of methylsulfonic acid (10 mL) in water (35 mL). Active carbon was added to the suspension. The mixture was boiled under reflux for a short time and passed through a sintered glass filter under suction. The resulting solution was cooled to 4 °C over night. Afterwards the colorless product was removed by suction (298 mg, 49 %). The product usually contained small amounts of $H_2C_6N_7(NH_2)_3(SO_3Me)_2 \cdot H_2O$.

FTIR (reflection, 25 °C, cm^{-1}) 3443 s, 3237 s br, 2600 sh br, 1611 m, 1510 w, 1467 m, 1320 w, 1204 w, 1185 m, 1148 m, 1042 m, 962 w, 779 m.

Colorless needle-shaped crystals of $HC_6N_7(NH_2)_3H_2C_6N_7(NH_2)_3(SO_3Me)_3 \cdot H_2O$ could best be collected after slow cooling / evaporation of a hot solution containing melem hydrate (150 mg), methylsulfonic acid (10 mL) and water (30 mL).

12.1.11 $\text{H}_2\text{C}_6\text{N}_7(\text{NH}_2)_3(\text{SO}_3\text{Me})_2 \cdot \text{H}_2\text{O}$

Melem hydrate (900 mg, 3.67 mmol) was suspended in a solution of methylsulfonic acid (20 mL) in water (30 mL). Active carbon was added to the suspension. The mixture was boiled under reflux for a short time and passed through a sintered glass filter under suction. The resulting solution was cooled to 4 °C over night. Afterwards the colorless product was removed by suction (278 mg, 18 %).

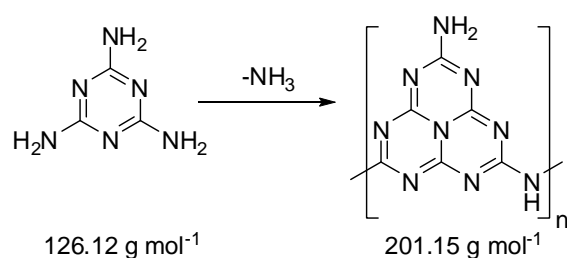
FTIR (reflection, 25 °C, cm^{-1}) 3558 m, 3302 m, 3063 s br, 2703 m br, 1717 w, 1650 s, 1619 s, 1541 m, 1494 m, 1437 m, 1410 m, 1342 w, 1312 w, 1150 s, 1127 s, 1040 s, 983 w, 964 w, 779 m.

Colorless needle-shaped crystals of $\text{H}_2\text{C}_6\text{N}_7(\text{NH}_2)_3(\text{SO}_3\text{Me})_2 \cdot \text{H}_2\text{O}$ could best be collected after slow cooling / evaporation of a hot solution containing melem hydrate (150 mg), methylsulfonic acid (20 mL) and water (30 mL).

12.1.12 $\text{H}_3\text{C}_6\text{N}_7(\text{NH}_2)_3(\text{HSO}_4)_3$

Melem (1.7 g, 7.80 mmol) was dissolved in hot H_2SO_4 (30 mL conc. H_2SO_4 + 20 mL H_2O). This was conducted as fast as possible to avoid decomposition. The solution was stored at 4 °C over night. The colorless crystals were collected by filtration using a sintered glass Schlenk frit. The product was dried at 10^{-3} mbar for 24 h to remove most of the remaining H_2SO_4 . The product is very sensitive to moisture and must be handled and stored in a dry inert gas atmosphere. Crystals were selected in an Ar-filled glove-box and measured in a sealed glass capillary.

12.1.13 $\text{C}_6\text{N}_7(\text{NH}_2)(\text{NH})$, Raw Melon from Melamine



A porcelain crucible was loaded with melamine (usually 20 – 60 g) and covered with a porcelain lid. The crucible was placed in a muffle furnace and maintained at 490 °C for 4 d. The product was ground to a powder and homogenized after the first day. This procedure was repeated if necessary. The resulting yellow solid was ground well before use in further reactions.

FTIR (reflection, 25 °C, cm^{-1}) 3249 m br, 3152 m br, 3082 m br, 1628 m, 1537 m, 1452 m, 1393 s, 1314 s, 1231 s, 1204 s, 1133 m, 890 w, 804 m; **Raman** (cm^{-1}) 3158 br w, 2420 br w, 1621 m, 1559 m, 1483 m, 1351 w, 1311 m, 1234 s, 1153 m, 1117 w, 1078 w, 978 w, 751 m, 707 s, 590 w, 474 m; **elemental analysis** for $\text{C}_6\text{N}_7(\text{NH}_2)(\text{NH})$ (wt.%) N: 62.67 (calcd. 62.67), C: 33.22 (calcd. 35.83), H: 1.83 (calcd. 1.50).

12.1.14 C₆N₇(NH₂)(NH), Highly Crystalline Melon

A well ground mixture (200 mg) consisting of raw melon (73 wt.%) melamine (25 wt.%) and ammonium chloride (2 wt.%) was placed in a Duran[®] ampoule and heated to 490 °C at a heating rate of 5 °C min⁻¹. The temperature was maintained for 900 min after which the ampoule was slowly cooled to room temperature (1 °C min⁻¹). Melon was yielded as a white solid with a slight hint of yellow (165.2 mg).

12.1.15 “Melon” from Sodium Thiocyanate

CAUTION: The handling of gaseous chlorine requires the respective security precautions.

Chlorine gas was passed through a solution of sodium thiocyanate (100 g, 1.23 mol) in water (250 ml). External cooling was applied to prevent overheating of the solution. The reaction was interrupted to collect resulting precipitate if the mixture got too thick to handle. The combined precipitate was washed thoroughly with water and dried at 120 °C under air overnight. So-called “pseudothiocyanogen” was yielded as an orange solid (18.2 g).

FTIR (reflection, 25 °C, cm⁻¹) 3050 m br, 2168 w, 2045 w, 1615 w, 1488 m, 1428 m, 1216 s, 1060 m, 908 m, 793 w, 672 w; **MS** (DEI⁺): M/Z (%) = 58.0 (10.85), 59.1 (75.62), 64.0 (100), 66.0 (8.81), 76.0 (82.47), 78.0 (7.44), 84.0 (19.39), 96.0 (17.56), 98.0 (2.46), 110.0 (1.36), 116.0 (2.37), 127.9 (8.67), 129.9 (1.55), 159.9 (22.03), 161.9 (4.95), 191.9 (20.34), 192.9 (1.04), 193.9 (5.57), 200.0 (1.97), 223.9 (9.37), 225.9 (2.99), 252.0 (1.66), 255.8 (3.82), 257.8 (1.41); **elemental analysis** (wt.%) N: 24.78, C: 19.99, H: 0.80, S: 52.15.

Further condensation of so-called “pseudothiocyanogen” was carried out by heating small batches (usually 100 mg) to temperatures ranging from 400 and 500 °C for 2 – 4 h.

12.1.16 “Melon” from Mercury(II) Thiocyanate

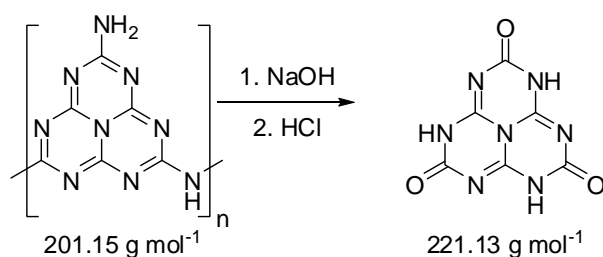
CAUTION: Mercury thiocyanate is very toxic and must be handled with appropriate care. All reaction steps must be conducted in a fume hood providing sufficient ventilation.

Mercury(II) thiocyanate (typically 5 - 10 g, 16 -32 mmol) was placed in a porcelain evaporation dish. Ignition was carried out with a hot glass rod. After the reaction had subsided potential unreacted parts were reignited until the reaction was complete. The yellow serpent-like structures were ground to a powder. For further purification the product was washed with water and dried in vacuo (10⁻¹ mbar) at ca. 100 °C for several hours.

FTIR (reflection, 25 °C, cm⁻¹) 2347 w br, 2118 w br, 1581 s br, 1417 s, 1312 s, 1213 s, 1083 w, 800 m; **elemental analysis** (wt.%) Hg: 64, S: 12.5.

The “Pharaoh’s serpents” were transformed into “melon” by heating to 400 °C under air using a muffle furnace. Reaction times were variable and largely dependent on sample size. Usually the reaction took between 6 h and 48 h for samples between 100 mg and 1 g.

12.1.17 $\text{H}_3\text{C}_6\text{N}_7\text{O}_3 \cdot 3\text{H}_2\text{O}$



Large quantities of synthetically pure cyameluric acid are best prepared by the following procedure:

Melon was suspended in 2 M NaOH and boiled under reflux for 1 h. The hot solution was immediately passed through a preheated, large sintered glass funnel into a cooled flask. The filtrate was cooled to RT. The solution was acidified ($\text{pH} \approx 1$) by drop-wise addition of conc. HCl (37 %) and stored at 4 °C for several hours. The product was collected by suction and washed thoroughly with ice water. Cyameluric acid was yielded as a white solid and dried on a piece of absorptive filter paper under air over night.

Highly crystalline samples are readily accessible by the following procedure:

Melon (1 g, 5 mmol) was suspended in 1.5 M NaOH (50 mL, freshly prepared from NaOH pellets) and boiled under reflux for 45 min. Sodium cyamelurate crystallized upon cooling to room temperature. The cyamelurate salt was collected by suction and dissolved in water (150 mL) and shortly heated until boiling. All insolubles were removed by filtration. Conc. HCl (37 %, 2 mL) was carefully added to the filtrate. Cyameluric acid trihydrate (420 mg) was yielded as a crystalline colorless solid after several days of crystallization.

FTIR (reflection, 25 °C, cm^{-1}) 3483 m, 3427 m, 3328 m, 3200 m, 2984 m, 2851 m, 2779 m, 1583 s, 1470 s, 1393 s, 1306 s, 1167 m, 932 m, 823 w, 784 s; **Raman** (cm^{-1}) 1705 s, 1560 s, 1475 m, 1403 m, 1327 m, 1102 m, 965 w, 737 m, 550 s, 450 m, 360 w, 247 w, 105 s; **^{13}C NMR** (solid-state, 25 °C, ppm) $\delta = 156.5 \text{ C(e)}$, 150.6 C(i) ; **^1H NMR** (solid-state, 25 °C, ppm) $\delta = 4.9$; **^{15}N NMR** (solid-state, 25 °C, ppm) -242.7 , -245.9 ; **elemental analysis** for $\text{H}_3(\text{C}_6\text{N}_7)\text{O}_3 \cdot 3\text{H}_2\text{O}$ (wt.%) N: 36.07 (calcd. 35.63), C: 26.26 (calcd. 26.19), H: 3.06 (calcd. 3.30).

12.1.18 $\text{Na}[\text{H}_2(\text{C}_6\text{N}_7)\text{O}_3] \cdot 4\text{H}_2\text{O}$

Melon was prepared in accordance to the abovementioned procedure. Melon (2 g, 10 mmol) was suspended in 1.3 M aqueous sodium hydroxide (50 mL) and boiled under reflux for 2 h. The solution was diluted by addition of water (100 mL) and boiled for an additional 2 h. All insoluble residues of melon were removed by filtration and the solution was cooled to RT. The solution was neutralized by drop-wise addition of conc. H_2SO_4 . A precipitate of cyameluric acid was removed by filtration. The resulting solution was allowed to crystallize at RT for several weeks after which crystals of $\text{Na}[\text{H}_2(\text{C}_6\text{N}_7)\text{O}_3] \cdot 4\text{H}_2\text{O}$ were collected.

12.1.19 $\text{CaNH}_4(\text{H}_2\text{C}_6\text{N}_7\text{O}_3)(\text{HC}_6\text{N}_7\text{O}_3) \cdot 6\text{H}_2\text{O}$

A saturated warm solution of cyameluric acid trihydrate in ca. 2.5 % aqueous ammonia containing Ca^{2+} ions (15.8 °dH = 281 ppm CaCO_3) was cooled to RT. The platelet-like crystals of the calcium salt were found among the fine needle-like crystals of ammonium cyamelurate. The crystals of $\text{CaNH}_4(\text{H}_2\text{C}_6\text{N}_7\text{O}_3)(\text{HC}_6\text{N}_7\text{O}_3) \cdot 6\text{H}_2\text{O}$ could be grown up to a size suitable for XRD by Ostwald ripening at about 40 °C for at least 48 h in a tightly sealed flask.

12.1.20 $[\text{Cu}(\text{NH}_3)_2]_3(\text{C}_6\text{N}_7\text{O}_3)_2 \cdot 2\text{H}_2\text{O}$

Cyameluric acid trihydrate (150 mg, 0.54 mmol) was suspended in water (30 mL). Aqueous ammonia (25 %, ca. 2 mL) was added until a clear solution had formed. $\text{CuSO}_4 \cdot 5\text{H}_2\text{O}$ (203 mg, 0.8 mmol) was dissolved in of water (8 mL). A 25 % ammonia solution (1 mL) was added to form the copper tetraammine complex. The two solutions were combined and placed in an open beaker glass allowing evaporation of ammonia. After about one hour a violet precipitate had formed which was collected by filtration (173 mg, 0.23 mmol, 85 %).

Part of this raw product was dissolved in concentrated ammonia and placed in an Erlenmeyer flask sealed with an hour glass allowing ammonia to dissipate slowly. After about a month large violet crystals of $[\text{Cu}(\text{NH}_3)_2]_3(\text{C}_6\text{N}_7\text{O}_3)_2 \cdot 2\text{H}_2\text{O}$ could be collected.

12.1.21 $(\text{NH}_4)_2[\text{Zn}(\text{H}_2\text{O})_6](\text{HC}_6\text{N}_7\text{O}_3)_2 \cdot 2\text{H}_2\text{O}$

ZnCl_2 (83.3 mg, 0.611 mmol) was dissolved in a small amount of water. A 25 % aqueous solution of ammonia was added until the initial precipitate of $\text{Zn}(\text{OH})_2$ had dissolved. This solution was added to a solution of cyameluric acid trihydrate (112.1 mg, 0.407 mmol) in aqueous ammonia (17 %, 50 mL). The combined solution was kept at 40 °C in an open flask over night. A microcrystalline precipitate was removed by filtration and discarded. After additional slow evaporation at RT for five days, the product was collected as a colorless solid. In order to yield suitable single-crystals $(\text{NH}_4)_2[\text{Zn}(\text{H}_2\text{O})_6](\text{HC}_6\text{N}_7\text{O}_3)_2 \cdot 2\text{H}_2\text{O}$ was recrystallized from 17 % ammonia at a temperature of about 70 °C. The structure of the recrystallized product is not altered according to PXRD.

12.1.22 $\text{H}_3\text{C}_6\text{N}_7\text{O}_3 \cdot \text{H}_2\text{NMe}_2\text{Cl} \cdot \text{H}_2\text{O}$

Poorly crystalline bulk material was prepared by dissolving cyameluric acid trihydrate (75 mg, 273 mmol) and dimethylammonium chloride (26 mg, 318 mmol) in DMF (5 mL) in an open round flask under prolonged stirring at room temperature. The solution was heated to 40 °C. After maintaining this temperature for 24 h the solvent had evaporated and the residual colorless solid was collected, ground and placed on an absorbing filter paper under air for additional 24 h (86 mg, 0.27 mmol, 98 %).

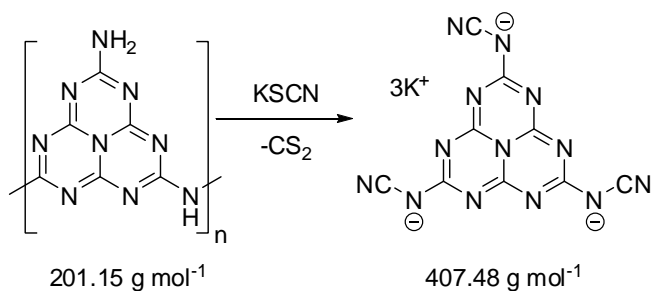
PXRD pattern was in agreement with the diagram simulated based one the single-crystal data. The product must be kept dry.

FTIR (reflection, 25 °C, cm^{-1}) 3444 m br, 2963 m br, 2891 m, 2824 m, 2745 s, 2463 sh, 1626 s, 1598 s, 1446 s, 1395 m, 1382 m, 1371 m, 1292 s, 1161 m, 1093 w, 1027 m, 938 m, 809 m, 777 s, 747 w, 617 w; **elemental analysis** for $\text{H}_3\text{C}_6\text{N}_7\text{O}_3 \cdot \text{H}_2\text{NMe}_2\text{Cl} \cdot \text{H}_2\text{O}$ (wt.%) N: 34.32 (calcd. 34.94), C: 30.44 (calcd. 29.96), H: 4.31 (calcd. 4.09).

For the growth of single-crystals cyameluric chloride was dissolved in an excess of DMF. The solution was allowed to crystallize by slow evaporation of the solvent in an open flask at room temperature. After several weeks the initially yellow solution lost its color and large needle-shaped crystals of $\text{H}_3\text{C}_6\text{N}_7\text{O}_3 \cdot \text{H}_2\text{NMe}_2\text{Cl} \cdot \text{H}_2\text{O}$ suitable for XRD were found.

12.1.23 $\text{K}_3\text{C}_6\text{N}_7(\text{NCN})_3$ from a Thiocyanate Melt

CAUTION: The reaction can be vigorous and results in the occurrence of open flames.



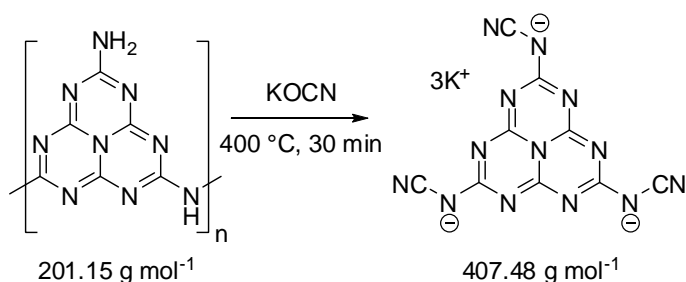
Potassium thiocyanate (14 g, 144 mmol) was molten in a ceramic evaporation dish using a Bunsen burner. Once the bottom of the dish had reached red heat, melon (6.9 g, 34 mmol) was added to the melt in small portions. The carbon disulfide liberated during the vigorous reaction was allowed to burn. After the reaction had ceased to evolve gases the temperature was maintained for approximately 10 min after which the melt was slowly cooled until it had completely solidified. Then the evaporation dish was quickly transferred into an argon glove-box where the crystals were collected from the melt.

For yielding bulk material potassium thiocyanate (4.0 g, 41 mmol) was molten in a ceramic evaporation dish using a Bunsen burner. Melon (1.66 g, 8.2 mmol) was added to the melt. After the vigorous reaction had ceased the product was dissolved in water (about 100 mL). A small amount of active carbon was added and the solution was boiled until it lost its slightly yellow color. After cooling to room temperature a small amount of ethanol was added and all insoluble parts were removed by filtration. The solution was completely precipitated using ethanol (about 200 mL were required). The product was collected by filtration and thoroughly washed with acetone. After drying overnight $\text{K}_3\text{C}_9\text{N}_{13} \cdot 5\text{H}_2\text{O}$ was collected as a white solid (1.04 g, 2.1 mmol, 32 %).^[u] Further purification is possible by recrystallization from water.

FTIR (reflection, 25 °C, cm^{-1}) 3392 s br, 2171 s, 2142 m, 1641 s, 1493 m, 1433 s, 1300 w, 1190 w, 1093 w, 793 m; **Raman** (cm^{-1}) 3392 w br, 2176 s, 1642 m, 1574 s, 1508 m, 1417 m, 1378 m, 1192 w, 1095 w, 1056 w, 775 m, 756 w, 709 w, 664 w, 574 w, 444 m, 422 m, 299 s; **^{13}C NMR** (270 MHz, D_2O , 25 °C): $\delta = 122.3, 156.1, 171.8$; **elemental analysis** for $\text{K}_3\text{C}_9\text{N}_{13} \cdot 5\text{H}_2\text{O}$ (wt.%) N: 37.04 (calcd. 36.60), C: 21.81 (calcd. 21.73), H: 2.04 (calcd. 2.03), K: 23.55 (calcd. 23.57).

[u] Percentage data given for yields is calculated under the assumption that the respective equations offered in Section 8.1.3 are applicable. Values are suspect to uncertainty, as this cannot be confirmed at the moment.

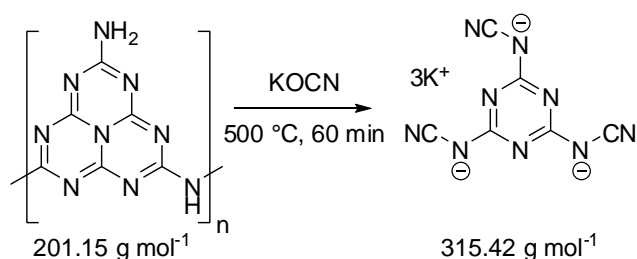
12.1.24 $\text{K}_3\text{C}_6\text{N}_7(\text{NCN})_3$ from a Cyanate Melt



Melon (500 mg, 2.47 mmol) and potassium cyanate (1000 mg, 12.3 mmol) were ground together and heated at 400 °C for about 30 min. The reaction mixture was cooled to room temperature and dissolved in water (about 50 mL). After boiling with a small amount of active carbon, insoluble components were removed by filtration. After cooling to room temperature, the product was precipitated by addition of at least three volume equivalents of ethanol. The precipitate was collected by filtration, washed with acetone and dried under steaming air. The product was yielded as white solid (515 mg, 1.04 mmol, 53 %).^[u] Recrystallization from water followed by drying at 40 °C was used for purification purposes.

FTIR (reflection, 25 °C, cm^{-1}) 3377 s br, 2166 s, 2137 m, 1636 s, 1491 m, 1427 s, 1301 w, 1187 w, 1090 w, 1045 w, 792 m; **^{13}C NMR** (270 MHz, D_2O , 25 °C): $\delta = 122.3$ (N-C \equiv N), 156.1 171.7 (C-NCN); **elemental analysis** for $\text{K}_3\text{N}_9\text{C}_{13} \cdot 5 \text{H}_2\text{O}$ (wt.%) N: 36.12 (calcd. 36.60) C: 21.57 (calcd. 21.73) H: 2.10 (calcd. 2.03).

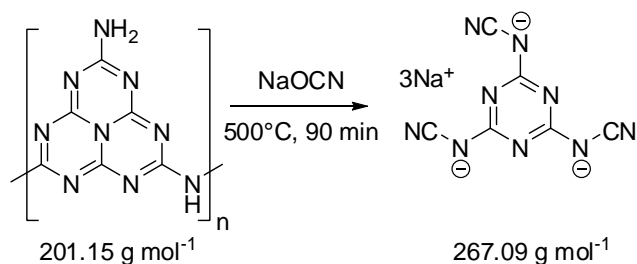
12.1.25 $\text{K}_3\text{C}_3\text{N}_3(\text{NCN})_3$ from a Cyanate Melt



Melon (500 mg, 2.47 mmol) and potassium cyanate (1000 mg, 12.3 mmol) were ground together and heated at 500 °C for about 60 min. The reaction mixture was cooled to room temperature and dissolved in water (about 50 mL). After heating to about 80 °C for a short time a small amount of active carbon was added and the solution was allowed to cool to room temperature. After filtration the product was precipitated by addition of at least three volume equivalents of ethanol. The precipitate was collected by filtration and recrystallized from water. $\text{K}_3\text{N}_6\text{C}_9 \cdot \text{H}_2\text{O}$ was yielded as a white solid (408 mg, 1.22 mmol, 37 %).^[u]

FTIR (reflection, 25 °C, cm^{-1}) 3534 w, 3014 w br, 2228 w, 2154 s 1644 w 1592 w, 1507 s, 1391 s, 1244 w, 1136 w, 1027 w, 982 w, 808 w; **^{13}C NMR** (270 MHz, D_2O , 25 °C): $\delta = 124.8$ (N-C \equiv N), 172.9; **elemental analysis** for $\text{K}_3\text{N}_6\text{C}_9 \cdot \text{H}_2\text{O}$ (wt.%) N: 35.55 (calcd. 37.81) C: 20.79 (calcd. 21.61) H: 0.83 (calcd. 0.60) K: 34.5 (calcd. 35.2).

12.1.26 Na₃C₃N₃(NCN)₃ from a Cyanate Melt

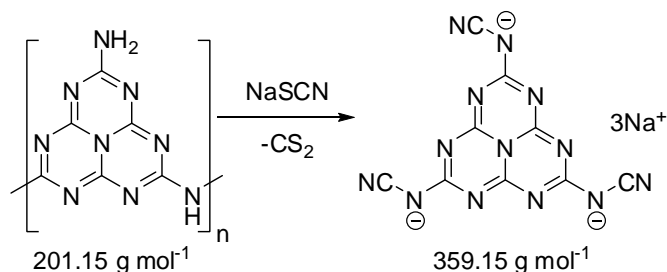


Melon (500 mg, 2.47 mmol) and NaOCN (800 mg, 9.88 mmol) were ground together and heated at 500 °C for about 90 min. After initial melting, the reaction mixture completely solidified again. The product was dissolved in about 20 mL of water. After addition of a small amount of active carbon and short boiling all insoluble impurities were removed by filtration. The product was precipitated from the solution after cooling to room temperature by addition of ethanol, collected by filtration and washed with acetone. Na₃N₆C₉ · 3 H₂O was yielded as a white solid (543 mg, 1.7 mmol, 52 %).^[u]

FTIR (reflection, 25 °C, cm⁻¹) 3615 m, 2930 m br, 2377 w, 2240 w, 2176 s, 1662 m, 1511 s, 1396 s, 1384 s, 1235 m, 1000 w, 802 m, 773 w 713 w; **¹³C NMR** (270 MHz, D₂O, 25 °C): δ = 124.9 (N-C≡N), 173.0; **elemental analysis** for Na₃N₆C₉ · 3 H₂O (wt.%) N: 38.48 (calcd. 39.25) C: 22.08 (calcd. 22.44) H: 1.94 (calcd. 1.88) Na: 21.2 (calcd. 22.4).

12.1.27 Na₃C₆N₇(NCN)₃ from a Thiocyanate Melt

CAUTION: The reaction can be vigorous and results in the occurrence of open flames.



Sodium thiocyanate (4.0 g, 50 mmol) was molten in a ceramic evaporation dish using a Bunsen burner. Melon (2.00 g, 10 mmol) was added to the melt. After the vigorous reaction had ceased the product was dissolved in water (about 100 mL). A small amount of active carbon was added and the solution was boiled until it lost its slightly yellow color. After cooling to room temperature a small amount of ethanol was added and all insoluble parts were removed by filtration. The solution was completely precipitated using ethanol (about 200 mL were required). The product was collected by filtration and thoroughly washed with acetone. After drying over night Na₃N₉C₁₃ · 6H₂O was collected as a white solid (0.82 g, 1.8 mmol, 23 %).^[u] Further purification is possible by recrystallization from water.

FTIR (reflection, 25 °C, cm⁻¹) 3366 m br, 2173 s, 2152 m, 1641 s, 1491 m, 1432 s, 1301 w, 1194 w, 1054 w, 794 m; **¹³C NMR** (270 MHz, D₂O, 25 °C): δ = 122.3, 156.1, 171.7; **elemental analysis** for Na₃N₉C₁₃ · 6H₂O (wt.%) N: 38.69 (calcd. 38.97) C: 22.70 (calcd. 23.13) H: 2.75 (calcd. 2.59) Na: 14.36 (calcd. 17.76)

12.1.28 Reactivity in KSCN melts

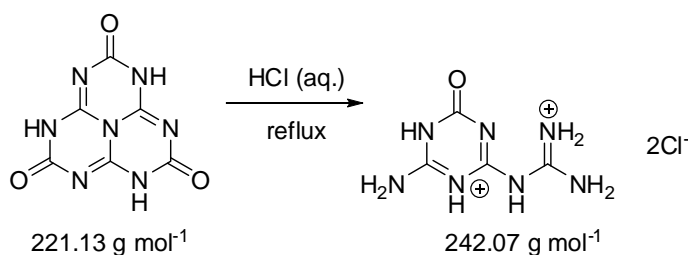
Experiments dealing with the reactivity of certain compounds in thiocyanate melts are listed below (cf. Table 45).

Table 45. Observations conducted for reactions in KSCN melts.

Substance added to KSCN melt ^[a]	Observations	Identified product(s)
Melon	evolution of gases, blue coloring of the melt, burning of CS ₂	K ₃ C ₆ N ₇ (NCN) ₃
Melem	evolution of gases, blue coloring of the melt, burning of CS ₂	K ₃ C ₆ N ₇ (NCN) ₃
NH ₄ Cl	evolution of gases, blue coloring of the melt, burning of CS ₂	yet unidentified crystalline compound(s), probably some sort of melam adduct
KHSO ₄	very vigorous reaction, blue coloring of the melt.	yet unidentified crystalline compound(s)
KOH	initial orange color of the melt quickly turns to blue, evolution of an inflammable gas (burning is however less intensive than observed for CS ₂)	yet unidentified crystalline compound(s)
Na ₂ S x H ₂ O	orange to red coloring of the melt, no evolution of CS ₂	
Urea	vigorous evolution of gases, no CS ₂ , blue coloring of the melt	none - probably no significant degree of reaction took place due to the low sublimation point of urea

[a] Reaction conditions were all chosen to be similar to the ones used for synthesizing melonates.

12.1.29 H₂(C₃N₃)=O(NH₂)NHC(NH₂)₂Cl₂



Cyameluric acid trihydrate (214 mg, 0.78 mmol) was suspended in conc. hydrochloric acid (37 %, 50 mL). The mixture was heated under reflux until most cyameluric acid had dissolved (about 1 h); however, a slight clouding remained. After cooling to RT small amounts of initial ill-defined precipitates were removed by filtration. The product was yielded as colorless crystals after 3 weeks of slow evaporation of the solvent at RT.

12.1.30 C₆N₇O₃ · 4.5H₂O

Melem hydrate (15 g, 62 mmol; cf. Section 12.1.1 for synthesis) was suspended in aqueous NaOH (2 M, 600 mL). After heating to reflux for 30 min to 1 h most melem was dissolved. The hot solution was quickly passed through a warm sintered glass funnel into an ice-

cooled flask under suction. After 12 h at 4 °C the colorless crystalline precipitate of $C_6N_7O_3 \cdot 4.5H_2O$ was collected and dried under air at RT.

12.1.31 $C_6N_7O_3 \cdot 4H_2O$

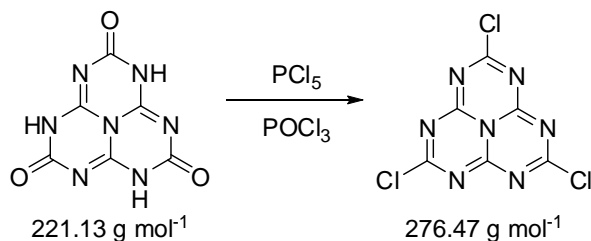
Method A

A saturated aluminum(III) solution is prepared by dissolving $Al_2(SO_4) \cdot 18H_2O$ in sodium hydroxide (1 M). The respective solution is added to solid $C_6N_7O_3 \cdot 4.5H_2O$ (73.6 mg, 0.2 mmol) until the product is completely dissolved at a temperature of ca. 60 °C. Evaporation at RT resulted in an initial ill-defined precipitate primarily consisting of $Al(OH)_3$. This precipitate was removed from the solution after 1 d. After 3 d another precipitate containing crystals of the new cyamelurate salt was collected. Later fractions contained large amounts of sulfate salts and were thus discarded.

Method B

$ZnCl_2$ (83.3 mg, 0.6 mmol) was dissolved in water (5 mL). A sodium hydroxide (2 M) solution was added until the initial precipitate had dissolved. A saturated solution of $C_6N_7O_3 \cdot 4.5H_2O$ (150 mg, 0.41 mmol) in water was added. Slow evaporation of the solvent resulted in an initial precipitate mainly consisting of ZnO , which was discarded. Further crystallization yielded the new cyamelurate salt as a colorless solid.

12.1.32 $C_6N_7Cl_3$



Cyameluric chloride is best prepared according to the following procedure. Other methods have shown significant disadvantages concerning yields and purity.

Anhydrous cyameluric acid was prepared by drying cyameluric acid trihydrate (2.0 g, 8.1 mmol) at 130 °C and 10^{-3} mbar for 12 h. In an atmosphere of dry argon, a mixture of the resulting anhydrous cyameluric acid and PCl_5 (5.63 g, 27 mmol) was suspended in freshly distilled $POCl_3$ (5 mL). The mixture was stirred under reflux for 2.5 h. A vigorous evolution of gases (HCl) and a yellow coloring was observed. Subsequently all volatile components were removed in vacuo (10^{-2} mbar, 100 °C). Cyameluric chloride was yielded as a yellow solid (2.18 g, 7.9 mmol, 98 %). The product is best stored in the absence of air and light.

FTIR (reflection, 25 °C, cm^{-1}) 2923 w, 1602 s, 1498 m, 1295 s, 1200 s, 1088 m, 978 w, 939 m, 822 m, 647 w.

12.2 Chemicals

The sources of supply as well as the purity of the chemicals used in this work are listed in Table 46. Additional purification steps are described in the respective sections. If not mentioned otherwise, chemicals were used as-supplied.

Table 46. Source of supply and purity of the chemicals used in this work.

Name	Formula	Purity	Supplier
acetic acid	HO ₂ CMe	purum	Bisterfeld-Graen
acetone	CO(Me) ₂	DAB	Bisterfeld-Graen
acetonitrile	MeCN	99.5 %	Acros
aluminum chloride hexahydrate	AlCl ₃ · 6H ₂ O	puriss	Applichem
ammonia (25 %)	NH ₃	purum	Bisterfeld-Graen
ammonium carbonate ^[a]	“(NH ₄) ₂ CO ₃ ”	ACS reagent	Sigma-Aldrich
ammonium chloride	NH ₄ Cl	p.a.	Fluka
ammonium thiocyanate	NH ₄ SCN	puriss	Grüssing
calcium chloride dihydrate	CaCl ₂ · 2H ₂ O	p.a.	Merck
chlorine	Cl ₂	2.8	Messer-Griesheim
copper(I) iodide	CuI	purum	Riedel-de Haën
copper(II) sulfate pentahydrate	CuSO ₄ · 5H ₂ O	p.a.	Applichem
cyanamide	H ₂ NCN	purum	Fluka
cyanuric chloride	C ₃ N ₃ Cl ₃	99 %	Acros
dicayandiamide	C ₂ N ₄ H ₄	99 %	Avocado
1,2-dichlorobenzene	C ₆ H ₄ Cl ₂	for synthesis	Merck
dimethylammonium chloride	HN(Me) ₂ Cl	for synthesis	Merck
DMF (anhydrous)	HCO(NMe ₂)	extra dry	Acros
DMF (general use)	HCO(NMe ₂)	purum	Roth
DMSO	SO(Me) ₂	99.3 %	Roth
ethanol (1 % isohexane)	EtOH	99 %	Bundesmonopolverwaltung für Brandwein
europium	Eu	99.99 %	Smart Elements
hydrochloric acid (37 %)	HCl	purum	Bisterfeld-Graen
melamine	C ₃ N ₃ (NH ₂) ₃	purum	Fluka
mercury	Hg	100 %	Riedel-de Haën
mercury(II) thiocyanate	Hg(SCN) ₂	not given	Sigma-Aldrich
1-methyl-2-pyrrolidone	C ₅ H ₉ NO	99.5 %	Riedel-de Haën
methylsulfonic acid	HSO ₃ Me	99.0 %	Fluka
palladium(II) acetate	Pd(OAc) ₂	purum	Fluka
perchloric acid (60 %)	HClO ₄	p.a.	Merck
phosphorus oxychloride	POCl ₃	99 %	Acros
phosphorus pentachloride	PCl ₅	purum	Fluka
potassium cyanate	KOCN	97 %	Acros
potassium cyanide	KCN	for synthesis	VWR
potassium hexacyanoferrate(II) trihydrate	K ₄ [Fe(CN) ₆] · 3H ₂ O	purum, p.a.	Fluka
potassium hydroxide	KOH	p.a.	Acros
potassium iodide	KI	p.a.	Merck
potassium thiocyanate	KSCN	p.a.	Acros
selenic acid	H ₂ SeO ₄	99.95 %	Aldrich

sodium cyanamide	Na_2NCN	purum	Fluka
sodium cyanate	NaOCN	96 %	Aldrich
sodium cyanide	NaCN	purum	Acros or VWR
sodium hydroxide	NaOH	≥ 99.9 %	VWR
sodium thiocyanate	NaSCN	purum	Riedel-de Haën
sulfuric acid	H_2SO_4	purum	Bisterfeld-Graen
thiourea	$\text{SC}(\text{NH}_2)_2$	99 %	Grüssing
toluene	$\text{C}_6\text{H}_5\text{Me}$	puriss	Riedel-de Haën
trimethylsilyl cyanide	Me_3SiCN	98 %	Acros
urea	$\text{OC}(\text{NH}_2)_2$	puriss p.a.	Riedel-de Haën
zinc chloride	ZnCl_2	purum	Ventron / Alfa

[a] So-called “ammonium carbonate” is in fact a mixture of ammonium hydrogencarbonate and ammonium carbamate.

12.3 Abbreviations and Acronyms

Abbreviations and acronyms used in this work are listed in Table 47. Translations are provided wherever applicable.

Table 47. List of abbreviations and acronyms used in this work.

Short Form	Expression / Word
ATR	attenuated total reflectance
a. u.	arbitrary units
ca.	circa
calcd.	calculated
CCD	charge coupled device
CCDC	Cambridge Crystallographic Data Centre
cf.	confer
COF	covalent organic framework
conc.	concentrated
CP	cross-polarization
CPPI	cross-polarization with polarization inversion
d	day
DEI	direct electron impact
DMF	N,N-dimethyl formamide
DMSO	dimethyl sulfoxide
DSC	differential scanning calorimetry
DTA	differential thermal analysis
ED	electron diffraction
EDX	energy dispersive X-ray analysis
Eq.	equation
FAB	fast atom bombardment
F_c	calculated structure factor
F_o	observed structure factor
FT	Fourier transformation
FTIR	Fourier-transformed infrared (spectroscopy)
FWHM	full width at half maximum
GooF	goodness of fit
h	hour
ICP-AES	inductively coupled plasma - atomic emission spectrometry
IPDS	imaging plate diffraction system
IR	infrared
IUPAC	International Union of Pure and Applied Chemistry
kHz	kilohertz
lit.	literature
MAS	magic angle spinning
mg	milligram
MHz	megahertz
min	minute
mL	milliliter
MOF	metal-organic framework
MS	mass spectroscopy
NMR	nuclear magnetic resonance
p.	page

p.a.	<i>pro analysis</i> , for analysis
pm	picometer
pp.	pages
ppm	parts per million
PTC	phase-transfer catalysis
PXRD	powder X-ray diffraction
R	residual
RT	room temperature
s	second
SEM	scanning electron microscope / microscopy
SQUID	superconducting quantum interference device
STA	simultaneous thermal analysis
t	time
TEM	transmission electron microscope / microscopy
TG	thermogravimetry
TMS	tetramethyl silane
UV / vis	ultraviolet / visible
wt.	weight
et al.	<i>et alii</i> , and others
XRD	X-ray diffraction

12.4 List of Publications

Major results of this thesis were published or are to be published in scientific journals by way of the following publications. Publications are listed in chronological order. References of previously published work are included separately below.

A - Published or to be published as part of this thesis

„Kristallstruktur von Natrium-Dihydrogencyamelurat-Tetrahydrat Na[H₂(C₆N₇)O₃] · 4H₂O“

“Crystal Structure of Sodium Dihydrogencyamelurate Tetrahydrate Na[H₂(C₆N₇)O₃] · 4H₂O“

A. Sattler, W. Schnick, *Z. Anorg. Allg. Chem.* **2006**, 632, 531.

„Zur Frage der Tautomerie von Cyamelursäure im Kristall“

“On the Question of the Tautomerism of Cyameluric Acid in the Crystal”

A. Sattler, W. Schnick, *Z. Anorg. Allg. Chem.* **2006**, 632, 1518.

“Preparation and Structure of Melemium Melem Perchlorate HC₆N₇(NH₂)₃ClO₄ · C₆N₇(NH₂)₃”

A. Sattler, W. Schnick, *Z. Anorg. Allg. Chem.* **2008**, 634, 457.

“C₆N₇H₃O₃ · H₂N(CH₃)₂Cl · H₂O - A Dimethylammonium Chloride Adduct of Cyameluric Acid – Synthesis, Structure and Properties”

A. Sattler, W. Schnick, *Z. Anorg. Allg. Chem.* **2008**, 634, 1063.

“Metal(II) Cyamelurates Prepared from Aqueous Ammonia”

A. Sattler, M. R. Budde, W. Schnick, *Z. Anorg. Allg. Chem.* **2009**, 635, 1933.

“Melamine Melem Adduct Phases – Investigating the Thermal Condensation of Melamine”

A. Sattler, S. Pagano, M. Zeuner, A. Zurawski, D. Gunzelmann, J. Senker, K. Müller-Buschbaum, W. Schnick, *Chem. Eur. J.* **2009**, 15, 13161.

“Melemium Methylsulfonates $\text{HC}_6\text{N}_7(\text{NH}_2)_3\text{H}_2\text{C}_6\text{N}_7(\text{NH}_2)_3(\text{SO}_3\text{Me})_3 \cdot \text{H}_2\text{O}$ and $\text{H}_2\text{C}_6\text{N}_7(\text{NH}_2)_3(\text{SO}_3\text{Me})_2 \cdot \text{H}_2\text{O}$ ”

A. Sattler, S. Schönberger, W. Schnick, *Z. Anorg. Allg. Chem.* **2010** *in print*.

“On the Formation and Decomposition of the Melonate Ion in Cyanate and Thiocyanate Melts and the Crystal Structure of Potassium Melonate ($\text{K}_3\text{C}_6\text{N}_7(\text{NCN})_3$)”

A. Sattler, W. Schnick, *Eur. J. Inorg. Chem.* **2009**, 4972.

Melamium Adduct Phases

A. Sattler, N. Bramel, B. Jürgens, W. Schnick

In preparation

The Melemiumhydrogensulfate $\text{H}_3\text{C}_6\text{N}_7(\text{NH}_2)_3(\text{HSO}_4)_3$

A. Sattler, W. Schnick

In preparation

B - Other Publications

„Synthese, Kristallstruktur und schwingungsspektroskopische Eigenschaften des Melem-Adduktes $C_6N_7(NH_2)_3 \cdot H_3PO_4$ und der Melemiumsalze $(H_2C_6N_7(NH_2)_3)SO_4 \cdot 2H_2O$ und $(HC_6N_7(NH_2)_3)ClO_4 \cdot H_2O$ “

“Synthesis, Crystal Structure and Vibrational Spectroscopic Properties of the Melem Adduct $C_6N_7(NH_2)_3 \cdot H_3PO_4$ and the Melemium Salts $(H_2C_6N_7(NH_2)_3)SO_4 \cdot 2H_2O$ and $(HC_6N_7(NH_2)_3)ClO_4 \cdot H_2O$ ”

A. Sattler, L. Seyfarth, J. Senker, W. Schnick, *Z. Anorg. Allg. Chem.* **2005**, 631, 2545.

„Zur Kenntnis der Kristallstruktur von Melem $C_6N_7(NH_2)_3$ “

“On the Crystal Structure of Melem $C_6N_7(NH_2)_3$ ”

A. Sattler, W. Schnick, *Z. Anorg. Allg. Chem.* **2006**, 632, 238.

12.5 Deposition Numbers

Further details on the crystal structures can be obtained free of charge on application to Cambridge Crystallographic Data Centre, 12 Union Road, Cambridge CB2 1EZ (UK) (fax: + (44) 1223-336-033); e-mail (fileserv@ccdc.cam.ac.uk). Table 48 holds the respective deposition numbers.

Table 48. Database deposition numbers for the contents of this thesis.

Compound	References	Deposition Number
$2\text{C}_3\text{N}_3(\text{NH}_2)_3 \cdot \text{C}_6\text{N}_7(\text{NH}_2)_3$	Section 3.1	CCDC 731626
$\text{C}_3\text{N}_3(\text{NH}_2)_3 \cdot \text{C}_6\text{N}_7(\text{NH}_2)_3$	Section 3.1	CCDC 731627
$\text{C}_3\text{N}_3(\text{NH}_2)_3 \cdot 3\text{C}_6\text{N}_7(\text{NH}_2)_3$	Section 3.1	CCDC 731628
$\text{C}_6\text{N}_7(\text{NH}_2)_3 \cdot \text{HC}_6\text{N}_7(\text{NH}_2)_3\text{ClO}_4$	Section 5.2	CCDC 659153
$\text{HC}_6\text{N}_7(\text{NH}_2)_3\text{H}_2\text{C}_6\text{N}_7(\text{NH}_2)_3(\text{SO}_3\text{Me})_3 \cdot \text{H}_2\text{O}$	Section 5.3	CCDC 738615
$\text{H}_2\text{C}_6\text{N}_7(\text{NH}_2)_3(\text{SO}_3\text{Me})_3 \cdot \text{H}_2\text{O}$	Section 5.3	CCDC 738616
$\text{H}_3\text{C}_6\text{N}_7(\text{NH}_2)_3(\text{HSO}_4)_3$	Section 5.4	in preparation
$\text{H}_3(\text{C}_6\text{N}_7\text{O}_3) \cdot 3\text{H}_2\text{O}$	Section 7.2	CCDC 603410
$\text{NaH}_2(\text{C}_6\text{N}_7\text{O}_3) \cdot 4\text{H}_2\text{O}$	Section 7.2	CCDC 290659
$\text{CaNH}_4(\text{H}_2\text{C}_6\text{N}_7\text{O}_3)(\text{HC}_6\text{N}_7\text{O}_3) \cdot 6\text{H}_2\text{O}$	Section 7.3	CCDC 717005
$[\text{Cu}(\text{NH}_3)_2]_3(\text{C}_6\text{N}_7\text{O}_3)_2 \cdot 2\text{H}_2\text{O}$	Section 7.3	CCDC 717006
$(\text{NH}_4)_2[\text{Zn}(\text{H}_2\text{O})_6](\text{HC}_6\text{N}_7\text{O}_3)_2 \cdot 2\text{H}_2\text{O}$	Section 7.3	CCDC 717007
$\text{C}_6\text{N}_7\text{H}_3\text{O}_3 \cdot \text{H}_2\text{N}(\text{CH}_3)_2\text{Cl} \cdot \text{H}_2\text{O}$	Section 7.4	CCDC 673219
$\text{K}_3\text{C}_6\text{N}_7(\text{NCN})_3$	Section 8.2	CCDC 732128

12.6 Crystallographic Data

Further details on the crystal structures of compounds unpublished as yet are summarized as follows. For all other compounds please refer to the respective deposited datasets listed in Section 12.5.

12.6.1 $C_6N_{11}H_{10}Cl \cdot 0.5NH_4Cl$

Table 49. Atom positions and isotropic displacement parameters for $C_6N_{11}H_{10}Cl \cdot 0.5NH_4Cl$. Standard deviations in parentheses.

Atom	<i>x</i>	<i>y</i>	<i>z</i>	U_{eq}
N12	0.5	1	1	0.0601(10)
H10	0.201(4)	0.247(4)	0.778(2)	0.031(6)
H4	0.257(4)	0.521(4)	1.004(2)	0.029(6)
H3	0.613(5)	0.985(4)	0.750(3)	0.044(7)
H9	0.211(5)	-0.266(5)	0.367(3)	0.047(8)
H8	0.097(5)	-0.420(5)	0.420(2)	0.037(7)
H6	-0.033(4)	-0.181(4)	0.834(2)	0.030(6)
H7	-0.089(5)	-0.364(5)	0.777(3)	0.048(8)
H5	0.166(5)	0.329(5)	0.958(3)	0.046(8)
H2	0.627(5)	0.915(4)	0.636(3)	0.043(7)
H1	0.396(4)	0.322(4)	0.525(2)	0.031(6)
H21	0.449(14)	1.075(10)	0.994(8)	0.081(15)
H23	0.457(14)	0.938(11)	1.053(5)	0.081(15)
H22	0.466(14)	0.926(10)	0.945(5)	0.081(15)
H24	0.630(3)	1.047(12)	1.005(7)	0.081(15)
Cl1	0	0	0	0.0359(2)
Cl2	0.29190(7)	0.69693(6)	0.17112(3)	0.03002(18)
N10	0.2359(3)	0.4398(2)	0.94505(12)	0.0309(3)
N9	-0.0362(3)	-0.2507(2)	0.77634(12)	0.0296(3)
N5	0.4632(3)	0.5847(2)	0.64346(11)	0.0260(3)
N7	0.4171(3)	0.6736(2)	0.83041(11)	0.0279(3)
N1	0.3306(3)	0.2758(2)	0.58747(11)	0.0261(3)
N6	0.0519(3)	-0.2858(2)	0.59885(11)	0.0272(3)
N8	0.1583(3)	-0.3038(2)	0.42368(12)	0.0312(3)
N11	0.5784(3)	0.8888(2)	0.70424(12)	0.0308(3)
N4	0.2620(3)	0.3617(2)	0.76389(11)	0.0266(3)
N2	0.2461(2)	-0.0114(2)	0.50448(11)	0.0263(3)
C5	0.3063(3)	0.4951(2)	0.84719(12)	0.0259(3)
C6	0.4839(3)	0.7123(2)	0.72745(14)	0.0271(3)
N3	0.1423(2)	0.0160(2)	0.68765(11)	0.0264(3)
C1	0.2342(3)	0.0840(2)	0.59513(13)	0.0245(3)
C3	0.1520(3)	-0.1985(2)	0.51074(13)	0.0258(3)
C2	0.3537(3)	0.4108(2)	0.66650(13)	0.0249(3)
C4	0.0536(3)	-0.1739(2)	0.68541(13)	0.0259(3)

Table 50. Anisotropic thermal displacement parameters for $C_6N_{11}H_{10}Cl \cdot 0.5NH_4Cl$. Standard deviations in parentheses.

Atom	U_{11}	U_{22}	U_{33}	U_{23}	U_{13}	U_{12}
N12	0.085(3)	0.0415(15)	0.0562(17)	0.0192(14)	0.0427(18)	0.0228(16)
Cl1	0.0514(4)	0.0259(3)	0.0249(3)	0.0014(2)	0.0096(2)	0.0080(3)
Cl2	0.0386(3)	0.0257(2)	0.0222(2)	0.00189(14)	0.00617(15)	0.00776(19)
N10	0.0406(9)	0.0246(7)	0.0211(6)	0.0019(5)	0.0074(6)	0.0046(7)
N9	0.0393(8)	0.0235(7)	0.0219(6)	0.0015(5)	0.0074(6)	0.0068(6)
N5	0.0321(7)	0.0223(6)	0.0207(5)	0.0019(5)	0.0042(5)	0.0068(6)
N7	0.0349(8)	0.0234(7)	0.0214(6)	0.0008(5)	0.0051(5)	0.0064(6)
N1	0.0325(8)	0.0218(6)	0.0206(6)	0.0023(5)	0.0061(5)	0.0058(6)
N6	0.0330(8)	0.0232(6)	0.0218(6)	0.0020(5)	0.0056(5)	0.0062(6)
N8	0.0421(9)	0.0227(7)	0.0241(6)	0.0022(5)	0.0103(6)	0.0062(6)
N11	0.0440(9)	0.0217(7)	0.0229(6)	0.0023(5)	0.0094(6)	0.0076(7)
N4	0.0316(7)	0.0229(6)	0.0220(6)	0.0012(5)	0.0053(5)	0.0065(6)
N2	0.0314(7)	0.0229(7)	0.0221(6)	0.0028(5)	0.0056(5)	0.0069(6)
C5	0.0297(8)	0.0256(7)	0.0201(6)	0.0019(5)	0.0032(6)	0.0076(7)
C6	0.0308(8)	0.0237(8)	0.0247(7)	0.0019(6)	0.0034(6)	0.0078(7)
N3	0.0308(7)	0.0228(6)	0.0219(6)	0.0014(5)	0.0039(5)	0.0059(6)
C1	0.0265(8)	0.0222(7)	0.0220(6)	0.0008(5)	0.0019(5)	0.0060(6)
C3	0.0295(8)	0.0246(8)	0.0213(6)	0.0021(6)	0.0042(6)	0.0078(7)
C2	0.0280(8)	0.0219(7)	0.0223(6)	0.0019(5)	0.0032(6)	0.0065(6)
C4	0.0286(8)	0.0235(7)	0.0232(7)	0.0024(6)	0.0031(6)	0.0072(7)

12.6.2 C₆N₁₁H₁₀SCN · 2C₃N₃(NH₂)₃.**Table 51.** Atom positions and isotropic displacement parameters for C₆N₁₁H₁₀SCN · 2C₃N₃(NH₂)₃. Standard deviations in parentheses.

Atom	<i>x</i>	<i>y</i>	<i>z</i>	<i>U</i> _{eq}
C1	0.0697(3)	0.8032(2)	0.57591(15)	0.0225(5)
C2	-0.0550(3)	0.6268(2)	0.62219(15)	0.0227(5)
C3	-0.0402(3)	0.8330(2)	0.70863(15)	0.0225(5)
N1	-0.0890(2)	0.70194(17)	0.69878(13)	0.0249(4)
N2	0.0232(2)	0.67111(17)	0.55794(12)	0.0240(4)
N3	0.0400(2)	0.88887(17)	0.64976(12)	0.0230(4)
N4	0.1500(3)	0.8539(2)	0.51636(15)	0.0291(5)
N5	-0.1012(3)	0.4961(2)	0.60743(16)	0.0332(5)
N6	-0.0765(3)	0.9117(2)	0.78161(15)	0.0304(5)
H4A	0.185(3)	0.930(3)	0.5317(18)	0.036
H4B	0.178(3)	0.795(2)	0.4754(18)	0.036
H5A	-0.143(3)	0.468(2)	0.6441(18)	0.036
H5B	-0.085(3)	0.441(3)	0.5568(19)	0.036
H6A	-0.041(3)	0.989(3)	0.7889(17)	0.036
H6B	-0.123(3)	0.880(2)	0.8235(18)	0.036
C11	0.7314(3)	0.8808(2)	-0.00265(15)	0.0228(5)
C12	0.7450(3)	0.6719(2)	-0.07712(15)	0.0226(5)
C13	0.6184(3)	0.7064(2)	0.04844(15)	0.0237(5)
N11	0.7816(2)	0.80249(17)	-0.07281(13)	0.0245(4)
N12	0.6654(2)	0.61715(17)	-0.01724(13)	0.0245(4)
N13	0.6479(2)	0.83872(17)	0.06067(12)	0.0240(4)
N14	0.7664(3)	1.01149(19)	0.00592(16)	0.0339(5)
N15	0.7891(3)	0.5900(2)	-0.14687(15)	0.0315(5)
N16	0.5372(3)	0.6549(2)	0.10968(14)	0.0298(5)
H14A	0.813(3)	1.041(2)	-0.0345(18)	0.036
H14B	0.740(3)	1.069(2)	0.0518(18)	0.036
H15A	0.827(3)	0.627(2)	-0.1907(18)	0.036
H15B	0.787(3)	0.511(3)	-0.1429(17)	0.036
H16A	0.492(3)	0.707(3)	0.1387(18)	0.036
H16B	0.482(3)	0.577(3)	0.0849(17)	0.036
C21	0.7009(3)	0.3295(2)	0.16474(15)	0.0228(5)
C22	0.5805(3)	0.1618(2)	0.22164(15)	0.0220(5)
C23	0.5967(3)	0.3729(2)	0.29807(15)	0.0220(5)
C24	0.6108(3)	0.5947(2)	0.39645(15)	0.0207(5)
C25	0.7440(3)	0.7839(2)	0.35956(15)	0.0228(5)
C26	0.6276(3)	0.7954(2)	0.48968(15)	0.0213(5)
N21	0.6589(2)	0.19964(17)	0.15482(12)	0.0235(4)
N22	0.5475(2)	0.24573(17)	0.29561(12)	0.0229(4)
N23	0.6728(2)	0.42202(17)	0.23570(12)	0.0241(4)
N24	0.5647(2)	0.46082(18)	0.37388(13)	0.0241(4)
N25	0.6899(2)	0.65108(18)	0.33733(13)	0.0242(4)
N26	0.5764(2)	0.66194(17)	0.47361(12)	0.0220(4)
N27	0.7140(2)	0.85829(16)	0.43631(12)	0.0223(4)
N28	0.5344(3)	0.03344(19)	0.21294(15)	0.0286(5)
N29	0.7781(3)	0.3740(2)	0.10146(15)	0.0293(5)
N210	0.5920(3)	0.86906(19)	0.56443(13)	0.0254(5)

N211	0.8274(3)	0.8361(2)	0.30328(14)	0.0285(5)
H28A	0.488(3)	0.012(2)	0.2530(18)	0.034
H28B	0.562(3)	-0.025(2)	0.1687(18)	0.034
H29A	0.792(3)	0.313(2)	0.0566(18)	0.034
H29B	0.793(3)	0.454(3)	0.1010(17)	0.034
H21C	0.631(3)	0.952(3)	0.5768(17)	0.034
H21D	0.544(3)	0.825(2)	0.6027(17)	0.034
H21A	0.875(3)	0.920(3)	0.3223(17)	0.034
H21B	0.833(3)	0.789(2)	0.2570(18)	0.034
H24	0.522(3)	0.429(2)	0.4151(17)	0.028(7)
H25	0.710(3)	0.593(3)	0.2841(19)	0.046(8)
S1	0.09076(9)	0.73601(7)	0.13984(5)	0.0423(2)
C31	0.2206(3)	0.7856(2)	0.2474(2)	0.0364(6)
N31	0.3087(3)	0.8227(3)	0.32317(19)	0.0602(7)

12.6 Crystallographic Data

Table 52. Anisotropic thermal displacement parameters for $C_6N_{11}H_{10}SCN \cdot 2C_3N_3(NH_2)_3$. Standard deviations in parentheses.

Atom	U_{11}	U_{22}	U_{33}	U_{23}	U_{13}	U_{12}
C1	0.0194(12)	0.0239(12)	0.0237(12)	0.0041(10)	0.0047(9)	0.0009(9)
C2	0.0192(12)	0.0238(12)	0.0245(12)	0.0016(10)	0.0056(9)	0.0023(9)
C3	0.0228(12)	0.0230(12)	0.0222(12)	0.0046(10)	0.0062(9)	0.0016(9)
N1	0.0289(11)	0.0231(10)	0.0254(11)	0.0032(8)	0.0126(8)	0.0024(8)
N2	0.0266(10)	0.0233(10)	0.0241(10)	0.0021(8)	0.0123(8)	-0.0005(8)
N3	0.0263(10)	0.0217(10)	0.0220(10)	0.0022(8)	0.0096(8)	0.0014(8)
N4	0.0370(12)	0.0231(10)	0.0300(12)	-0.0013(9)	0.0194(9)	-0.0029(9)
N5	0.0471(14)	0.0232(11)	0.0349(13)	0.0023(9)	0.0250(11)	-0.0039(9)
N6	0.0466(13)	0.0204(10)	0.0295(12)	0.0017(9)	0.0225(10)	0.0002(9)
C11	0.0220(12)	0.0262(12)	0.0221(12)	0.0050(10)	0.0083(9)	0.0029(9)
C12	0.0209(12)	0.0240(12)	0.0244(12)	0.0043(10)	0.0084(9)	0.0036(9)
C13	0.0225(12)	0.0269(12)	0.0226(12)	0.0058(10)	0.0066(9)	0.0003(9)
N11	0.0286(11)	0.0229(10)	0.0239(10)	0.0020(8)	0.0119(8)	0.0019(8)
N12	0.0260(10)	0.0231(10)	0.0275(10)	0.0032(8)	0.0132(8)	0.0022(8)
N13	0.0268(10)	0.0241(10)	0.0230(10)	0.0033(8)	0.0106(8)	0.0018(8)
N14	0.0535(14)	0.0216(11)	0.0349(13)	0.0044(9)	0.0285(11)	-0.0004(10)
N15	0.0458(13)	0.0222(10)	0.0338(12)	0.0035(10)	0.0248(10)	0.0043(10)
N16	0.0385(13)	0.0248(11)	0.0308(12)	0.0006(9)	0.0220(10)	-0.0017(9)
C21	0.0208(11)	0.0249(12)	0.0247(12)	0.0055(10)	0.0086(10)	0.0044(9)
C22	0.0203(12)	0.0230(12)	0.0233(12)	0.0039(10)	0.0063(9)	0.0041(9)
C23	0.0220(12)	0.0235(12)	0.0206(12)	0.0029(9)	0.0056(9)	0.0026(9)
C24	0.0207(12)	0.0222(11)	0.0211(12)	0.0043(9)	0.0084(9)	0.0017(9)
C25	0.0232(12)	0.0216(11)	0.0243(12)	0.0039(10)	0.0073(10)	0.0024(9)
C26	0.0176(11)	0.0245(12)	0.0230(12)	0.0054(10)	0.0066(9)	0.0017(9)
N21	0.0247(10)	0.0234(10)	0.0233(10)	0.0018(8)	0.0089(8)	0.0029(8)
N22	0.0266(10)	0.0196(10)	0.0238(10)	0.0022(8)	0.0101(8)	0.0011(8)
N23	0.0272(10)	0.0226(10)	0.0245(10)	0.0033(8)	0.0113(8)	0.0014(8)
N24	0.0318(11)	0.0210(10)	0.0231(11)	0.0022(8)	0.0155(9)	0.0007(8)
N25	0.0308(11)	0.0204(10)	0.0236(11)	0.0021(8)	0.0126(9)	0.0002(8)
N26	0.0235(10)	0.0194(10)	0.0236(10)	0.0017(8)	0.0084(8)	0.0012(7)
N27	0.0244(10)	0.0197(10)	0.0242(10)	0.0029(8)	0.0099(8)	-0.0007(8)
N28	0.0390(12)	0.0232(11)	0.0278(12)	0.0006(9)	0.0194(9)	0.0010(9)
N29	0.0381(12)	0.0251(11)	0.0298(12)	0.0033(9)	0.0196(9)	0.0027(9)
N210	0.0350(12)	0.0167(10)	0.0281(11)	0.0008(9)	0.0177(9)	-0.0004(8)
N211	0.0397(12)	0.0207(11)	0.0267(12)	-0.0028(9)	0.0179(10)	-0.0063(9)
S1	0.0433(4)	0.0418(4)	0.0398(4)	-0.0004(3)	0.0093(3)	0.0110(3)
C31	0.0310(14)	0.0376(15)	0.0455(17)	0.0089(12)	0.0167(13)	0.0085(11)
N31	0.0421(15)	0.084(2)	0.0515(16)	0.0156(15)	0.0019(13)	0.0131(13)

12.6.3 H₂C₆N₇(NH₂)₃(ClO₄)₂ · 1.5H₂O**Table 53** Atom positions and isotropic displacement parameters for H₂C₆N₇(NH₂)₃(ClO₄)₂ · 1.5H₂O. Standard deviations in parentheses.

Atom	<i>x</i>	<i>y</i>	<i>z</i>	<i>U</i> _{eq}
C1	0.78768(19)	-0.0298(10)	0.1994(6)	0.0390(18)
C2	0.78839(19)	-0.0444(9)	0.3839(6)	0.0381(17)
C3	0.7260(2)	-0.0016(11)	0.2470(7)	0.041(2)
C4	0.84770(19)	-0.0798(10)	0.3368(6)	0.0353(17)
C5	0.7278(2)	-0.0016(10)	0.4232(6)	0.0412(18)
C6	0.7277(2)	0.0071(10)	0.0789(7)	0.046(2)
C7	0.9783(2)	0.2526(10)	0.2468(6)	0.0342(17)
C8	1.03901(18)	0.2088(9)	0.2012(6)	0.0347(16)
C9	1.03999(19)	0.2044(10)	0.3866(6)	0.0379(17)
C10	1.0988(2)	0.1533(11)	0.3338(6)	0.0403(19)
C11	0.9806(2)	0.2516(11)	0.4312(7)	0.048(2)
C12	0.9796(2)	0.2456(11)	0.0801(6)	0.046(2)
N1	0.76739(15)	-0.0196(7)	0.2782(5)	0.0329(14)
N2	0.82782(17)	-0.0544(8)	0.2308(5)	0.0390(15)
H2	0.8417	-0.0547	0.1851	0.047
N3	0.76991(18)	-0.0134(9)	0.1038(6)	0.0514(18)
N4	0.70619(17)	0.0083(8)	0.1480(6)	0.0443(17)
N5	0.70766(16)	0.0037(8)	0.3240(5)	0.0414(16)
H5	0.6816	0.0109	0.3083	0.050
N6	0.76808(18)	-0.0317(10)	0.4572(5)	0.0513(18)
N7	0.82693(15)	-0.0747(7)	0.4099(4)	0.0353(14)
N8	0.88657(16)	-0.1084(10)	0.3603(5)	0.0471(17)
H8A	0.8998	-0.1248	0.4246	0.057
H8B	0.8991	-0.1110	0.3117	0.057
N9	0.70887(18)	0.0178(10)	-0.0215(6)	0.062(2)
H9A	0.6828	0.0254	-0.0409	0.074
H9B	0.7226	0.0172	-0.0677	0.074
N10	0.70811(19)	0.0172(11)	0.4963(6)	0.065(2)
H10A	0.6823	0.0328	0.4787	0.077
H10B	0.7211	0.0138	0.5614	0.077
N11	1.01928(16)	0.2245(8)	0.2797(5)	0.0357(14)
N12	0.95953(15)	0.2626(8)	0.3273(5)	0.0454(18)
H12	0.9336	0.2761	0.3119	0.054
N13	0.95686(18)	0.2638(9)	0.1511(5)	0.0436(16)
N14	1.02057(15)	0.2230(9)	0.1016(5)	0.0436(16)
N15	1.07844(17)	0.1741(9)	0.2324(5)	0.0432(16)
H15	1.0917	0.1644	0.1855	0.052
N16	1.07935(16)	0.1645(9)	0.4124(5)	0.0457(17)
N17	1.02019(16)	0.2195(9)	0.4574(5)	0.0452(16)
N18	0.9601(2)	0.2822(10)	0.4985(6)	0.063(2)
H18A	0.9720	0.2825	0.5644	0.076
H18B	0.9344	0.3023	0.4774	0.076
N19	0.9602(2)	0.2625(10)	-0.0187(6)	0.064(2)
H19A	0.9733	0.2590	-0.0660	0.077
H19B	0.9343	0.2770	-0.0363	0.077
N20	1.13623(17)	0.1272(9)	0.3631(6)	0.0476(17)

12.6 Crystallographic Data

H20A	1.1502	0.1217	0.3176	0.057
H20B	1.1480	0.1146	0.4286	0.057
Cl1	0.71930(6)	0.5025(3)	0.2228(2)	0.0550(6)
O1	0.68074(19)	0.5786(16)	0.2026(7)	0.128(4)
O2	0.7249(3)	0.3674(11)	0.3015(7)	0.117(3)
O3	0.7259(3)	0.4276(13)	0.1313(8)	0.120(3)
O4	0.7475(2)	0.6250(11)	0.2688(13)	0.199(7)
Cl2	0.85320(6)	0.4119(3)	0.30364(18)	0.0522(6)
O5	0.8393(3)	0.5576(10)	0.2383(6)	0.117(4)
O6	0.8200(3)	0.3162(10)	0.3206(10)	0.135(4)
O7	0.87507(19)	0.3003(10)	0.2475(6)	0.082(2)
O8	0.8807(3)	0.4698(12)	0.3959(7)	0.130(4)
Cl3	0.96690(6)	0.7672(4)	0.2207(2)	0.0580(6)
O9	0.9276(2)	0.834(2)	0.2004(7)	0.165(6)
O10	0.9747(3)	0.753(3)	0.1293(7)	0.251(11)
O11	0.9747(5)	0.6218(12)	0.2819(10)	0.205(7)
O12	0.9951(3)	0.8781(11)	0.2839(8)	0.158(5)
Cl4	1.10092(6)	0.6497(3)	0.30053(18)	0.0529(6)
O13	1.0900(3)	0.7921(12)	0.2393(7)	0.120(4)
O14	1.1248(2)	0.5287(11)	0.2663(12)	0.167(6)
O15	1.0671(3)	0.5548(11)	0.3133(10)	0.137(4)
O16	1.1276(4)	0.7140(17)	0.3994(9)	0.170(5)
OW1	1.1028(2)	0.2044(15)	0.0519(6)	0.120(4)
OW2	0.8517(2)	0.0141(15)	0.0509(6)	0.120(4)
OW3	0.8765(3)	0.402(4)	0.0090(14)	0.328(13)

Table 54. Anisotropic thermal displacement parameters for $\text{H}_2\text{C}_6\text{N}_7(\text{NH}_2)_3(\text{ClO}_4)_2 \cdot 1.5\text{H}_2\text{O}$. Standard deviations in parentheses.

Atom	U_{11}	U_{22}	U_{33}	U_{23}	U_{13}	U_{12}
C1	0.037(4)	0.051(4)	0.031(5)	0.002(3)	0.012(3)	0.005(3)
C2	0.031(3)	0.056(4)	0.025(5)	0.000(3)	0.003(3)	0.006(3)
C3	0.022(3)	0.053(5)	0.049(6)	0.008(4)	0.011(3)	0.001(3)
C4	0.030(3)	0.047(4)	0.031(5)	-0.006(3)	0.013(3)	0.001(3)
C5	0.042(4)	0.053(4)	0.032(5)	0.010(3)	0.014(3)	0.005(3)
C6	0.036(4)	0.060(5)	0.040(6)	0.006(4)	0.009(4)	0.001(3)
C7	0.039(4)	0.048(5)	0.015(4)	-0.001(3)	0.006(3)	0.005(3)
C8	0.029(3)	0.044(4)	0.032(5)	0.004(3)	0.010(3)	0.002(3)
C9	0.035(3)	0.049(4)	0.030(5)	0.004(3)	0.008(3)	0.002(3)
C10	0.038(4)	0.054(5)	0.023(5)	0.002(3)	-0.003(3)	0.004(3)
C11	0.039(4)	0.073(6)	0.031(6)	-0.003(4)	0.005(3)	0.014(4)
C12	0.043(4)	0.067(6)	0.025(5)	-0.005(3)	0.005(3)	0.009(3)
N1	0.031(3)	0.041(3)	0.023(4)	0.001(2)	0.000(2)	0.003(2)
N2	0.040(3)	0.051(4)	0.029(4)	0.002(3)	0.015(3)	0.009(3)
N3	0.046(3)	0.071(4)	0.039(5)	0.001(3)	0.014(3)	0.007(3)
N4	0.032(3)	0.049(4)	0.045(5)	0.003(3)	-0.002(3)	0.001(3)
N5	0.038(3)	0.070(4)	0.018(4)	-0.001(3)	0.011(3)	0.011(3)
N6	0.043(3)	0.093(5)	0.020(4)	-0.003(3)	0.010(3)	0.007(3)
N7	0.034(3)	0.050(3)	0.018(4)	0.001(2)	0.000(2)	0.005(2)
N8	0.035(3)	0.086(5)	0.019(4)	0.018(3)	0.004(2)	0.008(3)
N9	0.037(3)	0.115(6)	0.029(5)	0.003(4)	0.000(3)	0.015(3)
N10	0.043(3)	0.120(6)	0.037(5)	0.008(4)	0.020(3)	0.028(4)

N11	0.035(3)	0.053(4)	0.021(4)	0.002(2)	0.012(2)	0.001(2)
N12	0.024(3)	0.069(5)	0.042(5)	0.003(3)	0.006(3)	0.009(3)
N13	0.043(3)	0.070(5)	0.018(4)	0.006(3)	0.008(3)	0.008(3)
N14	0.030(3)	0.078(4)	0.021(4)	-0.005(3)	0.004(3)	0.001(3)
N15	0.034(3)	0.064(4)	0.032(4)	0.004(3)	0.010(2)	0.000(3)
N16	0.034(3)	0.065(4)	0.039(4)	0.010(3)	0.011(3)	0.007(3)
N17	0.030(3)	0.068(4)	0.039(5)	0.013(3)	0.012(3)	0.010(3)
N18	0.052(4)	0.111(6)	0.028(5)	0.002(4)	0.016(3)	0.018(4)
N19	0.048(4)	0.115(6)	0.028(5)	0.005(4)	0.006(3)	0.014(4)
N20	0.040(3)	0.067(4)	0.041(5)	0.001(3)	0.019(3)	0.007(3)
Cl1	0.0465(11)	0.0731(14)	0.0465(16)	-0.0012(11)	0.0143(9)	0.0028(10)
O1	0.054(4)	0.266(12)	0.065(6)	0.014(7)	0.021(3)	0.044(5)
O2	0.175(8)	0.094(6)	0.074(6)	0.026(5)	0.020(5)	-0.007(6)
O3	0.106(6)	0.154(8)	0.118(8)	-0.060(7)	0.061(5)	-0.008(6)
O4	0.058(4)	0.065(5)	0.43(2)	0.029(8)	-0.022(7)	-0.015(4)
Cl2	0.0489(11)	0.0618(13)	0.0485(15)	0.0046(11)	0.0171(9)	0.0078(9)
O5	0.165(8)	0.074(5)	0.069(6)	0.022(4)	-0.044(5)	-0.028(5)
O6	0.127(7)	0.070(5)	0.252(13)	-0.019(6)	0.127(8)	-0.008(4)
O7	0.080(4)	0.106(5)	0.071(5)	-0.017(4)	0.041(3)	0.001(4)
O8	0.148(7)	0.130(8)	0.069(6)	0.009(5)	-0.048(6)	0.004(6)
Cl3	0.0502(12)	0.0798(16)	0.0476(16)	0.0025(12)	0.0191(10)	-0.0006(10)
O9	0.069(5)	0.361(18)	0.069(6)	0.026(9)	0.027(4)	0.060(8)
O10	0.119(7)	0.61(3)	0.032(6)	0.047(10)	0.043(5)	0.151(12)
O11	0.339(17)	0.061(5)	0.148(11)	0.023(6)	-0.055(11)	-0.002(8)
O12	0.203(10)	0.072(5)	0.132(8)	-0.019(5)	-0.078(7)	-0.035(6)
Cl4	0.0444(10)	0.0574(12)	0.0558(16)	0.0048(11)	0.0110(9)	0.0053(9)
O13	0.136(7)	0.089(5)	0.097(7)	0.041(5)	-0.037(5)	0.007(5)
O14	0.055(4)	0.081(5)	0.388(19)	-0.009(7)	0.100(7)	0.012(4)
O15	0.128(7)	0.097(6)	0.232(13)	-0.006(7)	0.131(8)	-0.006(5)
O16	0.227(13)	0.152(10)	0.095(9)	0.021(7)	-0.023(8)	0.002(9)
OW1	0.076(4)	0.239(11)	0.057(5)	-0.009(6)	0.036(4)	0.054(6)
OW2	0.067(4)	0.253(11)	0.042(5)	-0.003(5)	0.020(3)	0.049(5)
OW3	0.041(3)	0.72(3)	0.214(12)	0.329(18)	0.021(5)	0.054(8)

12.6 Crystallographic Data

Table 55. Bond lengths and angles (in Å and °) for $\text{H}_2\text{C}_6\text{N}_7(\text{NH}_2)_3(\text{ClO}_4)_2 \cdot 1.5\text{H}_2\text{O}$. Standard deviations in parentheses.

Bond Lengths					
C1-N3	1.256(10)	C7-N13	1.288(9)	C11-O4	1.364(9)
C1-N2	1.337(9)	C7-N11	1.368(9)	C11-O1	1.398(7)
C1-N1	1.396(10)	C7-N12	1.381(10)	C11-O3	1.407(9)
C2-N7	1.291(8)	C8-N14	1.307(9)	C11-O2	1.439(8)
C2-N6	1.334(10)	C8-N15	1.327(8)	C12-O8	1.402(8)
C2-N1	1.406(9)	C8-N11	1.382(9)	C12-O5	1.409(7)
C3-N4	1.309(11)	C9-N17	1.295(9)	C12-O6	1.414(8)
C3-N5	1.326(10)	C9-N16	1.332(9)	C12-O7	1.456(7)
C3-N1	1.373(8)	C9-N11	1.412(9)	C13-O10	1.307(9)
C4-N8	1.300(8)	C10-N20	1.250(9)	C13-O11	1.355(10)
C4-N7	1.340(9)	C10-N15	1.348(10)	C13-O12	1.384(8)
C4-N2	1.401(10)	C10-N16	1.374(10)	C13-O9	1.393(8)
C5-N5	1.312(9)	C11-N18	1.289(11)	C14-O13	1.346(8)
C5-N10	1.321(10)	C11-N17	1.326(9)	C14-O14	1.381(8)
C5-N6	1.350(9)	C11-N12	1.376(10)	C14-O15	1.409(8)
C6-N9	1.317(10)	C12-N19	1.306(10)	C14-O16	1.467(12)
C6-N4	1.314(11)	C12-N14	1.365(9)		
C6-N3	1.399(9)	C12-N13	1.371(10)		
Angles					
N3-C1-N2	120.9(7)	N16-C9-N11	119.3(6)	C9-N17-C11	121.1(7)
N3-C1-N1	122.8(6)	N20-C10-N15	123.1(7)	O4-C11-O1	108.8(6)
N2-C1-N1	116.4(7)	N20-C10-N16	115.7(6)	O4-C11-O3	114.0(8)
N7-C2-N6	120.4(6)	N15-C10-N16	121.2(6)	O1-C11-O3	110.9(5)
N7-C2-N1	120.6(6)	N18-C11-N17	123.6(8)	O4-C11-O2	102.8(7)
N6-C2-N1	119.0(6)	N18-C11-N12	116.1(6)	O1-C11-O2	112.0(6)
N4-C3-N5	122.8(6)	N17-C11-N12	120.2(7)	O3-C11-O2	108.1(6)
N4-C3-N1	121.9(7)	N19-C12-N14	116.4(7)	O8-C12-O5	109.1(5)
N5-C3-N1	115.3(7)	N19-C12-N13	116.4(6)	O8-C12-O6	114.0(7)
N8-C4-N7	122.1(7)	N14-C12-N13	127.1(6)	O5-C12-O6	110.3(6)
N8-C4-N2	117.4(6)	C3-N1-C1	117.1(6)	O8-C12-O7	108.1(6)
N7-C4-N2	120.5(6)	C3-N1-C2	122.0(6)	O5-C12-O7	106.4(6)
N5-C5-N10	119.5(6)	C1-N1-C2	120.7(5)	O6-C12-O7	108.6(5)
N5-C5-N6	124.1(7)	C1-N2-C4	121.3(6)	O10-C13-O11	115.3(11)
N10-C5-N6	116.3(7)	C1-N3-C6	116.4(7)	O10-C13-O12	109.3(10)
N9-C6-N4	118.9(6)	C3-N4-C6	117.3(6)	O11-C13-O12	98.1(7)
N9-C6-N3	116.5(7)	C5-N5-C3	122.4(6)	O10-C13-O9	105.7(6)
N4-C6-N3	124.5(7)	C2-N6-C5	116.6(7)	O11-C13-O9	116.3(10)
N13-C7-N11	126.5(7)	C7-N11-C8	115.6(6)	O12-C13-O9	112.1(8)
N13-C7-N12	119.5(7)	C7-N11-C9	122.6(6)	O13-C14-O14	115.8(8)
N11-C7-N12	113.9(6)	C8-N11-C9	121.7(5)	O13-C14-O15	112.1(6)
N14-C8-N15	120.8(7)	C11-N12-C7	122.5(6)	O14-C14-O15	105.6(5)
N14-C8-N11	123.2(6)	C7-N13-C12	112.7(6)	O13-C14-O16	106.1(6)
N15-C8-N11	116.0(6)	C8-N14-C12	114.7(6)	O14-C14-O16	103.4(7)
N17-C9-N16	121.1(7)	C8-N15-C10	123.4(7)	O15-C14-O16	113.7(8)
N17-C9-N11	119.6(6)	C9-N16-C10	118.4(6)	C2-N7-C4	120.5(6)

12.6.4 H₃C₆N₇(NH₂)₃(HSO₄)₃**Table 56.** Atom positions and isotropic displacement parameters for H₃C₆N₇(NH₂)₃(HSO₄)₃. Standard deviations in parentheses.

Atom	<i>x</i>	<i>y</i>	<i>z</i>	<i>U</i> _{eq}
C1	0.6503(2)	0.12328(15)	0.10056(18)	0.0182(4)
C2	0.8596(2)	0.13002(14)	0.22358(18)	0.0177(4)
C3	0.6594(2)	0.13789(14)	0.30422(18)	0.0182(4)
C4	0.4591(2)	0.13219(16)	0.17177(18)	0.0218(5)
C5	0.8553(2)	0.11247(15)	0.03283(18)	0.0201(4)
C6	0.8536(2)	0.14150(15)	0.42433(18)	0.0199(4)
N1	0.72279(17)	0.13574(12)	0.20904(14)	0.0170(4)
N2	0.72034(18)	0.11146(14)	0.01491(16)	0.0210(4)
N3	0.92547(17)	0.12064(13)	0.13986(15)	0.0205(4)
N4	0.92139(18)	0.13590(13)	0.33351(15)	0.0196(4)
N5	0.72060(17)	0.14111(13)	0.40890(15)	0.0203(4)
N6	0.52720(18)	0.13635(14)	0.28141(16)	0.0215(4)
N7	0.52278(18)	0.12286(14)	0.08011(16)	0.0243(4)
N8	0.9164(2)	0.10492(17)	-0.05437(18)	0.0287(5)
N9	0.9178(2)	0.14578(16)	0.52901(17)	0.0285(5)
N10	0.33127(19)	0.13665(18)	0.15424(19)	0.0334(5)
O1	0.18894(17)	0.09933(15)	0.93992(15)	0.0400(5)
O2	0.2268(2)	0.03864(13)	0.7602(2)	0.0493(6)
O3	0.32596(18)	0.17964(13)	0.82333(18)	0.0372(5)
O4	0.09333(18)	0.17235(14)	0.76483(16)	0.0391(5)
O5	0.19066(17)	0.19123(13)	0.53622(15)	0.0345(4)
O6	0.2749(2)	0.04703(13)	0.51108(17)	0.0367(5)
O7	0.18835(16)	0.13499(15)	0.34385(14)	0.0378(5)
O8	0.39360(15)	0.17644(13)	0.45754(14)	0.0295(4)
O9	0.56955(18)	0.09813(16)	0.80697(15)	0.0415(5)
O10	0.5669(2)	0.19657(14)	0.64536(19)	0.0460(5)
O11	0.58005(18)	0.03639(12)	0.61925(15)	0.0327(4)
O12	0.76537(16)	0.12028(15)	0.72206(15)	0.0390(5)
S1	0.20087(5)	0.11801(4)	0.82002(5)	0.02236(14)
S2	0.26041(5)	0.14207(4)	0.46051(5)	0.02141(14)
S3	0.62351(6)	0.10751(4)	0.69979(5)	0.02595(15)
H1	1.007(3)	0.1069(19)	-0.046(2)	0.037(8)
H2	0.880(3)	0.1076(19)	-0.116(3)	0.027(8)
H3	0.680(3)	0.107(2)	-0.050(3)	0.050(10)
H4	0.284(3)	0.129(2)	0.082(3)	0.049(9)
H5	0.287(3)	0.1395(18)	0.208(2)	0.029(7)
H6	0.486(3)	0.1414(19)	0.339(2)	0.033(8)
H7	0.871(3)	0.1430(18)	0.590(2)	0.031(7)
H8	0.997(3)	0.1468(19)	0.540(2)	0.033(8)
H9	1.001(3)	0.135(2)	0.342(3)	0.050(10)
H10	0.391(5)	0.137(3)	0.819(4)	0.103(17)
H11	0.516(4)	0.185(3)	0.586(3)	0.063(11)
H12	0.323(4)	0.020(3)	0.475(4)	0.083(14)

12.6 Crystallographic Data

Table 57. Anisotropic thermal displacement parameters for $\text{H}_3\text{C}_6\text{N}_7(\text{NH}_2)_3(\text{HSO}_4)_3$. Standard deviations in parentheses.

Atom	U_{11}	U_{22}	U_{33}	U_{23}	U_{13}	U_{12}
C1	0.0139(9)	0.0231(11)	0.0170(9)	0.0012(8)	0.0010(8)	-0.0006(8)
C2	0.0125(9)	0.0209(11)	0.0195(10)	-0.0003(8)	0.0023(8)	-0.0010(8)
C3	0.0161(10)	0.0202(11)	0.0194(10)	0.0004(8)	0.0062(8)	-0.0026(8)
C4	0.0151(10)	0.0315(12)	0.0192(10)	0.0021(9)	0.0038(8)	-0.0005(9)
C5	0.0157(10)	0.0259(11)	0.0188(10)	0.0006(9)	0.0027(8)	-0.0003(9)
C6	0.0167(10)	0.0238(11)	0.0192(10)	0.0015(9)	0.0030(8)	-0.0014(9)
N1	0.0113(8)	0.0244(9)	0.0156(8)	0.0005(7)	0.0031(6)	0.0000(7)
N2	0.0133(9)	0.0344(11)	0.0153(9)	-0.0003(8)	0.0019(7)	0.0014(8)
N3	0.0132(8)	0.0300(10)	0.0187(9)	0.0005(8)	0.0039(7)	0.0004(7)
N4	0.0115(9)	0.0290(10)	0.0179(8)	-0.0014(8)	0.0011(7)	0.0007(8)
N5	0.0140(8)	0.0308(10)	0.0163(8)	0.0005(8)	0.0031(7)	-0.0026(8)
N6	0.0126(8)	0.0365(11)	0.0165(8)	-0.0014(8)	0.0054(7)	-0.0042(8)
N7	0.0133(8)	0.0423(12)	0.0172(8)	0.0011(8)	0.0024(7)	0.0006(8)
N8	0.0155(10)	0.0545(15)	0.0171(10)	0.0023(10)	0.0053(8)	0.0015(9)
N9	0.0161(10)	0.0506(14)	0.0184(9)	-0.0016(9)	0.0015(8)	-0.0035(9)
N10	0.0116(9)	0.0683(17)	0.0207(10)	-0.0011(11)	0.0036(8)	-0.0011(10)
O1	0.0208(9)	0.0752(15)	0.0238(9)	0.0066(9)	0.0031(7)	-0.0040(9)
O2	0.0653(15)	0.0270(10)	0.0627(14)	-0.0110(10)	0.0311(12)	-0.0046(10)
O3	0.0234(9)	0.0300(10)	0.0612(13)	-0.0047(9)	0.0160(9)	-0.0055(8)
O4	0.0255(9)	0.0527(12)	0.0381(10)	0.0075(9)	0.0021(8)	0.0060(9)
O5	0.0282(9)	0.0414(11)	0.0371(10)	-0.0074(8)	0.0147(8)	0.0041(8)
O6	0.0424(11)	0.0319(10)	0.0404(10)	0.0059(9)	0.0203(9)	0.0042(9)
O7	0.0159(8)	0.0758(15)	0.0207(8)	0.0011(9)	0.0000(7)	0.0004(9)
O8	0.0154(8)	0.0467(11)	0.0267(8)	0.0000(8)	0.0046(7)	-0.0042(7)
O9	0.0221(9)	0.0815(16)	0.0211(8)	-0.0027(9)	0.0045(7)	0.0028(9)
O10	0.0523(13)	0.0376(12)	0.0397(11)	-0.0077(10)	-0.0181(10)	0.0083(10)
O11	0.0313(10)	0.0365(10)	0.0305(9)	-0.0063(8)	0.0053(7)	0.0030(8)
O12	0.0166(8)	0.0750(15)	0.0249(9)	0.0003(9)	0.0017(7)	-0.0014(9)
S1	0.0189(3)	0.0267(3)	0.0229(3)	-0.0015(2)	0.0075(2)	-0.0023(2)
S2	0.0139(2)	0.0315(3)	0.0195(3)	0.0008(2)	0.0047(2)	0.0019(2)
S3	0.0173(3)	0.0410(4)	0.0192(3)	-0.0019(2)	0.0015(2)	0.0040(2)

12.6.5 Na₃C₆N₇O₃ · 4H₂O**Table 58.** Atom positions and isotropic displacement parameters for Na₃C₆N₇O₃ · 4H₂O. Standard deviations in parentheses.

Atom	x	y	z	U_{eq}
Na1	0.18466(7)	-0.04761(8)	0.7663(4)	0.0252(5)
Na2	0.0204(3)	0.5315(3)	0.3113(15)	0.0760(14)
O1	-0.08924(17)	0.2500	0.8357(11)	0.0261(9)
O2	0.19085(11)	0.04874(13)	0.2453(7)	0.0198(6)
OW1	0.18903(13)	-0.13953(16)	1.2690(8)	0.0285(7)
OW2	0.06468(17)	-0.0503(3)	0.8193(17)	0.0766(15)
N1	0.09483(18)	0.2500	0.4144(11)	0.0163(9)
N2	0.00058(13)	0.17813(16)	0.6403(9)	0.0200(7)
N4	0.09419(13)	0.10984(16)	0.4264(8)	0.0196(7)
N5	0.18886(14)	0.31856(16)	0.1692(9)	0.0212(7)
C1	0.06220(15)	0.17785(18)	0.4951(9)	0.0171(7)
C3	0.1583(2)	0.2500	0.2459(12)	0.0158(10)
C4	-0.0311(2)	0.2500	0.7089(14)	0.0186(10)
C5	0.15805(16)	0.11228(18)	0.2785(9)	0.0173(8)
H1	0.1577(15)	-0.169(2)	1.226(12)	0.026
H2	0.2239(14)	-0.158(2)	1.344(12)	0.026
H3	0.044(4)	-0.092(3)	0.78(2)	0.13(3)
H4	0.094(4)	-0.048(5)	0.654(19)	0.13(3)

Table 59. Anisotropic thermal displacement parameters for Na₃C₆N₇O₃ · 4H₂O. Standard deviations in parentheses.

Atom	U_{11}	U_{22}	U_{33}	U_{23}	U_{13}	U_{12}
Na1	0.0244(8)	0.0243(9)	0.0270(9)	-0.0025(6)	0.0004(6)	-0.0029(5)
Na2	0.091(3)	0.066(3)	0.072(3)	-0.009(3)	0.002(3)	-0.011(3)
O1	0.0157(17)	0.0217(17)	0.041(2)	0.000	0.0065(16)	0.000
O2	0.0185(12)	0.0130(12)	0.0277(14)	-0.0002(9)	0.0014(10)	0.0042(9)
OW1	0.0261(14)	0.0220(14)	0.0375(17)	0.0033(11)	-0.0087(12)	-0.0066(10)
OW2	0.0254(18)	0.078(3)	0.126(4)	-0.035(3)	-0.007(2)	0.0042(18)
N1	0.0167(19)	0.0118(18)	0.020(2)	0.000	0.0018(16)	0.000
N2	0.0159(14)	0.0160(14)	0.0282(15)	0.0029(13)	0.0039(12)	-0.0003(9)
N4	0.0189(14)	0.0154(13)	0.0246(15)	-0.0006(11)	0.0028(12)	0.0003(10)
N5	0.0193(14)	0.0131(14)	0.0313(16)	0.0008(12)	0.0037(13)	-0.0016(10)
C1	0.0157(15)	0.0161(16)	0.0195(16)	0.0008(13)	-0.0031(13)	-0.0025(11)
C3	0.013(2)	0.018(2)	0.017(2)	0.000	-0.0011(17)	0.000
C4	0.015(2)	0.018(2)	0.024(2)	0.000	-0.0011(18)	0.000
C5	0.0185(16)	0.0144(15)	0.0190(16)	-0.0019(12)	-0.0018(13)	0.0003(12)

12.6.6 $\text{H}_2(\text{C}_3\text{N}_3)=\text{O}(\text{NH}_2)\text{NHC}(\text{NH}_2)_2\text{Cl}_2$ **Table 60.** Atom positions and isotropic displacement parameters for $\text{H}_2(\text{C}_3\text{N}_3)=\text{O}(\text{NH}_2)\text{NHC}(\text{NH}_2)_2\text{Cl}_2$. Standard deviations in parentheses.

Atom	<i>x</i>	<i>y</i>	<i>z</i>	U_{eq}
Cl1	0.18810(10)	0.75455(4)	0.89101(6)	0.0458(2)
Cl2	0.88096(11)	0.61110(5)	0.09465(8)	0.0546(2)
O1	0.5155(3)	0.87180(12)	0.2069(2)	0.0477(4)
N1	0.4490(3)	0.71045(14)	0.1697(2)	0.0384(4)
N2	0.6016(3)	0.59542(13)	0.3347(2)	0.0366(4)
N3	0.6728(3)	0.76222(13)	0.3645(2)	0.0373(4)
N4	0.3744(4)	0.54703(17)	0.1427(3)	0.0502(6)
N5	0.8216(3)	0.65454(14)	0.5293(2)	0.0375(4)
N6	0.7852(3)	0.48547(15)	0.5454(2)	0.0423(5)
N7	0.9937(4)	0.57245(18)	0.7161(2)	0.0503(6)
C1	0.5428(4)	0.78732(15)	0.2449(2)	0.0362(5)
C2	0.4754(4)	0.61771(16)	0.2146(2)	0.0365(5)
C3	0.6945(3)	0.66851(15)	0.4057(2)	0.0334(4)
C4	0.8664(4)	0.56829(16)	0.5976(2)	0.0370(5)
H1	0.368(6)	0.725(3)	0.078(5)	0.070(11)
H2	0.285(7)	0.563(3)	0.065(6)	0.092(15)
H3	0.406(6)	0.489(3)	0.182(4)	0.068(11)
H4	0.743(5)	0.813(3)	0.435(4)	0.059(10)
H5	0.879(5)	0.702(3)	0.567(4)	0.056(9)
H6	0.701(6)	0.482(3)	0.463(4)	0.062(10)
H7	0.809(6)	0.434(3)	0.573(5)	0.070(12)
H9	1.059(6)	0.631(3)	0.760(5)	0.074(12)
H8	1.034(5)	0.518(3)	0.773(4)	0.072(11)

Table 61. Anisotropic thermal displacement parameters for $\text{H}_2(\text{C}_3\text{N}_3)=\text{O}(\text{NH}_2)\text{NHC}(\text{NH}_2)_2\text{Cl}_2$. Standard deviations in parentheses.

Atom	U_{11}	U_{22}	U_{33}	U_{23}	U_{13}	U_{12}
Cl1	0.0497(5)	0.0414(3)	0.0419(3)	-0.0001(2)	0.0058(2)	-0.0021(2)
Cl2	0.0592(5)	0.0453(4)	0.0519(4)	0.0127(3)	0.0041(3)	0.0066(2)
O1	0.0591(13)	0.0283(8)	0.0482(10)	0.0073(7)	0.0034(7)	0.0019(6)
N1	0.0443(13)	0.0306(9)	0.0356(10)	0.0015(7)	0.0043(7)	0.0000(7)
N2	0.0401(12)	0.0272(8)	0.0381(10)	0.0002(7)	0.0042(7)	-0.0015(6)
N3	0.0394(12)	0.0262(8)	0.0415(10)	0.0015(7)	0.0041(7)	-0.0013(6)
N4	0.0571(16)	0.0349(11)	0.0473(13)	-0.0033(9)	-0.0034(9)	-0.0060(8)
N5	0.0406(13)	0.0286(9)	0.0386(10)	0.0003(7)	0.0041(7)	-0.0034(7)
N6	0.0493(14)	0.0273(10)	0.0465(12)	0.0041(8)	0.0078(8)	-0.0007(7)
N7	0.0584(16)	0.0389(12)	0.0427(12)	0.0060(9)	-0.0031(9)	-0.0004(8)
C1	0.0395(14)	0.0281(10)	0.0384(11)	0.0021(8)	0.0071(8)	0.0003(7)
C2	0.0367(14)	0.0307(10)	0.0389(11)	-0.0017(8)	0.0060(8)	-0.0009(7)
C3	0.0332(13)	0.0282(9)	0.0382(11)	0.0008(7)	0.0093(8)	-0.0003(7)
C4	0.0369(14)	0.0329(10)	0.0396(11)	0.0024(8)	0.0086(8)	0.0008(8)

12.7 Curriculum Vitae

Personal Details

Name	Andreas Sattler
Date of birth	9 th of January 1979
Place of birth	Augsburg, Germany
Citizenship	German
Marital status	unmarried

Education /Occupation

1985 to 1989	Primary school education at Sankt-Ulrich-Volksschule, Schwabmünchen
1989 to 1998	High-school education at Leonhard-Wagner-Gymnasium, Schwabmünchen
26 th of June 1998	Abitur
1998 to 1999	Military service
1999 to 2001	Undergraduate studies in Chemistry at Ludwig-Maximilians-Universität, München
31 th of October 2001	Preliminary Diploma
2001 to 2005	Graduate studies in Chemistry at Ludwig-Maximilians-Universität, München
14 th of March 2005	Diploma Thesis in the group of Prof. W. Schnick (chair of solid-state chemistry) at Ludwig-Maximilians-Universität, München, entitled: “Zur Kenntnis von Melem und seinen Verbindungen” “On Melem and its Compounds”
2005 to 2010	Research assistant in the group of Prof. W. Schnick (chair of solid-state chemistry) at Ludwig-Maximilians-Universität, München; PhD thesis entitled: “Investigations into <i>s</i> -Heptazine-Based Carbon Nitride Precursors”

Bibliography

- [1] W. Schnick, *Angew. Chem.* **1993**, *105*, 846; *Angew. Chem. Int. Ed.* **1993**, *32*, 806.
- [2] E. Kroke, M. Schwarz, *Coord. Chem. Rev.* **2004**, *248*, 493.
- [3] W. Schnick, *Angew. Chem.* **1999**, *111*, 3511; *Angew. Chem. Int. Ed.* **1999**, *38*, 3309.
- [4] W. Schnick, *Phys. Status Solidi RRL* **2009**, *3*, A113.
- [5] N. V. Riggs, L. Radom, *Australian J. Chem.* **1985**, *38*, 835.
- [6] a) A. Y. Liu, M. L. Cohen, *Science* **1989**, *245*, 841; b) A. Y. Liu, M. L. Cohen, *Phys. Rev. B* **1990**, *41*, 10727, c) A. Y. Liu, R. M. Wentzcovitch, *Phys. Rev. B* **1994**, *50*, 10362.
- [7] D. M. Teter, R. J. Hemley, *Science* **1996**, *271*, 53.
- [8] C.-M. Sung, M. Sung, *Mater. Chem. Phys.* **1996**, *43*, 1.
- [9] L. Pauling, J. H. Sturdivant, *Proc. Natl. Acad. Sci. U.S.A.* **1937**, *23*, 615.
- [10] E. Horvath-Bordon, R. Riedel, A. Zerr, P. F. McMillan, G. Auffermann, Y. Prots, W. Bronger, R. Kniep, P. Kroll, *Chem. Soc. Rev.* **2006**, *35*, 987.
- [11] W. Schnick, *Angew. Chem.* **1993**, *105*, 1649; *Angew. Chem. Int. Ed.* **1993**, *32*, 1580.
- [12] E. Horvath-Bordon, R. Riedel, P. F. McMillan, P. Kroll, G. Miehe, P. A. van Aken, A. Zerr, P. Hoppe, O. Shebanova, I. McLaren, S. Lauterbach, E. Kroke, R. Boehler, *Angew. Chem.* **2007**, *119*, 1498; *Angew. Chem. Int. Ed.* **2007**, *46*, 1476.
- [13] D. Foy, G. Demazeau, P. Florian, D. Massiot, C. Labrugère, G. Goglio, *J. Solid State Chem.* **2009**, *182*, 165.
- [14] Z. Zhang, K. Leinenweber, M. Bauer, L. A. J. Garvie, P. F. McMillan, G. H. Wolf, *J. Am. Chem. Soc.* **2001**, *123*, 7788.
- [15] A. Thomas, A. Fischer, F. Goettmann, M. Antonietti, J.-O. Müller, R. Schlögl, J. M. Carlsson, *J. Mater. Chem.* **2008**, *18*, 4893.
- [16] E. Wirnhier, M. Döblinger, D. Gunzelmann, J. Senker, B. V. Lotsch, W. Schnick, *Chem. Eur. J.* (in preparation).
- [17] M. Döblinger, B. V. Lotsch, J. Wack, J. Thun, J. Senker, W. Schnick, *Chem. Commun.* **2009**, 1541.
- [18] J. R. Holst, E. G. Gillan, *J. Am. Chem. Soc.* **2008**, *130*, 7373.
- [19] a) T. Komatsu, *J. Mater. Chem.* **2001**, *11*, 802; b) T. Komatsu, *J. Mater. Chem.* **2001**, *11*, 474.
- [20] E. Kroke, M. Schwarz, E. Horath-Bordon, P. Kroll, B. Noll, A. D. Norman, *New J. Chem.* **2002**, *26*, 508.
- [21] J. Sehnert, K. Bärwinkel, J. Senker, *J. Phys. Chem. B* **2007**, *111*, 10671.
- [22] a) B. Jürgens, W. Milius, P. Morys, W. Schnick, *Z. Anorg. Allg. Chem.* **1998**, *624*, 91; b) B. Jürgens, E. Irran, J. Schneider, W. Schnick, *Inorg. Chem.* **2000**, *39*, 665. c) E. Irran, B. Jürgens, W. Schnick, *Chem. Eur. J.* **2001**, *7*, 5372.
- [23] J. L. Hoard, *J. Am. Chem. Soc.* **1938**, *60*, 1194.
- [24] W. Madelung, E. Kern, *Justus Liebig's Ann. Chem.* **1922**, *427*, 1.
- [25] B. Jürgens, H. A. Höpfe, W. Schnick, *Inorg. Chem.* **2002**, *41*, 4849.
- [26] B. V. Lotsch, J. Senker, W. Schnick, *Inorg. Chem.* **2004**, *43*, 895.
- [27] a) B. V. Lotsch, J. Senker, W. Kockelmann, W. Schnick, *J. Solid State Chem.* **2003**, *176*, 180; b) B. V. Lotsch, W. Schnick, E. Naumann, J. Senker, *J. Phys. Chem. B*, **2007**, *111*, 11680.
- [28] M. B. Frankel, E. A. Burns, J. C. Butler, E. R. Wilson, *J. Org. Chem.* **1963**, *28*, 2428.
- [29] B. V. Lotsch, W. Schnick, *New J. Chem.* **2004**, *28*, 1129.

- [30] B. V. Lotsch, W. Schnick, *Chem. Mater.* **2005**, *17*, 3976.
- [31] B. V. Lotsch, J. Senker, W. Kockelmann, W. Schnick, *J. Solid State Chem.* **2003**, *125*, 10288.
- [32] B. V. Lotsch, W. Schnick, *Chem. Mater.* **2005**, *17*, 3982.
- [33] B. V. Lotsch, W. Schnick, *Chem. Mater.* **2006**, *18*, 1891.
- [34] B. V. Lotsch, W. Schnick, *Chem. Eur. J.* **2007**, *13*, 4956.
- [35] a) B. Jürgens, E. Irran, J. Senker, P. Kroll, H. Müller, W. Schnick, *J. Am. Chem. Soc.* **2003**, *125*, 10288; b) A. Sattler, W. Schnick, *Z. Anorg. Allg. Chem.* **2006**, *632*, 238.
- [36] A. Sattler, L. Seyfarth, J. Senker, W. Schnick, *Z. Anorg. Allg. Chem.* **2005**, *631*, 2545.
- [37] A. Sattler, W. Schnick, *Z. Anorg. Allg. Chem.* **2008**, *634*, 1063.
- [38] A. Sattler, S. Schönberger, W. Schnick, *Z. Anorg. Allg. Chem.* **2010**, *in print*.
- [39] B. V. Lotsch, M. Döblinger, J. Sehnert, L. Seyfarth, J. Senker, O. Oeckler, W. Schnick, *Chem. Eur. J.* **2007**, *13*, 4969.
- [40] A. Sattler, W. Schnick, *Z. Anorg. Allg. Chem.* **2006**, *632*, 1518.
- [41] J. Wagler, N. E. A. El-Gamel, E. Kroke, *Z. Naturforsch.* **2006**, *61b*, 975.
- [42] E. Horvath-Bordon, E. Kroke, I. Svoboda, H. Fueß, R. Riedel, S. a Neeraj, A. K. Cheetham, *Dalton Trans.* **2004**, *22*, 3900.
- [43] L. Seyfarth, J. Sehnert, N. El-Gamel, W. Milius, E. Kroke, J. Breu, J. Senker, *J. Mol. Structure* **2008**, *889*, 217.
- [44] E. Horvath-Bordon, E. Kroke, I. Svoboda, H. Fuess, R. Riedel, *New J. Chem.* **2005**, *29*, 693.
- [45] S. J. Makowski, D. Gunzelmann, J. Senker, W. Schnick, *Z. Anorg. Allg. Chem.* **2009**, *635*, 2434
- [46] S. J. Makowski, W. Schnick, *Z. Anorg. Allg. Chem.* **2009**, *635*, 2197.
- [47] C. Clauss, J. Wagler, M. Schwarz, A. Schwarzer, E. Kroke, *Z. Anorg. Allg. Chem.* **2010**, *636*, 196.
- [48] S. Tragl, H.-J. Meyer, *Z. Anorg. Allg. Chem.* **2005**, *631*, 2300.
- [49] D. R. Miller, D. C. Swenson, E. G. Gillan, *J. Am. Chem. Soc.* **2004**, *126*, 5372.
- [50] R. S. Hosmane, M. A. Rossman, N. J. Leonard, *J. Am. Chem. Soc.* **1982**, *104*, 5497.
- [51] T. Saplinova, V. Bakumov, T. Gmeiner, J. Wagler, M. Schwarz, E. Kroke, *Z. Allg. Anorg. Chem.* **2009** in press; DOI: 10.1002/zaac.200900311.
- [52] H. Schroeder, E. Kober, *J. Org. Chem.* **1962**, *27*, 4262.
- [53] B. Traber, T. Oeser, R. Gleiter, M. Goebel, R. Wortmann, *Eur. J. Org. Chem.* **2004**, *21*, 4387.
- [54] N. E. A. El-Gamel, L. Seyfarth, J. Wagler, H. Ehrenberg, M. Schwarz, J. Senker, E. Kroke, *Chem. Eur. J.* **2007**, *13*, 1158.
- [55] M. R. Schwarz, H. Ehrenberg, M. A. Kloc, E. Kroke, *Heterocycles* **2006**, *68*, 2499.
- [56] A. K. Hau, T. H. Kwan, P. K. Li, *J. Am. Soc. Nephrol.* **2009**, *20*, 245.
- [57] Melamine based resins are the topic of many patents and their importance is stressed in several textbooks e.g. *Römpp Chemie Lexikon* (Eds. J. Falbe, M. Regitz), Georg Thieme Verlag; Stuttgart New York, 9th Edition, **1996**, vol. 2, pp 2677.
- [58] Compounds based on melamine or melem are mentioned in many patents concerning flame retardants; examples are:
a) T. Yosomiya, *JP-Pat.* 2003272451, **2003**; b) K. Furuta, *JP-Pat.* 20000198907, **2000**.
- [59] a) V. L. Matveev, A. I. Finkel'shtein, Y. I. Mushkin, S. M. Slonchak, *SU-Pat.* 697603, **1979**; b) V. L. Matveev, A. I. Finkel'shtein, V. A. Lukoyanov, S. M. Slonchak, *SU-Pat.* 616345, **1978**.
- [60] A considerable amount of works cover this field. A rather recent example is:
M. Yamauchi, T. Kimura, K. Takeda, K. Sakamoto, M. Ohata, T. Tabe, K. Nakano, S. Fujiwara, Seiji, Y. Takao, G. Toda, *Alcoholism: Clin. Exp. Res.* **2000**, *24*, 39S.

- [61] a) F. Goettmann, A. Fischer, M. Antonietti, A. Thomas, *Chem. Commun.* **2006**, 4530; b) F. Goettmann, A. Fischer, M. Antonietti, A. Thomas, *New. J. Chem.* **2007**, *31*, 1455; c) F. Goettmann, A. Thomas, M. Antonietti, *Angew. Chem.* **2007**, *119*, 2773; *Angew. Chem. Int. Ed.* **2007**, *46*, 2717.
- [62] X. Wang, K. Maeda, A. Thomas, K. Takanabe, G. Xin, J. M. Carlsson, K. Domen, M. Antonietti, *Nat. Mater.* **2009**, *8*, 76.
- [63] Y. Zhang, A. Thomas, M. Antonietti, X. Wang, *J. Am. Chem. Soc.* **2009**, *131*, 1384.
- [64] a) S. Ito, T. Murata, M. Hasegawa, Y. Bito, Y. Toyoguchi, *J. Power Sources* **1997**, *68*, 245; b) M. Koh, T. Nakajima, R. N. Singh, *Mol. Cryst. Liq. Cryst.* **1998**, *310*, 341.
- [65] S. Jahromi, U. Moosheimer, *Macromolecules* **2000**, *33*, 7582.
- [66] E. C. Franklin, *J. Am. Chem. Soc.* **1922**, *44*, 486.
- [67] D. R. Miller, J. R. Holst, E. G. Gillan, *Inorg. Chem.* **2007**, *46*, 2767.
- [68] S. Tragl, K. Gibson, H.-J. Meyer, *Z. Anorg. Allg. Chem.* **2004**, *630*, 2373.
- [69] S. Tragl, K. Gibson, J. Glaser, G. Heydenrych, G. Frenking, V. Duppel, A. Simon, H.-J. Meyer, *Z. Anorg. Allg. Chem.* **2008**, *634*, 2754.
- [70] S. Tragl, K. Gibson, J. Glaser, V. Duppel, A. Simon, H.-J. Meyer, *Solid State Commun.* **2007**, *141*, 529.
- [71] T. Gasparis-Ebeling, H. Nöth, *Angew. Chem.* **1984**, *96*, 301; *Angew. Chem. Int. Ed.* **1984**, *23*, 303.
- [72] a) W. Harrison, R. T. Oakley, N. L. Paddock, J. Trotter, *Chem. Commun.* **1971**, 357; b) W. Harrison, J. Trotter, *J. Chem. Soc., Dalton Trans.* **1972**, 623.
- [73] Several crystal structures of hexaborates have been published. For some recent papers please refer to:
a) Z. Liu, L. J. Li, M. Hu, *J. Alloys Compd.* **2005**, *394*, 277; b) T. Yue, L. Zhu, S. Xia, S. Gao, K. Yu, *J. Alloys Compd.* **2003**, *358*, 87; c) G. Heller, J. Schnellhaas, *Z. Kristallogr.* **1983**, *164*, 237; d) H. Behm *Acta Crystallogr.* **1983**, *C39*, 1156.
- [74] J. Liebig, *Ann. Chem. Pharm.* **1834**, *10*, 1.
- [75] J. Liebig, *Ann. Chem. Pharm.* **1844**, *50*, 337.
- [76] J. Liebig, *Ann. Chem. Pharm.* **1845**, *53*, 330.
- [77] J. Liebig, *Ann. Chem. Pharm.* **1847**, *61*, 262.
- [78] J. Liebig, *Ann. Chem. Pharm.* **1855**, *95*, 257.
- [79] L. Gmelin, *Ann. Pharm.* **1835**, *15*, 252.
- [80] W. Henneberg, *Ann. Chem. Pharm.* **1850**, *73*, 228.
- [81] J. Klason, *J. prakt. Chem.* **1886**, *33*, 285.
- [82] W. L. Burdick, *J. Am. Chem. Soc.* **1925**, *47*, 1485.
- [83] W. Madelung, E. Kern, *Justus Liebigs Ann. Chem.* **1922**, *427*, 26.
- [84] E. C. Franklin, *The Nitrogen System of Compounds*, The Reinhold Publishing Corp., New York, **1935**, p. 107.
- [85] E. W. Hugh, *J. Am. Chem. Soc.* **1941**, *63*, 1737.
- [86] a) E. H. Moerman, N. F. Wiebenga, *Z. Krist.* **1938**, *99*, 217; b) G. A. Croes, A. J. van Gent, R. P. van Oosten, D. W. Smits, *J. Am. Chem. Soc.* **1952**, *74*, 6156.
- [87] J. Biechler, *Compt. Rend.* **1936**, *203*, 568.
- [88] a) *Chem. Eng. News* **2000**, *Aug. 7*, 62; b) *Chem. Eng. News* **2000**, *Oct. 2*, 8; c) E. K. Wilson, „*Old Molecules, New Chemistry*“ *Chem. Eng. News, Latest News* **2004**, *May 26*.
- [89] A. I. Finkel'shtein, N. V. Spiridonova, *Russ. Chem. Rev.* **1964**, *33*, 400.
- [90] *SciFinder ScholarTM*, American Chemical Society, **2007**.
- [91] a) M. Schütze, *Angew. Chem.* **1958**, *70*, 679; b) M. Schulze (Badische Anilin- & Soda-Fabrik Akt.-Ges.), *DE-Pat* 869052, **1953**; c) M. Schulze (Badische Anilin- & Soda-Fabrik Akt.-Ges.), *DE-Pat.* 965634, **1957**.
- [92] C. Giacovazzo, H. L. Monaco, G. Artioli, D. Viterbo, G. Ferraris, G. Gilli, G. Zanotti, *Fundamentals of Crystallography*, IUCr Texts on Crystallography, 2nd Edition, Oxford University Press, New York **2002**.

- [93] B. K. Vainstein, *Fundamentals of Crystals. Symmetry and Methods of Structural Crystallography I*, Springer Verlag, Berlin, **1996**.
- [94] *BASREADER*, v2.13a, Raytest Isotopenmessgeräte GmbH, Straubenhardt, **1994**.
- [95] *TINA*, 2.10g, Raytest Isotopenmessgeräte GmbH, Straubenhardt, **1993**.
- [96] Z. Otwinowski, W. Minor, *Methods Enzymol.* **1997**, 276, 307.
- [97] G. M. Sheldrick, *XPREP, Data Preparation & Reciprocal Space Exploration*; v6.12, Siemens Analytical X-ray Instruments, **1996**.
- [98] L. J. Farrugia, *WinGX*, v1.61, University of Glasgow, **1998**.
- [99] a) A. L. Speck, *Acta Crystallogr.* **2003**, A46, c34; b) A. L. Speck, *PLATON, A multipurpose Crystallographic Tool*, Utrecht University, **2003**.
- [100] K. Brandenburg, *DIAMOND, Program for X-ray Structure Analysis*, v3.1a – v3.2c, Crystal Impact GbR, Bonn.
- [101] a) G. M. Sheldrick, *Acta Crystallogr.* **2008**, A64, 112; b) G. M. Sheldrick, *SHELX-97, Program package for the solution and refinement of crystal structures*, Release 97-2, Universität Göttingen, **1997**.
- [102] A. Altomare, M. C. Burla, M. Camalli, G. L. Cascarano, C. Giacovazzo, A. Guagliardi, A. G. G. Moliterni, G. Polidori and R. Spagna, *J. Appl. Cryst.* **1999**, 32, 115.
- [103] *STOE IPDS Software package*, v. 2.94, STOE & Cie GmbH, Darmstadt, **2000**.
- [104] *Win XPOW*, v2.12, STOE & Cie GmbH, Darmstadt, **2005**.
- [105] *OPUS, Programm zur Auswertung von Schwingungsspektren*, v3.0.2, Bruker Optics GmbH, Karlsruhe, **1996**.
- [106] A. Sattler, S. Pagano, M. Zeuner, A. Zurawski, D. Gunzelmann, J. Senker, K. Müller-Buschbaum, W. Schnick, *Chem. Eur. J.* **2009**, 15, 13161.
- [107] B. Jürgens, *Doctoral Thesis*, University of Munich (LMU), **2004**.
- [108] B. V. Lotsch, *Doctoral Thesis*, University of Munich (LMU), **2007**.
- [109] M. Zeuner, F. Hintze, W. Schnick, *Chem. Mater.* **2009**, 21, 336.
- [110] J. N. Varghese, A. M. O'Connell, E. N. Maslen, *Acta Crystallogr.* **1977**, B33, 2102.
- [111] A. Sattler, *Diploma Thesis*, University of Munich (LMU), **2005**.
- [112] a) E. N. Boitsov, A. I. Finkel'shtein, *Zh. Obsh. Chem.* **1962**, 32, 321; b) E. N. Boitsov, A. I. Finkel'shtein, *Zh. Obsh. Chem.* **1962**, 32, 3403.
- [113] The reaction has been established decades ago and several patents deal with this process see e.g.
a) F. Castillo-Welter, C. Steden, M. Mueller-Hasky, G. Ehring, D. Walter (Lurgi GmbH, Germany), *Ger. Offen.* DE 102008032425, **2010**; b) Van Hardeveld, Rudolf (Stamicarbon B. V., Neth.) *Ger. Offen.* DE 2802238, **1978**.
- [114] *Römpp-Lexikon Chemie*, (Eds J. Falbe, M. Regitz), Vol. 2, 10th Edition, Thieme, Stuttgart, **1997**, pp 2677.
- [115] a) A. I. Finkel'shtein, V. M. Karlik, L. N. Al'tshuler, M. V. Rozhnova, V. I. Zagranichnyi, *SU-Pat* 956481, **1982**; b) V. A. Gal'perin, V. M. Karlik, A. I. Finkel'shtein, V. I. Zagranichnyi, *SU-Pat* 386943, **1973**.
- [116] V. M. Karlik, L. N. Al'tshuler, V. I. Zagranichnyi, A. I. Finkel'shtein, A. A. Arakelyan, G. G. Kazaryan, *SU-Pat* 1490122, **1989**.
- [117] V. M. Karlik, V. A. Gal'perin, V. I. Zagranichnyi, A. I. Finkel'shtein, *SU-Pat* 413147, **1974**.
- [118] A. I. Finkel'shtein, M. V. Rozhnova, *Khimiya i Khimicheskaya Tekhnologiya* **1990**, 33, 113.
- [119] T. B. Gavrilova, Yu. S. Nikitin, T. A. Rudnitskaya, A. I. Finkel'shtein, *Zh. Fiz. Chem.* **1993**, 67, 1436.
- [120] B. V. Lotsch, W. Schnick, *Z. Naturforsch.* **2004**, 59b, 1229.
- [121] B. V. Lotsch, W. Schnick, *Z. Naturforsch.* **2005**, 60b, 377.
- [122] a) A. I. Finkel'shtein, *Russ. J. Gen. Chem.* **1961**, 31, 1046; *Zh. Obsh. Chem.* **1961**, 31, 1132; b) A. I. Finkel'shtein, N. V. Spiridonova, *Russ. Chem. Rev.* **1964**, 33, 400.
- [123] N. K. Garvriilva, V. A. Gal'perin, A. I. Finkel'shtein, A. G. Koryakin, *Russ. J. Org. Chem.* **1977**, 13, 616.

- [124] L. Costa, G. Camino, G. Martinasso, *Polym. Prepr. Am. Chem. Soc. Div. Polym. Chem.* **1989**, *30*, 531.
- [125] T. Steiner, *Angew. Chem.* **2002**, *114*, 50; *Angew. Chem. Int. Ed.* **2002**, *41*, 48.
- [126] H. Krall, *J. Chem. Soc., Trans.* **1913**, *103*, 1378.
- [127] *Gmelins Handbuch der anorganischen Chemie Kohlenstoff, D6, Verbindungen*, Springer-Verlag, Berlin, Heidelberg, New York, 8th Edition, **1978**, pp 91.
- [128] a) W. Klempt *Chem. Tech.* **1942**, *15*, 1; b) S. Kodama, S. Kukushima, S. Nose, J. Nakajima, *J. Chem. Soc. Japan Ind. Chem Sect.* **1953**, *56*, 49; c) T. Yanagimoto, *Rev. Phys. Chem. Japan* **1954**, *24*, 1.
- [129] J. Madarász, G. Pokol, *J. Therm. Anal. Calorim.* **2007**, *88*, 329.
- [130] A. I. Finkel'shtein, N. V. Spiridoova, *Russ. Chem. Rev.* **1964**, *33*, 400.
- [131] B. V. Lotsch, W. Schnick, *Z. Anorg. Allg. Chem.* **2007**, *633*, 1435.
- [132] *Handbook of Chemistry and Physics*, (Editor in Chief R. C. Weast) The Chemical Rubber Co., Cleveland, Ohio, 49th Edition, **1968**, p. D91.
- [133] B. V. Lotsch, M. Döblinger, *personal communications*.
- [134] A. Wöhler, *Ann. Phys.* **1821**, *69*, 273.
- [135] a) A. Hordvik, *Acta Chem. Scand.* **1961**, *15*, 1186; b) H. J. Emeléus, A. Haas, N. J. Shepperd, *J. Chem. Soc.* **1963**, 3165.
- [136] A. Goldberg, *J. Prakt. Chem.* **1901**, *63*, 41.
- [137] W. M. Lehmann, *Z. Kristallogr. Kristallgeom. Kristallphys. Kristallchem.* **1924**, *60*, 379.
- [138] a) E. H. Wiebenga, N. F. Moerman, *Nature* **1938**, *141*, 122; b) E. H. Wiebenga, N. F. Moerman, *Z. Kristallogr.* **1938**, *99*, 217.
- [139] E. H. Wiebenga, *J. Am. Chem. Soc.* **1952**, *74*, 6156.
- [140] A. Sattler, W. Schnick, *Z. Anorg. Allg. Chem.* **2006**, *632*, 531
- [141] A. Sattler, M. R. Budde, W. Schnick, *Z. Anorg. Allg. Chem.* **2009**, *635*, 1933.
- [142] N. I. Zhogrova, N. V. Spiridonova, A. I. Finkel'shtein, *Zh. Prikl. Spektrosk.* **1973**, *19*, 153.
- [143] C. E. Redemann, H. J. Lucas, *J. Am. Chem. Soc.* **1940**, *62*, 842.
- [144] H. Lueken, *Magnetochemie*, B. G. Teubner; Stuttgart, Leibzig, **1999**.
- [145] A. Sattler, W. Schnick, *Z. Anorg. Allg. Chem.* **2008**, *634*, 1063.
- [146] D. D. Perrin, W. L. F. Armarego, *Purification of Laboratory Chemicals*, Pergamon Press, Oxford, New York, Seoul, Tokyo, 3rd Edition, **1988**, p 157.
- [147] A. Sattler, W. Schnick, *Eur. J. Inorg. Chem.* **2009**, 4972.
- [148] C. E. Redemann, H. J. Lucas, *J. Am. Chem. Soc.* **1939**, *61*, 3423.
- [149] *Handbook of Chemistry and Physics*, (Editor in Chief D. R. Lide) The Chemical Rubber Co., Cleveland, Ohio, 88th Edition, **2008**, pp. 4-82 (KOCN), 4-83 (KSCN), 4-89 (NaOCN), 4-91 (NaSCN).
- [150] *Sicherheitsdatenblatt*, Kaliumcyanat zur Synthese, Merck Schuchard OHG, Hohenbrunn, **2005**, p. 3.
- [151] a) *Gmelins Handbuch der anorganischen Chemie Natrium*, Verlag Chemie GmbH, Weinheim, 8th Edition **1967**, pp. 1382 (NaOCN), pp. 1387 (NaSCN).
b) *Gmelins Handbuch der anorganischen Chemie Kalium*, Verlag Chemie GmbH, Weinheim, Berlin, 8th Edition **1937**, pp. 890 (KOCN), pp. 894 (KSCN).
- [152] S. Grimme, *Angew. Chem.* **2008**, *120*, 3478; *Angew. Chem. Int. Ed.* **2008**, *47*, 3430.
- [153] E. Horvath-Bordon, *Doctoral Thesis*, Technische Universität Darmstadt, **2004**.
- [154] M. Schwarz, H. H. Buschmann, E. Kroke, O. Jimenez Alonso, J. Holenz, J. Corbera Arjona, D. Payella, C. Pelejero, C. R. Trullas (Isdin, S.A., Spain). *Eur. Pat. Appl.* EP-1854797, **2007**.
- [155] *Handbook of Chemistry and Physics*, (Editor in Chief R. C. Weast) The Chemical Rubber Co., Cleveland, Ohio, 47th Edition, **1968**, p. B-227.
- [156] C. Gremmelmaier, J. Riethmann, (Ciba-Geigy Corp., USA) *U.S.-Pat* 4205167, **1980**.
- [157] E. Ott, *Ber. Deutsch. Chem. Ges.* **1919**, *52B*, 656.

- [158] E. Kroke, M. Schwarz, R. Riedel, I. Svoboda, H. Fuess, *Z. Kristallogr. - New Cryst. Struct.* **1999**, *214*, 111.
- [159] a) R. E. Del Sesto, M. Botoshansky, M Kaftory, A. M. Arif, J. S. Miller *Cryst. Eng. Commun.* **2002**, *4*, 117; b) R. E. Del Sesto, A. M. Arif, J. S. Miller, *Chem. Commun.* **2001**, 2730; c) R. E. Del Sesto, A. M. Arif, J. J. Novoa, I. Anusiewicz, P. Skurski, J. Simons, B. C. Dunn, E. M. Eyring, J. S. Miller, *J. Org. Chem.* **2003**, *68*, 3367.
- [160] G. Beck, *U.S.-Pat.* 5086172, **1992**.
- [161] M. Sundermeier, A. Zapf, M. Beller, *Eur. J. Inorg. Chem.* **2003**, 3513.
- [162] a) T. Schareina, A. Zapf, M. Beller, *J. Organomet. Chem.* **2004**, *689*, 4576; b) T. Schareina, A. Zapf, M. Beller, *Chem. Commun.* **2004**, 1388.
- [163] a) *Römpf-Lexikon Chemie*, (Eds J. Falbe, M. Regitz), Vol. 3, 10th Edition, Thieme, Stuttgart, **1997** p. 2161; b) J. Kjeldahl, *Z. Anal. Chem.* **1883**, *22*, 366.
- [164] A. Ranganathan, V. R. Pedireddi, C. N. R. Rao, *J. Am. Chem. Soc.* **1999**, *121*, 1752.
- [165] F. H. Herbstein, *J. Chem. Crystallogr.* **2003**, *33*, 527.
- [166] Y. Wang, B. Wei, Q. Wang, *J. Crystallogr. Spec. Res.* **1990**, *20*, 79.
- [167] a) G. M. Whitesides, E. E. Simanek, J. P. Mathias, C. T. Seto, D. N. Chin, M. Mammen, D. M. Gordon, *Acc. Chem. Res.* **1995**, *28*, 37; b) G. M. Whitesides, J. P. Mathias, C. T. Seto, *Science* **1991**, *254*, 1312.
- [168] B. V. Lotsch, W. Schnick, *Chem. Mater.* **2006**, *18*, 1891.